LEABHARLANN CHOLÁISTE NA TRÍONÓIDE, BAILE ÁTHA CLIATH | TRINITY COLLEGE LIBRARY DUBLIN
Ollscoil Átha Cliath | The University of Dublin

Terms and Conditions of Use of Digitised Theses from Trinity College Library Dublin

Copyright statement

All material supplied by Trinity College Library is protected by copyright (under the Copyright and Related Rights Act, 2000 as amended) and other relevant Intellectual Property Rights. By accessing and using a Digitised Thesis from Trinity College Library you acknowledge that all Intellectual Property Rights in any Works supplied are the sole and exclusive property of the copyright and/or other IPR holder. Specific copyright holders may not be explicitly identified. Use of materials from other sources within a thesis should not be construed as a claim over them.

A non-exclusive, non-transferable licence is hereby granted to those using or reproducing, in whole or in part, the material for valid purposes, providing the copyright owners are acknowledged using the normal conventions. Where specific permission to use material is required, this is identified and such permission must be sought from the copyright holder or agency cited.

Liability statement

By using a Digitised Thesis, I accept that Trinity College Dublin bears no legal responsibility for the accuracy, legality or comprehensiveness of materials contained within the thesis, and that Trinity College Dublin accepts no liability for indirect, consequential, or incidental, damages or losses arising from use of the thesis for whatever reason. Information located in a thesis may be subject to specific use constraints, details of which may not be explicitly described. It is the responsibility of potential and actual users to be aware of such constraints and to abide by them. By making use of material from a digitised thesis, you accept these copyright and disclaimer provisions. Where it is brought to the attention of Trinity College Library that there may be a breach of copyright or other restraint, it is the policy to withdraw or take down access to a thesis while the issue is being resolved.

Access Agreement

By using a Digitised Thesis from Trinity College Library you are bound by the following Terms & Conditions. Please read them carefully.

I have read and I understand the following statement: All material supplied via a Digitised Thesis from Trinity College Library is protected by copyright and other intellectual property rights, and duplication or sale of all or part of any of a thesis is not permitted, except that material may be duplicated by you for your research use or for educational purposes in electronic or print form providing the copyright owners are acknowledged using the normal conventions. You must obtain permission for any other use. Electronic or print copies may not be offered, whether for sale or otherwise to anyone. This copy has been supplied on the understanding that it is copyright material and that no quotation from the thesis may be published without proper acknowledgement.

Characterisation of the Role of the *Candida albicans* Tor1 Pathway in regulating Flocculation, Biofilm Formation & Hyphal Growth

A thesis submitted to The University of Dublin in fulfillment of the requirements for the degree of Doctor of Philosophy by

Peter Richard Flanagan

May 2016

Trinity College Dublin
The University of Dublin

Microbiology Research Unit,
Division of Oral Biosciences,
Dublin Dental University Hospital,
University of Dublin,
Trinity College.

PMJ
DENTAL SCIENCE

Declaration

I declare that this thesis has not been submitted as an exercise for a degree at this or any other university and it is entirely my own work. I agree to deposit this thesis in the University's open access institutional repository or allow the library to do so on my behalf, subject to Irish Copyright Legislation and Trinity College Library conditions of use and acknowledgement.

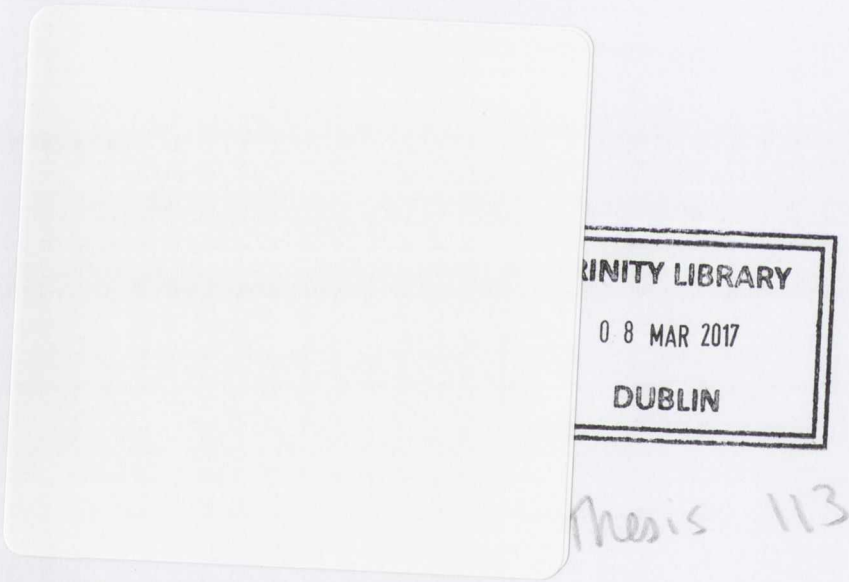
RINITY LIBRARY
0 8 MAR 2017
DUBLIN
Thesis 11314

Acknowledgments

Firstly, I'd like to thank everyone in our laboratory for always being there to help. Dr. John Haran and Dr. Peter Hyde, you both have been a fountain of knowledge when I needed advice about experiments and all the random questions I had! Dr. Emma-Louise McGinley and Dr. Maria Boyle, I'd like to thank you both for your help with tissue culture woes and Dr. Brenda McManus, who was on hand for PCR troubleshooting! I'd also like to thank Dr. Aisling Miller for taking some of the higher quality images for me and Dr. Sarah Teckelenbourg for the odd shots to calm the stressful days! I'd also like to thank Prof. David Coleman, Prof. Derek Sullivan, Dr. Mary O'Donnell and Dr. Peter Kinnevey whom I could always go to if ever I needed something as well as Dr. Eimear Connolly. Thanks for the laughs and awful smells in the back lab! Aoife O'Connor and Alexandros Lazaris, thanks for being great friends throughout and taking time points while I was demonstrating. Dr. Hannah Boyle, you may have beaten me to the viva, but I was happy to have you by my side as we did our PhD's together, and of course for correcting my grammar and spelling over the last few years. Associate Prof. Anna Shore, thank you for all your advise, the laughs, the "words of wisdom" to help me through the PhD blues and the "Pinot Noir"! They wont be forgotten.

Secondly, I'd like to Dr. Steven Bates of the University of Exeter Biosciences College of Life and Environmental Sciences for the use of the P_{ENO} promotor and our collaborator Dr. Julia Kohler of Harvard University for the P_{TET}*TOR1* strain.

Finally, I am extremely grateful and thankful to my supervisor Associate Professor Gary Moran. I am grateful of the chance you gave me to undertake this project and and for all the advice and help through out the last few years. Thank you.

Dedication

I'd like to dedicate this thesis to my closest friends (The Scoobies!) for supporting me throughout the last few years, especially the last year and a half. The girls, Beans, Moylo and Ned for the chats, cakes and copious cups of tea and coffee! The lads, Prior, Marco and Bren for the de-stressing poker nights, rugby games, chicken wings and nachos! And of course Fiadh and my goddaughter Éle, for all the hugs!

Finally to my family, my parents and my brother. From my undergrad in Maynooth, setting me up in the UK when I went to work at Oxford University and help when I decided to undertake a masters in London. You've always been there for me especially when it came to education and I'm extremely grateful.

Contents

1 General Introduction **1**

1.1 The Fungal Kingdom 2

1.2 Antifungal Drugs & Resistance 3

1.3 *Candida* Species and Candidosis 4

1.4 *Candida albicans* 6

1.5 Dimorphic Trait of *Candida albicans* & the Ability to Form Biofilms . . . 7

1.6 The Tor1 Kinase 11

1.6.1 Regulation of Nitrogen Metabolism 13

1.6.2 Regulation of Ribosome Biogenesis 14

1.6.3 Regulation of Filamentous Growth & Adhesion 17

1.6.4 The Putative Activators of Tor1 20

1.7 Overview and Aims of Doctoral Project 23

2 General Materials and Methods **25**

2.1 Chemicals, Buffers and Molecular Biological Reagents 26

2.2 General Laboratory Equipment and Plasticware 26

2.3 Microbial Cultures 29

2.3.1 *Candida albicans* Strains 29

2.3.2 Tissue cultures 30

2.4 DNA Techniques 30

2.4.1 DNA Extractions 30

2.5 RNA Techniques 32

2.5.1 Rapid RNA Isolation 32
2.5.2 Freeze-fracture Method 32
2.5.3 cDNA Synthesis 33
2.6 Polymerase Chain Reaction (PCR) 34
2.6.1 Standard PCR 34
2.6.2 Cleanup of PCR Products 34
2.6.3 Quantitative Real-Time PCR (qRT-PCR) 34
2.7 Transformations of *Candida albicans* 35
2.8 Growth Rate Determination 36
2.9 Hyphal Formation Assays (*Solid Medium*) 36
2.10 Enumeration of Free Yeast Cells in Flocculating Cultures of Filamentous Cells 37
2.11 Visual Flocculation Assays 37
2.12 Biofilm Assays 38
2.13 Adherence Assays 38
2.14 Two-Colour Microarray-Bassed Gene Expression Analysis (*Low Input Quick Amp Labeling*) 39
2.14.1 Sample Preparation 39
2.14.1.1 Preparation of Spike A & Spike B 39
2.14.1.2 Preparation of Labeling Reaction 40
2.14.1.3 Purifying Labeled/Amplified RNA 41
2.14.1.4 Quantification of cRNA 41
2.14.2 Hybridisation 42
2.14.2.1 Preparation of 10X Blocking Agent 42
2.14.2.2 Preparation of Hybridisation Samples 42
2.14.2.3 Preparation of Hybridisation Assembly & Hybridisation 42
2.14.3 Microarray Wash 43
2.14.3.1 Addition of Triton X-102 to Gene Expression Wash Buffers 43

2.14.3.2 Preparation of Equipment 43
2.14.3.3 Washing the Microarray Slide 43
2.14.4 Scanning & Feature Extraction 44
2.14.4.1 Scanning, Processing & Extraction of Data 44
2.14.4.2 Analysis of Data 44
2.15 Gene Set Enrichment Analysis 44

3 Over-expression & Phenotypic Analysis of Putative Activators of *Candida albicans* Tor1 **47**

3.1 Introduction 48
3.2 Materials and Method 49
3.2.1 Caffeine Resistant *Candida albicans* Transformations 49
3.2.2 Transformations of *Candida albicans* with the Enolase 1 Promoter (P_{ENO}) 49
3.3 Results 51
3.3.1 Generation of Caffeine Resistant Tor1 Hyperactive Mutants . . . 51
3.3.2 Use of the Enolase1 Promotor (P_{ENO}) to Overexpress Putative Tor1 Pathway Proteins as a Strategy for Generating a Constitutively Active Tor1 54
3.3.3 Determination of Cellular Growth of P_{ENO} Strains Compared to WT SC5314 56
3.3.4 Hyphal Formation Assays of P_{ENO} Strains Compared to WT SC5314 62
3.3.4.1 Formation of Hyphae on Solid Medium 62
3.3.4.2 Formation of Hyphae in Liquid Medium 63
3.3.4.3 Development of a Semi-Quantitative Assay to Enumerate Flocculation and Aggregation of *Candida* Strains in Filament Inducing Medium 66
3.3.4.4 Qualitative & Semi-Quantitative analysis of Aggregation of P_{ENO} Strains in a Filament Inducing Medium . . 70

3.3.5 Flocculation Assay of P_{ENO} Strains Compared to WT SC5314 . . 73
3.3.6 Effects of Rapamycin on P_{ENO} strains. Minimal Inhibitory Concentration Assay 73
3.3.7 Biofilm Formation of P_{ENO} Strains Compared to WT SC5314 . . . 76
3.3.8 Ability of P_{ENO} Strains to adhere to Human Buccal Epithelial (TR146) Cells Compared to WT SC5314 76
3.4 Discussion 79
3.4.1 Generation & Analysis of Constitutively Active Tor1 Mutants of *Candida albicans* 79
3.4.2 Growth Curve Analysis of P_{ENO} Strains Compared to WT SC5314 80
3.4.3 Hyphal Formation Analysis of P_{ENO} Strains Compared to WT SC5314 in Response to Nitrogen Starvation 82
3.4.4 Hyphal Formation and Enumeration of Free Yeast Cells in Liquid Culture of P_{ENO} Strains Compared to WT SC5314 83
3.4.5 Analysis of Flocculation of P_{ENO} Strains compared to WT SC5314 84
3.4.6 Analysis of Biofilm Formation of P_{ENO} Strains Compared to WT SC5314 85
3.4.7 Analysis of the ability of P_{ENO} Strains to Adhere to Human Buccal Epithelial TR146 Cells Compared to WT SC5314 86

4 Phenotypic Analysis of *GTR1* & *RHB1* mutants of *C. albicans* and a Conditional Mutant of *TOR1* **87**
4.1 Introduction 88
4.2 Materials and Methods 91
4.2.1 Cassette Generation and Gene Knockouts 91
4.2.2 *SAT1* Cassette Removal 91
4.2.3 Reintroduction of *GTR1* to the Δ*gtr1* Mutant Background 92
4.2.3.1 PCR amplification of *GTR1* Gene for Reintegration . . . 92

4.2.3.2 Ligation of *GTR1* to pCDRI Plasmid and *E. coli* transformation 92
4.2.3.3 Linearising pCDRI/*GTR1* plasmid and Transformation of Δ*gtr1* 93
4.3 Results 94
4.3.1 Generation of Δ*rhb*, Δ*gtr* & tetO-*TOR1*/*tor1* Mutants 94
4.3.1.1 Phospho-RPS6 (P-S6) Assay 95
4.3.2 Determination of Cellular Growth Rate of Δ*rhb1*, Δ*gtr1* & tetO-*TOR1*/*tor1* Compared to WT SC5314 98
4.3.2.1 Cellular Growth Rate of Δ*rhb1* & Δ*gtr1* 98
4.3.2.2 Cellular Growth Rate of tetO-*TOR1*/*tor1* 98
4.3.3 Hyphal Formation Assays of Δ*rhb1*, Δ*gtr1* & tetO-*TOR1*/*tor1* Compared to WT SC5314 103
4.3.3.1 Formation of Hyphae by Δ*rhb1* & Δ*gtr1* on Solid Medium 103
4.3.3.2 Qualitative & Semi-Quantitative analysis of Aggregation of Δ*rhb1* & Δ*gtr1* Strains in a Filament Inducing Medium 105
4.3.3.3 Qualitative & Semi-Quantitative analysis of Aggregation of tetO-*TOR1*/tor1 in a Filament Inducing Medium 105
4.3.4 Flocculation of Δ*rhb1*, Δ*gtr1* & tetO-*TOR1*/*tor1* Compared to WT SC5314 111
4.3.4.1 Flocculation of Δ*rhb1* & Δ*gtr1* 111
4.3.4.2 Flocculation of tetO-*TOR1*/*tor1* 111
4.3.5 Effects of *TOR1* Disruption on Cell Wall Integrity 116
4.3.5.1 Disruption of Cell Wall Integrity in Δ*rhb1* & Δ*gtr1* Strains 116
4.3.5.2 Disruption of Cell Wall Integrity in tetO-*TOR1*/*tor1* Strains 116
4.3.6 Analysis of the Response to Oxidative Stress in the Tor1 Pathway of Mutant Strains 121

4.3.6.1 Effects of Δ*rhb1* & Δ*gtr1* Disruption on the Response to Oxidative Stress . . . 121
4.3.6.2 Effects of tetO-*TOR1*/*tor1* Regulatable Strains on the Response to Oxidative Stress . . . 121
4.3.7 Effects of Rapamycin & Fluconazole on Δ*rhb1* & Δ*gtr1* Mutant Strains. (Minimal Inhibitory Concentration Assays) . . . 124
4.3.7.1 MIC of Rapamycin on Δ*rhb1* & Δ*gtr1* . . . 124
4.3.7.2 MIC of Fluconazole Δ*rhb1* & Δ*gtr1* . . . 124
4.3.8 Biofilm Formation of Δ*rhb1* & Δ*gtr1* Mutant Strains Compared with WT SC5314. . . . 124
4.4 Discussion . . . 129
4.4.1 Gtr1 is an Upstream Activator of Tor1 . . . 130
4.4.2 Effects on Cellular Growth . . . 130
4.4.3 Effects on Hyphal Formation, Aggregation and Flocculation . . . 132
4.4.4 Effects on Cell Wall Integrity & Responses to Oxidative Stress . . 133
4.4.5 Effects on Susceptibility to Rapamycin & Fluconazole of Δ*rhb1* and Δ*gtr1* . . . 134
4.4.6 Effects on Biofilm Formation . . . 135

5 Expression Analysis of a Homozygous *GTR1* Mutant Strain of *Candida albicans* & Comparative Analysis with a Homozygous *RHB1* Mutant Strain 137
5.1 Introduction . . . 138
5.2 Materials and Methods . . . 140
5.2.1 Gene Expression Levels of the Δ*gtr1* Mutant Strain . . . 140
5.3 Results . . . 141
5.3.1 Genes Expressed at Higher Levels in the Δ*gtr1* Mutant Strain . . 141
5.3.2 Genes Expressed at Lower Levels in the Δ*gtr1* Mutant Strain . . . 141
5.3.3 Gene Set Enrichment Analysis of the Δ*gtr1* Mutant Strain 142

5.3.4 qRT-PCR Confirmation of the Δ*gtr1* DNA Microarray Expression Analysis 142
5.3.5 Differentially Expressed Genes of the Δ*gtr1* Strain Compared with the Δ*rhb1* Strain 143
5.3.6 Heat Map Analysis 149
5.3.6.1 Genes Associated with Cell-Cell Adhesion, Nitrogen Uptake & Phosphate Utilisation 149
5.3.6.2 Genes Associated with Biofilm Formation, Cell Wall-Associated Proteins, Filamentous Growth, Cellular Amino Acid Biosynthesis & Metabolic Processes 150
5.4 Discussion 153
5.4.1 Differentially Expressed Genes in a *C. albicans* Homozygous *GTR1* Mutant 153
5.4.2 Dataset Comparison of the Δ*gtr1* & Δ*rhb1* Mutant Strains 154

6 Transcriptome Analysis of the Doxycycline Regulated Expression of *Candida albicans TOR1* **157**
6.1 Introduction 158
6.2 Materials and Methods 160
6.3 Results 161
6.3.1 Investigation of the Effects of a Doxycycline-Off *TOR1* 161
6.3.1.1 Genes Expressed at Higher Levels in the tetO-*TOR1/tor1* Strain 161
6.3.1.2 Genes Expressed at Lower Levels in the tetO-*TOR1/tor1* Strain 162
6.3.1.3 Genes Expressed at Higher Levels in the tetO-ΔN*TOR1* Strain 162
6.3.1.4 Genes Expressed at Lower Levels in the tetO-ΔN*TOR1* Strain 162

6.3.1.5 Genes Expressed at Higher Levels in the tetO-ΔN*TOR1* Compared with the *tor1/TOR1* Strain 163

6.3.1.6 Genes Expressed at Lower Levels in the tetO-ΔN*TOR1* Strain Compared with the *tor1/TOR1* Strain 163

6.3.1.7 Comparison of Differentially Expressed Genes in tetO-*TOR1/tor1* and tetO-ΔN*TOR1* Strains and Rapamycin Treated Cells 164

6.3.2 Gene Set Enrichment Analysis 172

6.3.2.1 Analysis of the tetO-*TOR1/tor1* strain by GSEA 172

6.3.2.2 Analysis of the tetO-ΔN*TOR1* JKC1441 strain by GSEA 172

6.3.3 Heat Map Analysis 178

6.3.3.1 Genes Associated with Ribosome Biogenesis & pre-RNA Processing & Assembly 178

6.3.3.2 Genes Associated with Oxidative and Osmotic Stress . . 178

6.3.4 qRT-PCR Confirmation of the DNA Microarray Expression Analysis 184

6.4 Discussion 186

7 General Discussion **189**

7.1 General Discussion 190

References **205**

List of Figures

1.1 Example of *C. albicans* morphology adapted from Sudbery (2011). . . . 10

1.2 Domain structure of a generic Tor protein. 12

1.3 A representation of the downstream effects of an active/inactive Tor1. 16

1.4 Control of Adhesin and Hypha Specific Gene (HSG) Promotors. 19

1.5 A representation of the activation of Tor1. 22

3.1 Chromatograms illustrating sequence from transformation to confer caffeine resistance and amino acid change. 53

3.2 Gene expression in WT SC5314 and JRB12 strains compared with P_{ENO} transformed strains. 55

3.3 Growth curve assays of WT SC5314 compared with P_{ENO} strains. . . . 58

3.4 Doubling times of P_{ENO} strains compared with WT SC5314. 59

3.5 Growth of WT SC5314 compared with P_{ENO} strains. 60

3.6 Expression levels of *MEP2*. 61

3.7 Hyphal formation on solid medium, spot plates. 64

3.8 True hyphae formation of P_{ENO} strains. 65

3.9 Qualitative images depicting the aggregation of WT SC5314 compared to strains with a defect in filamentation. 68

3.10 Semi-quantitative analysis of the aggregation of WT SC5314 compared to strains with a defect in filamentation. 69

3.11 Qualitative aggregation of WT SC5314 compared with P_{ENO} strains in YEPD and 10% serum. 71

3.12 **Semi-quantitative analysis of the aggregation of WT SC5314 compared with P_{ENO} strains at 2, 4 & 6 h.** 72

3.13 **Flocculation of WT SC5314 compared with P_{ENO} strains.** 74

3.14 **Rapamycin MIC assay.** 75

3.15 **Biofilm assay of P_{ENO} strains compared with WT SC5314.** 77

3.16 **Adherence levels of WT SC5314 compared with P_{ENO}strains.** 78

4.1 **Tetracycline regulated tetO promoter placed upstream of *TOR1*.** 90

4.2 **Confirmation of the genotypes of *GTR1* mutants of WT SC5314 by gel electrophoresis of PCR amplimers.** 96

4.3 **Phospho-S6 assay.** 97

4.4 **Growth curve of mutant strains compared with WT SC5314 in $(NH_4)_2SO_4$ and Urea.** 100

4.5 **Growth of doxycycline-regulatable strains in YEPD and a limiting medium.** 101

4.6 **Growth of doxycycline-regulatable strains in YEPD in the presence of doxycycline.** 102

4.7 **Hyphal formation on solid medium spot plate assay.** 104

4.8 **Qualitative image depicting the aggregation of WT SC5314 compared with mutant strains in YEPD and 10% (v/v) serum.** 107

4.9 **Semi-quantitative analysis of the aggregation of WT SC5314 compared to mutant strains in YEPD and 10 % (v/v) serum.** 108

4.10 **Qualitative image depicting the aggregation of WT JKC1361 & Heterozygous JKC1347 compared with doxycycline regulatable strains in YEPD and 10% (v/v) serum in the presence of doxycycline.** 109

4.11 **Semi-quantitative analysis of the aggregation of WT JKC1361 & Heterozygous JKC1347 compared with** doxycycline **regulatable strains in YEPD and 10% v/v serum in the presence of doxycycline.** 110

4.12 Flocculation (a) and microscopic appearance (b) of WT SC5314 compared with mutant strains in Spider medium. 113
4.13 Flocculation of WT JKC1361 and JKC1347 (*TOR1/tor1*) compared with tetO-*TOR1/tor1* strains in Spider medium. 114
4.14 Microscopic images of flocculate of WT JKC1361 and JKC1347 (*TOR1/tor1*) compared with tetO-*TOR1/tor1* strains. 115
4.15 Growth of WT SC5314 and mutants in the presence of Congo Red and Calcofluor White. 118
4.16 Growth of WT JKC1361, heterozygous *TOR1/tor1* JKC1347, tetO-*TOR1/tor1* JKC1549 and truncated tetO-ΔN*TOR1* JKC1441 in the presence of Congo Red and Calcofluor White and in the absence of 30 μg/ml doxycycline. 119
4.17 Growth of WT JKC1361, heterozygous *TOR1/tor1* JKC1347, tetO-*TOR1/tor1* JKC1549 and truncated tetO-ΔN*TOR1* JKC1441 in the presence of Congo Red and Calcofluor White and in the presence of 30 μg/ml doxycycline. 120
4.18 Effects of hydrogen peroxide on the growth of Δ*rhb1* & Δ*gtr1*. 122
4.19 Growth of WT JKC1361, heterozygous *TOR1/tor1* JKC1347, tetO-*TOR1/tor1* JKC1549 and truncated tetO-ΔN*TOR1* JKC1441 in the presence of hydrogen peroxide. 123
4.20 MIC assay. Effects of rapamycin & fluconazole on mutant Δ*rhb1* and Δ*gtr1* mutant strains. 126
4.21 Biofilm formation of the Δ*gtr1* & Δ*rhb1* mutants compared with WT SC5314. 127
4.22 Microscopic images of biofilms formed by the Δ*gtr1* & Δ*rhb1* mutants compared with WT SC5314. 128

5.1 GSEA of the genes differentially increased in the Δ*gtr1* mutant. 144
5.2 GSEA of the genes differentially decreased in the Δ*gtr1* mutant. 145
5.3 Enrichment plots of gene sets differentially expressed in Δ*gtr1*. 146
5.4 qRT-PCR data of the Δgtr1 mutant DNA microarray. 147

5.5 **Overview of overlap (2.0-fold increase & decrease) in DNA microarray data sets.** 148

5.6 **Heat map comparisons of differentially expressed genes involved in adhesion, nitrogen uptake and phosphate utilisation in Δ*gtr1* & Δ*rhb1*.** 151

5.7 **Heat map comparisons of differentially expressed genes involved in biofilm formation, cell wall associated proteins, filamentous growth and amino acid biosynthesis and metabolic processes in Δ*gtr1* & Δ*rhb1*.** 152

6.1 **Overview of overlap (1.5-fold increase) in DNA microarray datasets.** . 168

6.2 **Overview of overlap (1.5-fold decrease) in DNA microarray datasets.** . 169

6.3 **Enrichment map of the genes differentially expressed in the tetO-*TOR1*/*tor1* strain at 2 h.** 174

6.4 **Enrichment map of the genes differentially expressed (2 h v 8 h) in the tetO-*TOR1*/*tor1* strain.** 175

6.5 **Enrichment map of the genes differentially expressed in the tetO-ΔN*TOR1* strain at 2 h.** 176

6.6 **Enrichment map of the genes differentially expressed (2 h v 8 h) in the tetO-ΔN*TOR1* strain.** 177

6.7 **Heat maps of differentially expressed genes involved in ribosomal biogenesis and assembly.** 180

6.8 **Heat maps of differentially expressed genes involved in pre-RNA processing and assembly.** 181

6.9 **Heat maps of differentially expressed genes involved in oxidative stress.** 182

6.10 **Heat maps of differentially expressed genes involved in osmotic stress.** 183

6.11 **qRT-PCR data of the DNA microarray.** 185

7.1 **Suggested Gtr1 and Rhb1 down stream targets via the Tor1 kinase.** . . 197

7.2 **DNA microarray comparison of the tetO-ΔN*TOR1* and *tor1*/*TOR1* strains.** 200

List of Tables

2.1 List of plasticware used during the course of experimentation. 27

2.2 List of equipment used during course of experimentation. 28

2.3 **List of *C. albicans* strains.** 31

6.1 **GO-Slim mapper results of the tetO-*TOR1*/*tor1* expressed at higher levels.** 165

6.2 **GO-Slim mapper results of the tetO-*TOR1*/*tor1* expressed at lower levels.** 165

6.3 **GO-Slim mapper results of the tetO-ΔN*TOR1* expressed at higher levels.** 166

6.4 **GO-Slim mapper results of the tetO-ΔN*TOR1* expressed at lower levels.** 166

6.5 **GO-Slim mapper results of the tetO-ΔN*TOR1* compared with the *tor1*/*TOR1* strain expressed at higher levels.** 167

6.6 **GO-Slim mapper results of the tetO-ΔN*TOR1* compared with the *tor1*/*TOR1* strain expressed at lower levels.** 167

6.7 **GO-Slim mapper results of the tetO-*TOR1* strains with similar gene expression to the rapamycin treated strain (> 1.5-fold).** 170

6.8 **GO-Slim mapper results of the tetO-*TOR1* strains with similar gene expression to the rapamycin treated strain (< 1.5-fold).** 171

Abbreviations

°C	Degrees centigrade
Δ	Deletion (of a gene or part thereof)
aa	Amino acid
BEC	Buccal epithelial cell
bp	Base Pair
BSA	Bovine serum albumin
CDMEM	Complete Dulbecco's modified Eagle's medium
cDNA	Complementary DNA
cfu	Colony forming unit
CGD	Candida Genome Database
CFW	Calcafluor white
CO_2	Carbon dioxide
DNA	Deoxyribonucleic acid
DNase	Deoxyribonulease
dNTPs	di-Nucleotide triphosphate
DTT	Dithiothreitol
DMEM	Dulbecco's modified Eagle's medium
DOX	Doxycycline

DEPC	Diethylpyrocarbonate
EDTA	Ethylenediamine tetraacetic acid
et	*al.* And others
FCS	Foetal calf serum
g	Gram
GlcNAc	N-actylglucosamine
GO	Gene Ontology
GSEA	Gene Set Enrichment Analysis
h	Hour(s)
i.e.	That is
kb	Kilobase
kg	Kilogram
L	Litre(s)
M	Molar
MAPK	Mitogen activated protein kinase
mg	Milligram
min	Minute
ml	Millilitre
mM	Milliemolar

MPA	Mycophenolic acid
mTOR	Mammalian Tor
NAT	Nourseothricin
NAT200	YEPD (agar/broth) with 200μg/ml nourseothricin
ng	Nanogram
nm	Nanometer
O_2	Oxygen
OD_x	Optical Density at x nm
rpm	Revolutions per minute
v/v	volume per volume (ml/100ml)
YEPD	Yeast Extract Peptone Dextrose
YNB	Yeast nitrogen base with ammonium sulfate and aa
YNB-aa	Yeast nitrogen base without aa
YNB-aa-	Yeast nitrogen base without aa or ammonium sulfate
YPDS	YEPD with 10% (v/v) FCS
β	Beta
βMe	β-Mercaptoethanol
μg	Microgram
μl	Microlitre

Summary

Candida species are responsible for a wide range of superficial and life threatening infections and are the fourth most common cause of nosocomial bloodstream infections. *Candida albicans* is an opportunistic pathogen that is a commensal inhabitant of the alimentary canal. The ability to adapt to various nutritive environments presented by the host is essential to its survival as a commensal or pathogen. Thus, understanding how cell growth is controlled in response to environmental signals remains an active field of research.

Target of rapamycin (Tor1) is a highly conserved protein kinase from mammalian to yeast cells. In eukaryotes, Tor is responsible for regulating metabolism and the cell cycle. In *Saccharomyces cerevisiae*, Tor is stimulated by amino acids and an active Tor kinase promotes ribosome biogenesis and glycolysis, as well as repressing genes involved in nitrogen scavenging. Current literature presents several lines of evidence indicating that in *Candida* spp., Tor may play a role in the transition of yeast-to-hyphae. This study aims to determine if the Tor1 fungal kinase is a central regulator of virulence by characterising the role of Tor1 and the putative upstream activators of Tor1. In *S. cerevisiae*, the G-protein complex Gtr1/Gtr2 activates Tor1 in response to amino acid signals via a guanine-nucleotide exchange factor, Vam6. Homologues of these are found in *C. albicans*. A second activator, the recently characterised G-protein Rhb1 has also been described in *C. albicans*.

It is hypothesised that an active kinase represses virulence and filament formation. Therefore, initial studies focused on overexpression of the putative upstream activators of Tor1 and Tor1 itself using the strong, constitutive Enolase 1 promoter (*ENO1*p). The work presented here has shown that phenotypically, the overexpression strains are indistinguishable from wild-type SC5314 on a nutrient rich medium such as YEPD. However, on nutrient poor medium (100 mM urea & ammonium sulphate), these strains exhibited a reduction in filamentous fringing com- pared to wild-type SC5314. Additionally, assays of hyphal aggregation (in liquid YEPD 10 % v/v FCS) and yeast

cell flocculation (in liquid Spider medium) showed that the *ENO1*p overexpression strains demonstrated a reduction in aggregation and flocculation compared to WT SC5314. Moreover, biofilm formation was affected, with the *ENO1*p overexpression strains demonstrating a reduction in the formation of biofilm on an abiotic surface in liquid Spider medium. Next, homozygous gene deletion studies of *GTR1* and *RHB1* were performed and their phenotypes assessed in relation their ability to aggregate, flocculate and form biofilms. Differences were observed between both the Δ*gtr1* and Δ*rhb1* mutants. The Δ*gtr1* mutant strain exhibited greater hyphal aggregation compared with the Δ*rhb1* mutant. Furthermore, the Δ*gtr1* mutant flocculated in liquid Spider medium and the Δ*rhb1* mutant did not, suggesting that Gtr1 may have specific downstream responses via the Tor1 kinase. A DNA microarray was performed to examine the differentially expressed genes between both the Δ*gtr1* and Δ*rhb1* mutants and analysis confirmed that both Gtr1 and Rhb1 interact with Tor1 resulting in different downstream signalling of responses.

Finally, in order to confirm the essentiality of Tor1 with regards to growth in *C. albicans*, a heterozygous *tor1* mutant containing a tetracycline promoter (tetO) upstream of the intact *TOR1* allele was obtained. Additionally, a heterozygous mutant containing the tetO promoter upstream of a truncated copy of *TOR1* encoding an N-terminally truncated copy Tor1 was analysed. DNA microarrays were performed comparing the tetO-*TOR1* /*tor1* strains with the heterozygous *tor1*/*TOR1* strain. Furthermore, the DNA microarrays were compared with rapamycin treated cells and heat map analysis of all data sets has shown that the tetO-*TOR1* strains and rapamycin treated cells differ with regards to the expression of genes associated with ribosome biogenesis. This study indicates an important role for Tor1 and is upstream sensors in regulating important pathogenic traits in C. albicans, namely biofilm formation and nutrient acquisition. The study highlights the potential of Tor1 and its accessory proteins as potential targets for novel antifungal drugs.

Chapter 1

General Introduction

1.1 The Fungal Kingdom

Fungi were once believed to be part of the plant kingdom due to the similarities in their lifestyles. However, advances in molecular methods and phylogenetic analysis resulted in the identification of the kingdom fungi. The fungal kingdom is vast and diverse and reproduction can be asexual or sexual [1, 2]. The kingdom includes approximately 1.5 to as many as 5 million species. These consist of unicellular yeasts, filamentous fungi, lichens and mushrooms and are believed to have diverged from plants and animals approximately one billion years ago [3, 4].

Fungi play an important role in most ecological systems. In nearly all terrestrial ecosystems they are the major biological decomposers, playing an essential role in nutrient recycling as symbionts or saprotrophs [5, 6]. Additionally, fungi are beneficial in industrial applications. Many species are used for the production of antibiotics, vitamins or anti-cancer drugs. Many produce metabolites, such as penicillins, which are major sources of pharmacologically active drugs. Genetic engineering techniques have enhanced the production pharmaceutical products from fungi [7]. Furthermore, fungi have been used as pest control to eliminate harmful plant pathogens and they have also been used for the degradation of herbicides and pesticides [8, 9].

However, not all fungi are beneficial. While the ability to grow in a filamentous state allows for explorative and exploitative growth in many environments, this form of growth can be associated with pathogenesis. Many pathogenic fungi cause infection to both plants and animals, including humans.

Although some fungi can be primary pathogens of humans, e.g. *Coccidioides immitis*, the majority of fungal pathogens are opportunists. Infections caused by these opportunistic fungal pathogens have been increasing in recent decades. There are many factors that have contributed to the rise in infection, some of which include advances in medical technologies resulting in a longer lifespan, immunosuppression (intrinsic or extrinsic), and the development of acquired immunodeficiency after contraction of human immunodeficiency virus (HIV) [10, 11].

1.2 Antifungal Drugs & Resistance

As mentioned earlier, the fungal kingdom is remarkably diverse and fungi have indispensable roles in many ecosystems. However, approximately 150 are capable of causing disease in mammals. Three of which, *Candida albicans*, *Cryptococcus neoformans*, and *Aspergillus fumigatus*, are considered the predominant pathogenic fungi of humans [12]. These pathogenic fungi evolved strategies that allow them to survive in the host environment and can thrive when the immune system is compromised. Therefore, in a compromised host, drug therapy is needed to combat infection. In the United States of America, it has been estimated that $2.6b is spent annually to treat invasive fungal infections with an average per-patient cost attributed to $31,200 [13].

Fungi, which are eukaryotic organisms, share a close evolutionary relationship with humans making it a therapeutic challenge with regards to drug design. Therefore, drug therapy must ensure that toxicity to the host is minimised while acting effectively upon their target. The majority of antifungals currently used target ergosterol, a functional fungal analogue of cholesterol. Additionally, the cell wall of fungi is not shared by humans and thus acts as an additional target for antifungal therapy. Of the antifungals available, there are three main classes; the azoles, polyenes and echinocandins.

The azoles have been the most widely used group of antifungals for the last two decades [12]. These can be further divided into two subclasses; the imidazoles and triazoles. The imidazoles are used topically due to their toxicity and bioavailability problems, which limits their potential as systemic agents. For invasive fungal disease, the triazoles are available for clinical use and consist of fluconazole, itraconazole, voriconazole, and posaconazole. The triazoles contain 3 nitrogens bound to a five-membered aromatic azole ring. This specific structure allows for binding to a variety of enzymes and receptors in biological system [14]. The azoles target lanosterol demethylase, the ergosterol biosynthetic enzyme, encoded by Erg11 in *C. albicans*. The nitrogen atom in the azole ring binds to the active site of Erg11, inhibiting catalytic activity. This results in the prevention of the demethylation of lanosterol and blocks production of ergosterol. Fur-

thermore, it causes the build up of a toxic sterol that exerts severe membrane stress [12, 15].

The second class, the polyenes, intercalate into the cell membrane, forming a membrane-spanning channel resulting in the leakage of intracellular contents. The third class, the echinocandins, are a relatively new class and include the drug caspofungin [16]. β(1,3)-D-glucan is a polysaccharide and cell wall component of many fungi. The echinocandins inhibit the synthesis of this polysaccharide causing swelling and resulting in cell lysis [17].

In recent years however, resistance has emerged in clinical isolates due to increased drug use. Many available drugs are fungistatic rather than fungicidal, resulting in large populations of survivor cells [18]. These are exposed to strong directional selection for resistance. Furthermore, the overexpression of drug transporters, alterations of the drug target and alteration of metabolism, can result in a high rate of mutation yielding a resistant phenotype [19, 20].

Like other fungal pathogens, *C. albicans* is a eukaryotic organism. As a result, it shares biological processes with humans. This means that novel antifungal drug targets are difficult to identify and existing drugs can cause deleterious side effects. Furthermore, a major drawback in *C. albicans* treatment is resistance to common azole antifungals. Resistance following prolonged exposure to azoles has been well recognised [21, 22]. Many mechanisms are known to contribute to drug resistant phenotypes including alterations in drug import and in intracellular drug processing, as well as alterations in the target enzyme and in efflux pumps [21]. Therefore, identifying antifungal targets and understanding the biology of these targets are critical from a therapeutic perspective.

1.3 *Candida* Species and Candidosis

Candida species are a member of the Saccharomycetaceae with approximately 150 species. They can cause a wide variety of human infections, ranging from superficial to

life threatening infections. *C. albicans* is by far the most common species and can be found in approximately 80 - 90 % of cases of vaginal candidosis [23]. Approximately 70 % of woman experience vaginal infections, of which 20 % will suffer from recurrent infections [24]. The clinically relevant species exist as commensal organisms residing mainly in the oral and vaginal cavities as well as in the gastrointestinal (GI) tract [25]. Competition with the host microflora and the immune system of the host maintain *Candida* species as commensals. However, extensive treatments with antibacterials or an impaired immune system may enable overgrowth of the organism and result in a pathogenic mucosal infection. In individuals with severely compromised immunity, such as individuals with neutropenia, patients undergoing deep tissue surgery or individuals with invasive devices, *C. albicans* can disseminate into the bloodstream and invade other organs, resulting in life threatening infections with a mortality rate of 30 - 40 %.

Of the clinically relevant *Candida* species, the pathogenicity of *C. albicans* and *tropicalis* is most thoroughly studied. Both species haven been shown to be pathogenic in mouse infection models of and the liver or the kidneys have been identified as the major targets of infection depending on the route of transmission [26]. To be invasive, adhesion to the host tissues is vital. Microbial adherence is important for pathogenesis, and yeast cells possess the ability to adhere to host cells, tissues and abiotic surfaces. In *Candida* species, adhesion is conferred by cell wall proteins referred to as adhesins [27]. In *C. albicans*, adhesion is greater than that of *C. tropicalis*, *C. glabrata*, *C. pseudotropicalis*, and *C. krusei* [28]. Furthermore, the dimorphic trait of *C. albicans* to switch from yeast-to-hyphal form is an additional contributing factor to its success as a pathogen over other *Candida* species. This trait may contribute to the higher frequency of *C. albicans* in clinical settings.

1.4 *Candida albicans*

A commensal inhabitant of the surfaces of the oral, vaginal and gastrointestinal mucosa, *Candida albicans* is capable of opportunistic infections in a debilitated or compromised host [29]. Responsible for a wide range of superficial infections such as oral or vaginal thrush, to systemic life treating infections, *Candida* spp. are the fourth most common cause of nosocomial bloodstream infections [30].

C. albicans is a diploid organism with a genome divided across eight pairs of chromosomes [31]. Its genome displays a high degree of plasticity, exhibiting genomic changes such as aneuploidy and loss of heterozygosity. While it primarily reproduces asexually through clonal division, sexual mating has recently been described [32, 33]. Sequencing of the *C. albicans* genome began in 1996 with its completion in 2004 [34]. The availability of the *C. albicans* genome sequence has enabled us to extensively research and expand our knowledge of this pathogen [35].

It has been noted that *C. albicans* exists in 30-70% of healthy individuals without considerable disease, however approximately 75% of women suffer from *Candida* infection at least once in their lifetime [36, 34]. In those who are immunocompromised or immunologically weak, there is an inability to control colonisation of mucosal surfaces and prevent epithelial invasion, thus leading to life-threatening and systemic infections with a mortality rate of approximately 30-40% [34, 37, 38]. These include individuals undergoing chemo/immunosuppressive therapy, transplant patients or AIDS patients who have a low $CD4^+$ T Cell count.

The ability to switch from budding yeast to hyphae allows for the formation of biofilms. The production of hyphae and the formation of biofilms is commonly associated with *C. albicans* virulence. In the hyphal form, *C albicans* expresses adhesins, proteins that enable adherence to abiotic and biotic surfaces. Of these adhesins, the *ALS* gene family has been actively researched (Section 1.5). Furthermore, the hyphal wall protein 1 (*HWP1*) is an additional adherence protein only observed in the hyphal growth state. This presents a serious issue for those with prostheses and implanted medical devices

such as intravascular catheters or dentures, seeing as these biofilms are more resistant to common anti-fungal drugs compared with their planktonic counterparts [39]. Furthermore, the secretion of degradative enzymes have been shown to promote virulence in *C. albicans*. The secreted aspartyl proteinases LIPASEZ are necessary for the degradation of host proteins and *SAP*1-3 have been shown to be of importance in oral candidosis [40]. Therefore, although candidosis is rarely seen in healthy individuals, in recent decades it has become a serious medical threat.

1.5 Dimorphic Trait of *Candida albicans* & the Ability to Form Biofilms

C. albicans is a polymorphic organism that can interchange between yeast, pseudohyphae or true hyphae [41]. Unlike hyphae, which are elongated branching tubular filaments, pseudohyphae are ellipsodal elongated yeast cells (Fig 1.1.). The ability to transition to true hyphae is a critical factor in the virulence of *C. albicans*. In the bloodstream, yeast cells can disseminate easily, however, it is the hyphae that can penetrate host tissues during initial infection. This yeast-to-hyphal switch has been considered to be an important factor for pathogenesis. Mutants that have a defect in hyphal growth are less virulent [42, 43]. The yeast-to-hyphal switch is induced by a number of environmental cues. A shift in temperature from 30 °C to 37 °C, a shift from a low pH to pH7 or from a nutrient rich environment to a nutrient poor environment can induce the yeast-to-hyphal switch. However, perhaps the most critical, is the induction by serum or macrophages [42, 44]. Serum induced hyphal growth at 37 °C is perhaps the most studied inducing condition and results in a combination of stimuli, including alkaline pH, temperature and nutrient depletion, activating the G-protein Ras1 which initiates a cAMP signalling cascade to activate the transcription factor Efg1. In addition to positive regulation, genes involved in hyphal growth are also subject to repression under conditions of low temperature or high nutrients. The main repressor is Nrg1, which re-

cruits the Tup1 repressor complex to hyphal genes. Regulation of repression is poorly understood, but recent evidence suggests the involvement of Tor1 kinase regulated transcription factors (Section 1.6).

C. albicans hyphae are key in the development of biofilms and present significant problems clinically due to their potential to resist antifungal drugs. Yeast and hyphal cells aggregate to form a biofilm, a complex population of surface-associated cells embedded in an extracellular matrix, possessing distinct phenotypes to that of planktonic cells. Quorum-sensing molecules, available nutrients and surface contact are contributory factors for biofilm formation [39]. The formation of *C. albicans* biofilm, as noted *in vitro* [45], begins with the adherence of yeast cells to a substrate. These cells proliferate to form form microcolonies and produce elongated projections of hyphae and pseudohyphae. An extracellular matrix forms as the biofilm matures and shows drug resistant characteristics. Bound yeast cells are then released from the biofilm to allow for the colonisation of the surrounding environment.

Of the genes governing the formation of biofilms, many are involved in the production of hyphae. These genes can be grouped into several broad categories consisting of those encoding cell wall-related proteins, drug efflux pumps and transcription factors [45]. Critical to the process of biofilm formation are gene products that have a direct role in cell-substrate or cell-cell adherence and studies have indicated that agglutinin-like sequence 1 (Als1) and Als3, as well as hyphal wall protein 1 (Hwp1) have such roles [46, 47].

Other *C. albicans* genes encode transcription factors or protein kinases, functioning indirectly to control biofilm properties. The transcription factor Bcr1, which is a biofilm and cell wall regulator is required for biofilm formation [48]. Expression analysis of Bcr1 has shown that it activates cell surface proteins and adhesin genes. It has also been shown that Als3 mediated adherence is a fundamental property under the control of Bcr1 [49]. Its expression is up-regulated in hyphae, indicating that Bcr1-dependent gene products may be the hyphal components required for biofilm formation.

In addition to the aforementioned signals, several genes are involved in the response of the quorum sensing molecule farnesol, which can inhibit morphogenetic processes [50]. Quorum sensing is a means of stimulus and response correlated with population density. Studies have shown that this quorum sensing molecule is used by *C. albicans* to inhibit filamentation [50]. Additionally, it alters biofilm density and morphology at high concentrations. If provided early during adherence, exogenous farnesol can inhibit biofilm formation [51, 52].

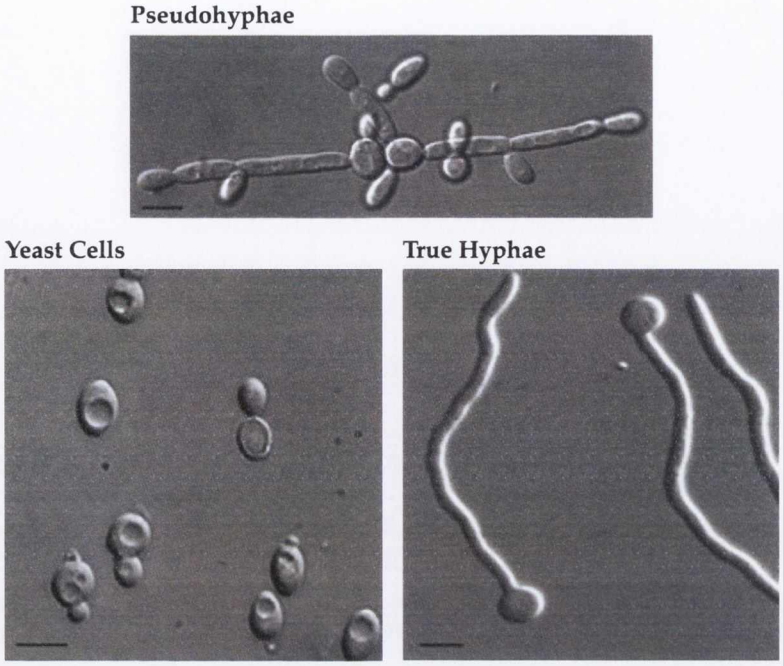

Figure 1.1: **Example of *C. albicans* morphology adapted from Sudbery (2011).**

The image above has been adapted from Sudbery (2001) "Growth of *C. albicans* hyphae" and illustrates the different morphological states seen in *C. albicans*. The scale bars inset on the photos represents 5 μm. The top image illustrates pseudohyphal growth while the bottom left illustrates budding yeast cells and the righ true hyphae. The pseudohyphal cells are due to the daughter cells remaining attached to the mother resulting in a constriction at the septa. True hypha have paralleled walls.

1.6 The Tor1 Kinase

The Tor1 (Target of Rapamycin) kinase (Fig. 1.2) is a central regulator in a nutrient-sensing pathway in eukaryotic cells. It was first identified in *Saccharomyces cerevisiae* in 1991 [53] following analysis of mutants conferring resistance to the drug rapamycin. Rapamycin is a macrolide produced by *Streptomyces hygroscopicus* that was initially investigated as an antifungal agent. However, it was not introduced to treat fungal infections due to its immunosuppressive characteristics. It is used however, to suppress immunity in transplant patients as it inhibits the activation of B-cells and T-cells. In all eukaryotic cells rapamycin diffuses into the cells and associates with FKBP12, a peptidylprolyl isomerase, inhibiting the activity of FKBP12. The FKBP12-rapamycin complex binds to the FRB domain of the Tor kinase resulting in inhibition of the kinases [54, 55].

Tor1 is a highly conserved eukaryotic kinase related to the phosphatidylinositol-3-kinase (PI3K) family of kinases. Tor proteins are large ($\approx$282 kDa), contain a C-terminal kinase domain as well as several protein-protein interaction sites. These include approximately 20 HEAT repeats in the N-terminus, a FAT/FATC domain and an FRB domain (Fig. 1.2) [55]. The HEAT repeat is a protein domain, found in a number of cytoplasmic proteins including the four that the give rise to the acronym HEAT (Huntington, elongation factor 3 (EF3), protein phosphatase 2A (PP2A), and the yeast kinase TOR1) [56]. HEAT repeats are involved in intracellular transport. The HEAT motifs contain approximately 39 amino acid sequences that form a pair of antiparallel α-helices once the protein changes its conformational shape [57]. The FAT/FATC domains are characteristic of the phosphatidylinositol kinase (PIK) related kinase family and thought to serve a scaffolding function. The FRB (FKB-rapamycin binding) domain is the site of rapamycin inhibition. [54]. Biochemical processes fundamental to cell growth and proliferation are governed by the Tor1 signalling pathway [55].

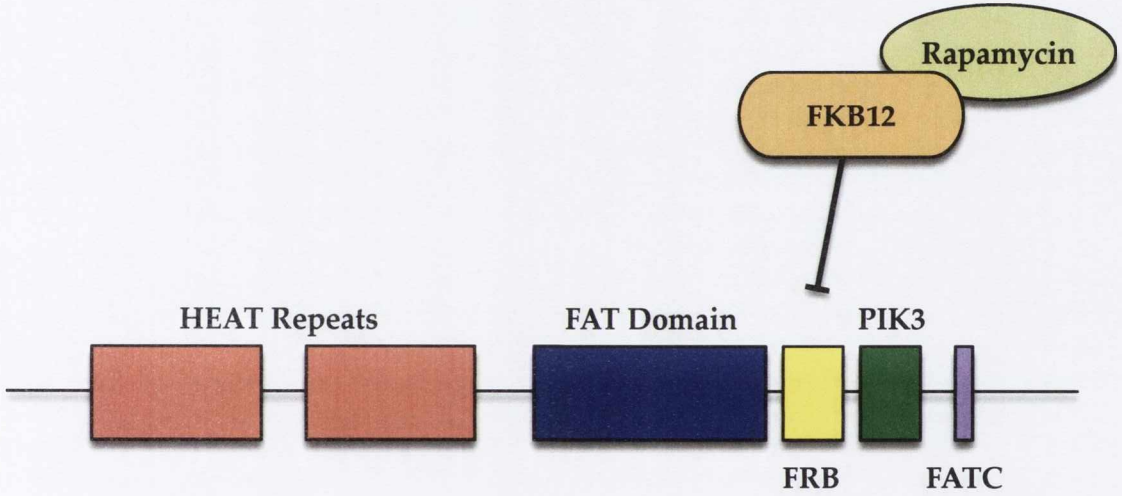

Adapted from Hall *et al.* Genetics, vol. 189, pp. 1177-1201, 2011

Figure 1.2: **Domain structure of a generic Tor protein.**

The image shows the functional domains conserved in the Tor proteins. Shown above are the N-terminus heat repeats, the central FAT domain, FKBP12-rapamycin binding domain (FRB), the PIK3 kinase domain and FATC domain.

1.6.1 Regulation of Nitrogen Metabolism

In *S. cerevisiae*, Tor1 is stimulated by nutrients and an active Tor1 kinase phosphorylates target proteins which promote ribosome biogenesis and glycolysis (Fig 1.3 and section 1.6.2). During growth in nitrogen rich medium (e.g. YEPD), genes involved in utilising alternative nitrogen sources such as *GAP1* are repressed by Tor1. Gap1 is a general amino acid permease, expression of which is controlled by nitrogen catabolite repression (NCR). In nitrogen poor conditions, the expression of *GAP1* is greatly increased, resulting in accumulation at the plasma membrane, allowing the high-affinity high-capacity uptake of amino acids. The transcription of *GAP1* is regulated by the GATA transcription factors Gat1 and Gln3, both of which are active during nitrogen limiting conditions by the Tor1-repressed phosphatase Sit4. [58, 59, 60, 61]. In the presence of rich nitrogen sources, these GATA transcriptional factors are phosphorylated and restricted to the cytoplasm via the protein Ure2. However, in nitrogen poor environments, or when treated with the drug rapamycin, Tor1 activity is inhibited and Sit4 is released from Tor1 repression. Sit4 in turn dephosphorylates Gat1 and Gln3, allowing the translocation of these transcription factors to the nucleus and the transcriptional activation of genes involved in the metabolism of poor nitrogen sources. These transcriptional activators regulate genes such as *GAP1*, *PUT1*, *PUT2* and *CAR1*.

GATA transcription factors are also involved in the regulation of the expression of *MEP2*, an ammonium permease [62]. The deletion of these GATA transcription factors results in the inhibition of *MEP2* expression, thus impacting on nitrogen-induced starvation filamentation. Furthermore, in *C. albicans*, *MEP2* expression appears to be regulated by Gat1 and Gln3 since a $\Delta gln3$ and $\Delta gat1$ mutant resulted in reduced *MEP2* expression, while a double mutant containing both resulted in the elimination of *MEP2* expression [63]. Mep2 is a transceptor, acting as both as a transporter and receptor of ammonium [64]. Transceptor activity has been documented for Gap1, a general amino acid permease and to a lesser extent for Mep1 and Mep2 [65, 66]. Nuland *et al.* (2006) showed that in *S. cerevisiae*, the protein kinase A (PKA) pathway is activated in nitrogen

starved cells by Mep2 [65].

In *C. albicans*, nitrogen availability is important in regulating the phenotypes that may contribute to virulence such as filamentous growth and protease secretion. As mentioned previously, in a limiting nutrient environment, *C. albicans* can switch from a yeast to filamentous growth. Mep2, an ammonium permease, facilitates this switch. It mediates the uptake of ammonium, a preferred nitrogen source [67]. When placed in a nitrogen-limiting environment, *MEP2* is highly expressed. The cytoplasmic C-terminal tail of Mep2 appears to stimulate the cAMP-PKA and MAP kinase pathways promoting filamentation [68].

Furthermore, *SAP2* and oligopeptide transporter (*OPT*) gene expression is reliant on the GATA transcription factors Gln3 and Gat1. Sap2, a secreted aspartic protease has also been associated with virulence in *C. albicans* [69]. *SAP2* is induced when *C. albicans* is grown in a medium that contains protein as the sole nitrogen source and Δ*sap2* mutants are incapable of growing in these conditions [70]. In addition to Sap2, oligopeptide transporters are required for the utilisation of protein as a sole nitrogen source. Furthermore, the expression *SAP2* and that of the oligopeptide transporters is controlled by the transcription factor Stp1 [71, 72].

1.6.2 Regulation of Ribosome Biogenesis

Tor1 is involved in multiple cellular responses, allowing for cellular proliferation, inhibition of stress responses, amino acid import and ribosome biogenesis. Signaling to downstream effectors is proposed to be through direct phosphorylation of downstream targets as well as the repression of phosphatase activity. Active growth requires numerous ribosomes, and ribosome biosynthesis requires major energy expenditure. Ribosomal biosynthesis in *S. cerevisiae* requires the transcription of more than 100 different genes [73]. In a nutrient rich environment, Tor1 signals the transcription of rRNA via Pol I and Pol III as well as mRNAs via Pol II in *S. cerevisiae* [74, 75]. Opposingly, in a nutrient-depleted environment ribosomal production is reduced.

Ribosome biogenesis is important for cellular proliferation and the Tor kinase is a signalling pathway that links stress and nutritional signals to ribosome biogenesis (Fig. 1.3). In *S. cerevisiae*, the transcriptional activator Sfp1 is phosphorylated by Tor1, promoting nuclear localisation that results in the transcriptional activation of genes involved in ribosome biogenesis [76]. Increased *SFP1* expression results in reduced phosphorylation of Sch9, a protein kinase that is involved in growth control and the expression of genes associated with ribosomal proteins and ribosome biogenesis. In *S. cerevisiae*, TORC1 directly phosphorylates 6 amino acids in the C-terminus of Sch9 and upon nitrogen starvation or rapamycin treatment, this phosphorylation is lost [77]. Additionally, Sfp1 appears to negatively regulate the phosphorylation of Sch9 and a Δ*sfp1* mutant displays a hyper-phosphorylation phenotype of Sch9. This suggests a feedback mechanism that controls the activity of genes associated with ribosome biogenesis. [78].

A well-characterised Tor1 substrate is the ribosomal protein *RPS6*. Ruvinsky *et al.* (2005) showed that the phosphorylation of Rps6 is critical downstream of mTor in relation to cell size and it is used as a marker of mTor activity in oncologic research [79, 80]. Phosphorylation of Rps6 (P-S6) is controlled by Tor and work by Chowdhury *et al.* (2015) has shown that the signal from Rps6 is a marker for *TOR*-dependent anabolic activity in *C. albicans*. Nutritional modulation resulted in corresponding P-S6 levels [81]. Additionally, phosphorylation of Rps6 can be measured using a phospho-S6 antibody to measure Tor activity. Furthermore, the ribosomal S6 kinase downstream of Tor1 is involved in signal transduction and it regulates translation of ribosomal protein mRNAs [82]. It is suggested that two substrates of the S6 kinase are involved in the regulation of ribosomal protein translation, the ribosomal S6 protein and eIF4B, a translation initiation factor. Finally, inhibitors of PIK3 as well as rapamycin have been shown to inhibit S6 kinase, thus indicating that mTor and PIK3 are necessary for the S6 kinase [83].

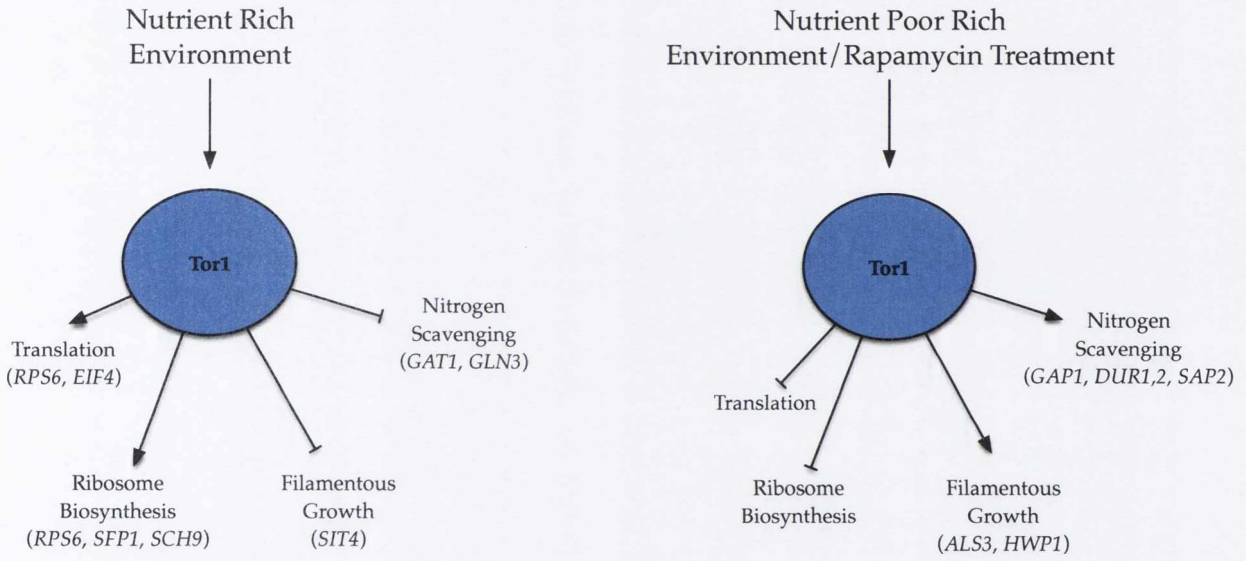

Figure 1.3: **A representation of the downstream effects of an active/inactive Tor1.**

The image above depicts the downstream effects when Tor is active or inactive. In an active state, Tor permits for the general proliferation of the cell, allowing translation, ribosome biogenesis and the stability of high affinity amino acid permeases. Alternatively, in an inactive state, starvation induced gene transcription occurs.

1.6.3 Regulation of Filamentous Growth & Adhesion

Recent studies suggest that in *C. albicans* Tor1 may control adhesion and hyphal elongation. Work by Liu *et al.* (2012) has shown that reduced Tor1 signalling during hyphal initiation results in the increased expression of the GATA transcription factor Brg1. Brg1 promotes hyphal growth by relieving Nrg1 repression of hypha-specific genes. It promotes hyphal gene expression by recruiting the histone deacetylase Hda1 to the promoters of these genes, which results in nucleosome repositioning that blocks Nrg1 from binding to the promoters (Fig. 1.4) [84]. Work by Cleary *et al.* (2012) has also shown that expression of *BRG1* influences the stability of the *NRG1* transcript, thus controlling filamentation through a feedback loop [85]. It is unclear what downstream effectors of the Tor1 pathway are responsible for the expression of *BRG1* as well as sustained hyphal development. However, recent work has shown, that reduced Tor1 signalling lowers the activity of the Hog1 MAP kinase, which results in increased *BRG1* expression and hyphal elongation [41]. In *C. albicans*, the Hog1 pathway has been shown to play a role in oxidative, osmotic and heavy metal stress responses [86, 87].

Mds3 is required for growth and hyphal formation at alkaline pH. Zacchi *et al.* (2010) suggest that Mds3 is another downstream Tor1 signalling component promoting filamentous growth [88]. A Δ*mds3* mutant has similar morphological and transcriptional defects as a Δ*sit4* mutant, encoding a Tor1 repressed phosphatase (Section 1.6.1.). Additionally, both Δ*sit4* and Δ*mds3* mutants display increased sensitivity to an alkaline pH., which suggests that the defects seen are as a results of an increased Tor1 kinase activity, given that rapamycin treatment is sufficient to rescue the filamentous growth defects in Δ*sit4* and Δ*mds3* mutants. Moreover, they show that both the Mds3 and Sit4 proteins coimmunoprecipitate suggesting that they both interact with the same complex. Furthermore, Lee *et al.* (2004) demonstrated that the disruption of *MDS3* resulted in reduced growth rate as well as reduced hyphal growth [89].

Recent work by Bastidas *et al.* (2009) has shown that Tor1 has a role in the expression of the adhesins *ALS1*, *ALS3* and *HWP1* and their transcriptional repressors Nrg1 and

Tup1 [90]. The group demonstrated that rapamycin induced cellular aggregation of *C. albicans* in an adhesin-dependent manner, demonstrating that adhesin gene induction and cellular aggregation of rapamycin-treated cells were strongly dependent on the transactivators Bcr1 and Efg1. Their findings support models in which Tor1 negatively controls cellular adhesion by governing the activities of Bcr1 and Efg1 (Fig 1.4).

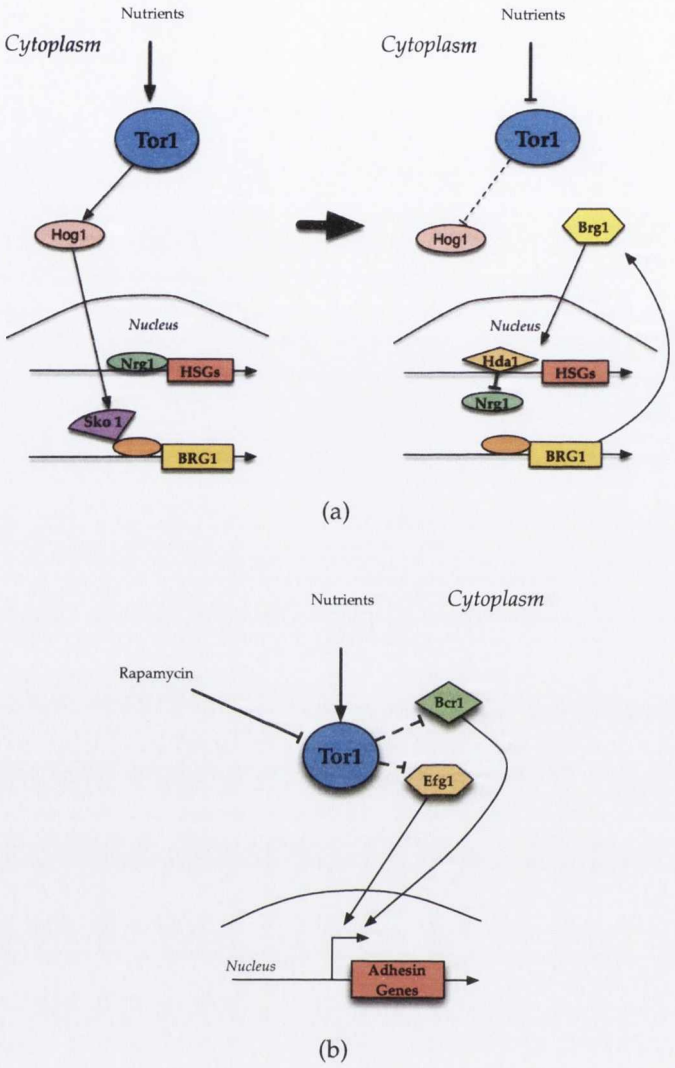

Figure 1.4: **Control of Adhesin and Hypha Specific Gene (HSG) Promotors.**

Shown above is a simplistic representation of the activation of hypha specific gene promotors (a) and those of adhesin specific promotors (b). In nutrient rich environments, Hog1 recruits Sko1 in repressing the expression of Brg1 by binding to the *BGR1* promoter. However, in a nutrient poor environment, reduced Tor1 signaling lowers Hog1 activity allowing for the dissociation of Sko1 from the *BRG1* promoter. *BRG1* is expressed and Brg1 recruits Hda1 to the nucleus allowing for the expression of hypha specific genes. (b) illustrates the expression of adhesin genes. In a nutrient rich environment, the transactivators Bcr1 and Efg1 are maintained in the cytoplasm by Tor1 activity. When nutrients are limiting, Tor1 activity is repressed and these transactivators promote the expression of adhesin genes.

1.6.4 The Putative Activators of Tor1

There are many activators of Tor1. In *S. cerevisiae*, these putative upstream activators (Fig. 1.5) include the G-protein complex Gtr1/Gtr2, which activate Tor1 in response to amino acid signals via the guanine-nucleotide exchange factor Vam6 [91]. Homologs to these exist in *C. albicans* but have not yet been characterised. Additionally, a second activator, the recently characterised G-protein Rhb1, has been described in *C. albicans*[92]. First identified in mammals as Rheb, this protein functions as a positive regulator of mammalian Tor (mTor) [93]. Rheb is activated by the binding of GTP and the Rheb/GTP complex stimulates the kinase activity of mTor, triggering downstream signaling cascades. In *C. albicans*, Rhb1 is involved in nitrogen starvation-induced morphogenesis, possibly by controlling the expression of Mep2, a permease and ammonium sensor [94, 95].

As mentioned above, in *S. cerevisiae* Gtr1 and Vam6 are putative activators of Tor1. *S. cerevisiae* Gtr1 is a member of the RagA subfamily of the GTPase superfamily and is a GTP-binding protein that is essential for amino acid signaling and TORC1 activation [96]. Gtr1 shares 52 % protein and 47 % sequence similarity with the mammalian GTPases RagA and RagB [97]. It has recently been shown that conversion of GDP-bound Gtr1 to the GTP-bound Gtr1 is facilitated by Vam6, a guanine nucleotide exchange factor [91]. Furthermore, it has been shown that mutants unable to escape from rapamycin-induced growth arrest (EGO) resulted in the identification of the EGO complex as an activator of TORC1. This complex, consisting of Ego1, Ego3, Gtr1 and Gtr2 is vacuolar bound and thought to signal amino acid levels to TORC1 via the Gtr1 guanine-nucleotide exchange factor Vam6 [98, 99]. Furthermore, studies in *Schizosaccharomyces pombe* have shown that the deletion of *GTR1* or *GTR2* result in promotion of mating, mating, meiosis and sporulation. This is consistent with down-regulation of TORC1. Moreover, the same study showed that Gtr1 and Gtr2 function downstream of Vam6 but upstream of TORC1 and that *GTR1* and *GTR2* are colocalised with TORC1 to vacuoles [100].

Rhb1 is an additional Tor1 activator. Originally identified in mammalian cells, Rheb is a small G-protein of the RAS superfamily and a direct upstream regulator mTor . Rheb is the down stream target of Tsc1/Tsc2, a complex that negatively activates mTORC1 by promoting GTP hydrolysis of Rheb, thus inhibiting Rheb [101, 99]. In *C. albicans*, Rhb1-Tor1 signaling is involved in nitrogen starvation-induced morphogenesis, presumably via *MEP2* [102]. Recent work by Chen *et al.* (2012) suggests that Rhb1 is regulates cell growth in media where protein is the sole nitrogen source via the control of *SAP2* expression [92]. Work by Naglik *et al.* (2003) suggested that Sap2 is critical for growth in the human host by degrading host proteins, destroying barriers, thus allowing for penetration into the tissue and the bloodstream [103]. Chen et al. (2012) suggest a model where, in the absence of Rhb1 or with the addition of rapamycin, Tor1 directly or indirectly signals the expression of *SAP2*. This occurs by transmitting signals from Gat1 and Gln3 to activate the expression of the transcription factor *STP1*, and Stp1 activates *SAP2* expression [92].

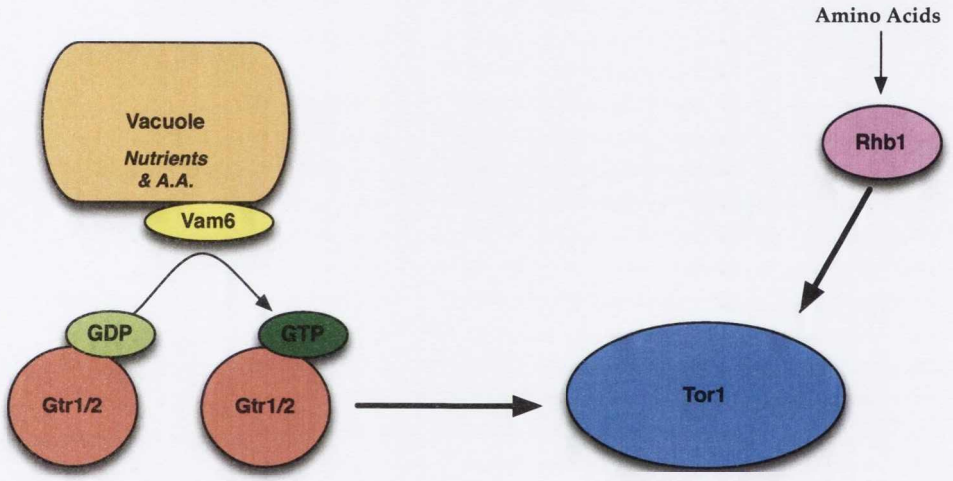

Figure 1.5: **A representation of the activation of Tor1.**

The image above represents the activation of Tor1. Intravacuole amino acid levels are sensed via Vam6, a guanine-nucleotide exchange factor of the GTPase Gtr1. A GTP activated Gtr1 bind and activates Tor1 allowing for cellular proliferation and suppressing starvation-induced gene transcription. Additionally, the GTPase Rhb1 activates Tor1.

1.7 Overview and Aims of Doctoral Project

C. albicans has the ablity to cause both superficial and bloodstream infections. The ability to form hyphae that can penetrate and invade tissue is a key factor in the virulence of this organism. Additionally, characteristic traits such as adhesins and secreted proteinases enhance its ability to adhere to and colonise mucosal surfaces [40]. The ability to switch from yeast cells to a filamentous hyphal form is the most studied virulence factor given that hyphae are more adherent and can penetrate and invade tissue.

Evidence described in section 1.6.3 suggests that Tor1 may play a role in the yeast-to-hyphal switch in *C. albicans*. Previous work carried out in our laboratory studied the yeast-to-hypha transition of *C. dubliniensis*. *C. dubliniensis* is the closest known relative of *C. albicans*. However, *C. dubliniensis* is less virulent and less invasive than *C. albicans*. Furthermore, it forms hyphae less efficiently. Our laboratory has shown that the transition from yeast-to-hyphae in *C. dubliniensis* is nutrient sensitive and that media rich in amino acids or peptides are capable of repressing filamentation in an alkaline environment and at a temperature of 37 °C. Furthermore, this repression of filamentation could be relieved by depletion of the amino acids and peptides or the addition of rapamycin [104, 105]. This rapamycin-sensitive inhibition of filamentation in *C. dubliniensis* suggests a role for Tor1 kinase-mediated nutrient repression and that this may partly explain the reduced virulence of *C. dubliniensis* relative to *C. albicans*.

Based on these data and the work described here, we propose a role for the Tor1 kinase as a critical regulator of host-pathogen interactions. In nutrient rich conditions, the Tor1 kinase is activated, resulting in the repression of filamentation and biofilm formation in *Candida* species. We hypothesise that this will result in a hyperactive Tor1 phenotype, suppressing virulence functions which would be of major importance for the control of fungal infections. If this is true, agonists that activate the putative upstream nutrient sensors that regulate Tor1 could potentially be used as agents to control infection by preventing the switch from a commensal to invasive organism.

Each chapter will study different aspect of this hypothesis. In order to investigate if

increased Tor1 activity resulted in a hyperactive Tor1 phenotype suppressing virulence and filamentation we generated overexpressed strains using the Enolase 1 promoter. We generated strains with an overexpressed *RHB1*, *GTR1*, *VAM6* and *TOR1* itself. Additionally, we generated a Δ*gtr1* mutant strain and compare it to a previously generated Δ*rhb1* mutant strain. Phenotypic analysis was carried out on both the over expression strains and mutant strains to determine the effects on hyphal production, aggregation, flocculation and ultimately biofilm formation. Furthermore, we carried out phenotypic tests on a doxycycline regulatable Tor1 (P_{TET}*TOR1*/*tor1*) generated by Julia Koehler's group at Harvard. Tor1 is essential and therefore both alleles cannot be deleted. Finally, DNA microarray analysis was performed on the Δ*gtr1* mutant and compared with previously published data on a Δ*rhb1* mutant in order to determine what effect these strains had on the whole transcriptome. Additionally, a DNA microarray was performed on a strain in which one allele of *TOR1* is under the control of the P_{TET} promoter (Fig 4.1). By the conclusion, we hope to have a better understanding of the role of Tor1 and its' putative activators.

Chapter 2

General Materials and Methods

2.1 Chemicals, Buffers and Molecular Biological Reagents

All chemicals used in the experiments detailed below were of analytical grade and unless otherwise stated, were purchased from Sigma-Aldrich (Arklow, Ireland). DNA primers were custom synthesised by Sigma-Aldrich and 10 mM stocks stored at -20°C. Additionally, all water used for the preparation of buffers and solutions was purified using a Milli Q Biocel system (Millipore Ireland, Carrigtwohill, Ireland).. Molecular Biology Reagent water was purchased from Sigma-Aldrich and used in all polymerase chain reactions (PCR) and DNA elutions. Diethylpyrocarbonate (DEPC) treated water was made by placing 1 ml of DEPC into 1 l of ultra-pure H_2O followed by incubated overnight at 37°C. Following incubation, the DEPC in the solution was inactivated by autoclaving.

2.2 General Laboratory Equipment and Plasticware

All plastics used for experimental procedures are listed in table 2.1. Additionally, all machinery used in the laboratory for experimental procedures are listed in table 2.2.

Table 2.1: List of plasticware used during the course of experimentation.

Plastic Ware	Make	Part No.	Size/Volume
Microcentrifuge Tube	Eppendorf (*Hamburg, Germany*)		1.5 ml
Micro Tube (Screw Cap)	Sarstedt (*Hildesheim, Germany*)	72.694.006	2 ml
PCR Tubes	Molecular BioProducts (*San Diego, CA, USA*)	3412	0.2 ml
Conical Centrifuge Tubes	Greiner Bio-One (*Kremsmünster, Austria*)	227270	50 ml
Tissue Culture T75 Plates	Corning (*Corning, NY, USA*)	3972XX1	75 cm^2
96 Well Plate	Applied Biosystems (*Carlsbad, CA, USA*)	4346906	0.1 ml
96 Well Plate	Greiner Bio-One (*Kremsmünster, Austria*)	655-160	340 µl
Filter Membranes	PALL Life Science (*Port Washington, NY, USA*)	AP-4001T	10 µm
6 Well Plate	Greiner Bio-One (*Kremsmünster, Austria*)	657-160	5 ml

Table 2.2: List of equipment used during course of experimentation.

Machine	Make	Model	Rotor Radius (cm)	Rotor Model
Centrifuge	Eppendorf (*Hamburg, Germany*)	5417 C/R	9.5	FA-45-30-11
Centrifuge	Eppendorf (*Hamburg, Germany*)	5810 R	18	A-4-81
Centrifuge	Hettich (*Tuttlingen, Germany*)	Universal 320	146	1624
Electroporation Apparatus	Bio Rad (*Hercules, CA, USA*)	MicroPulsar 165-2100	N/A	N/A
Thermocycler	Kyratec (*Queensland, Australia*)	SC200	N/A	N/A
Thermocycler	G-Storm (*Somerset, UK*)	GS1	N/A	N/A
Real-Time Thermocycler	Applied Biosystems (*Carlsbad, CA, USA*)	7500 Fast Real-Time PCR System	N/A	N/A
Spectrophotometer	Thermo Scientific (*Waltham, MA, USA*)	NanoDrop 2000c	N/A	N/A
Spectrophotometer	Thermo Scientific (*Waltham, MA, USA*)	Evolution 60S	N/A	N/A
Cell Disrupter	BioSpec (*Bartlsville, OK, USA*)	Mini-BeadBeater 24	N/A	N/A
Water Bath	Nickel - Electro LTD. (*Weston-super-Mare, UK*)	Clifton NE5-28	N/A	N/A
Water Bath	Nickel - Electro LTD. (*Weston-super-Mare, UK*)	Clifton NE4-P	N/A	N/A
Water Bath	Grant (*Cambridge, UK*)	GD100	N/A	N/A
Orbital Incubator	Sanyo (*Leicestershire, UK*)	Gallenkamp 10X 400	N/A	N/A
Bead Beater	Sartorius (*Goettingen, Germany*)	Mikro-Dismembrator S	N/A	N/A

2.3 Microbial Cultures

All broth cultures were grown in 250 ml Erlenmeyer flasks (Fisher Scientific, Blanchardstown, Ireland) and incubated at 200 rpm in an orbital incubator.

2.3.1 *Candida albicans* Strains

C. albicans strain SC5314 as well as JRB12, a rapamycin resistant derivative of SC5314, were used throughout the course of experiments described below [106, 107]. Overexpression strains containing the Enolase 1 promoter (P_{ENO}) upstream of *VAM6*, *TOR1*, *RHB1* and *GTR1* were also used. Mutant *GTR1* and *RHB1* strains were also used as well as doxycycline-regulatable *TOR1* strains. Strains were primarily cultured from stocks maintained at -80°C on Microbank beads (Pro-Lab Diagnostics, ON, Canada), onto yeast extract peptone dextrose (YEPD) agar (1 % w/v Yeast Extract, 2 % w/v Peptone, 2 % v/v Glucose) plates and incubated overnight at 37°C. For doxycycline-regulatable *TOR1* strains, 0.5 mg/ml uridine was additionally added to YEPD medium. For experimentation with P_{ENO} or mutant $\Delta gtr1$ or $\Delta rhb1$ strains , colonies were used from plates that were no older than 24 h. Plates were subsequently stored at 4°C for a maximum of one month and additional colonies were sub-cultured as required. For experimentation with doxycycline-regulatable TOR1 strains, colonies were used from plates that were no older than 24 h. Plates were subsequently stored at 4°C for a maximum of one week and additional colonies were sub-cultured as required. A list of all strains used in this study are in table 2.3.

2.3.2 Tissue cultures

Human Buccal Epithelial cell line TR146 was cultured in T75 flasks at 37°C with 5 % (v/v) CO_2. Cells were routinely cultured in Dulbecco's Modified Eagle's Medium (DMEM) supplemented with 10 % (v/v) fetal calf serum (FCS) and 1 % (v/v) penicillin-streptomycin to form complete DMEM (CDMEM). Monolayers were allowed to reach 80-90 % confluency and treated with trypsin-EDTA in order to detach the monolayer. Detached cells were spun at 250 *x* g, washed in CDMEM and resuspended in CDMEM. An aliquot of suspended cells was stained with trypan blue and cells counted on an improved Neubauer haemocytometer and approximately 1 x 10^5 cells/ml were seeded into new T75 flask.

2.4 DNA Techniques

2.4.1 DNA Extractions

DNA extractions were performed using the phenol/chloroform method. Cells were subcultured from plates no older than 48 h and incubated overnight in YEPD broths at 37 °C with shaking at 200 rpm. Following incubation, cells were harvested in 1.5 ml microcentrifuge tubes at 18,000 *x* g for 1 min. Supernatants were removed and the pellets resuspended in 200 µl breaking buffer (2 % Triton X-100, 1 % SDS, 10 mM Tris HCl [pH 8.0], 1 mM EDTA, 100 mM NaCl).

This suspension was transferred to a 2 ml screw capped tube containing 0.3 g glass beads previously washed in HCl. A further 200 µl of phenol:chloroform:isoamyl alcohol (24:24:1) was added. Tubes were shaken for 1 min at a setting of 5.5 in a BeadBeater (Mini-BeadBeater 24, BioSpec Products, OK, USA). Samples were centrifuged for 10 min at 18,000 *x* g. After centrifugation, the aqueous phase was extracted with equal volumes of chloroform:isoamyl alcohol (24:1) into a fresh 1.5 ml microcentrifuge tube. Samples were vortexed briefly ensuring adequate mixing and centrifuged for 3 min at 18,000 *x* g. The aqueous phase was removed to a fresh 1.5 ml microcentrifuge tube and

Table 2.3: **List of *C. albicans* strains.**

Strain Name	Parent Strain	Genotype	Reference
SC5314	N/A	Wild Type	[106]
JRB12	SC5314	*TOR1-1/TOR1*	[107]
P_{ENO}*VAM6*	SC5314	Ca*NAT1*::*ENO1*p::*VAM6*	This study
P_{ENO}*TOR1*	SC5314	Ca*NAT1*::*ENO1*p::*TOR1*	This study
P_{ENO}*RHB1*	SC5314	Ca*NAT1*::*ENO1*p::*RHB1*	This study
P_{ENO}*GTR1*	SC5314	Ca*NAT1*::*ENO1*p::*GTR1*	This study
Δ*gtr1*	SC5314	Δgtr1::*SAT1*/Δgtr1::*SAT1*	This study
Δ*rhb1*	SC5314	Δ*rhb1*::*FRT*/Δ*rhb1*::*FRT*	[102]
Δ*gtr1*::*GTR1*	Δ*gtr1*	Δgtr1::GTR1/Δgtr1::*GTR1*	This study
Δ*rhb1*::*RHB1*	Δ*rhb1*	Δ*rhb1*::RHB1/Δ*rhb1*::*RHB1*	[102]
JKC1361	N/A	*his1*/*his1*::tetR-FRT;*arg4*/*arg4*;*ura3*/*ura3*	[81]
JKC1347	JKC1361	*TOR1*/*tor1*::*ARG4*;*his1*/*his1*::tetR-FRT;*arg4*/*arg4*;*ura3*/*ura3*	[81]
JKC1549	JKC1347	tetO-*TOR1*/*tor1*::*ARG4*;*his1*/*his1*::tetR-FRT;*arg4*/*arg4*;*ura3*/*ura3*	[81]
JKC1441	JKC1347	tetO-Δ*NTOR1*/*tor1*::*ARG4*;*his1*/his1::tetR-FRT;*arg4*/*arg4*;*ura3*/*ura3*	[81]

nucleic acids precipitated with 20 µl of a 3 M sodium acetate solution and 400 µl of ice cold 70 % ethanol. Samples were centrifuged at 18,000 *x* g for a further 10 min. A final wash was performed with an additional 500 µl ice cold 70 % ethanol and centrifuged at 18,000 *x* g for 1 min and the DNA resuspended in 50 µl of sterile ultra-pure water.

2.5 RNA Techniques

2.5.1 Rapid RNA Isolation

RNA extractions were carried out using an RNeasy® Mini Kit (Qiagen, Crawley, England). Prior to performing the extraction, colonies were subcultured from plates no older than 48 h and incubated overnight at 37 °C with shaking at 200 rpm in YEPD. Following incubation, a sample of each strain was placed into a 1.5 ml microcentrifuge tube, centrifuged at 18,000 *x g* for 1 min and the supernatants discarded. RNA extractions proceeded as per Part 1 of the manufacturers instructions. However, it must be noted that slight adjustments were made to the protocol. When lysing the cells in the BeadBeater, samples were shaken for 30 s at a setting of 5.5, stored on ice for 1 min to prevent over-heating, then shaken for an additional 30 s. Additionally, the optional spin step to ensure full removal of ethanol from the membrane was performed.

2.5.2 Freeze-fracture Method

In order to obtain adequate RNA concentrations for microarray analysis, the freeze-fracture method was employed. On day 0, cells were grown to the necessary cell density, centrifuged at 15,000 *x* g for 3 min and the supernatant discarded. The pellet was resuspended in the residual supernatant that remained and the cell slurry was then added slowly in a drop wise fashion to a 50 ml Falcon tube containing 25 ml liquid nitrogen to allow for flash freezing of cells. Samples were then placed into a -80 °C freezer until the following day.

On day 1, polytetrafluoroethylene (PTFE) vessels and grinding balls were placed in

RNase Away solution (Molecular BioProducts, CA, San Diego) for 1 h prior to use. Following this, PTFE vessels and grinding balls were placed into DEPC water for 5 min and then transferred to liquid nitrogen until needed.

RNA was extracted one sample at a time. Frozen pellets were removed from - 80 °C and placed into the pre-frozen PTFE vessels along with a grinding ball. Vessels were placed into a high-performance laboratory ball mill (Mikro-Dismembrator S) and samples homogenised for 1 min at 3,000 rpm. The sample was removed, tapped on the bench top to loosen the contents and homogenised for a further minute. Following homogenisation, 700 µl of buffer RLT (RNeasy® Mini Prep) containing 10 µl/ml β-Mercaptoethanol (βMe) was added to each half of the vessel in order to thaw the homogenised sample. Each 700 µl sample was aliquoted into 2 separate 2 ml Starsted screw cap tubes and 700 µl of ice cold 70 % ethanol was added to each tube and subsequently placed on ice. Samples were centrifuged through an RNeasy® Mini Prep column for 30 s at 15,000 *x* g. Following centrifugation, RNA extraction continued according to manufacturers instructions in the Qiagen RNeasy® Mini Prep protocol.

2.5.3 cDNA Synthesis

Extracted RNA was treated with the TURBO DNase kit (Applied BioSystems, Life Technologies Corporation, California, USA). A 5 µl aliquot of the supplied buffer and 1 µl of the supplied enzyme were added to the RNA samples and these samples were incubated at 37 °C for 30 min. Following incubation, 5 µl of the supplied inactivation solution was added, samples centrifuged at 15,000 *x* g and the supernatant transferred to a new 1.5 ml microcentrifuge tube.

cDNA synthesis was performed with RNA at a concentration of 10 µg/µl. A 1 µl volume of Oligo dT (Promega, Madison, Wisconsin, USA) and 1 µl of dNTPs (Promega, Madison, Wisconsin, USA) was added to a 0.2 ml PCR tube. Additionally, 10 µl of RNA (1 µg) was added and the sample run on a thermal cycler block for 5 min at 65 °C. Upon completion of this cycle, 5 µl First Strand Buffer (5X), 1 µl DTT (0.1 M), 1 µl RNase out

(40 U/μl), 1 μl Superscript III (200 μg/μl) (Invitrogen, Life Technologies Corporation, California, USA) and 1 μl H2O was added to each sample which was run on a thermal cycler at 50°C for 1 h followed by 70°C for 15 min.

2.6 Polymerase Chain Reaction (PCR)

2.6.1 Standard PCR

Polymerase chain reactions (PCR) were performed in order to generate transformation cassettes, confirm transformations and the generation of gene knockout strains. All primers used are listed in the supplementary table S1 and S2. Unless otherwise stated, the conditions used for each cycle consisted of a preliminary denaturation step at 95 °C for 30 s. Following this, 35 cycles were run consisting of a denaturation step at 95 °C, an annealing step of 55-58 °C depending on composition and length of primer and an elongation step of 72 °C for 30 s up to 2 min depending on expected product size. A final elongation step of 72 °C for 8 min was also added and the the reaction stored at 4 °C.

2.6.2 Cleanup of PCR Products

In order to send samples for sequencing, PCR products were cleaned using the GenElute PCR Clean-Up Kit (Sigma-Aldrich, Arklow, Ireland) according to manufacturers instructions.

2.6.3 Quantitative Real-Time PCR (qRT-PCR)

qRT-PCR was carried out on the Applied Biosystem 7500 Fast Real Time PCR System. Samples were run on 96-well plates in a 15 μl volume reaction. This consisted of 7.5 μl Fast SYBR Green Master Mix (Applied Biosystems, Life Technologies Corporation, California, USA), 0.375 μl of both forward and reverse primers (10 mM) (See Appendix

X) and 5.75 µl of H_2O. To this, 1 µl of cDNA, previously diluted 1:100, was added before running the reaction. A preliminary denaturation step at 95 °C for 20 s was run before a 40 round cycle consisting of a denaturation step at 95 °C for 3 s and an elongation step at 60 °C for 30 s.

Primers targeting *ACT1* were used as an endogenous control in all qRT-PCR reactions. Before performing qRT-PCR, target primers along with the endogenous primers were optimised to ensure the amplification efficacies were similar.

Following the primer optimisation, each sample was examined. Plates were set up in triplicate with the endogenous control, *ACT1*, run alongside each target. Results were exported into Microsoft Excel and the delta Ct values calculated for each sample. These were ultimately graphed using GraphPad Prism version 6 (San Diego, California, USA, www.graphpad.com).

2.7 Transformations of *Candida albicans*

Transformations were performed according to the method described by Staib *et al*[108]. Cells were subcultured from plates no older than 48 h and incubated overnight in YEPD broths at 37 °C with shaking at 200 rpm. After incubation, the OD_{600} nm of the cultures was determined and the culture was diluted accordingly to obtain an OD_{600} nm between 1.6 and 2.0 (~1.0 x 10^7cells/ml). The cells were pelleted by centrifugation at 2,500 *x* g for 5 min, resuspended in 8 ml H2O and 1 ml 10X TE (100 mM Tris-HCl, 10 mM EDTA [pH 7.5]) and 1 ml 1 M lithium acetate added. Cells were incubated at 30 °C with shaking at 200 rpm for 1 h. After incubation, 250 µl of 1 M dithiothreitol (DTT) was added and the cells were incubated at 30 °C with shaking at 200 rpm for a further 30 min. A 40 ml volume of H2O was then added and cells pelleted by centrifugation at 2,500 x g for 5 min. The pellet was resuspended in 50 ml H2O and pelleted again by centrifugation at 2,500 *x* g. This pellet was resuspended in 10 ml ice-cold 1 M sorbitol and pelleted a further time by centrifugation at 3,000 *x* g for 3 min. All traces of supernatant were removed and the cells were finally resuspended in 50 µl 1 M sorbitol. A

40 µl suspension was used for each transformation. To each sample, 1 µg of DNA was added, mixed gently and transferred to a chilled 0.2 cm electroporation cuvette. A negative, non-DNA containing control was also transferred to an electroporation cuvette. Each cuvette was electroporated at 1.6 kV, 200 W, 25 µF on the fungi setting using the BioRad Micropulser (Biorad). After pulsing, 800 µl YEPD was added to each cuvette and the suspension transferred to a 1.5 ml microcentrifuge tube. Following incubation at 30 °C with shaking at 200 rpm for 4 h, 100 µl was plated onto YEPD agar containing 200 µg/ml nourseothricin (NAT) and incubated for 3 days at 37 °C. Colonies that formed were sub-cultured and prepped for DNA extraction (section 2.4.1). Confirmation PCR was performed with forward and reverse primers specific to the gene of interested and samples were run on a 1 % agarose gel.

2.8 Growth Rate Determination

C. albicans cells were subcultured from 24 h old plates and grown overnight in broth at 37 °C with shaking at 200 rpm. Following incubation, cells were diluted in fresh broth to OD_{600} nm 0.01 (~2 x 10^6 cells/ml) in a 50 ml volume in a 250 ml Erlenmeyer flask and incubated at 37 °C with shaking at 200 rpm. The media utilised differed according to the experimental protocol. A 1 ml sample was taken hourly and the OD_{600} nm determined. The OD_{600} nm readings were analysed using GraphPad Prism version 6.

2.9 Hyphal Formation Assays (*Solid Medium*)

Hyphal formation assays were performed in order to distinguish differences in ability of *Candida* strains to form hyphae. Single colonies were subcultured from 24 h plates and incubated in YEPD broth overnight at 37°C with shaking at 200 rpm. Following incubation, cells were washed with 1X PBS and resuspended in 1 ml 1X PBS. A 1 ml suspension containing 2 x 10^6 cells was prepared of which 2 µl was spotted onto SLD agar plates containing varying nitrogen and amino acid (aa) sources and incubated for

7 days at 37°C

2.10 Enumeration of Free Yeast Cells in Flocculating Cultures of Filamentous Cells

Filamentous growth and flocculation was induced in *C. albicans* cultures by dilution of cells grown overnight at 30 °C in YEPD to either fresh YEPD at 37 °C (referred to as a cell density/temperature shift) or to YEPD supplemented with 10 % serum at 37 °C (serum induction). Following overnight growth in YEPD at 30 °C with shaking at 200 rpm, cells were washed in 1X PBS, counted and resuspended in 25 ml of each media type at 2 x 10^6 cells/ml. In order to quantify the number of free yeast cells in culture, a 1 ml sample of culture was taken at 2 and 4 h and filtered through a 10 μm Versapor® membrane. Filtrates were centrifuged at 20,000 *x* g for 1 min and the pellet resuspended in 100 μl. Cells were counted on a haemacytometer and compared. Additionally, a 1 ml sample was taken and left unfiltered in order to determine qualitatively, the appearance of each strain. 1 ml samples were spun at 20,000 *x* g and resuspended in 1 μl of a 1X PBS solution.

2.11 Visual Flocculation Assays

For visual assessment of flocculation, cells were grown in YEPD medium to OD_{600} nm of 0.5, washed twice in 1X PBS and resuspended in YEPD containing 10 % serum. Cultures were treated with and without the addition of 0.5 nM rapamycin and incubated at 37 °C with shaking at 200 rpm for 2 hours. After incubation, samples were removed from the incubator, vortexed briefly, placed into a test-tube rack and the level of flocculation photographed.

2.12 Biofilm Assays

In order to determine biofilm formation, cells were grown in YEPD at 37 °C overnight with shaking at 200 rpm. Following overnight incubation, 100 µl was removed and transferred to YNB with 100 mM glucose and incubated overnight at 37 °C overnight with shaking at 200 rpm. Following the second night of incubation, cells were washed in 1X PBS and resuspended in 1 ml of YNB with 100 mM glucose at a cell density of 2 x 10^6 cells/ml. 100 µl of each strain was placed in triplicate into a 96 well plate and incubated at 37 °C for 90 min. Following incubation, the medium was aspirated and cells washed twice with 150 µl 1X PBS. Medium of interested for biofilm formation was placed into each well and plates incubated at 37 °C for 24 or 48 hr respectively.

2.13 Adherence Assays

Quantification of fungal cell adherence to epithelial cells was assessed using Human Buccal Epithelial TR146 cells according to that described by Rotrosen *et al.* TR146 cells were cultured in 75 cm^2 tissue culture flasks at 37 °C with 5 % (v/v) CO2 until monolayers reach 80-90 % confluency. Cells were treated with trypsin-EDTA in order to detach the monolayer and centrifuged at 250 x g, washed in CDMEM and resuspended in CDMEM. An aliquot of suspended cells were stained with trypan blue and cells counted on an improved Neubauer haemocytometer. Approximately 1 x 10^4 cells/ml were seeded into 6 well plates in triplicate and incubated until 90 % confluency was reached. *Candida* strains subcultured from 48 h old YEPD agar were grown overnight in YEPD broth at 37 °C with shaking at 200 rpm. Cultures were pelleted by centrifugation at 15,000 *x g* for 1 min, washed in 1X phosphate buffered saline (PBS) and resuspended in 1 ml 1X PBS. Cells were suitably diluted and cell densities counted using an improved Neubauer haemocytometer. A suspension of 100 *Candida* cells in 1 ml CDMEM was prepared in triplicate for each strain corresponding to each well of the 6 well plates. The TR146 monolayers were washed with 2 ml 1X PBS and the 1 ml CDMEM containing the

100 *Candida* cells transferred to the corresponding wells. These plates were incubated for 30 min and 1 h time points at 37 °C with 5 % (v/v) CO_2. The same number of cells, in 1X PBS in 100 µl volume, was added to YEPD agar in triplicate and incubated overnight at 37 °C.

After the 30 min and 1 h co-inubation of *Candida* cells with TR146 monolayers, the medium was removed and monolayers gently washed with 10 ml 1X PBS in 2 ml aliquots with rotation in order to remove any non adherent fungal cells. Each monolayer was covered with 2 ml YEPD agar cooled to approximately 37 °C and left to incubate overnight at 37 °C. After approximately 24 h, colony-forming units (cfu) for each well were counted and an average expressed as a percentage of the average cell counts of the control YEPD agar plates.

2.14 Two-Colour Microarray-Bassed Gene Expression Analysis (*Low Input Quick Amp Labeling*)

In order to compare and contrast the transcriptome expression in mutant strains, two-colour microarrays were performed using the Agilent Technologies method.

2.14.1 Sample Preparation

2.14.1.1 Preparation of Spike A & Spike B

Spike A and Spike B are synthetic RNA transcripts provided by Agilent Technologies and are used to calibrate measurements in the DNA microarray by hybridising with a specific control probe on the target DNA microarray. The degree of the hybridisiation between the spike-in and control probes is used to normalise the hybridisation measurements for the target probes.

Water baths were equilibrated to 37 °C, 40 °C, 65 °C, 70 °C and 80 °C. Spike mix A & B, used to calibrate the DNA microarray, were mixed vigorously on a vortex mixer

and heated at 37 °C for 5 min and vortexed once more. Both mixes were prepared to the manufacture's instructions for 100 ng of RNA. 2 µl of spike A and Spike B were placed into separate microcentrifuged tubes labeled A and B. 38 µl of dilution buffer was then added. A serial dilution of both A and B was carried out at 1:40, 1:16 and 1:2 respectively and stored on ice.

2.14.1.2 Preparation of Labeling Reaction

To a microcentrifuge tube, 100 ng of total RNA was added in a 1.5 µl volume. A total of 8 samples, 4 wild type and 4 experimental were set up. To each, 2 µl of spike A was added to 2 wild type samples and 2 experimental samples. Additionally, 2 µl of spike B was added to 2 wild type samples and 2 experimental samples. Samples were placed on ice and T7 Primer mixed was prepared. To a microcentrifuge tube, 8 µl of T7 primer was added along with 10 µl of nuclease free water. 1.8 µl of the mix was added to each wild type and experimental sample and each were incubated at 65 °C for 10 min. Following incubation, samples were placed on ice for 5 min while the 5X first strand buffer was pre-warmed at 80 °C.

A cDNA master mix was performed containing 20 µl 5X first strand buffer, 10 µl DTT (0.1 M), 5 µl dNTP (5 mM) and 12 µl Affinity script RNase block mix. To each sample, 4.7 µl of the cDNA master mix was added and all samples were incubated for 2 h at 40 °C. Following incubation, samples were transferred to a 70 °C water bath and incubated for a further 10 min. Following incubation samples were placed on ice and a transcription master mix prepared. A 10 µl master mix was prepared consisting of 7.5 µl nuclease free water, 32 µl 5X transcription buffer, 6 µl DTT (0.1 M) 10 µl NTP mix and 2.1 µl T7 RNA polymerase blend. To each sample, 5.76 µl of the master-mix was added. Additionally, to each sample containing spike A, 0.24 µl of cyanine 3-CTP dye was added. Respectively, 0.24 µl of cyanine 5-CTP was added to samples containing spike B. Samples were incubated for 2 h at 40 °C.

2.14.1.3 Purifying Labeled/Amplified RNA

Following the labeling reaction at 40 °C, samples were removed and placed on ice. 84 µl of nuclease free water was added to each along with 350 µl of buffer RLT (RNeasy® Mini Kit, Qiagen) containing 10 µl/ml βMe. An Additional 250 µl of ice cold ethanol was added. Each sample was next transferred to an RNeasy® mini prep column and centrifuged at 4 °C for 30 s at 13,000 rpm, supernatant discarded and 500 µl of buffer RPE added. Samples were centrifuged at 4 °C for 30 s at 13,000 rpm, supernatant discarded and an additional 500 µl of buffer RPE added and re-centrifuged. The supernatant was discarded and samples were centrifuged one last time time at 4 °C for 30 s at 13,000 rpm to insure all buffer RPE removed. Purified cRNA was eluted with 30 µl RNase-free water and all samples kept on ice.

2.14.1.4 Quantification of cRNA

cRNA was quantified using a NanoDrop 2000c Spectrophotometer (Thermo Scientific, Waltham, MA, USA). 1 µl of each sample was measured using the RNA-40 as the sample type under the microarray measurements tab. The cyanine 3 and 5 dye concentration along with the RNA absorbance ratio and cRNA concentration was noted. The yield and specific activity of each sample was calculated using the following formulas:

a) $$\frac{(Concentration\ cRNA) \times 30\,\mu l\ (Elution\ Volume)}{1000} = \mu g\ cRNA$$

b) $$\frac{Concentration\ Cy3/5}{Concentration\ cRNA} \times 1000 = pmol\ Cy3/5\,\mu g/cRNA$$

The minimal recommended yields and specific activity values should be 0.825 µg of cRNA and 6 pmol Cy3/5 per µg cRNA.

2.14.2 Hybridisation

2.14.2.1 Preparation of 10X Blocking Agent

500 µl of nuclease free water was added was added to the 10X Gene Expression Blocking Agent, mixed gently and heated at 37 °C for 5 min.

2.14.2.2 Preparation of Hybridisation Samples

A water bath was equilibrated to 60 °C and for a 4-pack microarray, both the cyanine 3- and 5-labeled dyes, 10X blocking agent, nuclease-free water and 25X fragmentation buffer were added according to the manufactures specifications. Samples were mixed gently on a vortex and incubated at 60 °C for 30 min. Following incubation, samples were placed on ice for 1 min and 55 µl of 2X Hi-RPM Hybridization buffer was added. Samples were mixed by pipette ensuring not to introduce air bubbles. Samples were centrifuged at 13,000 rpm in a microcentrifuge.

2.14.2.3 Preparation of Hybridisation Assembly & Hybridisation

A clean gasket slide was placed into the Agilent SureHub chamber base with the label facing upwards. A 100 µl of the hybridised sample was placed into each corresponding well on the gasket slide and the DNA microarray slide with the "active side" down facing placed on top of the gasket. The SureHub chamber cover was placed on top and clamped firmly in place. In order to ensure no leaks during hybridisation, the assembled chamber was rotated vertically and inspected for leaks. Additionally, the mobility of any bubbles were assessed insuring equal slide to hybridise solution interaction. Each assembled chamber was placed into an oven rotor rack rotating at 10 rpm at 65 °C for 17 h.

2.14.3 Microarray Wash

2.14.3.1 Addition of Triton X-102 to Gene Expression Wash Buffers

A 0.005 % of Triton X-102 was added to each wash buffer in order to reduce the possibility of microarray wash artifacts. A 2 ml volume of Triton X-102 was added to both wash buffer 1 and wash buffer 2 and mixed carefully and thoroughly. Prior to washing the DNA microarray, Wash buffer two was pre-warmed over night in a water bath at 37 °C.

2.14.3.2 Preparation of Equipment

Prior to washing the DNA microarray, all wash staining dishes, slide racks, stir bars and forceps were washed with isopropyl alcohol to avoid wash artifacts on the DNA microarray slide. Each piece of equipment was left in isopropyl alcohol for 5 min. Following this, each was washed with Milli-Q water 5 times and dried.

2.14.3.3 Washing the Microarray Slide

Three staining dishes were set up side by side. Staining dish one and two contained wash buffer 1 and staining dish three wash buffer 2 at the elevated temperature of 37 °C. Staining dish two contained the slide rack and bar stirrer and was placed on a magnetic stir plate. Stain dish three was also had a stir bar and placed on a magnetic stir plate. The hybridisation chamber was removed from the incubator after 17 h and the chamber disassembled. The microarry-gasket sandwich was removed and placed into staining dish one. Once submerged the microarry-gasket sandwich was pried apart and the microarray slide transferred to the slide rack in staining dish two for 1 min. After the 1 min wash, the slide rack, containing the microarray slide, was transferred to staining dish three and washed for a following minute. After the 1 min wash, the slide rack was carefully removed in order to minimise droplets adhering to the slide and the slide placed into a light-free slide holder.

2.14.4 Scanning & Feature Extraction

2.14.4.1 Scanning, Processing & Extraction of Data

The microarray slide was placed into the scanning chamber of a Genepix 4100A scanner and scanned at 5 µM pixel resolution with wavelengths 635 nm and 532 nm. The combined image file and *C. albicans* template .GAL file were saved. Each of the four image files was aligned separately with the .GAL settings file. Aligning was performed automatically using the Genepix Pro software (v6.1.0.4). Individual microarray spots were annotated based on signal to noise ratio (SNR) flags and background fluorescence and microarray spots with a SNR of < 1 were excluded. The gene expression levels were converted to numerical results and were saved as GenePix Results (.GPR) files.

2.14.4.2 Analysis of Data

The .GPR files were imported into the Agilent Technologies software package GeneSpring GX (v11.0). The software was programmed to interpret the correct microarrays for dye-swap inclusion and subjected to normalisation based on the Lowess method [109]. The data were then transformed logarithmically to base 2 for display purposes and filtered on the flags present, marginal and absent based on the SNR values described in section 2.14.4.1. Absent data were excluded and the results subjected to a range of statistical tests. Gene expression values were filtered by fold-change and represented visually using hierarchical organisation heat maps using the default settings.

2.15 Gene Set Enrichment Analysis

Gene set enrichment analysis software (Broad Institute GSEA v2.2.2) was used in conjunction with Cytoscape v3.3.0 in order to generate a network of functional clusters of genes exhibiting increased and decreased gene expression in DNA microarray experiments. GSEA was used to identify significant enrichments in differentially expressed genes by comparing them to a database of published gene sets. This database contains

gene sets for microarray data, predicted protein-protein interactions, Gene Ontologies and global ChIP data. To visualize these enrichments and to identify related gene sets, the data were exported to the Cytoscape suite. Once exported to Cytoscape, enrichment maps were generated selecting only those enrichments that were highly significant (P value <0.005 and False Discovery FDR Q-value cutoff set at 0.1). Each node in the map represents a cluster of genes associated with a specific function with red indicating genes up-regulated and blue down-regulated. Enrichments associated with a common protein-protein interaction have the ending 'BIND' after the interaction partner. Those enrichment labelled 'BIO' and 'MOL' relate to GO terms, those with UP or DN relate to sets of up or down-regulated genes identified in Microarray experiments.

Chapter 3

Over-expression & Phenotypic Analysis of Putative Activators of *Candida albicans* Tor1

3.1 Introduction

The ability to adapt to various nutritive environments presented by the host is essential to the survival of *Candida albicans* as commensal or pathogen. For that reason, understanding how cell growth is controlled in response to environmental signals remains an active field of research. Current literature presents several lines of evidence indicating that in *Candida* spp., Tor1 may play a role in the transition of yeast-to-hyphae [?, 41]. This chapter asks whether the Tor1 fungal kinase is a central regulator of virulence and whether strategies to increase Tor1 activity could suppress virulence and filamentation. In order to address this, we set out to determine if overexpression of upstream activators of Tor1 resulted in strains with phenotypes characteristic of a Tor1 hyperactive state. These upstream activators of Tor1 include of Vam6, Gtr1 and Rhb1.

Vam6, a guanine nucleotide exchange factor (GEF), directs GEF activity towards Gtr1, a putative GTP-binding protein (Fig. 1.3) [110]. Binda *et al.* demonstrated that Vam6 activates Gtr1, a yeast homolog of the mammalian Rag GTPase, in a component of the vacuolar-membrane-associated EGO complex that interacts with and activates Tor1 in an amino acid sensitive manner [91].

In order to generate overexpression strains, the Enolase1 promotor (P_{ENO}) was used. Work by Bates *et al.* (2011) has shown that P_{ENO}, placed upstream of a gene, results in the stable overexpression of the gene. Therefore, P_{ENO} was placed upstream of *VAM6*, *RHB1* and *GTR1*, the putative upstream activators of Tor1. P_{ENO} was also placed upstream of *TOR1* itself. Once confirmed by qRT-PCR, phenotypic assays were carried out to characterise the effects of overexpression of these putative upstream activators and determine whether Tor1 is indeed in a constitutively active state.

In an additional approach to create a constitutively active Tor1 strain, base substitutions were incorporated into regions of *TOR1* FRB domain resulting in specific amino acid changes (I1954V & A1957V). Previous studies in *S. cerevisiae* [111] have shown that these substitutions conferred resistance to caffeine and also results a hyperactive Tor1 phenotype.

3.2 Materials and Method

3.2.1 Caffeine Resistant *Candida albicans* Transformations

Transformation experiments to generate caffeine resistant SC5314 mutant derivatives were carried out using oligonucleotide probes homologous to the *TOR1* gene. The 81 mer oligonucleotides contained point mutations to introduce a single amino acid substitution of an isoleucine to valine at position 1954 or an alanine to valine at position 1957 within the FRB and kinase domains of Tor1 [111]. A third oligonucleotide with both substitutions was also used. For ease of identification these strains are referred to as Ca*TOR* Mut1, Ca*TOR* Mut2 and Ca*TOR* Mut3 respectively. The sequence of these oligonucleotides can be found in the supplemental table S1. Preliminary work prior to transformations involved determining the optimal caffeine concentration in YNB agar at which growth of WT SC5314 would be inhibited. Transformations were carried out on plates containing 3, 6, 9, 12 and 15 mM of caffeine. Transformations were performed as outlined in section 2.7

3.2.2 Transformations of *Candida albicans* with the Enolase 1 Promoter (P_{ENO})

Transformations were carried out as stated in section 2.7. Using this method, the P_{ENO} promoter was placed upstream of genes encoding putative upstream activators of Tor1 (*VAM6*, *RHB1* and *GTR1*), and *TOR1* itself. Cassettes containing both P_{ENO} and the *C. albicans*/nourseothricin (CaNAT) selectable marker, with flanking regions homologous to the gene to be overexpressed, were generated using PCR with primers in table S2. PCRs to confirm integration were performed with forward and reverse primers at a working concentration of 10 mM complementary to both P_{ENO} and within the gene of interest (*VAM6*, *TOR1*, *RHB1* or *GTR1*). A 1 µl volume of a 100 ng/µl of stock DNA was added to each reaction. An initial denaturation step at 95°C for 1 min was run before 35 cycles of 95°C for 30 s, 68°C for 30 s and 72°C for 30 s. A final elongation step of 72°C

for 8 min was also added to the program. Amplimers were visualised on a 1 % agarose gel stained with gel-red (1/10,000).

3.3 Results

3.3.1 Generation of Caffeine Resistant Tor1 Hyperactive Mutants

Using custom oligonucleotides to incorporate single and double amino acid substitutions at positions 1954 and 1957 of *TOR1*, transformations were carried out to generate mutant SC5314 strains resistant to caffeine [111]. These substitutions were expected to yield an isoleucine to valine (I1954V) and an alanine to valine (A1957V) mutation. Preliminary work prior to transformation involved determining the caffeine concentrations that inhibited WT SC5314 for selection of caffeine resistant transformants. Reinke *et al.* (2006) reported that in the *S. cerevisiae* strain W303, a caffeine concentration of 9 mM was sufficient to impede growth. Therefore, multiple caffeine concentrations in YNB agar, ranging from 3 mM to 15 mM were used to determine which concentrations inhibit growth of *C. albcans* SC5314.

After 48 h incubation at 37°C, growth was observed on plates containing 3 mM and 6 mM of caffeine. Upon examination the 9 mM plates, light background growth was observed. Less growth was observed on the 12 mM and 15 mM plates. Therefore, YNB agar containing 12 mM, 15 mM and 20 mM caffeine was used for selecting transformants.

Following electroporation of WT SC5314 with the Mut1-3 primers, control transformations that contained no DNA were negative for growth on the 15 mM and 20 mM plates. Transformations that contained DNA and plated on 12 mM caffeine exhibited high levels of background growth preventing individual colonies to be picked and sub-cultured. However, plates containing 20 mM caffeine allowed for individual colonies to be picked and sub-cultured onto additional YEPD plates containing 20 mM caffeine. Colonies that formed on these plates were subsequently picked, grown overnight in YEPD broth at 37°C and the DNA extracted. PCR was used to amplify the region of Tor1 where integration of the oligonucleotides was predicted to occur. The product was purified and sent for sequencing to confirm the single base pair substitution or double sub-

stitution. Figure 3.1a below represents a fragment of sequences obtained from Source Bioscience for all transformants in order to confirm base substitution. It was expected that CaTOR Mut1 transformants would be heterozygous at position 4753bp with alleles containing both A and G, CaTOR Mut2 transformants heterozygous at position 4763bp with both C and T and for both heterozygous variant to be present in CaTOR Mut3 transformants. The sequence trace of each putative transformant was identical to that of the parent CaTOR WT strain, with no evidence of heterozygosity and incorporation of the mutagenic oligonucleotide onto either allele of TOR1. While it was noted that these derivatives could grow at higher caffeine concentrations compared to WT (20 mM), the expected base changes could not be detected. Multiple caffeine MIC assays (not shown) were also carried out resulting in non-reproducible data.

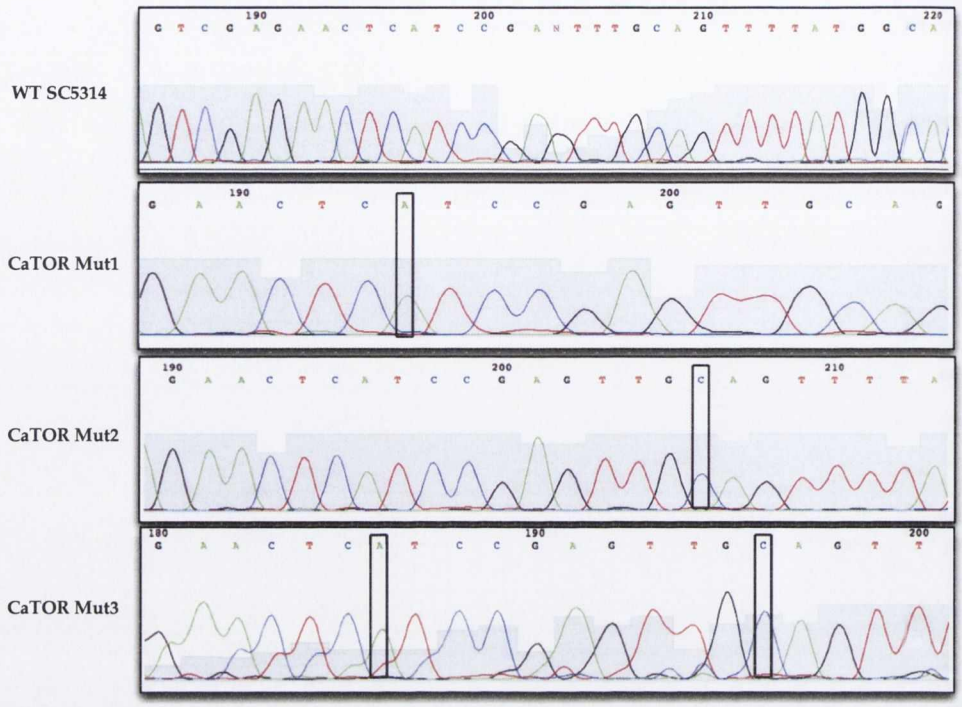

(a)

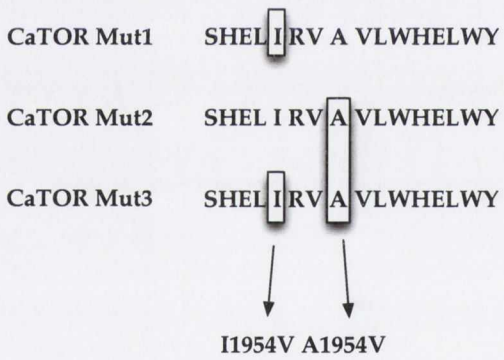

(b)

Figure 3.1: **Chromatograms illustrating sequence from transformation to confer caffeine resistance and amino acid change.**

(a) All 3 transformants, Ca*TOR* Mut1-3, along with WT SC5314 were sequenced to determine whether base mutations were incorporated. A base change of an adenine to guanine was needed to obtain the I1954V in Ca*TOR* Mut1 at position 194 bp and a cytosine to thymine to obtain the A1957V in Ca*TOR* Mut2 at position 206 bp. Ca*TOR* Mut3 relied on the base change occurring in both. This is at position 186 bp and 196 bp respectively. Note, in Ca*TOR* WT, an "N" can be seen. This is normally indicative of multiple peaks in the chromatogram. However, upon inspection the base is a guanine. (b) Section of the amino acid sequence of *TOR1* and the locations where the I1954V and A1957V mutations should have occurred.

3.3.2 Use of the Enolase1 Promotor (P_{ENO}) to Overexpress Putative Tor1 Pathway Proteins as a Strategy for Generating a Constitutively Active Tor1

A different approach to generate a constitutively active Tor1 was investigated using the Enolase1 promoter (P_{ENO}) to overexpress genes of interest. P_{ENO} was placed upstream of *VAM6* and *RHB1* since both are putative upstream activators of Tor1 (Fig. 3.3). Additionally, it was decided to place P_{ENO} upstream of *GTR1* since *VAM6* phosphorylates *GTR1* which in turn activates Tor1. Subsequently, *TOR1* itself was overexpressed with P_{ENO}. Cassettes consisting of P_{ENO} and the nourseothricin resistance marker (*NAT1*) gene were amplified from the plasmid vector pCR2.1, kindly donated by Dr. Steven Bates from the University of Exeter. These cassettes were generated using primers with homology to the upstream sequences of *VAM6*, *GTR1*, *TOR1* and *RHB1* respectively. Following electroporation of WT SC5314 or the rapamycin resistant derivative JRB12, DNA free control plates were negative for growth while transformed strains yielded colonies on YEPD containing 200 µg/ml NAT. These colonies were picked, subcultured onto solid YEPD and then grown in YEPD broth overnight. DNA extractions were carried out and PCR confirmations performed with primers specific to amplify the P_{ENO}-*VAM6/TOR1/RHB1/GTR1* insertion respectively. These PCR products confirmed the upstream insertion of P_{ENO}. Subsequently, qRT-PCR was carried out to assess the level of expression.

Figure 3.2 shows the expression levels of the indicated genes in WT SC5314 in comparison to the respective P_{ENO} strains. A 5.8-fold increase in the expression of P_{ENO}*TOR1* is seen while P_{ENO}*VAM6* exhibited a significantly larger (39.6-fold) increase, thus confirming the effects of P_{ENO} insertion. Additionally, an increase in gene expression (99.7-fold) was observed in P_{ENO}*RHB1* as well as an increased expression (5.9-fold) in P_{ENO}*GTR1*. These further confirmed P_{ENO}-*VAM6/TOR1/RHB1/GTR1* cassettes were successfully transformed into WT SC5314. Additionally, overexpression of each gene was observed in the rapamycin resistant derivative JRB12 [107].

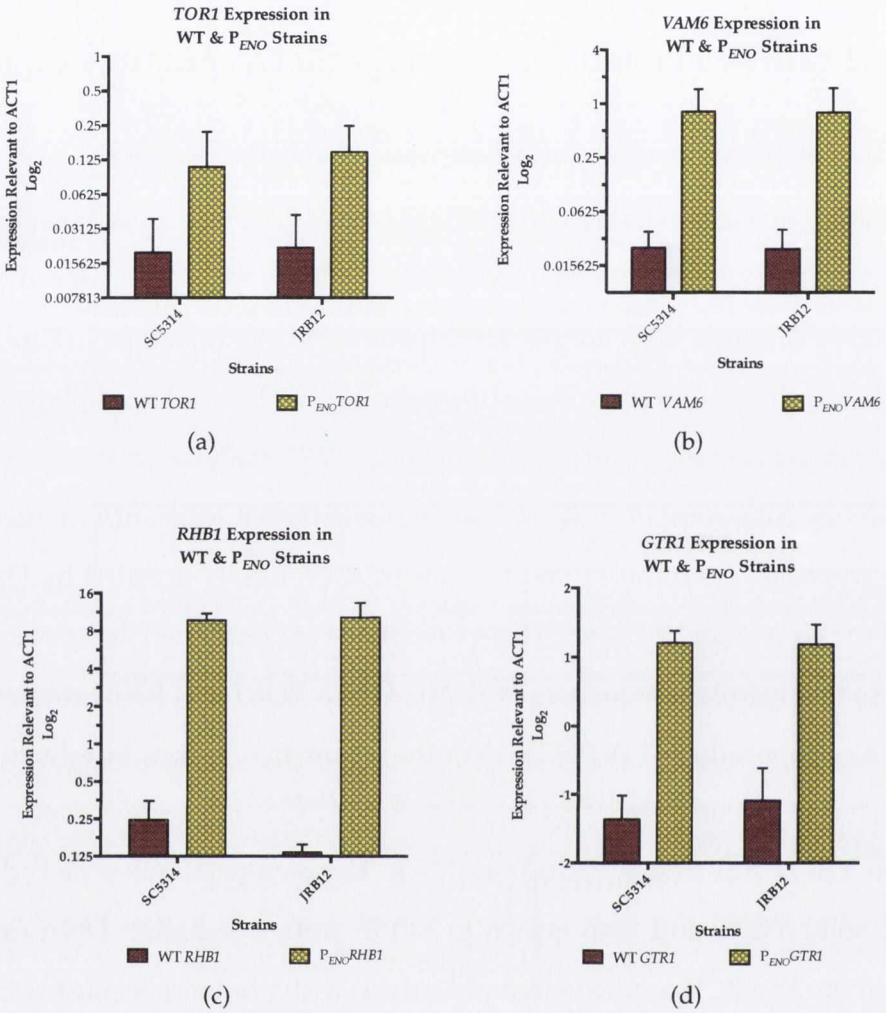

Figure 3.2: **Gene expression in WT SC5314 and JRB12 strains compared with P_{ENO} transformed strains.**

(a) WT gene expression of *TOR1* compared to P_{ENO}*TOR1*, (b) WT *VAM6* compared to P_{ENO}*VAM6*, (c) WT *RHB1* compared to P_{ENO}*RHB1* and (d) WT *GTR1* compared to P_{ENO}*GTR1*.

3.3.3 Determination of Cellular Growth of P_{ENO} Strains Compared to WT SC5314

In order to determine whether there was a statistically significant difference in the growth of each P_{ENO} strain, growth curve assays were employed to examine their doubling times compared with WT SC5314. Growth curve assays were set up in multiple nitrogen sources (YEPD or YNB supplemented with either 100 mM urea, 100 mM proline or 100 mM ammonium sulfate $(NH_4)_2SO_4$). As shown previously in Figure 1.2, when Tor1 is in an active state, cell proliferation is maximized and uptake mechanisms for alternative nitrogen sources are inhibited. Therefore, we hypothesised, that the P_{ENO} strains would grow poorly in the presence of proline or urea.

Figure 3.4 shows the growth of P_{ENO} strains compared with WT SC5314. A student t-test was carried out on the doubling times of each P_{ENO} strain compared with WT SC5314 using the statistical package GraphPad Prism. In each case, no P-value of less than 0.05 was obtained. However, it was noted that in our YEPD experiment, the doubling time of the P_{ENO} strains were shorter than that of the WT SC5314. In 100 mM urea, doubling times of P_{ENO} strains were longer than that of WT SC5314. In 100 mM $(NH_4)_2SO_4$, the doubling times were slightly shorter with the exception of P_{ENO}*GTR1*. Additionally, in 100 mM proline, doubling times of P_{ENO} strains were slightly shorter than that of WT SC5314 with the exception of P_{ENO}*VAM6*. Figure 3.4 illustrates the doubling times of all P_{ENO} strains and WT SC5314.

P_{ENO} strains were also grown in a yeast carbon base medium supplemented with bovine serum albumen (YCB-BSA). Chen *et al.* (2012) showed that a derivative of SC5314 overexpresing *RHB1* exhibited a slower growth rate in medium where BSA was the sole nitrogen source compared with wild-type cells. Following incubation in YCB-BSA, P_{ENO}*VAM6* and P_{ENO}*TOR1* showed reduced growth from 30 h compared with WT SC5314. However, P_{ENO}*RHB1* and P_{ENO}*GTR1* showed reduced growth from 10 h compared to WT SC5314 (Fig. 3.5).

We also examined whether overexpression of these regulators could suppress the ex-

pression of transporters of alternative nitrogen transporters. Tsao *et al.* (2009) showed that in a strain overexpressing *RHB1*, the expression of *MEP2* is lower than in a wild-type cell. We also analysed the expression of *MEP2* in the P_{ENO} strains compared with WT SC5314. The expression of *MEP2* was lower in P_{ENO}*RHB1* consistent with what Tsao *et al.* (2009) observed. Moreover, all P_{ENO} strains showed a reduction in the level of *MEP2* expression. Furthermore, the reduction in expression levels was significant in the P_{ENO}*RHB1*, P_{ENO}*GTR1*, and P_{ENO}*VAM6* strains (Fig. 3.6).

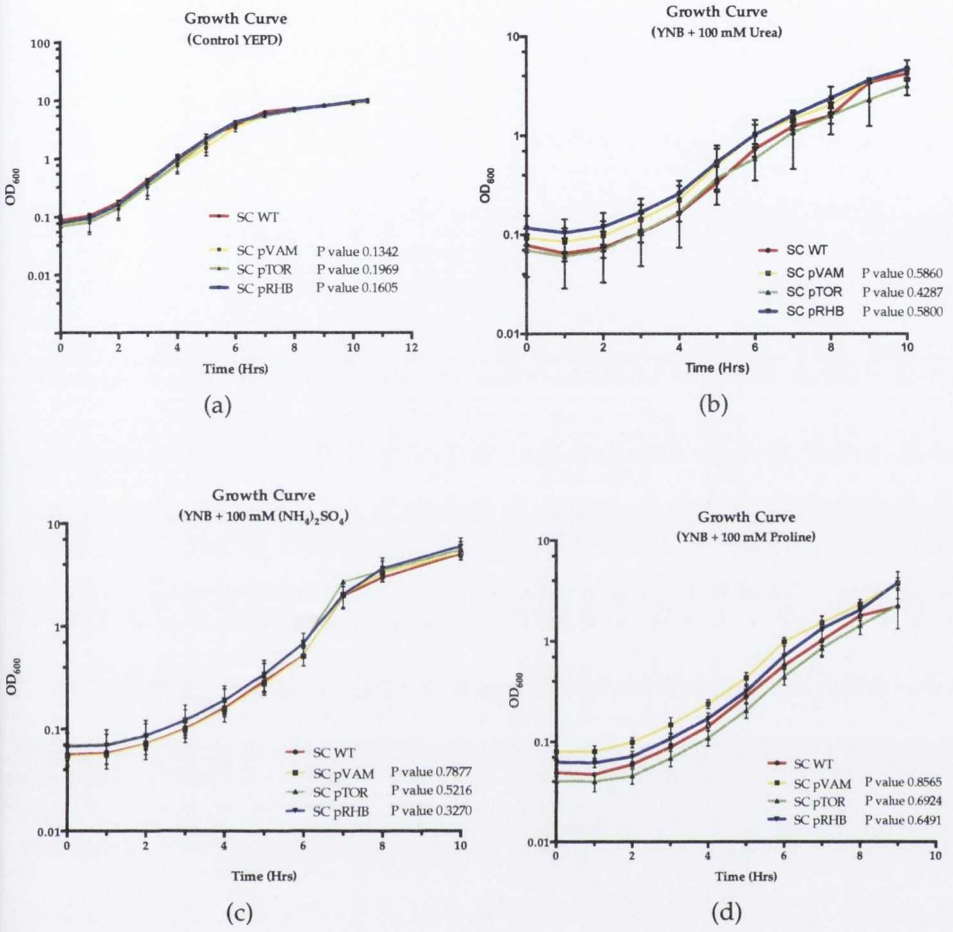

Figure 3.3: **Growth curve assays of WT SC5314 compared with P_{ENO} strains.**

All strains were grown in YEPD as a control and subsequently tested in nitrogen poor medium to determine the doubling rate. All growth rates appears similar to WT SC5314 and no statistical significance was noted.

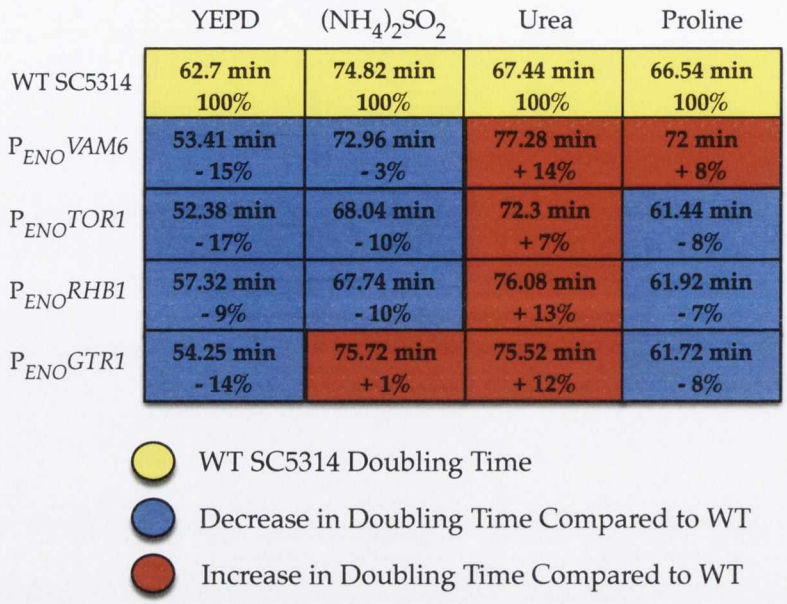

Figure 3.4: **Doubling times of P_{ENO} strains compared with WT SC5314.**

In 100 mM urea, all P_{ENO} strains exhibited a decrease in the rate of cellular proliferation. Additionally, $P_{ENO}VAM6$ experienced an decrease compared to WT SC5314 in 100 mM proline as did $P_{ENO}GTR1$ in 100 mM $(NH_4)_2SO_4$.

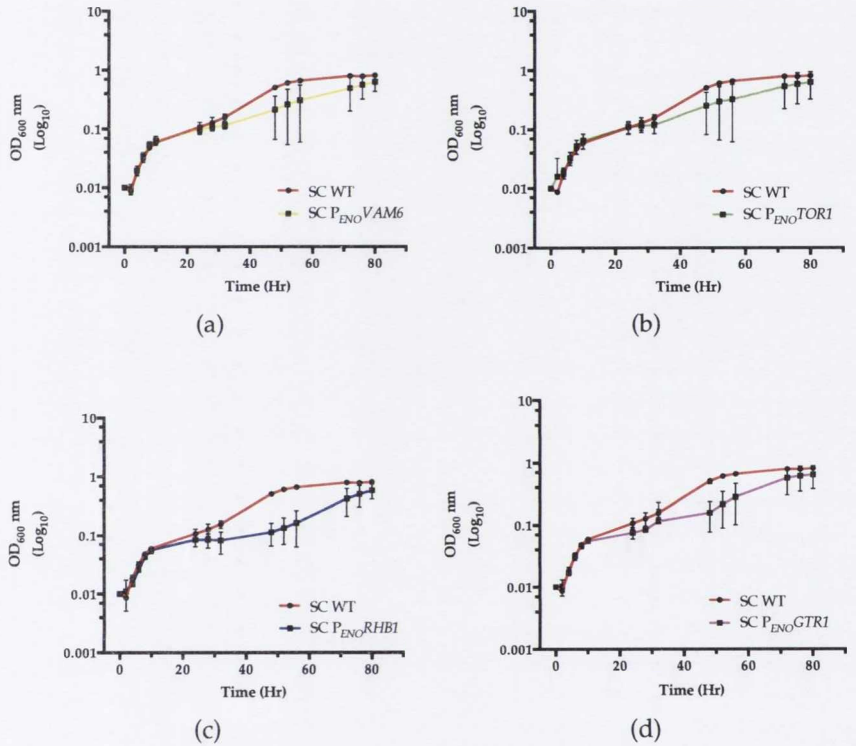

Figure 3.5: **Growth of WT SC5314 compared with P_{ENO} strains.**

(a) Growth rate of P_{ENO}*VAM6*, (b), P_{ENO}*TOR1*, (c) P_{ENO}*RHB1* and (d) P_{ENO}*GTR1* in YCB-BSA medium over the course of 80 h.

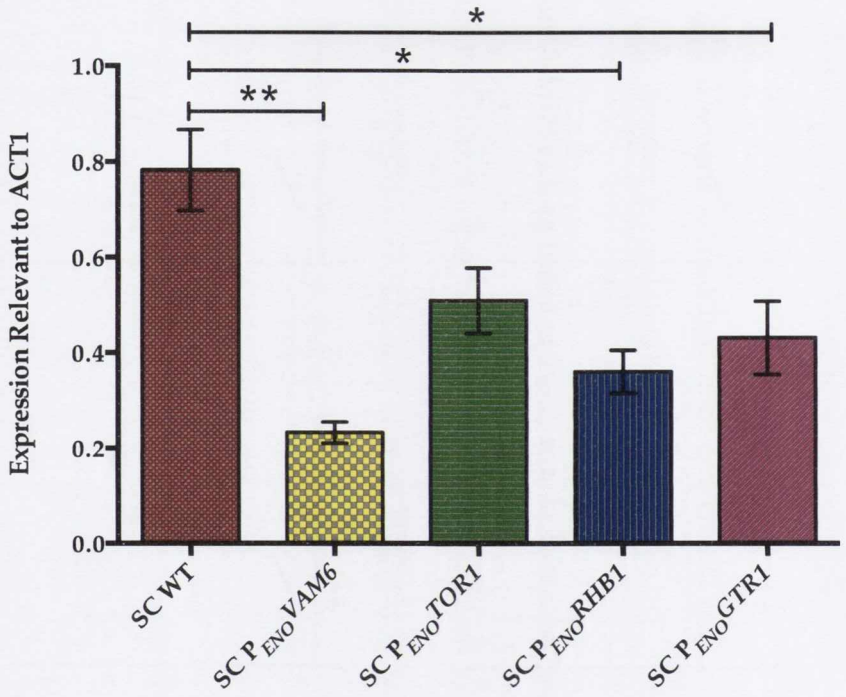

Figure 3.6: **Expression levels of *MEP2*.**

Expression of *MEP2* relative to *ACT1* in all P_{ENO} strains compared with WT SC5314. With the exception of P_{ENO}*TOR1*, all P_{ENO} strains show a statistical difference in the level of *MEP2* expression.

3.3.4 Hyphal Formation Assays of P_{ENO} Strains Compared to WT SC5314

3.3.4.1 Formation of Hyphae on Solid Medium

In order to examine nitrogen starvation-induced filamentous growth in WT SC5314 compared with the P_{ENO} strains, spot plate assays on nitrogen poor media were set up. YNB agar, without amino acids or $(NH_4)_2SO_4$, but supplemented with a poor source of nitrogen (100 µM urea) or a limiting amount of $(NH_4)_2SO_4$(100 µM) was used. We hypothesised, that the P_{ENO} strains would exhibit less filamentation as Tor1 should be constitutively active and starvation induced gene transcriptions dampened.

Figure 3.7 shows the difference in the filamentous growth of the WT SC5314 when compared with the P_{ENO} strains. WT SC5314 exhibits a hyphal fringe surrounding the entire colony in both the 100 µM urea and 100 µM $(NH_4)_2SO_4$. In the 100 µM urea and 100 µM $(NH_4)_2SO_4$, P_{ENO}*VAM6* shows a decreased hyphal fringe compared with WT SC5314, suggesting that P_{ENO}*VAM6* suppresses filamentous growth. However, a greater difference was noted between P_{ENO}*VAM6* grown on 100 µM urea compared with 100 µM $(NH_4)_2SO_4$. Additionally, while P_{ENO}*VAM6* exhibited a reduced hyphal fringe grown on 100 µM urea and $(NH_4)_2SO_4$, the reduction was not as extensive as that observed with other P_{ENO} strains.

The largest difference in colony morphology was noted with the P_{ENO}*TOR1*, P_{ENO}*RHB1* and P_{ENO}*GTR1* strains. On both the 100 µM urea and 100 µM $(NH_4)_2SO_4$, little evidence of a hyphal fringe was seen, indicating that overexpression of these genes strongly inhibits nitrogen starvation induced filamentation. In order to confirm whether the observed phenotype was due to increased Tor1 activation, a sub-inhibitory concentration of rapamycin (0.5 mM) was added to the medium to reduce the level of Tor1 activity. This resulted in reversal of the inhibition of hyphal growth in all P_{ENO} strains, resulting in a similar phenotype to a WT SC5314 phenotype. An additional 2 biological replicates were performed confirming the same results.

3.3.4.2 Formation of Hyphae in Liquid Medium

In order to determine whether P_{ENO} strains could form true hyphae, each strain was grown in YEPD supplemented with 10 % serum (v/v) and incubated at 37°C for 2 h. Upon microscopic analysis, all strains could form true hyphae and were similar to WT SC5314 in appearance (Fig. 3.8). Of interest, following careful observation it was noted that the hyphae formed by the P_{ENO} strains exhibited less cell-cell adherence compared with hyphae formed by WT SC5314. Additionally, it was observed that the number of free yeast cells in the culture appeared greater in those of the P_{ENO} strains compared with WT SC5314. Therefore, in order to determine the number of free, non-adherent cells in these cultures, we developed a semi-quantitative assay.

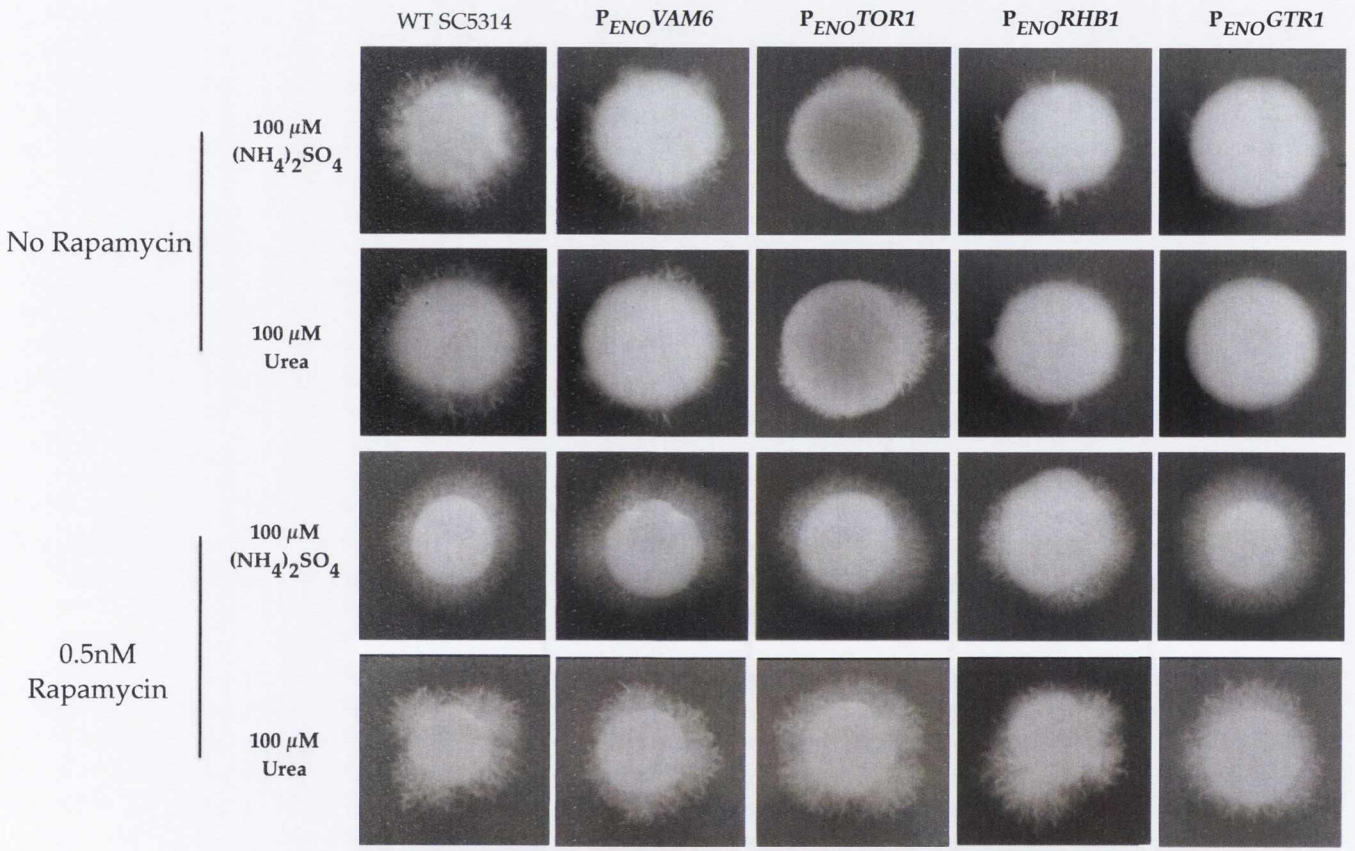

Figure 3.7: **Hyphal formation on solid medium, spot plates.**

Hyphal fringe formation by WT SC5314 compared with P_{ENO} strains on YNB agar plates supplemented with 100 μM $(NH_4)_2SO_4$ and 100 μM urea. Plates were incubated at 37°C for 5 days. P_{ENO} strains grown without the addition of rapamycin showed a decrease level in hyphal formation compared to WT SC5314. In the presence of 0.5 nM rapamycin, hyphal formation was restored to levels seen in WT SC5314

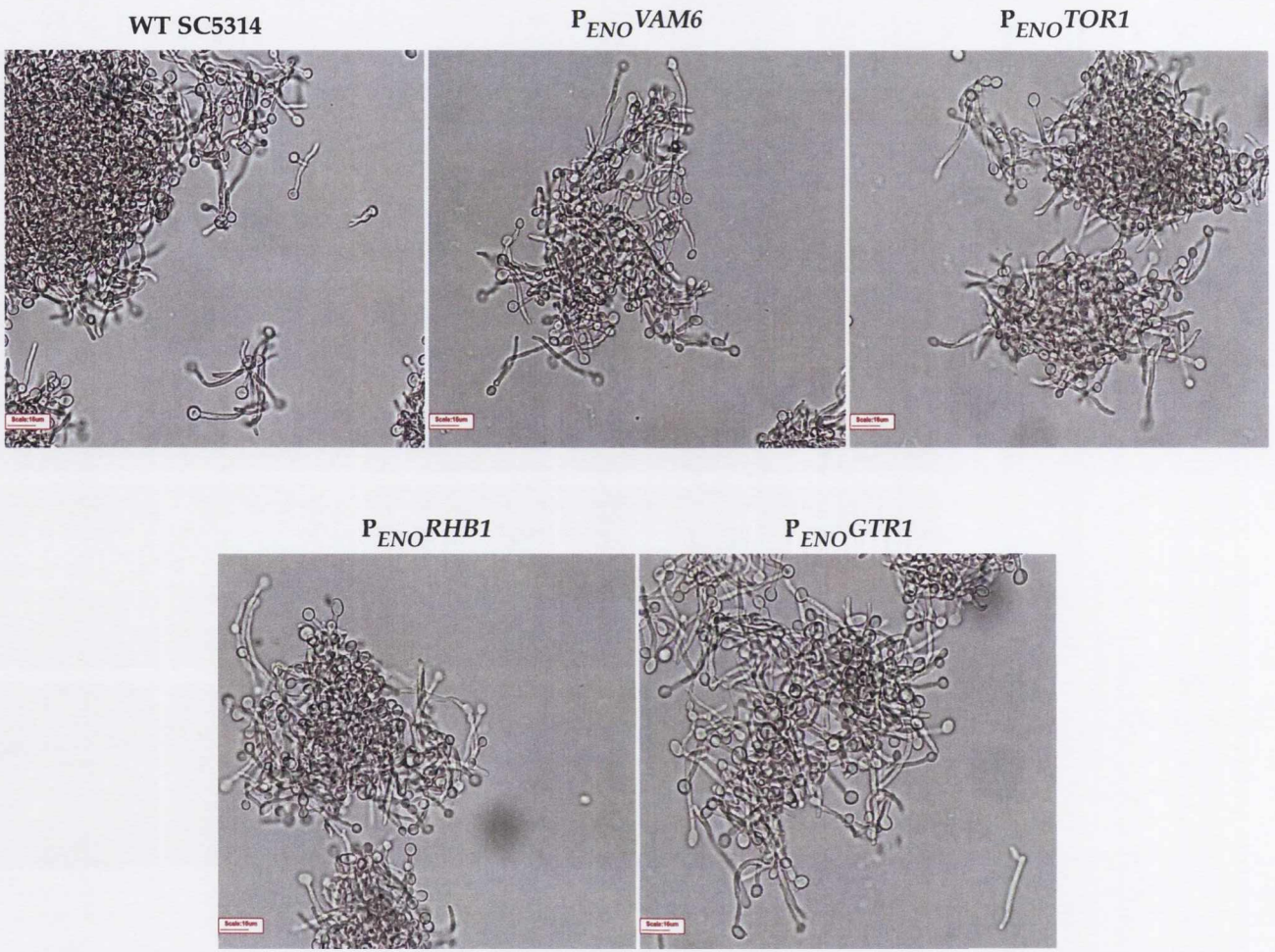

Figure 3.8: **True hyphae formation of P$_{ENO}$ strains.**

All P$_{ENO}$ strains were capable of forming true hyphae in YEPD supplemented in 10 % serum (v/v).

3.3.4.3 Development of a Semi-Quantitative Assay to Enumerate Flocculation and Aggregation of *Candida* Strains in Filament Inducing Medium

Due to the qualitative nature of the observations made in 3.3.4.2, we developed a semi-quantitative assay to estimate the level of flocculation of our strains. The assay was first tested with WT SC5314 compared with characterised mutants (Δ*eed1*, Δ*sfl2* and Δ*efg1*) with known defects in filamentation and flocculation. The Δ*efg1* strain is not capable of forming true hyphae so we predicted that this strain would exhibit greatly reduced levels of flocculation compared to WT SC5314. *SFL2* is an activator of filamentation and deletion of this gene also impairs filamentation [112]. *EED1* is crucial for extension and maintenance of filamentous growth [113]. Therefore, it was expected that a higher number of free yeast cells would be observed in these filament defective strains.

Time points were taken at 2, 4, 6 and 8 h and the morphology observed (Fig 3.9). All strains, with the exception of Δ*efg1* were capable of forming hyphae at 2 h and each aggregated together (Fig. 3.10a). At 4 h (Fig. 3.10b), a difference was seen in hyphal formation. WT SC5314 had distinct elongated true hyphae and aggregated as expected. Δeed1 and Δ*sfl2* had a higher proportion of pseudohyphae and these strains exhibited less aggregation than WT SC5314. The Δ*efg1* strain, while showing some aggregation, had no true hyphae. Instead, the strain formed pseudohyphae. At 6 h (Fig. 3.10c), WT SC5314 aggregated to a higher degree than the mutant strains and true hyphae were still visible. The Δ*sfl2* and Δ*efg1* strains had no discernible true hyphae remaining and exhibited greatly reduced aggregation compared with WT SC5314. Additionally, Δ*eed1* showed no remaining true hyphae but instead some pseudohyphae. However, it showed a higher degree of aggregation than Δ*sfl2* and Δ*efg1* but less than WT SC5314. At 8 h (Fig. 3.10d), WT SC5314 still showed the greatest level of aggregation. While free yeast cells were noted, elongated true hyphae were seen emerging from the mass of aggregates. By this later time-point, Δ*eed1*, Δ*sfl2* and Δ*efg1* showed no true hyphae and with the exception of Δ*sfl2*, no aggregation. While Δ*sfl2* appeared to form some aggregates, a number of free yeast cells were also noted. Δ*eed1* did, however, demonstrate

to some extent, a number of pseudohyphae and a small degree of aggregation but an observable number of free yeast cells were still seen. In order to quantify this, an assay was developed to allow for the enumeration of free yeast cells in the medium (Section 2.10).

Figure 3.10 illustrates the number of free yeast cells counted for each strain at each of the time points that visual inspection was carried out at. At 2 h, Δ*efg1* has a significantly higher cell count compared with WT SC5314. This was expected since Δ*efg1* cannot form true hyphae. No significance was seen for Δ*eed1* and Δ*sfl2*. While these strains have defects in hyphal growth, at 2 h, the strain exhibits the onset of filamentation. This early filamentation was reversed by 4 h as Δ*eed1* and Δ*sfl2* exhibit significantly greater numbers of free cells counted at 4 h. As expected, Δ*efg1* also had a higher count of free cells compared with WT SC5314 at the 4 h time point. At 6 h, Δ*eed1* and Δ*efg1* had a statistically significant higher number of free cells counted compared with WT SC5314. Unfortunately, Δ*sfl2* did not return a statistical significance when a t-test was performed. This is due to the discrepancies between the 3 biological replicates. However, by 8 h, all mutant strains demonstrate significance in the number of cells counted compared with WT SC5314. The significance in counts correlate with the qualitative visual inspection of each strain at each chosen time point thus suggesting our method of counting the number of free yeast cells provides a semi-quantitative analysis of aggregation.

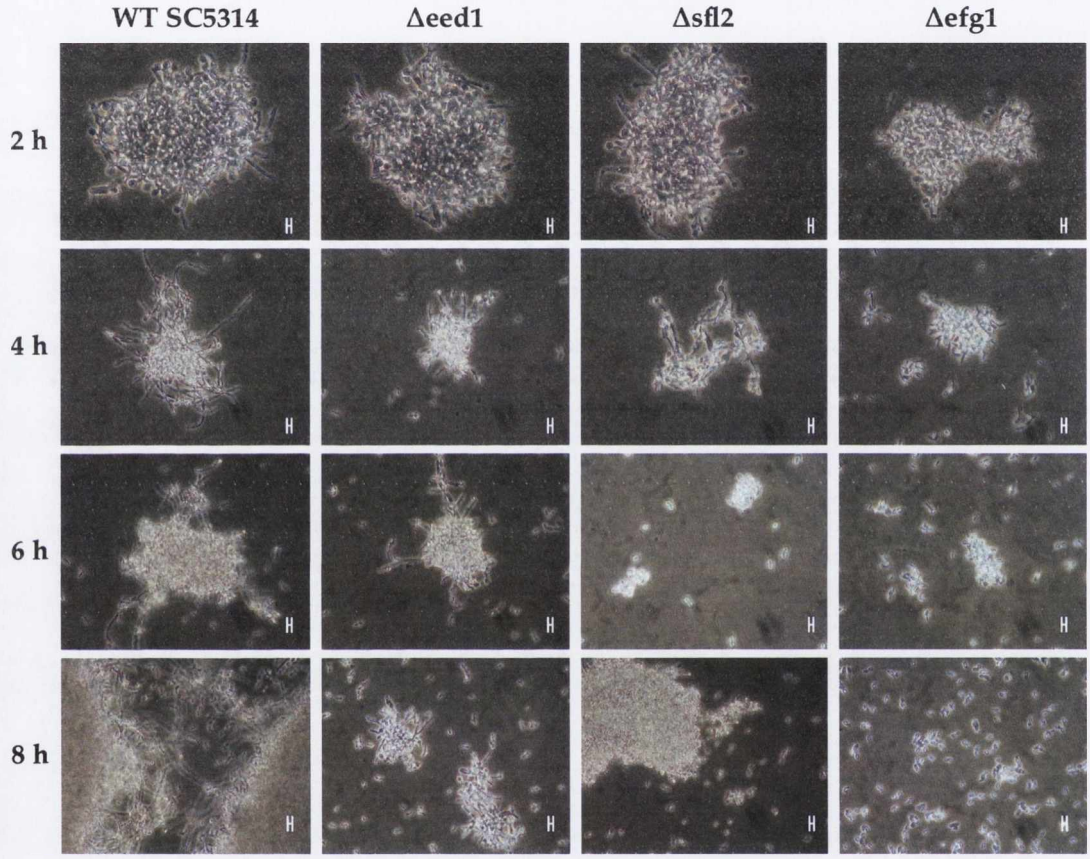

Figure 3.9: **Qualitative images depicting the aggregation of WT SC5314 compared to strains with a defect in filamentation.**

Aggregates of WT SC5314 compared to strains which have a known defect in filamentation at 2, 4, 6 and 8 h in YEPD supplemented with 10% (v/v) serum. WT SC5314 appears to aggregate more than the mutant strains. Mutant strains appear to have less aggregation compared with WT SC5314 and a greater number of free yeast cells. The scale bar is equivalent to 10 µm.

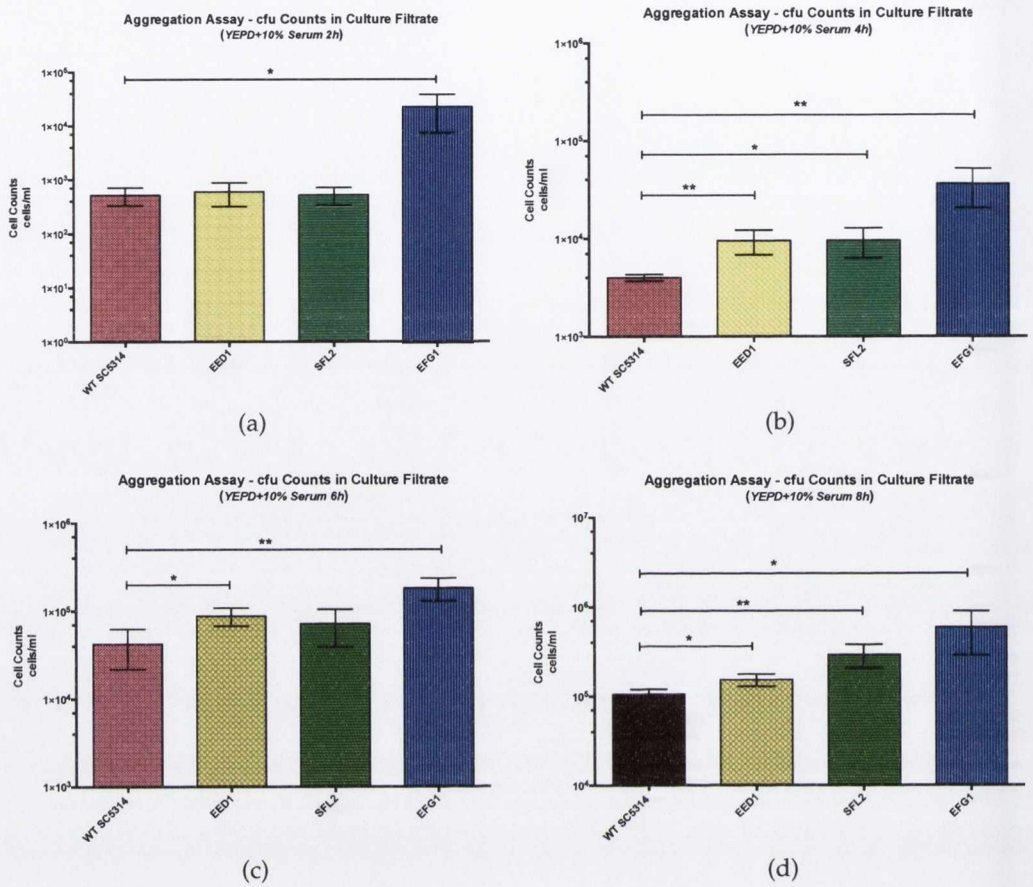

Figure 3.10: **Semi-quantitative analysis of the aggregation of WT SC5314 compared to strains with a defect in filamentation.**

Free yeast cell counts after aggregation at 2 (a), 4 (b), 6 (c) and 8 (d) h time points. Samples were filtered through a 0.12 μm membrane to remove hyphae. The assay was performed with an initial inoculum of an OD_{600} of 0.01 nm.

3.3.4.4 Qualitative & Semi-Quantitative analysis of Aggregation of P_{ENO} Strains in a Filament Inducing Medium

In the knowledge that the assay in section 3.3.4.3 allowed for the filtration of free yeast cells from hyphal cells in a semi-quantitative analysis (Fig 3.8 & 3.9), we decided to carry out the assay with our P_{ENO} strains. Upon qualitative inspection, all strains were capable of forming true hyphae (Fig 3.11) and aggregated at 2 and 4 h. However, the aggregates in P_{ENO} strains were less dense compared with WT SC5314. At 8 h, aggregation was prevalent in all strains, however, the level of aggregation in P_{ENO}*VAM6*, P_{ENO}*GTR1* and P_{ENO}*RHB1* appeared less than WT SC5314. Additionally, the number of free yeast cells was greater in the P_{ENO} strains compared to WT SC5314.
Using the semi-quantitative assay developed in section 3.3.4.3, P_{ENO}*TOR1* and P_{ENO}*GTR1* had significantly higher counts (3.6-fold and 3.2-fold change respectively) of free yeast cells at 2 h in liquid YEPD containing 10% (v/v) serum (Fig. 3.12). At 4 h, no statistical significance was noted and all counts were similar to WT SC5314. In order to determine if this reduction in aggregation required increased Tor1 activity, we carried out the assay in 0.5 nM rapamycin while this would inhibit Tor1 activity and negate the effects of the constitutive Tor1 activation. In the presence of rapamycin, all strains exhibited similar levels of aggregation and cell counts (Fig. 3.12) indicating that the P_{ENO} phenotype required activation of Tor1.

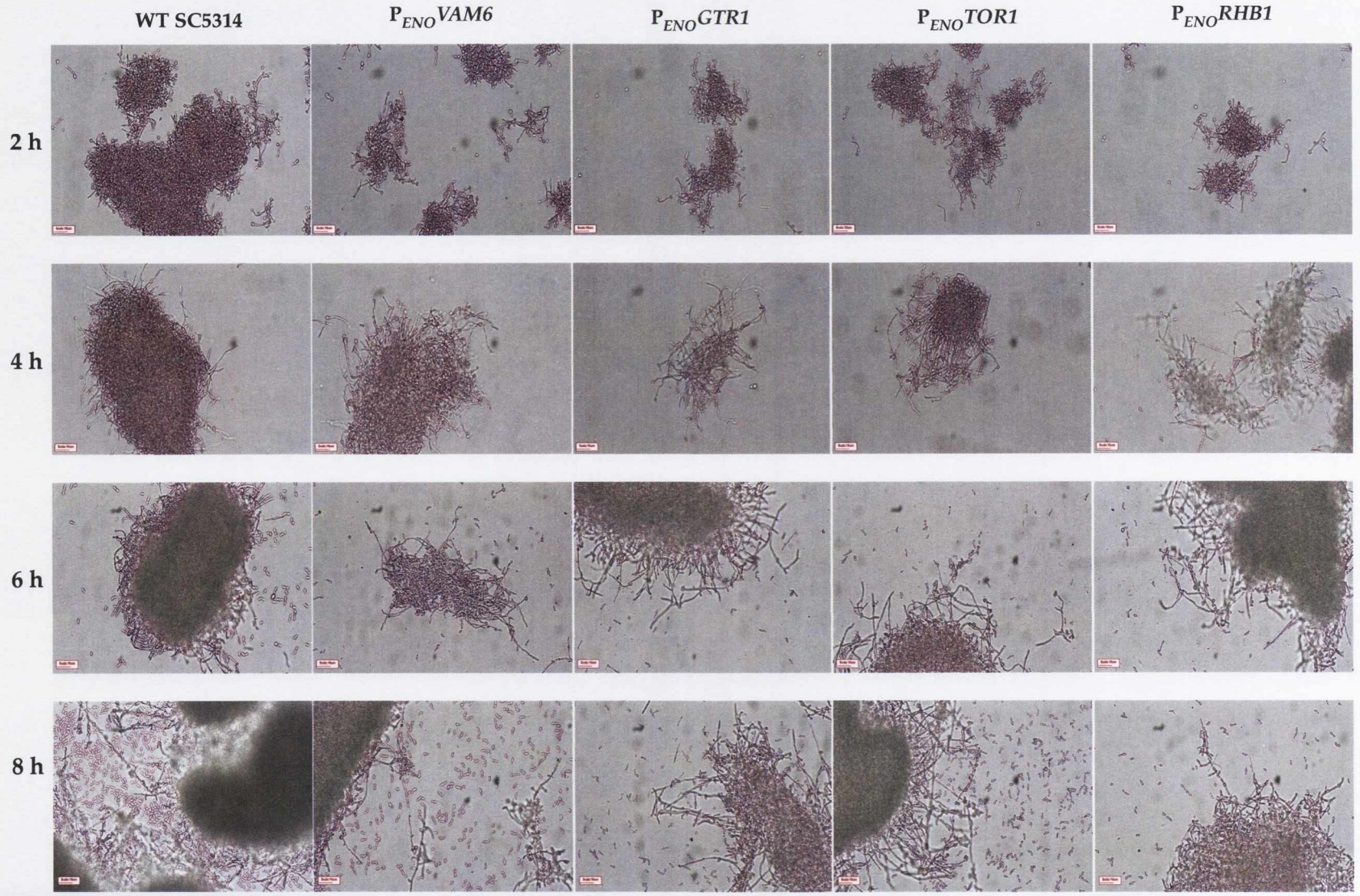

Figure 3.11: **Qualitative aggregation of WT SC5314 compared with P_{ENO} strains in YEPD and 10% serum.**
Aggregates of WT SC5314 compared with P_{ENO} strains at 2, 4, 6 & 8 h in YEPD supplemented with 10% serum (v/v). WT SC5314

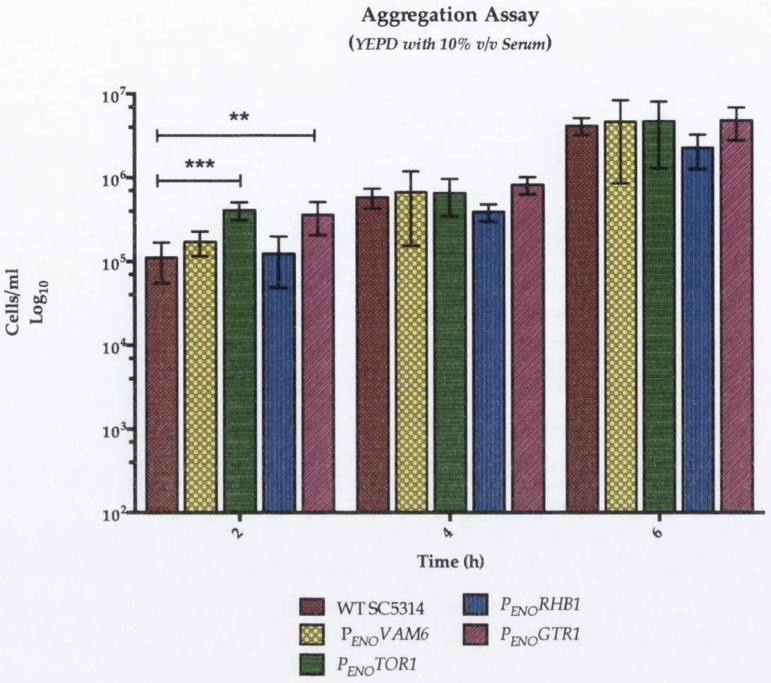

Figure 3.12: **Semi-quantitative analysis of the aggregation of WT SC5314 compared with P_{ENO} strains at 2, 4 & 6 h.**

(a) Growth in YEPD supplemented with 10 % serum (v/v). $P_{ENO}TOR1$ and $P_{ENO}GTR1$ show a statistical significance in the number of free yeast cells counted. (b) Upon the addition of 0.5 nM rapamycin, this phenotype was reversed and levels equivalent to wild type where seen. The assay was performed with an initial inoculum of an OD_{600} of 0.1 nm.

3.3.5 Flocculation Assay of P_{ENO} Strains Compared to WT SC5314

Aggregation and enumeration of free yeast cells demonstrated that P_{ENO} strains aggregated less than WT SC5314 (section 3.3.6). Bastidas *et al.* (2011) [90] also demonstrated that flocculation of *C. albicans* in liquid Spider medium was induced by rapamycin, indicating this was a Tor1-regulated phenotype. Therefore, in order to confirm the results of section 3.3.6, we analysed the flocculation of the P_{ENO} strains compared to WT SC5314 using Spider medium. A simple assay was carried out in 13 ml test tubes. Strains were incubated at 200 rpm for 2 hr, after which, they where left stationary to allow cells to flocculate (Fig. 3.12). WT SC5314 flocculated and settled at the bottom of the tube more rapidly than the P_{ENO} strains (~ 20 min.), indicative of the expression of cellular adhesins allowing greater aggregation. In order to confirm this, an additional assay was carried out in which 0.5 nM rapamycin was added to the medium, resulting in the flocculation of all strains.

3.3.6 Effects of Rapamycin on P_{ENO} strains. Minimal Inhibitory Concentration Assay

In order to determine whether these P_{ENO} strains were resistant to rapamycin, an MIC assay was performed, as shown in figure 3.13. All strains were grown in the presence of rapamycin in doubling dilutions from 40 ng/ml to 0.08 ng/ml and incubated for 24 h. WT SC5314, P_{ENO}*TOR1*, P_{ENO}*RHB1* and P_{ENO}*GTR1* all had an 80 % inhibitory concentration (IC_{80}) in the range of 8 ng/ml to 11 ng/ml rapamycin. WT SC5314 had an IC_{80} of 9.8 ng/ml, P_{ENO}*TOR1* an IC_{80} of 11 ng/ml, P_{ENO}*RHB1* an IC_{80} of 8.2 ng/ml and P_{ENO}*GTR1* an IC_{80} of 9.2 ng/ml. P_{ENO}*VAM6* has an IC_{80} of 6.3 ng/ml rapamycin were as P_{ENO}*TOR1* has an IC_{80} of 6 ng/ml rapamycin, the lowest of all P_{ENO} strains.

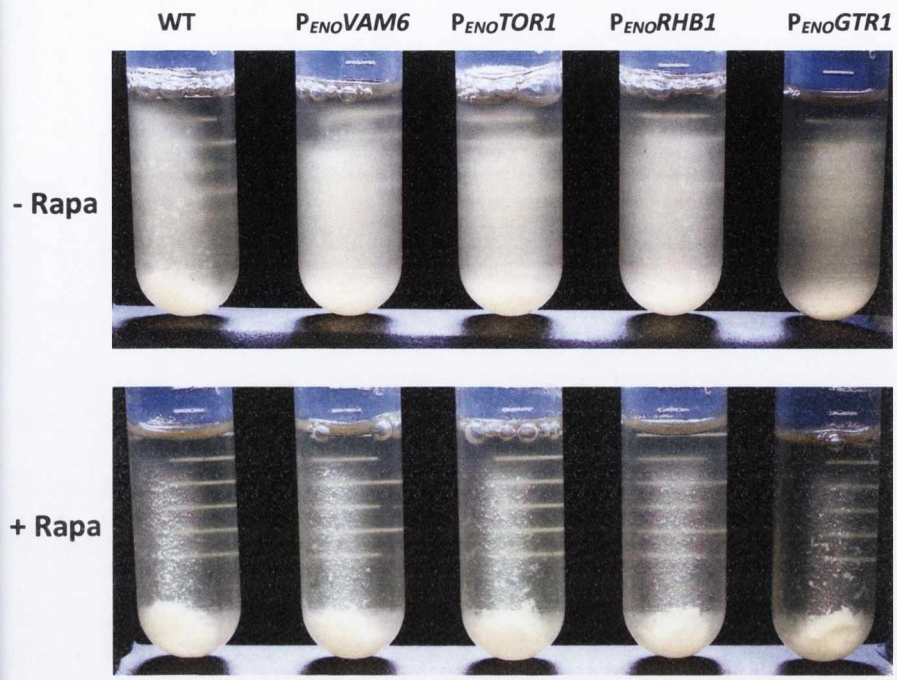

Figure 3.13: **Flocculation of WT SC5314 compared with P_{ENO} strains.**
Left to right, WT SC5314, P_{ENO}*VAM6*, P_{ENO}*TOR1*, P_{ENO}*RHB1* and P_{ENO}*GTR1*. The top image represents all strains grown in Spider. The WT SC5314 strain settles before the P_{ENO} strains. The bottom image represents all strains grown in Spider with the addition of 0.5 nM rapamycin.

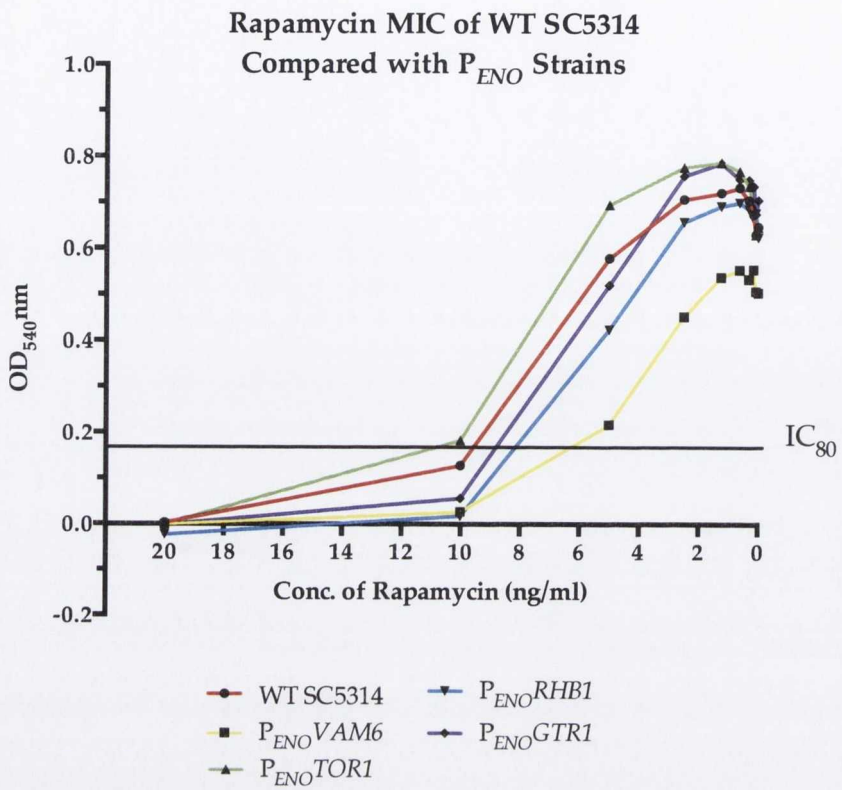

Figure 3.14: **Rapamycin MIC assay.**
Effects of rapamycin on P_{ENO} strains compared with WT SC5314.

3.3.7 Biofilm Formation of P_{ENO} Strains Compared to WT SC5314

In order to establish whether P_{ENO} strains were less proficient at forming biofilms when compared with WT SC5314, biofilm assays were carried out on 96-well plates and tested by way of a colourmetric assay using 0.4 % crystal violet.
At 24 h, P_{ENO}*TOR1*, P_{ENO}*RHB1* and P_{ENO}*GTR1* showed significant reduction in biofilm formation compared with WT SC5314 (fig. 3.14). Although P_{ENO}*VAM6* also showed a decrease in biofilm formation compared to WT SC5314, this result was not statistically significant. At 48 h, all strains showed a decrease in biofilm compared with 24 h counterparts. However, biofilm growth by strain P_{ENO}*GTR1* was still significantly lower than wild-type.

3.3.8 Ability of P_{ENO} Strains to adhere to Human Buccal Epithelial (TR146) Cells Compared to WT SC5314

Previous assays demonstrated that P_{ENO} strains aggregated and flocculated less than WT SC5314. In order to test the adherence ability of P_{ENO} strains, an adherence assay using TR146 cells was carried out. It was hypothesised that P_{ENO}strains would not adhere as effectively compared with WT SC5314. Figure 3.15 below represents the percentage adherence of each strain to the TR146 monolayer. No discernible difference was noted between WT SC5314 and the P_{ENO} strains. Discrepancies between biological replicates account for the large error bars seen.

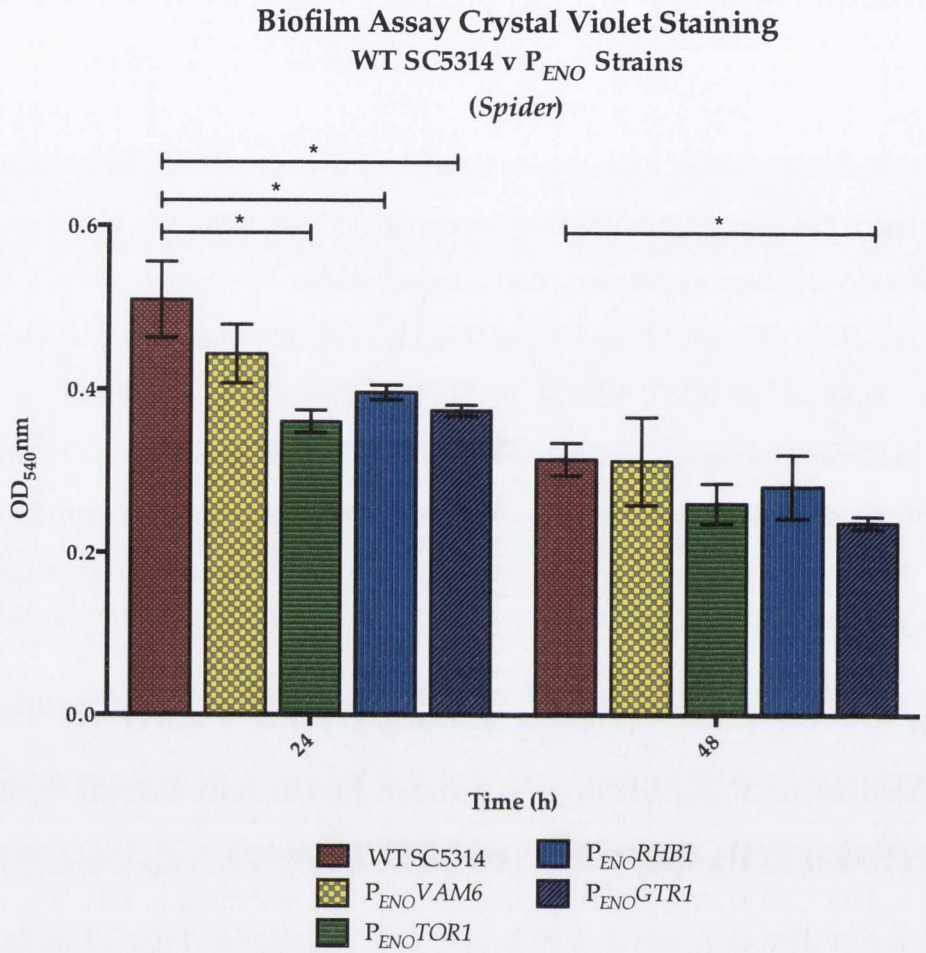

Figure 3.15: **Biofilm assay of P_{ENO} strains compared with WT SC5314.**
The biofilm assay was performed in Spider medium and the biomass measured using a Crystal Violet assay.

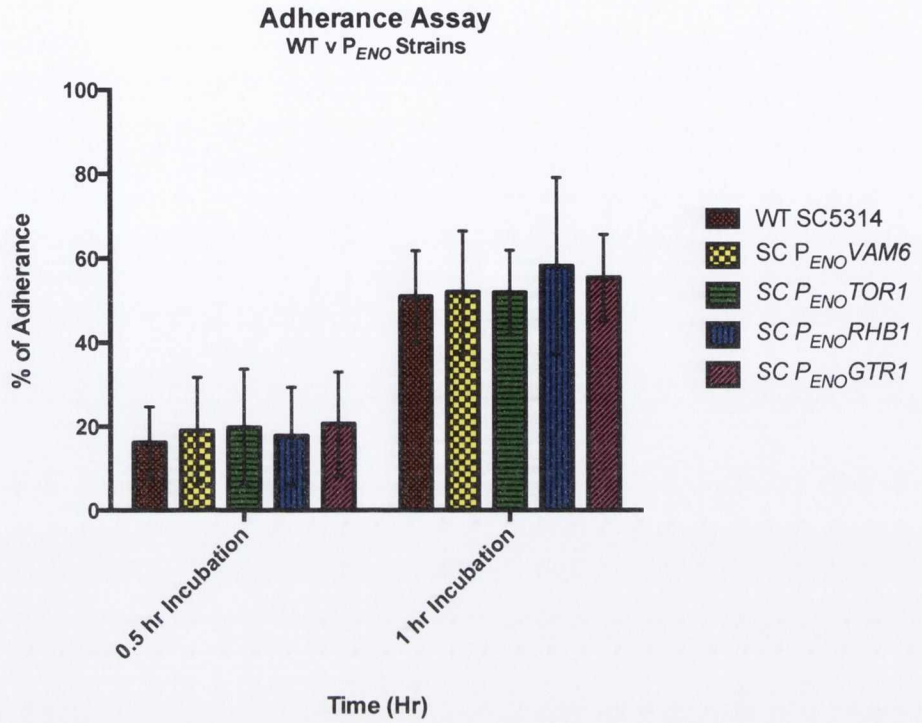

Figure 3.16: **Adherence levels of WT SC5314 compared with P_{ENO}strains.**

The level of adherence of WT SC5314 compared to P_{ENO} strains on an epithelium monolayer of TR146 cells.

3.4 Discussion

3.4.1 Generation & Analysis of Constitutively Active Tor1 Mutants of *Candida albicans*

Target of rapamycin (TOR), a protein kinase, is highly conserved from mammalian to yeast cells. In eukaryotes, mTor is responsible for regulating metabolism and the cell cycle. In *Saccharomyces cerevisiae*, Tor1 is stimulated by amino acids and an active Tor kinase promotes ribosome biogenesis and glycolysis, as well as repressing genes involved in nitrogen scavenging.

In *C. albicans*, global transcriptional profiling has shown roles for Tor1 in ribosome biogenesis and nitrogen scavenging. Current literature presents several lines of evidence indicating that in *Candida* species, Tor1 may play a role in the transition of yeast-to-hyphae [90]. Therefore, it is hypothesised that an active Tor1 kinase may repress virulence and filament formation. Subsequently, we aim to determine whether strategies to activate this kinase could be valuable in controlling infection. The work presented above has involved testing this hypothesis by generating constitutively active Tor1 mutants of *C. albicans*.

According to Reinke *et al.* (2006), a single base substitution in the *Saccharomyces cerevisiae TOR1* confers resistance to caffeine. They noted that this single base substitution in the *TOR1* gene, converting either an isoleucine at position 1954 to valine or alanine at position 1957 to valine, not only confers caffeine resistance but also a hyperactive Tor1 phenotype. In our study, attempts here to generate similar mutants in *C. albicans* SC5314 yielded derivatives that could grow on inhibitory concentrations of caffeine, however the isolated transformants did not contain either the I1954V or A1957V substitution (Fig. 3.5a). A possible explanation is that the base substitution was lost when cells were subcultured in an environment free of caffeine. Pre-transformation, caffeine inhibition concentrations were ~12-15 mM. However, MIC assays confirmed that the inhibitory concentrations of caffeine in transformed strains were ~27 mM. Further MIC

assays were carried out but were not reproducible. We therefore suggest that the transformed cells either lost the cassette inserted or the cassette may have inserted in a different location. Alternatively, if the cassette was not inserted, *C. albicans* may have a natural inducible resistance to caffeine. Due to this, a second approach was used, focusing on the putative upstream activators of Tor1. This approach involved using the Enolase1 promotor (P_{ENO}) to induce overexpression of these genes in order to achieve a constitutively active Tor1 phenotype.

Bates *et al.* (2011) showed that P_{ENO} is a useful, strong promotor for gene overexpression [114]. Therefore, we chose to overexpress the putative upstream activators of Tor1 as well as Tor1 itself, using P_{ENO}. Firstly, we looked at genes encoding proteins homologous to the EGO complex in *S. cerevisiae*, including the orthologues of *VAM6* and *GTR1*. As previously mentioned, *VAM6* encodes a protein reported to control Tor complex 1 in *S. cerevisiae*. It is a guanine nucleotide exchange factor coupled to the vacuole acting upon the GTPase Gtr1, the second target for overexpression. Work on both has been described in *S. cerevisiae* but not in *C. albicans*. The third upstream activator, Rhb1, is a recently characterised protein shown to regulate sensitivity to rapamycin thus suggesting association with Tor1 signalling. Additionally, Rheb (mammalian homolog of Rhb1) is known to stimulate the kinase activity of mTor. Finally, Tor1 itself was additionally overexpressed using P_{ENO}.

Data obtained by qRT-PCR (Fig. 3.6), confirmed overexpression of the genes of interest P_{ENO} and the generation of overexpressing strains. The phenotypes of the overexpressing strains were characterised and it was determined whether overexpression resulted in constitutively active Tor1 phenotype.

3.4.2 Growth Curve Analysis of P_{ENO} Strains Compared to WT SC5314

In a nutrient rich environment Tor1 is active, thereby suppressing nitrogen scavenging. Therefore, in YEPD, normal growth and proliferation was expected in both the P_{ENO} strains and WT SC5314 in YEPD experiments. Figure 3.7 shows the rate of growth in

a nutrient rich YEPD medium. It was observed that the doubling times of all P_{ENO} strains were marginally shorter (i.e. faster) than that of WT SC5314. YEPD is a nutrient rich medium source, resulting in an active Tor1 and increased proliferation. Overexpression of the putative upstream activators may drive even greater proliferation under these conditions and result in the decrease in the doubling times observed. P_{ENO} strains and WT SC5314 were also grown in a nitrogen limiting medium (YNB supplemented with either 100 mM proline, 100 mM urea or 100 mM $(NH_4)_2SO_2$). In a limiting nitrogen source, Tor1 activation of ribosome biogenesis and glycolysis is suppressed and nitrogen scavenging mechanisms become more active. Cells grown in an environment without a readily available nitrogen source would show a reduced rate of growth. We hypothesised that if the putative upstream activators of Tor1 are overexpressed, a constitutively active Tor1 phenotype would be seen. Therefore, we expect a slower rate of proliferation of the P_{ENO} strains since mechanisms involved in utilising poorer nitrogen sources are suppressed.

P_{ENO} strains showed slightly shorter doubling times than that of WT SC5314 in the 100 mM proline and the 100 mM $(NH_4)_2SO_2$, however these differences were not significant. Nonetheless, in 100 mM urea, P_{ENO} strains grown had a slightly longer doubling time than that of WT SC5314. The variation in doubling times between strains may be due to the different transporter systems involved in the uptake of proline, urea and $(NH_4)_2SO_2$. For example, Dur3 is the major urea transporter system in *C. albicans* and suppression of *DUR3* expression could account for the longer doubling times observed in the presence of urea, although qRT-PCR would be required to confirm this [115].

When grown in YCB-BSA, P_{ENO} strains showed a slower rate of growth compared with WT SC5314. As previously mentioned, work by Chen *et al.* (2012) showed that an overexpressed *RHB1* (P_{ADH1}*RHB1*) resulted in growth slower than a wild-type strain in YCB-BSA. They showed that Rhb1 overexpression suppressed the expression of *SAP2*, a virulence factor required for the degradation of protein substrates in *C. albicans*. The P_{ENO}*RHB1* strain generated here also likely exhibits a reduced level of *SAP2* expression

due to the reduced growth levels observed in YCB-BSA, and we hypothesise that the P_{ENO}*GTR1* strain may also exhibit this defect. Attempts to measure *SAP2* expression were performed. Unfortunately we could not determine the expression of *SAP2* as RNA extractions failed to yield a), a high concentration and b), a high quality of RNA.

3.4.3 Hyphal Formation Analysis of P_{ENO} Strains Compared to WT SC5314 in Response to Nitrogen Starvation

We sought to analyse the nitrogen starvation induced filamentous growth of the P_{ENO} strains compared to WT SC5314. All strains were plated onto poor or limiting sources of nitrogen (100 μM ammonium sulphate [$(NH_4)_2SO_4$] or 100 μM urea). After 7 days incubation, a discernible difference was noted in the ability of each P_{ENO} strain to filament compared to WT SC5314 (Fig 3.8). Full filamentation was seen around WT SC5314 colonies as expected.

As nitrogen sources on this medium are limiting, Tor1 activity is decreased, initiating the expression of hypha specific genes (Fig 3.4) and nitrogen scavenging systems such as the ammonium permease, Mep2. Mep2 has a dual role as it mediates the uptake of ammonium and induces filamentous growth in *C. albicans* in response to nitrogen limitation [116]. This occurs via the C-terminal cytoplasmic tail of Mep2 which acts as a signalling domain activating the cAMP-PKA pathway [117]. Tsao *et al.* (2009) showed that Rhb1 and Tor1 partly regulate nitrogen starvation-indudced morphogenesis by controlling *MEP2* expression. We decided to confirm whether this observation was seen in our P_{ENO}*RHB1* strain and other P_{ENO} strains. When qRT-PCR was performed on the level of *MEP2* expression, it was shown that expression of *MEP2* was significantly less in P_{ENO}*RHB1* strain. Furthermore, *MEP2* expression was significantly less in P_{ENO}*GTR1* and P_{ENO}*VAM6* than WT SC5314 (Fig 3.6).

As expected, P_{ENO} strains showed a distinguishable difference in filamentation, notably the P_{ENO}*TOR1*, P_{ENO}*RHB1* and P_{ENO}*GTR1* strains. Under poor nitrogen conditions, these strains failed to filament to the same degree as their WT SC5314 counterpart.

WT SC5314 showed large dense filament formation surrounding the colony. However, P_{ENO}*TOR1*, P_{ENO}*RHB1* and P_{ENO}*GTR1* strains showed limited areas of filamentation that were less dense. This indicates that the overexpression of these putative upstream activators are in turn, resulting in a constitutively active Tor1 phenotype.

Interestingly, P_{ENO}*VAM6* exhibited intermediate levels of filamentation in comparison to P_{ENO}*TOR1*, P_{ENO}*RHB1* and P_{ENO}*GTR1*. Presumably, this is due to the fact that it does not interact with Tor1 directly but instead works via an intermediate protein, Gtr1. Nevertheless, filamentation did not completely encompass the entire colony and the fringing of P_{ENO}*VAM6* appeared more reduced compared to WT SC5314.

In order to confirm the observed phenotypes required for Tor1 activity, 0.5 nM rapamycin was added to the solid medium. Rapamycin inhibits Tor1 thus mimicking a nitrogen poor environment. When P_{ENO} strains were grown in the presence of rapamycin, full filamentous growth was observed on the P_{ENO} colonies, indicating that the suppression of filamentous growth required the activity of Tor1.

3.4.4 Hyphal Formation and Enumeration of Free Yeast Cells in Liquid Culture of P_{ENO} Strains Compared to WT SC5314

After analysis of hyphal formation on solid medium, we carried out similar tests in liquid medium to determine whether hyphal growth was affected in the P_{ENO} strains. P_{ENO} strains and WT SC5314 were grown in YEPD supplemented with 10% serum. WT SC5314 and P_{ENO} strains were grown in serum and subjected to a temperature shift from 30°C to 37°C in order to induce hyphae.

We determined that the P_{ENO} strains were able to form hyphae in a hyphal induced environment (Fig. 3.8). However, a difference in the number of free yeast cells was observed in the WT SC5314 cells compared with the P_{ENO} strains at 2 h and 4 h. No free yeast cells were seen in WT SC5314 at 4 h. Yeast cells may have been present but due to tight clumping, were aggregated within the mass of hyphae. Interestingly, the P_{ENO} strains appear to have a larger number of free-floating yeast cells and less compact hy-

phal aggregation compared to WT SC5314. The higher number of free yeast cells suggests that a constitutively active Tor1 may be suppressing hypha specific genes such as the adhesins *ALS1*, *ALS3* and *HPW1* (Fig 1.4). This reduction in the compactness of the aggregate in the P_{ENO} strains suggests that, while P_{ENO} strains are capable of filamenting, there was a difference in the mechanisms by which the hyphae aggregate. This effect on the ability to aggregate could indicate that drugs acting as Tor1 agonists could be useful in combating biofilm formation . Ultimately, microarray analysis of global gene transcription would be of benefit in order to determine whether the expression of genes involved in filamentation and adhesion have been altered.

In order to quantify this phenotype, we filtered each time point to remove clumped hypha and counted the free yeast cells. In YEPD medium, the initiating factor for hyphal formation was a shift in temperature (30°C to 37°C) and the addition of 10% serum. In this medium, a difference was observed in the number of free yeast cells in P_{ENO}*TOR1* and P_{ENO}*GTR1* at 2 h compared with WT SC5314 (Fig. 3.12). This suggests that these P_{ENO} strains have reduced clumping due to a constitutively active Tor1 phenotype. This result correlates with the the qualitative inspection preliminarily undertaken where the P_{ENO} strains appeared to visually contain the largest number of free yeast cells. Therefore, the lack of aggregation and the number of free yeast cells led us to hypothesise that the P_{ENO} strains would flocculate less than WT SC5314.

Additionally, in order to determine whether the observed phenotype was Tor1 mediated, 0.5 nM rapamycin was added to cultures of each strain. Rapamycin inhibits Tor1 thus mimicking a nitrogen poor environment. Figure 3.12 illustrates that the addition of rapamycin reverts the phenotype noted in the P_{ENO} strains.

3.4.5 Analysis of Flocculation of P_{ENO} Strains compared to WT SC5314

After observing the lack of filamentation on solid medium as well as the decrease in flocculation and hyphal aggregation in YEPD, we investigated whether P_{ENO} strains flocculated less when compared with WT SC5314 cells in Spider broth. Bastidas *et al.*

(2009) have shown that flocculation in Spider broth is Tor1 dependent [90].

P_{ENO}strains and WT SC5314 were grown in Spider broth and after 2 h of incubation, samples were examined for flocculation. WT SC5314 exhibited flocculation (Fig. 3.13) and settling of the yeast suspension after approximately 10 min whereas the P_{ENO} strains did not flocculate and took longer (25 min) to settle at the bottom of the tube. This suggests reduced expression of adhesins in the P_{ENO} strains and supports the qualitative and quantitative results observed in the earlier experiments. Additionally, 0.5 nM rapamycin was added to the medium in order to determine whether the observed phenotype could be reversed, indicating that the phenotype is a Tor1 mediated phenotype.

3.4.6 Analysis of Biofilm Formation of P_{ENO} Strains Compared to WT SC5314

The reduction in cellular aggregation and flocculation (Fig. 3.11, 3.12 & 3.13) of the P_{ENO} strains compared with WT SC5314 suggested a potential defect in the ability of the P_{ENO} strains to form biofilms successfully. Therefore, we sought to investigate biofilm formation in the P_{ENO} strains compared to WT SC5314.

Biofilm analyses were performed in 96 well plates using an colourimetric assay involving crystal violet staining. At 2 h, all P_{ENO} strains exhibited a decrease in biofilm formation with P_{ENO} - *TOR1, RHB1* and *GTR1* having the greatest decrease. This result was keeping in line with the decrease in aggregation and flocculation previously seen. Additionally, at 48 h all three strains continued to demonstrate a decrease in biofilm formation with P_{ENO}*GTR1* having the greatest defect. It would be of interest to perform the biofilm assay in a flow system in order to determine the effect a constitutively active *TOR1* has on biofilm formation in a more in vivo-like environment.

3.4.7 Analysis of the ability of P_{ENO} Strains to Adhere to Human Buccal Epithelial TR146 Cells Compared to WT SC5314

With the results observed in biofilm formation, the negative effect of hyphal formation on solid media containing poor nitrogen sources as well as the reduction in aggregation and flocculation, we investigated the ability of P_{ENO} strains to adhere to human buccal epithelial cells. It was suspected that the P_{ENO}strains would show less adherences than WT SC5314.

Unfortunately there were large discrepancies between biological replicates in this assay. At 30 min and 1 h incubation periods, no discernible difference was observed between strains. While it was noted that aggregation was less in P_{ENO} strains compared to WT SC5314, this difference may not be large enough to translate to a reduction in adherence on epithelial cells or may involve differnet adhesins.

Therefore, the results presented here demonstrate that the overexpression of *VAM6*, *GTR1* and *RHB1* are indicative of a Tor1 hyperactive phenotype. These strains showed a reduction in hyphal formation as well as aggregation and flocculation when compared with wild-type. Moreover, to confirm that these observed phenotypes were in fact due to increased Tor1 activation, the phenotypes were reversed with the addition of the Tor1 inhibiting drug rapamycin. Finally, a defect in biofilm formation was noted suggesting a possible role for these Tor1 activators as potential targets in combating and controlling infection.

Chapter 4

Phenotypic Analysis of *GTR1* & *RHB1* mutants of *C. albicans* and a Conditional Mutant of *TOR1*

4.1 Introduction

Tor1 plays a central role in cellular proliferation and is regulated by environmental cues, nutrient availability and stress conditions [59, 77]. Upstream activators of Tor1 have been described in *S. cerevisiae*, including *RHB1* and *GTR1* which are involved in cell wall integrity, and control of filamentous growth under nitrogen starvation and phosphate transport respectively [118, 110].

As stated previously, Tsao *et al.* (2009) suggest that *RHB1* is associated with Tor1 signalling in *C. albicans* due to the enhanced sensitivity of a mutant Δ*rhb1* strain to rapamycin. Furthermore, they suggest that *RHB1* is involved in nitrogen starvation-induced filamentation, potentially by controlling the expression of *MEP2*, an ammonium permease and sensor of nitrogen availability [92]. In *S. cerevisiae*, *GTR1* has been proposed to be involved in the epigenetic control of gene expression in the TOR signalling pathway. Gtr1 has also been proposed to mediate amino acid signalling to the target of rapamycin complex 1 (TORC1) [119, 120]. *GTR1* is part of the EGO (escape from rapamycin-induced growth arrest) complex that resides on the vacuolar membrane, transducing amino acid signals to TORC1 [98]. The nucleotide binding status of *GTR1* is regulated by Vam6, a conserved guanine nucleotide exchange factor. When expressed in a constitutively active "GTP-bound state", *GTR1* has been shown to interact strongly with TORC1, whereas in a "GDP-bound state" exhibits low TORC1 activating activity [91].

Highly conserved orthologues of *RHB1* and *GTR1* have been identified in *C. albicans* and overexpression studies in chapter 3 of the current study demonstrated that in nutrient poor environments, an overexpression of *GTR1* or *RHB1* results in a constitutively active Tor1 strain, resulting in decreased filamentous growth and a reduction in flocculation and aggregation (Chapter 3).

We have previously proposed genetic means to generate Tor1 constitutively active strains. Although this has allowed us to generate proof of concept that Tor1 restricts hyphal formation, aggregation and flocculation, it does not provide us with information on the normal pathways of Tor1 activation. As stated previously, Tor1 is highly conserved

and elements upstream of this pathway may prove to be potential targets for Tor1 activating antifungal agents. Therefore, we have sought to delete the upstream activators *RHB1* and *GTR1* in order to determine the downstream effects on Tor1 signalling. We have generated mutant strains that contain either homozygous *RHB1* or *GTR1* deletions. However, due to the essentiality of Tor1, a homozygous mutant could not be generated as it would be lethal to the cell. In order to analyse the effects of Tor1 depletion, we have obtained a conditional Tor1 mutant from the laboratory of Dr. Julia Koehler (Harvard, Boston). This strain has one copy of Tor1 deleted and a tetracycline inhibitable promoter placed upstream of the intact *TOR1* allele (Fig. 4.1). Here we use the mutant to examine the effects of *TOR1* depletion on flocculation and biofilm formation.

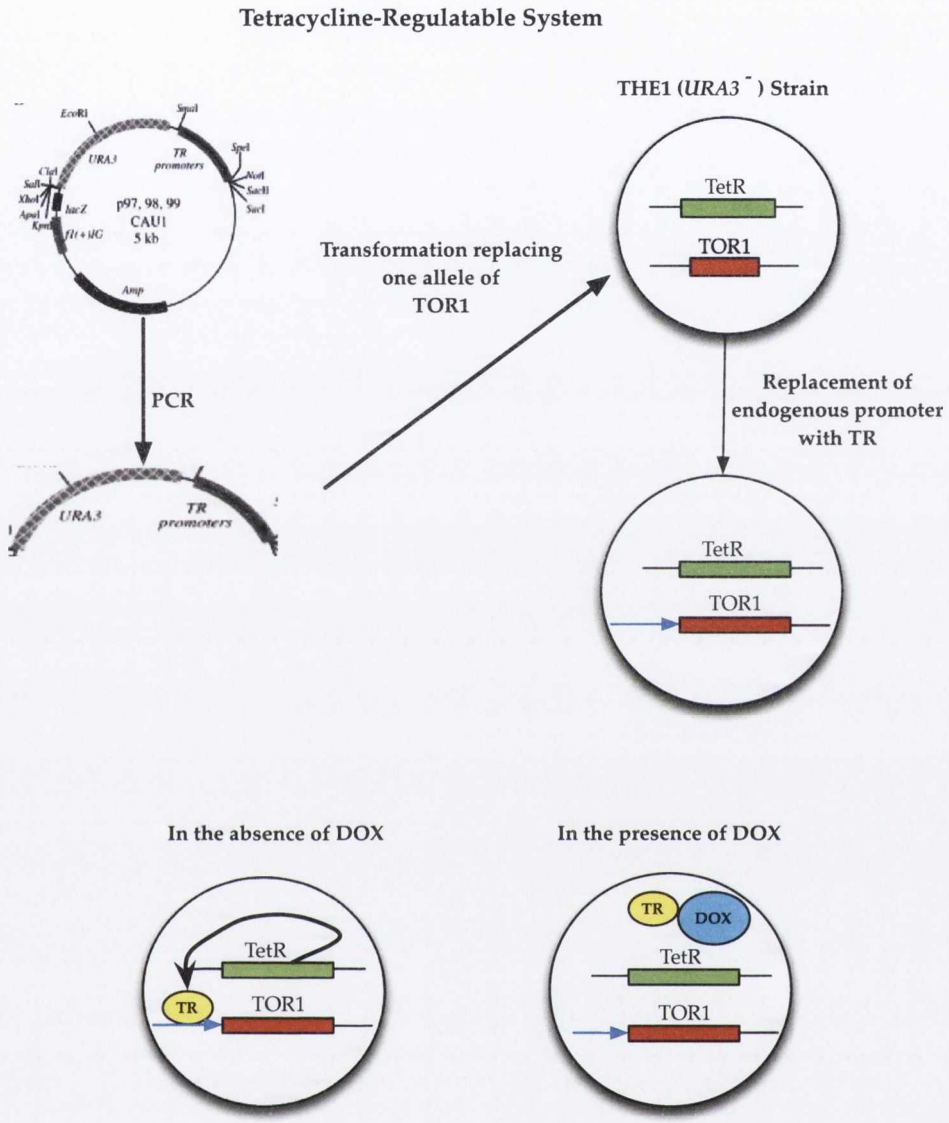

Figure 4.1: **Tetracycline regulated tetO promoter placed upstream of *TOR1*.**

The first allele of *TOR1* is deleted using the *SAT1* cassette. The tetracycline regulatable tetO promoter is amplifed from the pCAU1 plasmid (Nakayama *et al.* 2000) with flanking regions homologous to sequences upstream of *TOR1*. Transformation with the tetracycline promoter is then performed on the heterozygous *tor1/TOR1* mutant placing it upstream of the intact *TOR1* allele. In the absence of doxycycline, the tetR protein activates *TOR1* transcription. In the presence of doxycycline, the tetR activator protein binds to doxycycline, preventing binding to the tetO sequence preventing *TOR1* expression.

4.2 Materials and Methods

4.2.1 Cassette Generation and Gene Knockouts

In order to knock out *RHB1* and *GTR1*, a *SAT1* cassette was generated with flanking regions homologous to either *RHB1* or *GTR1*. Primers (Table S2) targeting the *SAT1* cassette with the flanking regions homologous to either *RHB1* or *GTR1* were used in a 2 step PCR reaction. The first PCR step consisted of 7 cycles containing a denaturation step at 95 °C for 30 s, an annealing step of 58 °C for 30 s and elongation step of of 72 °C for 4 min. The second PCR step consisted of 28 cycles containing a denaturation step at 95 °C for 30 s and an elongation step at 66 °C for 5 min. Once completed, the reaction was held at 4 °C. PCR products were run on a 1 % agarose gel, cleaned as stated in section 2.6.2 and transformations were performed according to section 2.7

4.2.2 *SAT1* Cassette Removal

In order to knock out the second allele of either *RHB1* or *GTR1*, the first copy of the *SAT1* cassette was removed from the heterozygous knockouts. Cells were grown overnigh in 4% YPM at 37 °C with shaking at 200 rpm. Following overnight growth, 4 µl was removed and placed into fresh 4% YPM and incubated overnight at 37 °C with shaking at 200 rpm. Following overnight incubation, cells were centrifuged at 15,000 rpm and washed in 1X PBS. These cells were counted and a 1 ml sample containing 2 x 10^6 cells was prepared. A serial dilution of this was carried out from 2 x 10^6 cells to 2 x 10^3cells. From the 2 x 10^3suspension, 100 µl of each strain was plated onto YEPD plates containing 100 µg/ml or 200 µg/ml nourseothricin (NAT100 or NAT200) and incubated overnight at 37 °C. Following overnight incubation, plates were screened for sensitive revertants, i.e. derivatives that had lost the SAT1 cassette due to homologous recombination of the FRT regcognision sequence. Colonies that were susceptible to nourseothricin were smaller in size compared to those that were still resistant and containing the *SAT1* cassette. To confirm this phenotype, small colonies were picked

and subcultured onto YEPD containing NAT200 and NAT-free YEPD and incubated overnight at 37 °C. Mutants that failed to form colonies on the NAT200 plates were characterised as NAT-sensitive and were subcultured from the YEPD plates and DNA extractions performed. A PCR targeting flanking regions of the gene of interest was carried out. The PCR conditions consisted of an initial denaturation step at 95 °C for 1 min. Following this, a 35 cycle containing a denaturation step at 95 °C for 30 s, an annealing step at 58 °C for 2 min and an elongation step at 72 °C for 30 sec was carried out. A final elongation step at 72 °C for 8 min was also added and the reaction stored at 4 °C. PCR products were run on a 1 % agarose gel stained with gel-red (1/10,000).

4.2.3 Reintroduction of *GTR1* to the Δ*gtr1* Mutant Background

4.2.3.1 PCR amplification of *GTR1* Gene for Reintegration

In order to confirm the phenotype associated with deleting *GTR1*, a single copy of the gene was reintroduced to the mutant strain. In order to reintroduce *GTR1*, PCR primers (Table S2) targeting the gene were used to amplify *GTR1* from WT SC5314. The PCR consisted of an initial denaturation step at 95 °C for 20 s. Following this, a 30 cycle PCR consisting of a denaturation step at 95 °C for 30 s, an annealing step at 58°C for 30 s and elongation step at 72 °C for 150 s was performed and a final elongation step at 72 °C for 10 min. was carried out. Upon completion, the reaction was held at 4 °C. The PCR product was electrophoresed on a 1 % agarose gel to confirm the expected band size of approximately 2 kb. Once confirmed, the product was cleaned using the GenElute PCR Clean-Up Kit (section 2.6.2)

4.2.3.2 Ligation of *GTR1* to pCDRI Plasmid and *E. coli* transformation

In order to reintroduce the single copy of *GTR1*, the product amplified in section 4.2.3.1 was cloned into the pCDRI-MPA plasmid. Purified pCDRI plasmid DNA and *GTR1* were digested with the restriction endonuclease enzymes *Xho*I and *Hind*III at 37 °C in a shaking water bath for 4 h. Digests were carried out in 100 µl volumes consisting of 80

μl of sterile ultra pure H_2O, 5 μl of template DNA (1 μg/μl), 1 μl bovine serum albumen (10 μg/μl) 2 μl of each restriction enzyme (10 U/μl) and 10X Promega Buffer B (6 mM Tris-HCl pH 7.8, 6 mM $MgCl_2$, 50 mM NaCl and 1 mM DTT). The digested DNA was purified using the GenElute PCR Clean-Up kit (section 2.6.2). Digested fragments were loaded on a 1.0 % agarose gel stained with gel-red (1/10,000) to visualise products. Purification of products was carried out using the GenElute PCR Clean-Up Kit (section 2.6.2). The ligation of the *GTR1* gene fragment to pCDRI plasmid was carried out using T4 DNA ligase (Promega) and reactions were set up containing sterile ultra pure H_2O, Promega 10X Ligase Buffer (300 mM Tris-HCl pH 7.8, 100 mM $MgCl_2$, 100 mM DTT and 10 mM ATP), the vector and insert to be ligated and T4 DNA ligase in a final reaction volume of 30 μl. Molar ratios of vector to insert were used (1:1, 1:3 and 1:0) and reactions incubated at 16 °C for 2 h followed by an overnight incubation at 4 °C.

Transformation of ligated reactions were performed using *E. coli* XL10 High Efficiency Electrocompetent cells. Once cells were thawed on ice, 200 μl was added to each ligation reaction and samples were left on ice for 5 min. Ligation reaction/*E. coli* mixes were heat shocked for exactly 2 min at 42 °C. Following heat shock, samples were placed on ice for 2 min., followed by the addition of 1 ml of pre-warmed SOC medium (2 % tryptone, 5 % yeast extract, 10 mM sodium chloride, 2.5 mM potassium chloride, 10 mM magnesium chloride, 10 mM magnesium sulphate and 20 mM glucose). Samples were left to incubate at 37 °C for 1.5 h in a shaking water bath. Following incubation, antibiotic selection was used to identify the uptake of plasmid containing the ampicillin resistance gene. A 100 μl suspension of cells were plated onto pre-warmed L_{amp100} agar plates (Luria-Bertani agar containing 100 μl/ml ampicillin) and incubated overnight at 37 °C.

4.2.3.3 Linearising pCDRI/*GTR1* plasmid and Transformation of Δ*gtr1*

Following overnight incubation on L_{amp100}agar plates at 37 °C, transformants were sub-cultured onto fresh L_{amp100}agar plates. Plasmid DNA was extracted from each trans-

formant and digested with *Nco*I as described above. Following digestion, the linearised plasmid was electrophoresed on a 1 % agarose gel stained with gel-red (1/10,000) to confirm a product size of approximately 6 kb. Once confirmed, the product was cleaned using the GenElute PCR Clean-Up Kit (section 2.6.2) and transformed into Δ*gtr1* as described in section 2.7. Transfromants were selected on YEPD containing X /ml of mycophenolic acid.

4.3 Results

4.3.1 Generation of Δ*rhb*, Δ*gtr* & tetO-*TOR1*/*tor1* Mutants

Transformation experiments were also performed on WT SC5314 in order to generate a Δ*rhb1* and Δ*gtr1* knockout mutant. Additionally, transformation experiments were performed to delete one copy of *TOR1*. Figure 4.2 illustrates gel electrophoresis confirming the deletion of both copies of the *GTR1* gene. Several attempts were made to delete *RHB1* yielding negative results. PCR reactions to confirm the genotypes of transformants yielded multiple bands. Multiple primer sets were used along with temperature curves to help minimise the spurious bands. However, all attempts failed to yield definitive results. Due to the failure to generate a null Δ*rhb1* mutant and a Tor1 regulatable strain in the current study, we obtained a gift of a published Δ*rhb1* mutant from Prof. Lan (University of Taiwan) and identified a collaborator in Harvard School of Medicine (Prof, Julia Koehler) who agreed to share unpublished strains including a tetO-*TOR1*/*tor1* strain. Julia Koehler's group provided a tetO-*TOR1*/*tor1* strain (JKC1549) with a full length copy of *TOR1* under the control of the tetO promoter and a second strain with a truncated allele of *TOR1* (JKC1441) under the control of the same promoter. This latter strain, JKC1441, is missing approximately the first 380 amino acids in the heat repeats of the N-terminal region. The N-terminal region consists of 20 tandemly repeated HEAT motifs (Fig 1.1) that comprise of 40-50 amino acids that are thought to act as a protein-protein interaction surface[76]. Therefore, this N

terminal truncation leaves the kinase domain unaffected while allowing the functions of the N-terminal to be assessed.

4.3.1.1 Phospho-RPS6 (P-S6) Assay

RPS6 is a ribosomal protein, a component of the 40S ribosomal subunit involved in regulating translation and is a target of the Tor1 kinase activity. A Phospho-RPS6 (P-S6) assay, developed and carried out in the Koehler Lab (Harvard, Boston) was used to investigate the phosphorylation of *RPS6* in the Δ*gtr1* mutant. In this assay, wild-type, homozygous Δ*gtr1*, heterozygous Δ*gtr1* and overexpressed P_{ENO}*GTR1* were grown in a nutrient poor environment (YNB [without amino and ammonium sulfate] and 1 % glucose) for 4 h to starve them. Following starvation, either water, 10 mM glutamine or 10 mM proline was added to the medium (Fig. 4.3). Following the addition of water, no P-S6 was seen. However, after the addition of 10 mM glutamine or 10 mM proline, distinct bands were observed. WT SC5314 and heterozygous Δ*gtr1* showed bands of similar intensity while homozygous Δ*gtr1* exhibited a much weaker band. Furthermore, P_{ENO}*GTR1* showed the most intense band of all four strains. As a control for the Western blot, tubulin was used. This is expressed at high-levels and is also expressed at consistent levels thus ensuring equal loading of the gel between strains.

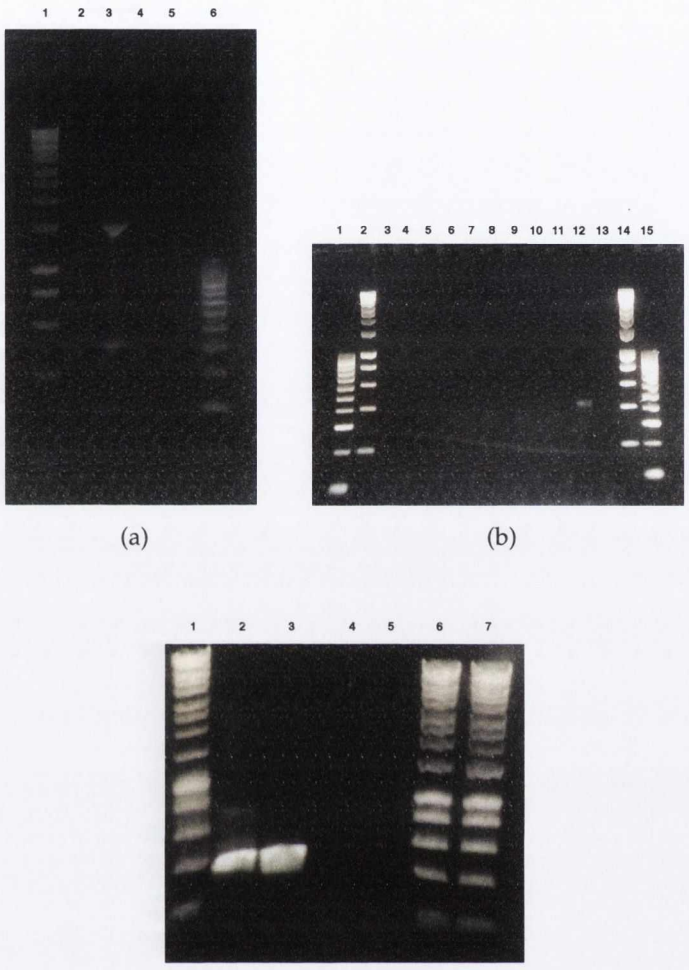

Figure 4.2: **Confirmation of the genotypes of *GTR1* mutants of WT SC5314 by gel electrophoresis of PCR amplimers.**

(a) Confirmation of a heterozygous *GTR1/gtr1* using *GTR1* flanking primers *GTR/SAT* Flip F4 and *GTR* Flank R1. From left to right, lane 1 Hyperladder™ 1kb, lane 3 *GTR1/gtr1* mutant, lane 5 negative control and lane 6 Hyperladder™ 100 bp. (b) Confirmation of homozygous *gtr1/gtr1* (Δ*gtr1*) mutant using internal primers *GTR*inF3 and *GTR*inR4. From left to right, lane 1 Hyperladder™ 100bp, lane 2 Hyperladder™ 1kb, lane 3-11 positive transformants, lane 12 positive control for internal *GTR1* segment of 426bp, lane 13 negative control, lane 14 Hyperladder™ 1kb and lane 15 Hyperladder™ 100bp. (c) Re-insertion of *GTR1* into the Δ*gtr1* mutant. From left to right, lane 1 Hyperladder™ 1kb, lane 2 Δ*gtr1*::*GTR1*, lane 3 WT SC5314, lane 4 Δ*gtr1*, lane 5 negative control and lane 6 and 7 Hyperladder™ 1kb.

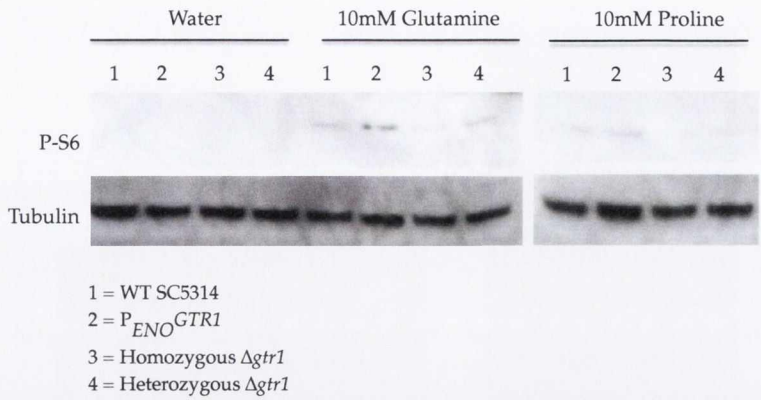

Figure 4.3: **Phospho-S6 assay.**

Nutrient deprived cells had water, 10 mM glutamine or 10 mM proline re-introduced after 4 h of starvation (YNB [without amino and ammonium sulfate] and 1 % glucose). Under water conditions, no P-S6 protein was seen. When 10 mM glutamine was added, WT SC5314 and heterozygous Δ*gtr1* showed equal levels of P-S6 while homozygous Δ*gtr1* showed none. P$_{ENO}$*GTR1* showed the greatest level of P-S6.

4.3.2 Determination of Cellular Growth Rate of Δ*rhb1*, Δ*gtr1* & tetO-*TOR1/tor1* Compared to WT SC5314

4.3.2.1 Cellular Growth Rate of Δ*rhb1* & Δ*gtr1*

We compared the growth rates of homozygous mutant strains with WT SC5314. Growth curve assays were set up in multiple nitrogen sources (YNB supplemented with either 100 mM urea or 100 mM ammonium sulfate $[NH_4]_2SO_4$) and controlled growth experiments were performed in YEPD nutrient rich broth.

In YEPD and $(NH_4)_2SO_4$ all growth rates appeared similar to WT SC5314 (Fig. 4.4). Additionally, in urea, the rate of growth of Δ*gtr1* was similar to WT SC5341. However, in the presence of urea, the growth rate of Δ*rhb1* was marginally reduced at the 8 h and 10 h time point compared with WT SC5314.

4.3.2.2 Cellular Growth Rate of tetO-*TOR1/tor1*

The growth of JKC1549 and JKC1441 were compared to JKC1316 and a heterozygous *TOR1* mutant (JKC1347) in nitrogen rich (YEPD) and nitrogen limiting medium. Strains were grown in YEPD and YNB with either 100 mM ammonium sulfate $(NH_4)_2SO_4$ or 100 mM urea (Fig. 4.5a, 4.5b & 4.5c). In the absence of doxycycline the growth rate of the tetO-Δ*NTOR1* strain was reduced compared with JKC1361, the heterozygous *tor1/TOR1* mutant and the tetO-*TOR1/tor1* strains. In both $(NH_4)_2SO_4$ and urea, JKC1347 and JKC1549 also exhibited reduced growth relative to wild-type. However, growth of JKC1441was significantly lower than all other strains investigated.

Next, growth was assessed in the presence of doxycycline in order to determine the optimal amounts to inhibit growth. Upon the addition of 2.5 μg/ml doxycycline, the growth of tetO-Δ*NTOR1* strain JKC1441 was inhibited (Fig. 4.6a). However, in contrast the growth of the tetO-*TOR1/tor1* strain JKC1549 was not significantly inhibited in the presence of 10, 20 or 40 mg/ml doxycycline in liquid medium (Fig 4.6b). In order to reduce the rate of growth in the tetO-*TOR1/tor1* strain with the addition of doxycycline,

overnight cultures were grown in the presence of low amounts of doxycycline (10 or 100 ng/ml) to limit expression of Tor1 and these were used to inoculate cultures for growth curve analysis in YEPD containing 10 ng/ml doxycycline as well as 20 or 30 mg/ml doxycycline. Pre-incubation in 10 or 100 ng/ml doxycycline resulted in a decrease in growth in both the 20 or 30 mg/ml doxycycline broths (Fig 4.6c). Pre-incubation in 100 ng/ml resulted in a greater decrease in growth than pre-incubation in 10 ng/ml doxycycline.

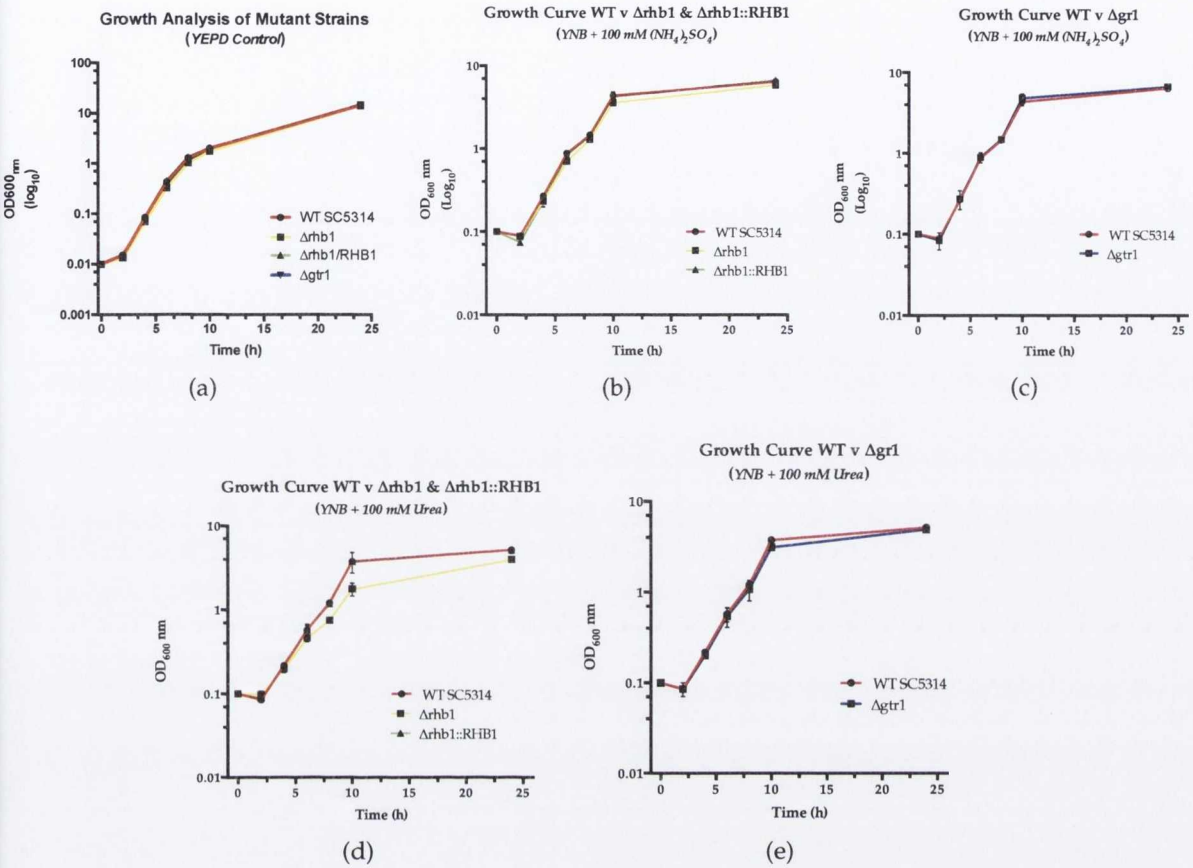

Figure 4.4: **Growth curve of mutant strains compared with WT SC5314 in $(NH_4)_2SO_4$ and Urea.**

All strains were grown in YEPD as a control and subsequently tested in nitrogen poor medium to determine the rate of growth. All growth rates appear similar to WT SC5314 in YEPD (a) and $(NH_4)_2SO_4$ (b). In urea (c), Δ*rhb1* had a marginally slower rate of growth compared with WT SC5314.

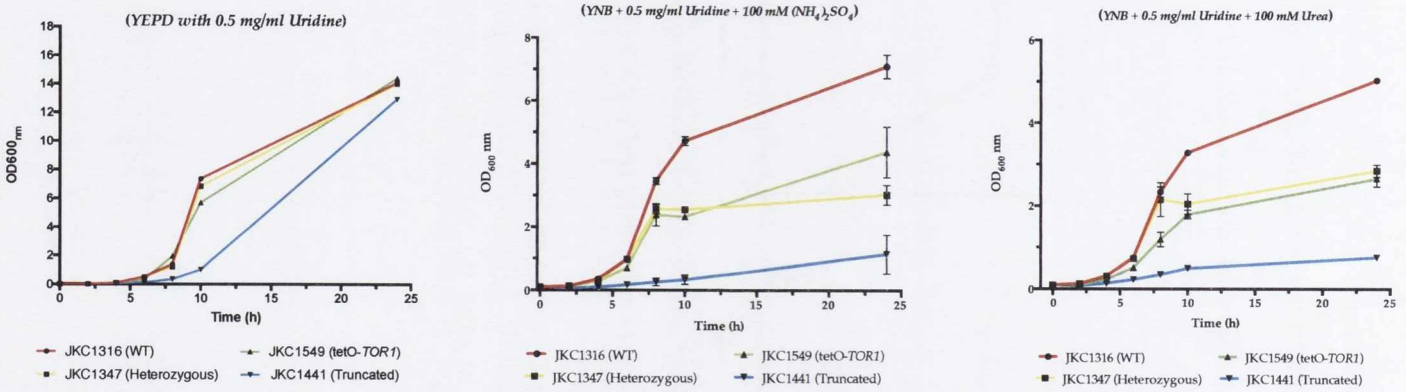

Figure 4.5: **Growth of doxycycline-regulatable strains in YEPD and a limiting medium.**

Figure (a) shows growth of both the tetO-*TOR1*/*tor1* and tetO-ΔN*TOR1* strains and the WT JKC1316 and tor1/TOR1 JKC1347 in YEPD without the addition of doxycycline. (b) show growth in 100 mM $(NH_4)_2SO_4$ and while (c) shows growth in 100 mM urea.

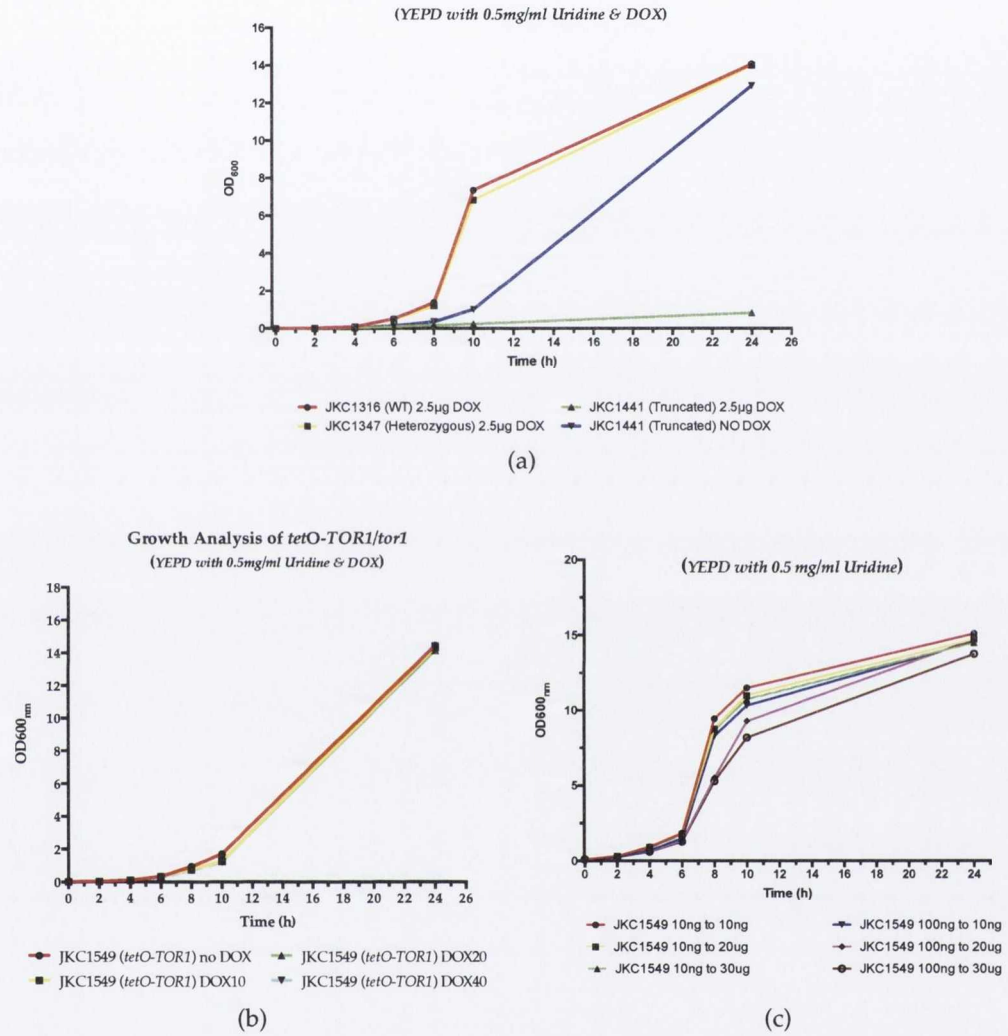

Figure 4.6: **Growth of doxycycline-regulatable strains in YEPD in the presence of doxycycline.**

Figure (a) illustrates the tetO-Δ*NTOR1* strain grown in the presence of 2.5 µg/ml doxycycline. (b) The tetO-*TOR1/tor1* strain grown in the presence of 10, 20 and 40 µg/ml doxycycline. Neither concentration was capable of decreasing growth of the strain. (c) The tetO-*TOR1/tor1* strain was pre-incubated overnight in the presence of 10 or 100 ng/ml doxycycline prior to growth in 10, 20 and 30 µg/ml doxycycline.

4.3.3 Hyphal Formation Assays of Δ*rhb1*, Δ*gtr1* & tetO-*TOR1*/*tor1* Compared to WT SC5314

4.3.3.1 Formation of Hyphae by Δ*rhb1* & Δ*gtr1* on Solid Medium

In order to examine nitrogen starvation-induced filamentous growth of WT SC5314 compared with the mutant strains, spot plate assays were set up. YNB agar without amino acids or $(NH_4)_2SO_4$, but supplemented with a limiting amount of $(NH_4)_2SO_4$ (100 µM) was the medium used. We hypothesised, that the mutant strains would exhibit more, if not equal rates of filamentation as the WT SC5314. Figure 4.7 shows the filamentous growth of each strain. All strains showed similar rates of filamentation compared with WT SC5314.

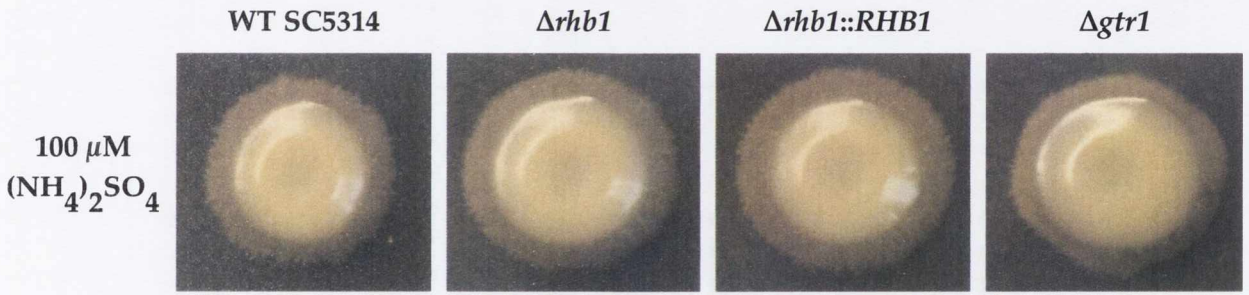

Figure 4.7: **Hyphal formation on solid medium spot plate assay.**

Hyphal fringe formation in WT SC5314 compared with Δ*rhb1* and Δ*gtr1* mutant strains on YNB agar plates supplemented with 100 μM $(NH_4)_2SO_4$. Plates were left at 37°C for 5 days. After incubation, equal rates of filamentation was observed on all strains.

4.3.3.2 Qualitative & Semi-Quantitative analysis of Aggregation of Δ*rhb1* & Δ*gtr1* Strains in a Filament Inducing Medium

Previously we developed an assay to allow for the filtration of yeast cells from hyphal cells in order to determine the level of aggregation in a semi-quantitative analysis (Section 3.3.4.2). Therefore this assay was performed on the mutant strains in YEPD with 10% v/v serum.

Upon qualitative inspection, all strains were capable of forming true hyphae and aggregating at 2 h (Fig 4.8). At 4 h, WT SC5314 and the Δ*rhb1*::*RHB1* complemented strain demonstrated a decreased aggregated mass when compared with Δ*rhb1* and Δ*gtr1*. By 6 h, WT SC5314 shed free yeast cells as too did the Δ*rhb1*::*RHB1* complemented strain. Cultures of the Δ*rhb1* and Δ*gtr1* strains showed the presence of fewer free yeast cells and maintained tight aggregates in culture. By 8 h, WT SC5314 and the Δ*rhb1*::*RHB1* complemented strain appear to have a greater number of free yeast cells compared with the Δ*rhb1* and Δ*gtr1* strain.

In the semi-quantitative analysis (Fig 4.9), Δ*gtr1* had a significant lower count (4.7 fold change) of free yeast cells at 2 h. By 4 h, a significance (1.9-fold and 17-fold respectively) was noted in the number of free yeast cells in the Δ*rhb1* and Δ*gtr1* strains compared with WT SC5314.

4.3.3.3 Qualitative & Semi-Quantitative analysis of Aggregation of tetO-*TOR1*/tor1 in a Filament Inducing Medium

Using our previously developed assay to allow for filtration of yeast cells from hyphal aggregates, we performed the assay on our tetO-*TOR1/tor1* strains. This was carried out in YEPD supplemented with 10 % (v/v) serum in the presence of 30 μg of doxycycline. At 4 h, 6 h and 8 h post inoculation, a significantly reduced number of free yeast cells were observed in cultures of JKC1441 compared with WT JKC1316 was shown (Fig 4.11) correlating with the qualitative inspection in figure 4.10. Additionally, a significant reduction was shown in the number of free yeast cells in JKC1549 incubated in

the presence of 30 μg/ml doxycycline compared with WT JKC1316 at 8 h. Furthermore, both the tetO-*TOR1*/*tor1* JKC1549 and tetO-ΔN*TOR1* JKC1441 extended longer hyphae from aggregates compared with WT JKC1316 and *tor1*/*TOR1* JKC1347.

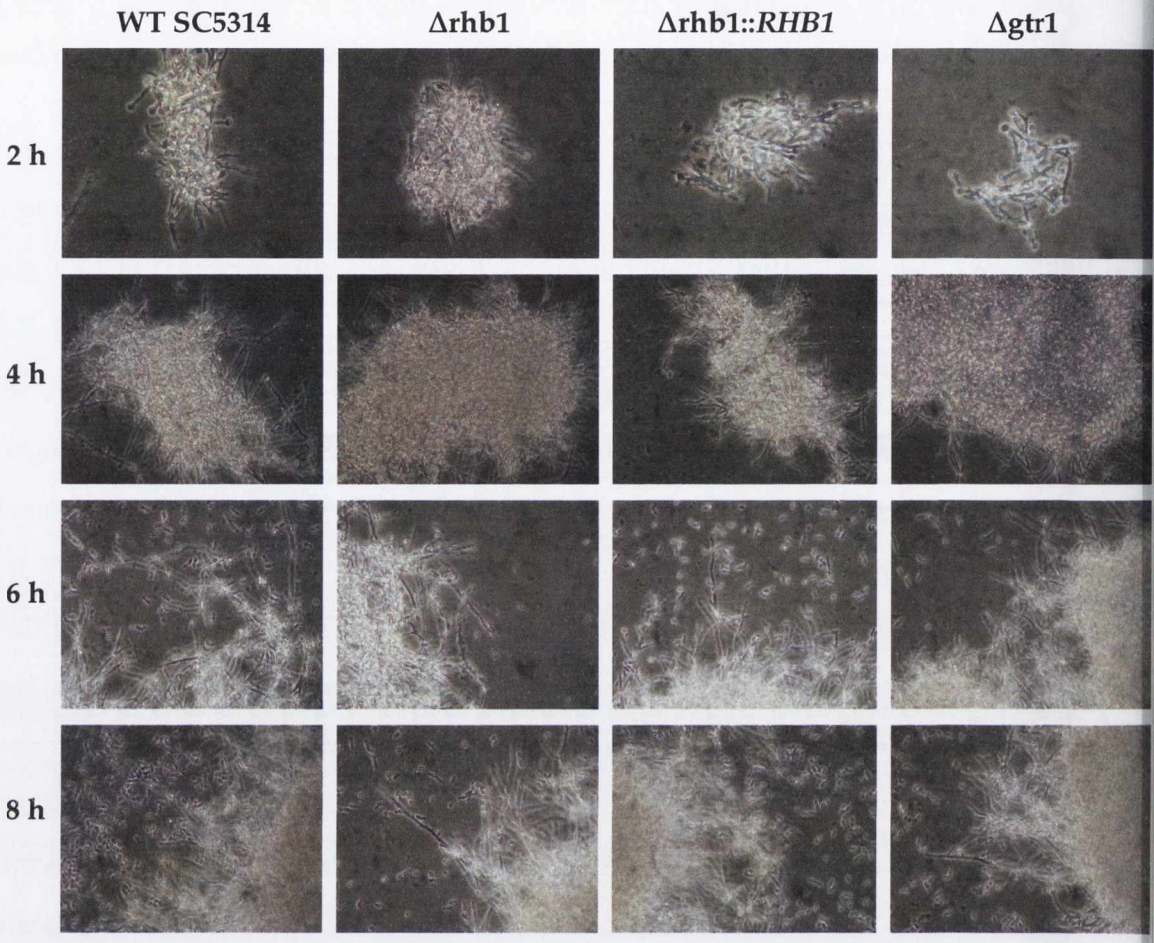

Figure 4.8: **Qualitative image depicting the aggregation of WT SC5314 compared with mutant strains in YEPD and 10% (v/v) serum.**

At 2 h, Δ*rhb1* and Δ*gtr1* are capable of forming true hyphae and are similar in appearance to WT SC5314 and Δ*rhb1*::*RHB1*. At 4 h, Δ*rhb1* and Δ*gtr1* have a higher degree of aggregation compared with WT SC5314 and Δ*rhb1*::*RHB1*. By 6 and 8 h, WT SC5314 and Δ*rhb1*::*RHB1* appear less aggregated than Δ*rhb1* and Δ*gtr1* with higher free yeast cells seen in the wild-type and recombinant.

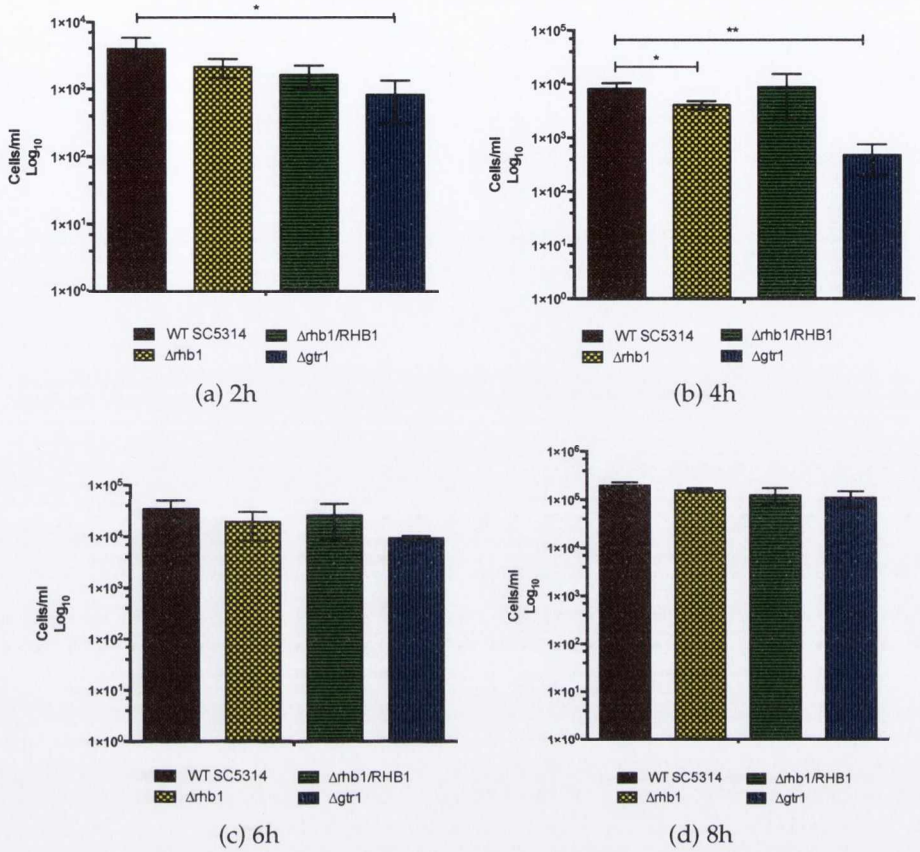

Figure 4.9: **Semi-quantitative analysis of the aggregation of WT SC5314 compared to mutant strains in YEPD and 10 % (v/v) serum.**

Semi-quantitative anlaysis of WT SC5314 and mutant strains at 2 (a), 4 (b), 6 (c) and 8 (d) h. At 2 and 4 h, mutant strains had a statistically lower number of free yeast cells compared with WT SC5314 and Δ*rhb1*::*RHB1*.

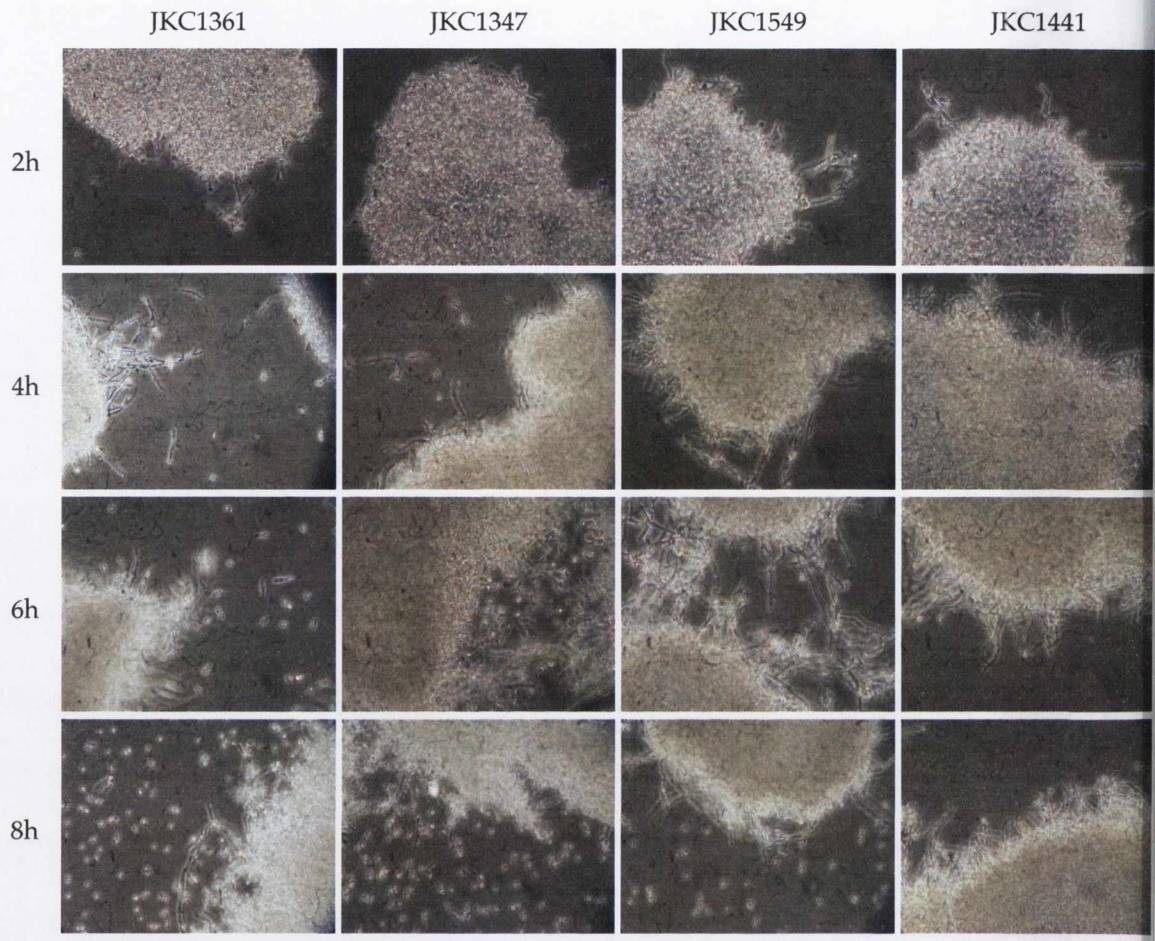

Figure 4.10: **Qualitative image depicting the aggregation of WT JKC1361 & Heterozygous JKC1347 compared with doxycycline regulatable strains in YEPD and 10% (v/v) serum in the presence of doxycycline.**

At 2, 4, 6 and 8 h, all strains were capable of aggregating. By 4 and 6 h, JKC1361 and JKC1347 had free yeast cells in the medium while JKC1549 and JKC1441 did not. By 8 h, JKC1361 and JKC1347 had a significant number of free yeast cells compared with JKC1549. However, JKC1441 did not have any free yeast cells.

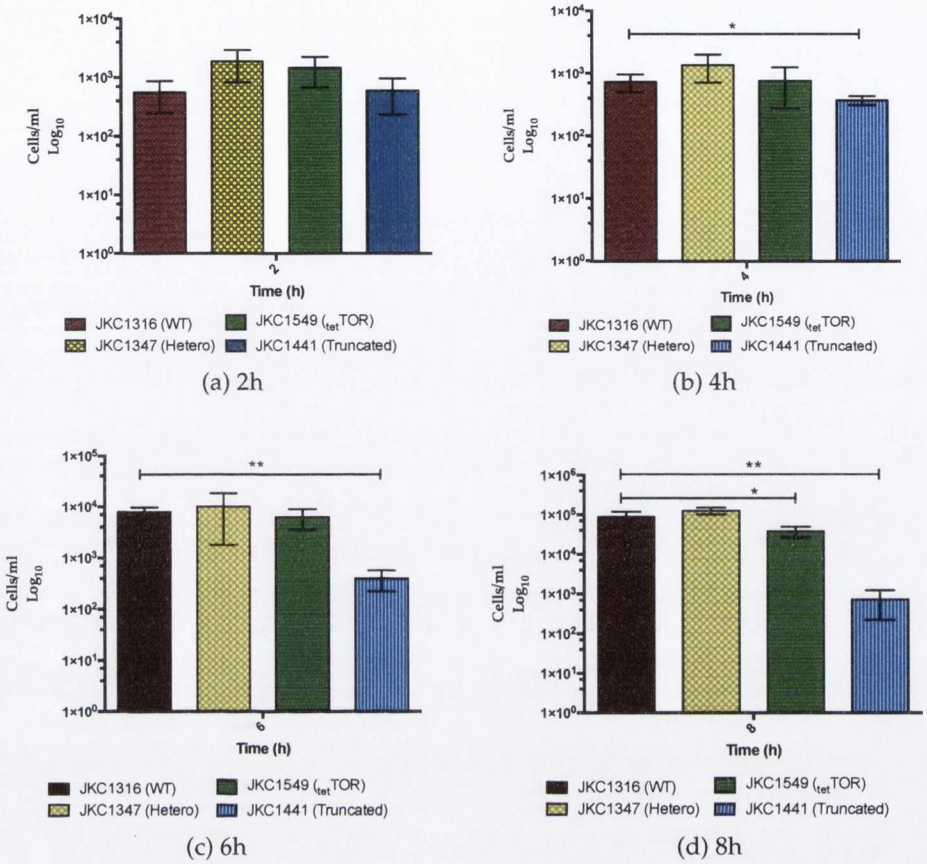

(a) 2h (b) 4h

(c) 6h (d) 8h

Figure 4.11: **Semi-quantitative analysis of the aggregation of WT JKC1361 & Heterozygous JKC1347 compared with** doxycycline **regulatable strains in YEPD and 10% v/v serum in the presence of doxycycline.**

Figure (a) represents 2 h, (b) 4 h, (c) 6 h and (d) 8 h. doxycycline inhibition of JKC1441 resulted in fewer free yeast cells and lower cell count compared with WT JKC1316 at 4, 6 and 8 h. Additionally, JKC1549 had a lower cell count compared to WT JKC1316 at 8 h.

4.3.4 Flocculation of Δ*rhb1*, Δ*gtr1* & tetO-*TOR1*/*tor1* Compared to WT SC5314

4.3.4.1 Flocculation of Δ*rhb1* & Δ*gtr1*

Following on from the semi-quantitative assay of aggregation in YEPD containing 10% (section 4.3.3.2), flocculation of the mutant strains was carried out in liquid Spider medium. Figure 4.12a shows that Δ*gtr1* flocculated compared with WT SC5314 and the Δ*rhb1* strain. WT SC5314, Δ*rhb1* and the Δ*rhb1*::*RHB1* complemented strain (~ 20 min). Following flocculation of each strain, 10 µl of each flocculate was visulised under the microscope in order to assess the appearance of the cells (Fig. 4.12b). WT SC5314, Δ*rhb1* and Δ*rhb1*::*RHB1* produced short true hyphae with very little aggregation compared to the Δ*gtr1* strain which had elongated hyphal cells and large aggregates. The Δ*rhb1* mutant produced long hyphal filaments that clustered together.

4.3.4.2 Flocculation of tetO-*TOR1*/*tor1*

Analysis of hyphal aggregation by visual inspection and using the semi-quantitative assay demonstrated that the truncated tetO-*TOR1*/*tor1* strain JKC1441 exhibited reduced cell counts and greater aggregation compared to the WT JKC1361 and heterozygous mutants JKC1347 (*tor1*/*TOR1*) and JKC1549 (tetO-*TOR1*/*tor1*). Flocculation of these strains were compared in liquid Spider medium with and without 30 µg/ml of doxycycline. Figure 4.13a shows after a 2 h incubation period in the absence of doxycycline, the truncated tetO-ΔN*TOR1*/*tor1* strain JKC1441 exhibited greater flocculation (~ 10 min.) compared to WT JKC1361 and the heterozygous JKC1347 and JKC1549 (~ 20 min). However, in the presence of 30 µg/ml of doxycycline (Fig. 4.12b), the tetO-*TOR1*/*tor1* strain JKC1549 exhibited greater flocculation than the WT JKC1361 and the heterozygous JKC1347. However, the phenotype was not as strong as that observed in the truncated tetO-ΔN*TOR1*/*tor1* strain JKC1441.

Following visual inspection of the flocculation phenotype, 10 µl of the flocculate of was

removed and viewed under the microscope in order to assess the appearance of the cells. Figure 4.14a represents the cells grown in Spider for 2 h without the addition of doxycycline and figure 4.14b the cells grown in the presence of 30 μg of doxycycline. Whether grown in 30 μg/ml of doxycycline or without, the WT JKC1361 and heterozygous JKC1347 strains appeared similar and were primarily pseudohyphal. However, the tetO-*TOR1*/*tor1* strain JKC1549, while similar in aggregation to the WT JKC1361 and heterozygous *TOR1*/*tor1* JKC1347 strains appeared hyphal. The truncated tetO-Δ*NTOR1*/*tor1* strain JKC1441 had longer hyphae, indicative of a biofilm.

Similarly, when grown in the presence of 30 μg/ml of doxycycline, the WT JKC1361 and heterozygous *tor1*/*TOR1* JKC1347 strains appeared similar to their non-DOX counterparts. However, in the presence of 30 μg/ml of doxycycline, the tetO-*TOR1*/*tor1* strain JKC15491 had a higher propensity to aggregate compared to growth in non-doxycycline medium. The cells appeared pseudohyphal compared to their non-DOX counterparts. In the presence of 30 μg/ml of doxycycline, the truncated tetO-Δ*NTOR1*/*tor1* strain JKC1441 continued to aggregate to the same levels seen in non-DOX samples and microscopy images revealed similar levels of extended hyphal growth.

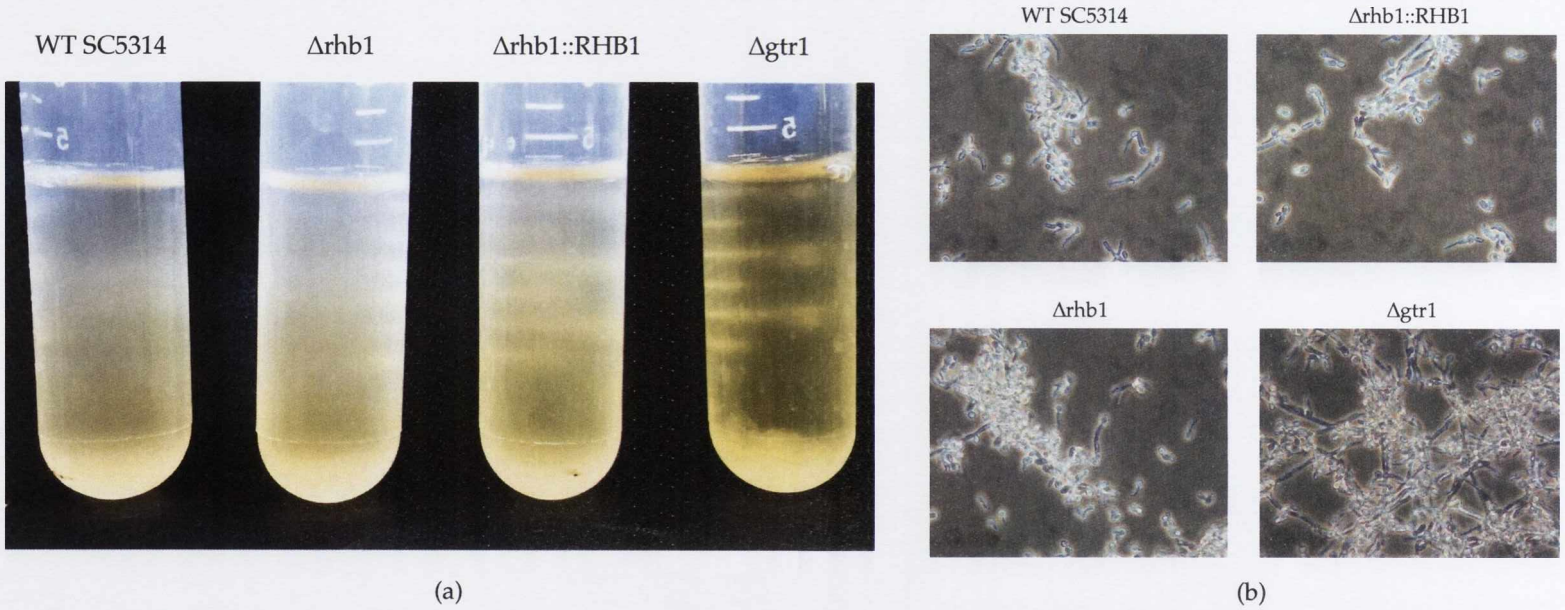

Figure 4.12: **Flocculation (a) and microscopic appearance (b) of WT SC5314 compared with mutant strains in Spider medium.** Left to right, WT SC5314, Δ*rhb1*, Δ*rhb1*::*RHB1* and Δ*gtr1*. All strains with the exception of Δ*gtr1* did not flocculate.

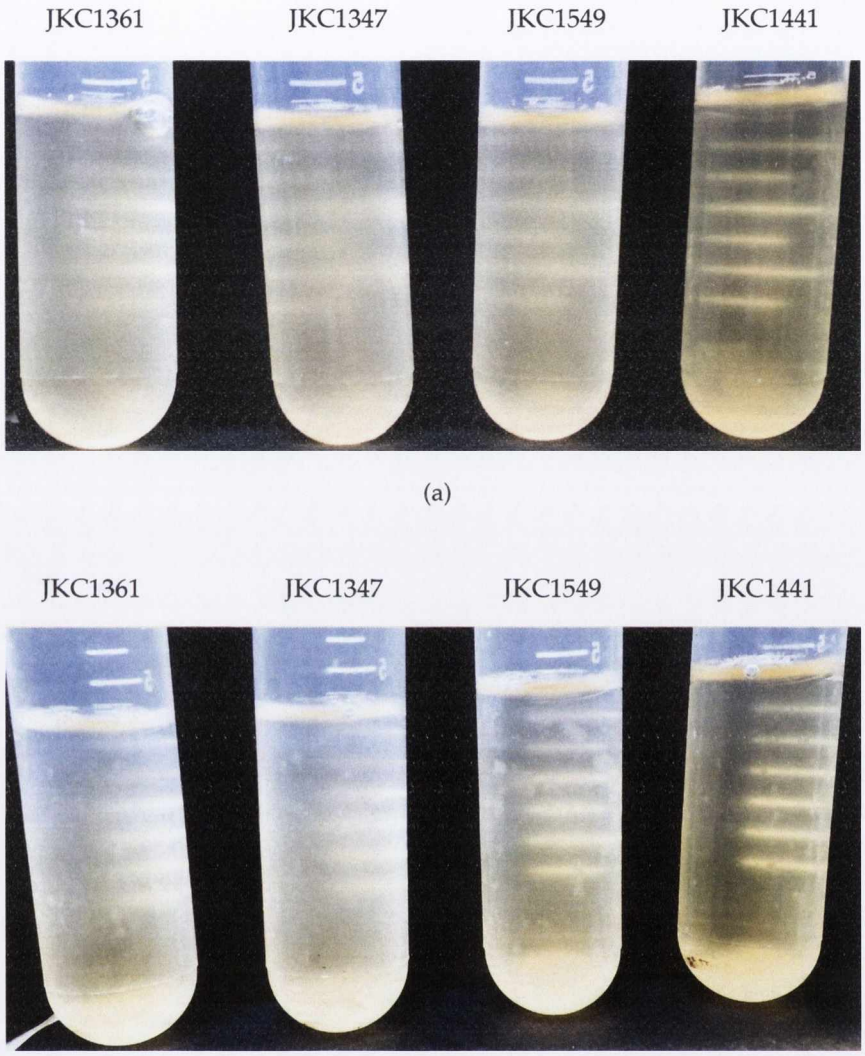

Figure 4.13: **Flocculation of WT JKC1361 and JKC1347 (*TOR1/tor1*) compared with tetO-*TOR1/tor1* strains in Spider medium.**

Panel (a) shows flocculation in the absence of doxycycline and (b) in the presence of 30 μg/ml doxycycline. Left to right, WT JKC1361, heterozygous JKC1347, tetO-*TOR1* JKC1549 and truncated tetO-*TOR1* JKC1441.

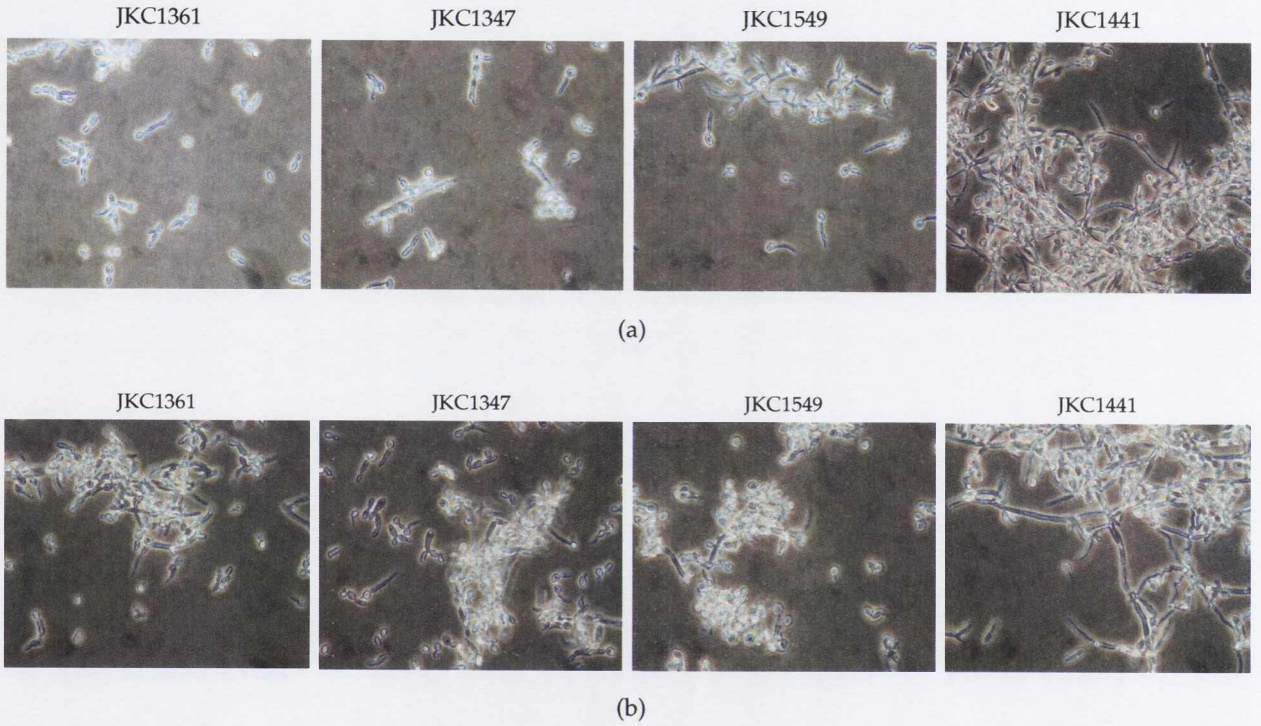

Figure 4.14: **Microscopic images of flocculate of WT JKC1361 and JKC1347 (*TOR1/tor1*) compared with tetO-*TOR1/tor1* strains.**

Samples were viewed microscopically to assess formation of hyphae in the absence (a) and presence (b) of doxycycline. In the absence and presence of 30 μg/ml doxycycline, JKC1441 qualitatively demonstrated a higher degree of hyphae and aggregation. JKC1361 & JKC1347 appeared pseudohyphal. JKC1549, in the absence of doxycycline formed hyphae while in the presence of doxycycline appeared pseudohyphal, aggregating to a greater extent than when grown in the absence of doxycycline.

4.3.5 Effects of *TOR1* Disruption on Cell Wall Integrity

In order to determine whether the Δ*gtr1* and Δ*rhb1* strains, as well as the tetO-*TOR1* exhibited defects in cell wall integrity, spot plate assays were set up using the cell wall-perturbing compounds Congo Red and Calcofluor White.

4.3.5.1 Disruption of Cell Wall Integrity in Δ*rhb1* & Δ*gtr1* Strains

Both Congo Red and Calcofluor White were added to YEPD agar at concentrations of 100, 200 and 300 μg/ml. A series of dilutions of each strain were prepared and approximately 10^4 to 10^1 cells/ml were spotted onto the surface of the agar plates (Fig. 4.15). A YEPD control agar plate confirmed that all strains could grow at the dilutions tested.

On Congo Red plates, WT SC5314 was capable of growing on all concentrations tested. The Δ*rhb1* strain exhibited reduced growth compared with WT SC5314 and the complemented Δ*rhb1*::*RHB1* strain. However, unlike the Δ*rhb1* strain, the Δ*gtr1* strain was capable of growth on all concentrations of Congo Red. However, the Δ*rhb1* strain did not exhibit any growth at this concentration. Growth was restored in the complemented Δ*rhb1*::*RHB1* strains. However, unlike the Δ*rhb1* strain, the Δ*gtr1* mutant did not exhibit any defect in growth on Calcofluor White.

4.3.5.2 Disruption of Cell Wall Integrity in tetO-*TOR1*/*tor1* Strains

In order to determine whether modulating *TOR1* expression resulted in defects in cell wall integrity, the WT JKC1361, heterozygous *TOR1*/*tor1* strain JKC1347, tetO-*TOR1*/*tor1* strain JKC1549 and truncated tetO-ΔN*TOR1*/*tor1* strain JKC1441 were grown on YEPD agar containing either Congo Red or Calcofluor White in the absence (Fig. 4.16) and presence (Fig. 4.17) of 30 μg/ml of doxycycline. A control YEPD plate confirmed that all strains could grow normally. A second control plate containing 30 μg/ml of doxycycline confirmed doxycycline repression of *TOR1* expression inhibited the growth of the tetO-*TOR1* strain JKC1549 and truncated tetO-ΔN*TOR1* JKC1441.

In the absence of 30 μg/ml doxycycline, and on Congo Red, the WT JKC1361, the heterozygous *tor1/TOR1* strain JKC1347 and the tetO-*TOR1/tor1* strain JKC1549 grew on all concentration of Congo Red tested. However, the truncated tetO-ΔN*TOR1* strain JKC1441 showed considerably decreased growth on 100 μg/ml of Congo Red and growth was arrested on subsequent concentrations. On Calcofluor White, the WT JKC1361 and heterozygous *tor1/TOR1* strain JKC1347 showed equal growth on 50 μg/ml calcofluor white with arrested growth on subsequent concentrations. The tetO-*TOR1/tor1* strain JKC1549 showed less growth compared with both of these on 50 μg/ml and no growth on subsequent concentrations. However, 50 μg/ml Calcofluor White was enough to completely inhibit the growth of the tetO-ΔN*TOR1* strain JKC1441. On agar plates containing Congo Red and Calcofluor White in the presence of 30 μg/ml doxycycline, the homozygous tetO-*TOR1/tor1* strain JKC1549 showed greatly reduced growth, however this was not any greater than the effect of doxycycline alone (Fig. 4.17).

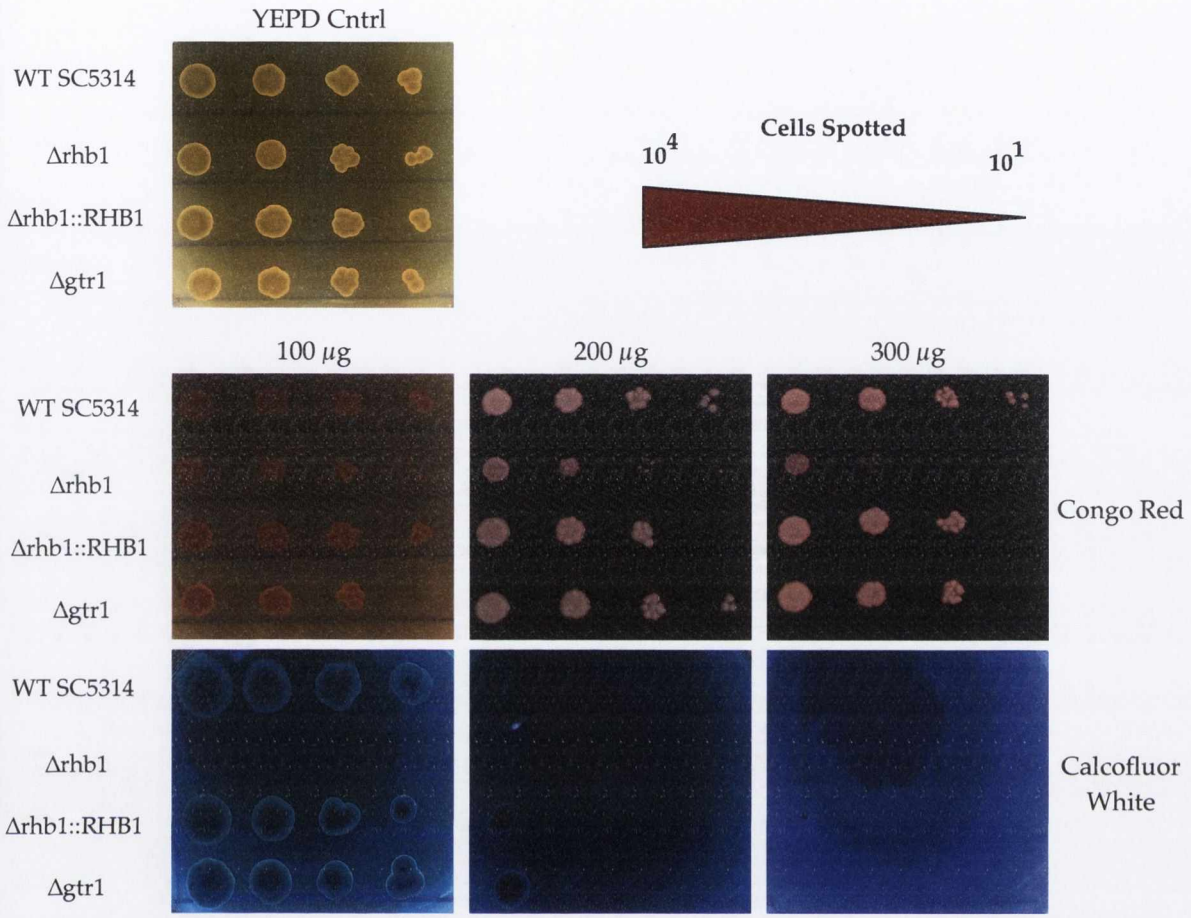

Figure 4.15: **Growth of WT SC5314 and mutants in the presence of Congo Red and Calcofluor White.**

Cells (10^4 to 10^1) were spotted (left to right) on plates containing Congo Red and Calcofluor White at the concentrations shown.

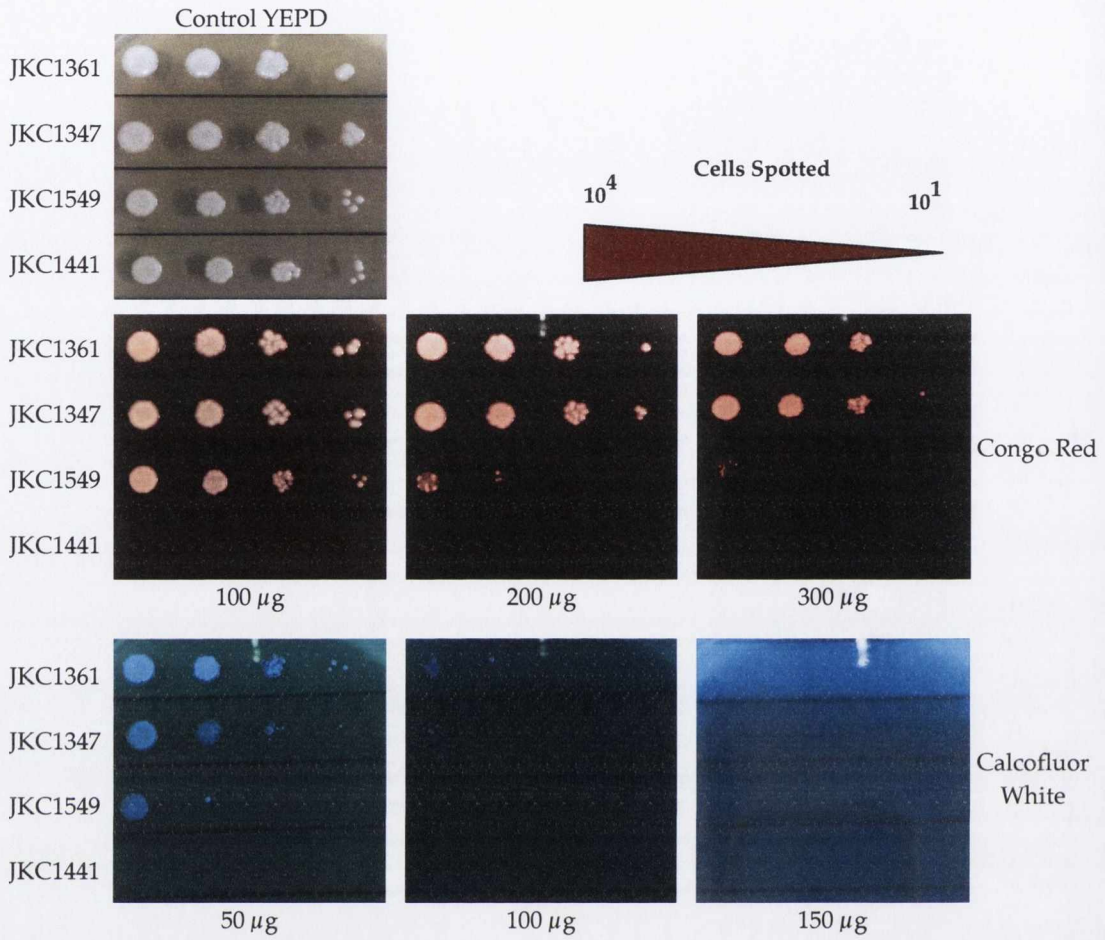

Figure 4.16: **Growth of WT JKC1361, heterozygous *TOR1/tor1* JKC1347, tetO-*TOR1/tor1* JKC1549 and truncated tetO-ΔN*TOR1* JKC1441 in the presence of Congo Red and Calcofluor White and in the absence of 30 μg/ml doxycycline.**

Cells (10^4 to 10^1) were spotted (left to right) on plates containing Congo Red and Calcofluor White at the concentrations shown.

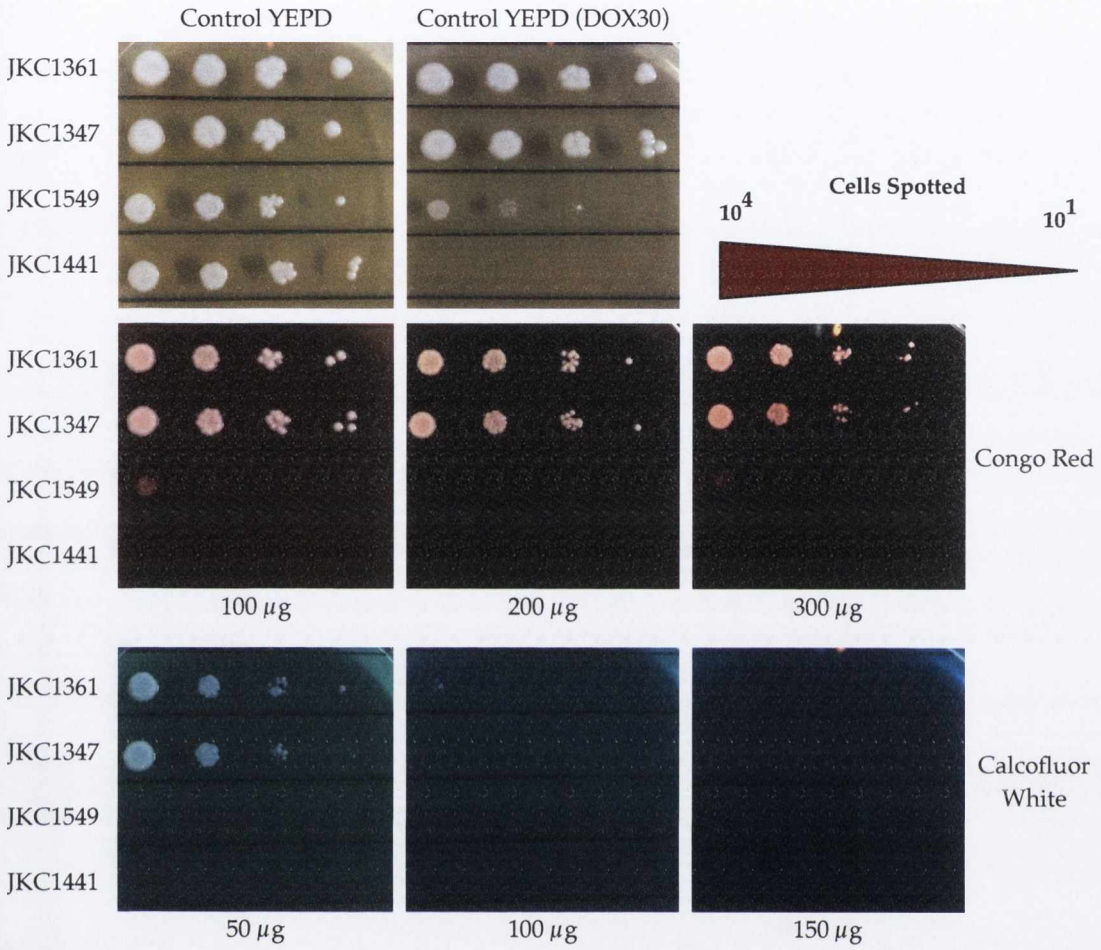

Figure 4.17: **Growth of WT JKC1361, heterozygous *TOR1/tor1* JKC1347, tetO-*TOR1/tor1* JKC1549 and truncated tetO-ΔN*TOR1* JKC1441 in the presence of Congo Red and Calcofluor White and in the presence of 30 μg/ml doxycycline.**

Cells (10^4 to 10^1) were spotted (left to right) on plates containing Congo Red and Calcofluor White at the concentrations shown.

4.3.6 Analysis of the Response to Oxidative Stress in the Tor1 Pathway of Mutant Strains

In order to determine whether the Δ*gtr1* and Δ*rhb1* mutant strains, as well as the tetO-*TOR1* strains were susceptible to oxidative stress, spot plate assays were set up using a range of hydrogen peroxide (H_2O_2) concentrations.

4.3.6.1 Effects of Δ*rhb1* & Δ*gtr1* Disruption on the Response to Oxidative Stress

WT SC5314, Δ*rhb1*, Δ*rhb1*::*RHB1* and Δ*gtr1* strains were plated on YEPD and YEPD containing 4, 6, 8 and 10 mM H_2O_2 (Fig. 4.18). On control YEPD, all strains grew at each dilution spotted (10^4 cells to 10^1 cells). Similar growth was observed on agar containing 4 mM H_2O_2. On 6 mM and 8 mM H_2O_2, all strains grew at each dilution with the exception of Δ*gtr1* which did not grow at the lowest dilution

4.3.6.2 Effects of tetO-*TOR1*/*tor1* Regulatable Strains on the Response to Oxidative Stress

On control YEPD agar, all strains were capable of growth while on control YEPD with the addition of 30 μg/ml of doxycycline, the WT JKC1361 and heterozygous *tor1*/*TOR1* JKC1347 strains were capable of full growth (Fig. 4.19). The homozygous tetO-*TOR1*/*tor1* strain JKC1549 had reduced growth while the truncated tetO-ΔN*TOR1* strain JKC1441 had no growth. On YEPD agar containing either 2, 4 or 6 mM H_2O_2, none of the strains appeared affected by the H_2O_2. With the addition of 30 μg/ml of doxycycline on these plates, growth on all plates was similar in appearance to the control YEPD containing 30 μg/ml of doxycycline. The WT JKC1361 and *tor1*/*TOR1* JKC1347 strains grew at each cell dilution while the homozygous JKC1549 and truncated JKC1441 strains had reduced in growth and no growth respectively.

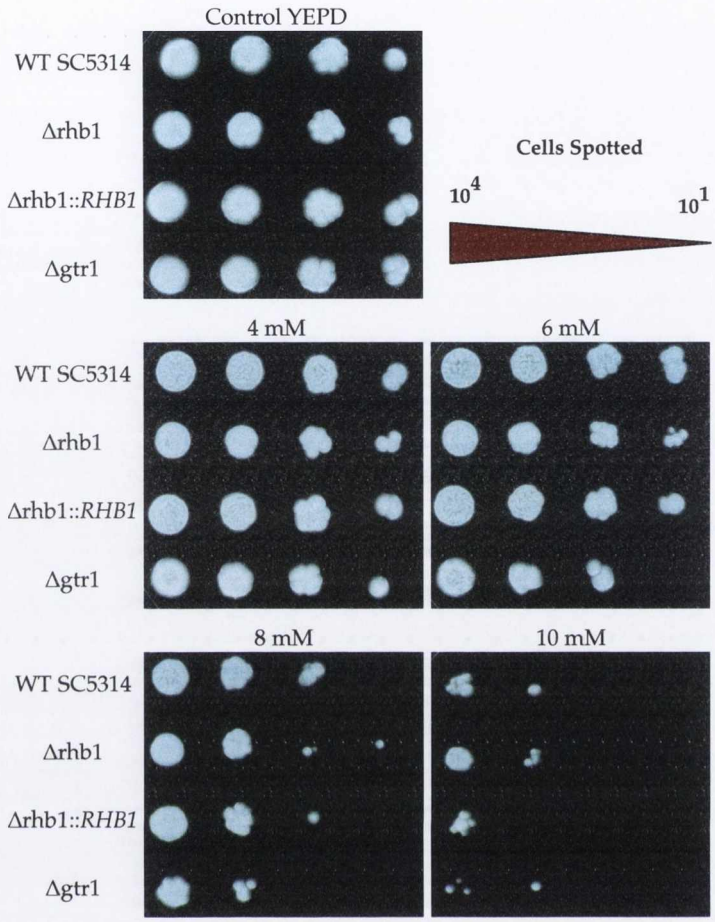

Figure 4.18: **Effects of hydrogen peroxide on the growth of Δ*rhb1* & Δ*gtr1*.**

10-fold serial dilutions (left to right) of 2 x 10^4 cells to 2 x 10^1 cells were spotted on YEPD agar containing 2, 4 or 6 mM of H_2O_2. Plates were incubated for 48 h at 30 °C.

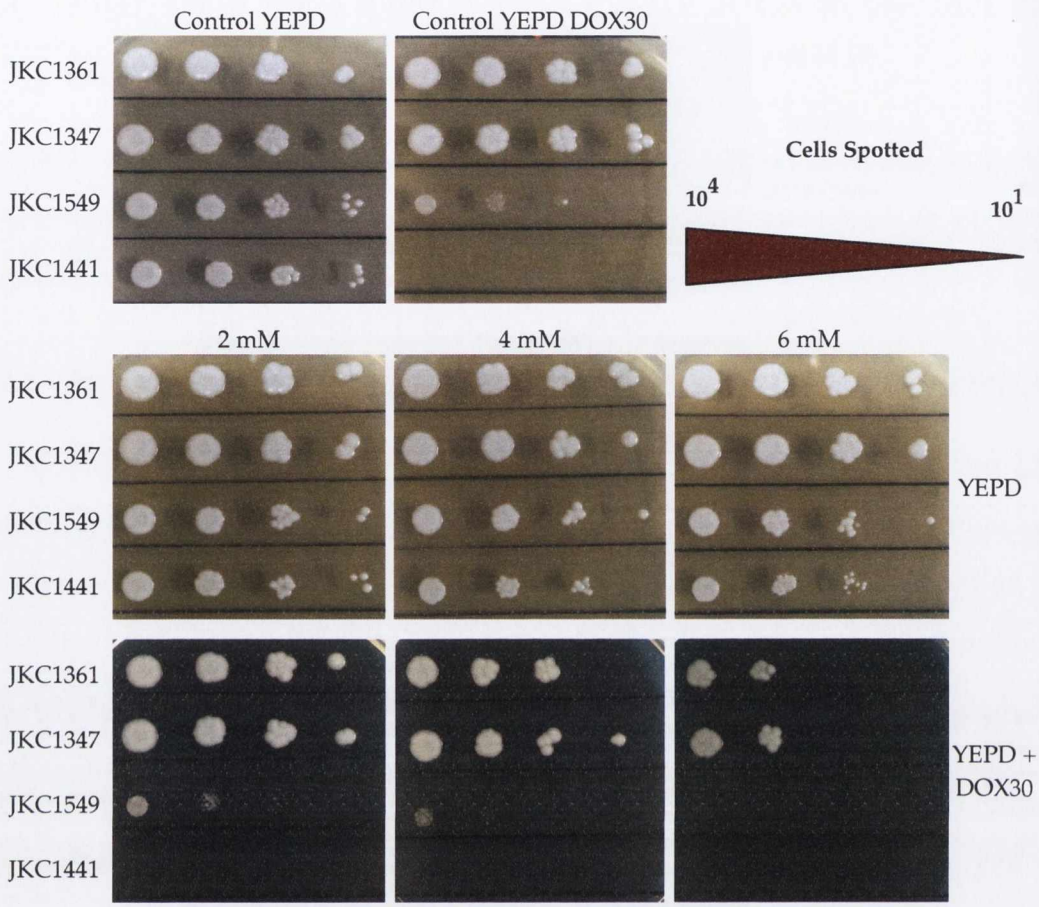

Figure 4.19: **Growth of WT JKC1361, heterozygous *TOR1/tor1* JKC1347, tetO-*TOR1/tor1* JKC1549 and truncated tetO-ΔN*TOR1* JKC1441 in the presence of hydrogen peroxide.**

10-fold serial dilutions (left to right) of 2 x 10^4 cells to 2 x 10^1 cells were spotted on YEPD agar containing 2, 4 or 6 mM of H_2O_2. Plates were incubated for 48 h at 30 °C. Two sets, one containing 30 μg/ml of doxycycline and one without, were incubated alongside one another.

4.3.7 Effects of Rapamycin & Fluconazole on Δ*rhb1* & Δ*gtr1* Mutant Strains. (Minimal Inhibitory Concentration Assays)

4.3.7.1 MIC of Rapamycin on Δ*rhb1* & Δ*gtr1*

In order to determine what effect the Tor1 inhibiting drug rapamycin had on the Δ*gtr1* and Δ*rhb1* strains, and whether they exhibited hypersensitivity, MIC assays were performed as shown in figure 4.20a. All strains were grown in the presence of rapamycin in doubling dilutions from 10 ng/ml to 0 ng/ml and incubated for 24 h. The WT SC5314 and Δ*rhb1*::*RHB1* strains had an 80 % inhibitory concentration (IC_{80}) of ~ 9.7 ng/ml rapamycin. Additionally, the Δ*gtr1*::*GTR1* had an IC_{80} of 9 ng/ml while Δ*rhb1* and Δ*gtr1* had an IC_{80} of 6 ng/ml and 8.5 ng/ml respectively.

4.3.7.2 MIC of Fluconazole Δ*rhb1* & Δ*gtr1*

The effects of the Δ*rhb1* and Δ*gtr1* mutations on fluconazole sensitivity was also examined using an MIC assay as shown in figure 4.20b. All strains were grown in the presence of fluconazole in doubling dilutions from 100 μg/ml to 0 μg/ml and incubated for 24 h. All strains, with the exception of Δ*rhb1*, had an 80% inhibitory concentration (IC_{80}) of ~ 40 μg/ml. The Δ*rhb1* strain had an IC_{80} of ~ 20 μg/ml.

4.3.8 Biofilm Formation of Δ*rhb1* & Δ*gtr1* Mutant Strains Compared with WT SC5314.

The ability to form biofilm was examined in Spider medium on plastic surfaces following 24 h and 48 h growth. Strains were inoculated into 96 well plates in a 1/100 dilution of a YNB with 100 mM glucose culture grown to an OD_{520} of 0.38 nm (10^7 cells). At 24 h, both the Δ*gtr1* and Δ*rhb1* mutants demonstrated an increase in the level of biofilm formed (Fig. 4.21) compared with WT SC5314 and their complemented counterparts. At 48 h, the Δ*rhb1* mutant exhibited the largest increase in the level of biofilm formed compared with WT SC5314 and the complemented Δ*rhb1*::*RHB1* strain. The

Δ*gtr1* mutant also exhibited an increase in the level of biofilm formed compared with WT SC5314 and the complemented Δ*gtr1*::*GTR1* strain, albeit not to the same extent as Δ*rhb1*. Furthermore, upon microscopy analysis (Fig. 4.22), it was observed that the Δ*gtr1* and Δ*rhb1* mutants had a dense biofilm mass in comparison to WT SC5314 and their complemented counterparts. WT SC5314 and complemented strains exhibited a number of free yeast cells along with hyphal filaments. However, the biomass was less than that observed in the mutant strains.

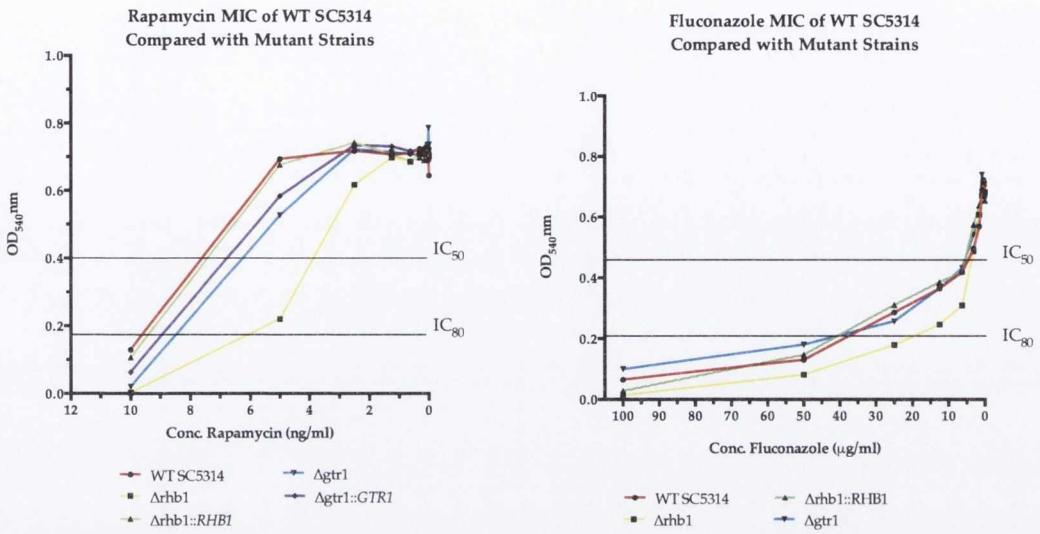

Figure 4.20: **MIC assay. Effects of rapamycin & fluconazole on mutant Δ*rhb1* and Δ*gtr1* mutant strains.**

Figure (a) shows the MIC of mutant strains in the presence of rapamycin and (b) in the presence of fluconazole.

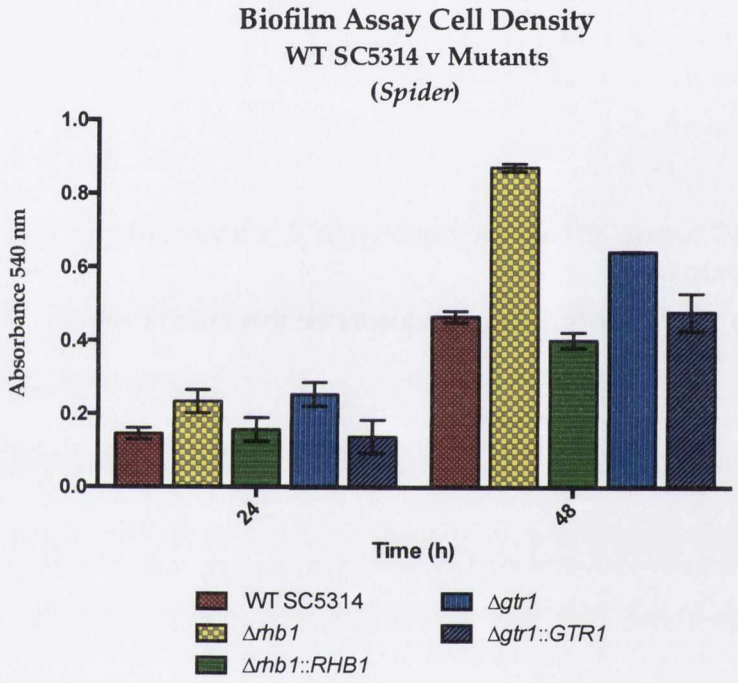

Figure 4.21: **Biofilm formation of the Δ*gtr1* & Δ*rhb1* mutants compared with WT SC5314.**

The biofilm assay was performed in Spider medium and the biomass measured using a Crystal Violet assay.

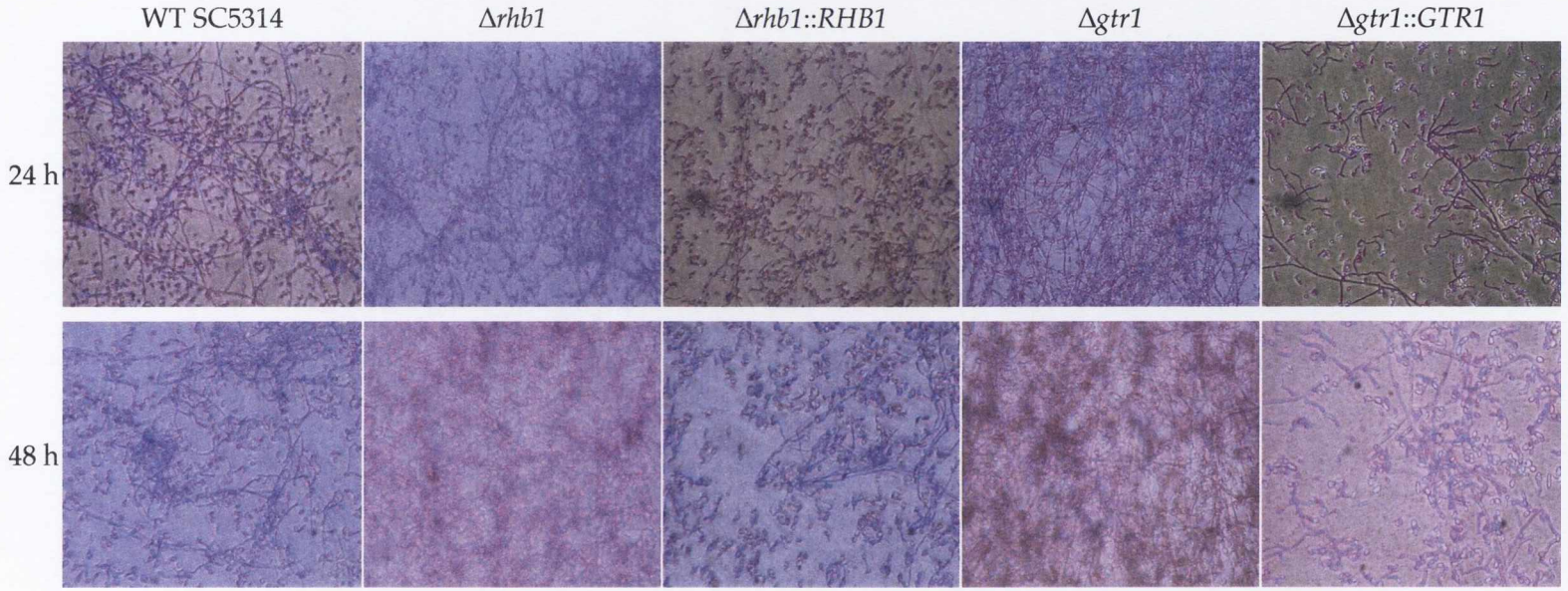

Figure 4.22: **Microscopic images of biofilms formed by the Δ*gtr1* & Δ*rhb1* mutants compared with WT SC5314.** Microscopic images were taken of biofilms formed on 96 well plates at 24 h and 48 h.

4.4 Discussion

Overexpression of *GTR1*, *RHB1* and *TOR1* was previously carried out in order to generate strains exhibiting a hyperactive Tor1 phenotype (chapter 3). This allowed us to generate a proof of concept that Tor1 hyperactivity restricts fungal virulence by way of reducing filamentation, flocculation and biofilm formation. However, this does not provide information on the pathways by which Tor1 is activated.

Tor1 itself is a highly conserved protein, and therefore is an unsuitable antifungal target. Therefore, upstream pathways may have more potential as antifungal targets. As discussed previously, Gtr1, a GTPase and Rhb1, a G protein from the Ras superfamily, are putative upstream activators of Tor1. Previously it has been shown that Gtr1 colocalises to vacuoles with Tor complex 1 (TORC1) [100]. Presumably, it is here that vacuolar amino acid levels are signaled to TORC1, allowing for its activation and stimulating growth. Additionally, previous studies have shown that deletion of *RHB1* increases sensitivity to rapamycin, suggesting association with the Tor1 pathway [102]. Further analysis showed involvement in nitrogen starvation-induced filamentation [102].

Here, we generated a Δ*gtr1* strain and carried out comparative analysis with a Δ*rhb1* strain donated by Prof. Lan (University of Taiwan). We assessed the phenotypes associated with both of these strains in relation to their growth in a nitrogen-limiting medium and their ability to aggregate and flocculate. Furthermore, we assessed their ability to form biofilms and whether there were defects in relation to cell wall integrity. Finally, we looked at their susceptibility to rapamycin and fluconazole.

In addition to characterising the phenotypes of the Δ*rhb1* and Δ*gtr1* strains, we characterised the phenotypes associated with a doxycycline regulatable tetO strains. Tor1 is essential for cellular proliferation and therefore a mutant Δ*tor1* strain could not be generated. To overcome this, we obtained a gift of a tetO-*TOR1*/*tor1* doxycycline-regulatable strain. Additionally, we used a truncated tetO-Δ*N-TOR1* strain where the tetO promoter replaced the 5′ end of the TOR1 gene coding for the N-terminus of the Tor1. Here we analysed the phenotypes associated with a repressed *TOR1*.

4.4.1 Gtr1 is an Upstream Activator of Tor1

As mentioned in section 1.6, the ribosomal protein *RPS6* is a well characterised Tor1 substrate. Its phosphorylation is critical downstream of mTor and an antibody targeting Rps6 phosphorylation can be used to measure Tor1 activity. Therefore, in order to confirm that Gtr1 acts upstream of Tor1, we carried out a phosphorylation assay to determine whether Rps6 is phosphorylated in a Δ*gtr1* mutant strain. Additionally, the assay was carried on our overexpressed P_{ENO}*GTR1* strain.

The WT SC5314, homozygous and heterozygous Δ*gtr1* and the overexpressed P_{ENO}*GTR1* were all subjected to the P-S6 assay and confirmed that Gtr1 as an upstream activator of Tor1. From the results seen in figure 4.3, the WT SC5314 and heterozygous Δ*gtr1* mutant strain showed equal band intensities for the phosphorylation of Rps6. Homozygous Δ*gtr1* showed a fainter band suggesting a role for Gtr1 upstream of Tor1. Furthermore, the P_{ENO}*GTR1* strain showed the greatest intensity, indicative of a Tor1 hyperactive phenotype. This is further evidence for the role of Gtr1 upstream of Tor1.

4.4.2 Effects on Cellular Growth

As previously mentioned, Tor1 is active in a nutrient rich environment and it is the upstream activators that signal to Tor1, thus activating the Tor1 kinase. Here, we looked at the effects of growth on the Δ*rhb1* and Δ*gtr1* mutant strains. Additionally, we looked at the effects on growth in a doxycycline-regulatable tetO-*TOR1* strain.

In YEPD medium, both the Δ*rhb1* and Δ*gtr1* mutants were capable of growth with similar levels to wild-type cells in figure 4.4a. In 100 mM $(NH_4)_2SO_4$, the Δ*rhb1* and Δ*gtr1* mutants grew to similar levels to WT SC5314 and Δ*rhb1*::*RHB1*. Neither strain were affected by the limited nitrogen source. However, when grown in 100 mM urea, the Δ*rhb1* mutant showed a lag in growth compared with WT SC5314 and Δ*rhb1*::*RHB1*, while the Δ*gtr1* mutant grew at a similar rate to WT SC5314. Previously, *RHB1* has been linked to a signaling response due to nitrogen availability in *C. albicans* [102]. While no difference was seen in 100 mM $(NH_4)_2SO_4$, the difference in growth in 100 mM urea

may be attributed to different nitrogen uptake mechanisms.

The catabolism of urea is known to aid in the virulence of bacterial pathogens and furthermore, urea degradation is exploited by some fungal pathogens [121, 122]. In *C. albicans*, Dur3 is a major urea transporter which is co-regulated by *DUR1,2*, a urea amidolyase allowing for the use of urea as a nitrogen source [123]. The decreased rate of growth of the Δ*rhb1* mutant compared with WT SC5314, Δ*rhb1*::*RHB1* and the Δ*gtr1* mutant may provide a link between *RHB1* and *DUR3/DUR1,2*. Navarathna *et al.* (2011) state that in *C. albicans*, *DUR1,2* has five (A/T) GATA (A/G) sites upstream of the open reading frame that are putative binding sites for the GATA transcription factors Gln3 and Gat1, that work downstream of Tor1 via Rhb1 [102]. Therefore, these results along with the ability of Δ*gtr1* to grow in urea at the same rate of WT SC5314, suggest a role for Rhb1 in growth in urea as a nitrogen source.

The essentiality of Tor1 for growth was confirmed using tetO-*TOR1* strains where expression can be suppressed by the addition of doxycycline. The addition of 2.5 μg/ml of doxycycline was enough to inhibit growth in the truncated tetO-Δ*NTOR1* strain JKC1441 strain while the homozygous tetO-*TOR1* strain JKC1549 was capable of growth even with the addition of 40 μg/ml of doxycycline. However, after pre-incubation overnight with 100 ng/ml doxycycline the rate of growth was lowered when grown in 30 μg/ml of doxycycline. Unlike the tetO-Δ*NTOR1* strain, growth was not fully inhibited but rather reduced. A possible explanation for this may be due to residual available Tor1 proteins in the cell. The truncated tetO-Δ*NTOR1* strain has a reduced rate of growth compared with the full length tetO-*TOR1/tor1* strain in the absence of doxycycline. Therefore, any residual protein remaining prior to doxycycline treatment are not fully functioning in the tetO-Δ*NTOR1* strain where as in the tetO-*TOR1/tor1* strain, the residual proteins are in tact and thus fully functional.

The growth of the full length and truncated tetO-*TOR1* mutants was assessed using a limited nitrogen source (YNB + 0.5 mg/ml uridine with either (NH4)2SO or urea) without the addition of doxycycline. The truncated tetO-ΔN-*TOR1* strain JKC1441

strain grew poorly compared to JKC1549 in either medium, suggesting that the HEAT repeat domain in the N-terminal, involved in intracellular transport, is necessary in signaling nutrient availability. The reduced activity of the truncated allele of *TOR1* in JKC1441 likely explains why lower concentration of doxycycline were required to inhibit growth.

4.4.3 Effects on Hyphal Formation, Aggregation and Flocculation

Hyphal formation, aggregation and flocculation was determined in each mutant strain. In YEPD supplemented with 10% (v/v) serum, it was shown that the Δ*rhb1* and Δ*gtr1* mutants had the ability to form true hyphae (Fig. 4.7). Additionally, microscopic analysis indicated that the Δ*rhb1* and Δ*gtr1* strains formed tight aggregates with less free yeast cells when compared with WT SC5314 and Δ*rhb1*::*RHB1* (Fig. 4.8 & 4.9). Presumably, this is due to an increase in genes associated with adhesion, therefore having a greater propensity to aggregate and resulting in the decreased number of free yeast cells. Semi-quantitative analysis by filtration confirmed this at 2 h and 4 h. Furthermore, examination of flocculation in Spider medium (Fig. 4.12) indicated that the Δ*gtr1* strain exhibited a greater ability to aggregate and flocculate compared with WT SC5314 and the Δ*rhb1* mutant. These results indicate that the Δ*gtr1* strain has a greater effect than the Δ*rhb1* mutant on the Tor1 activation of genes associated with adhesion, suggesting a role for *GTR1* in the transcription of adhesins via Tor1 signaling.

Doxycycline-regulatable strains were also tested for their ability to form hyphae, aggregate and flocculate in YEPD supplemented with 10% (v/v) serum (Fig 4.10 & 4.11). The tetO-*TOR1* strain JKC1549 and the truncated tetO-ΔN*TOR1* strain JKC1441 strains were capable of forming hyphae and aggregating when compared with WT JKC1361 and *TOR1*/*tor1* JKC1347 respectively. As time progressed from 2, 4, 6 and 8 h, it was observed that the WT JKC1316 and heterozygous JKC1347 aggregates yielded a higher number of yeast cells were seen. However, the tetO-*TOR1*/*tor1* strain JKC1549 and truncated tetO-ΔN*TOR1* strain JKC1441 did not exhibit a similar phenotype. Both

strains aggregated tightly and few to no free yeast cells were observed. Additionally, both extended longer hyphae from the aggregates. A semi-quantitative assay showed a significantly greater number of free yeast cells in the truncated tetO-Δ*NTOR1* strain JKC1441 strain at 4, 6 and 8 h. Furthermore, a significantly greater number of cells were recorded at 8 h for the tetO-*TOR1/tor1* strain JKC1549 strain.

In all aspects, the tetO-Δ*NTOR1* strain JKC1441 struggles in comparison to JKC1549. This was evident from the qualitative images and semi-quantitative cell counts as well as their ability to flocculate (Fig. 4.13). With or without the addition of doxycycline, the tetO-Δ*NTOR1* strain JKC1441 flocculated to a greater extent than the tetO-*TOR1/tor1* strain JKC1549. Visual inspection of the flocculate confirmed this. The tetO-Δ*NTOR1* strain JKC1441 had greater extended hyphae and a network of hyphal cells similar to that of a biofilm. These differences between both strains further imply a role for the HEAT domain in signaling nutrient availability.

4.4.4 Effects on Cell Wall Integrity & Responses to Oxidative Stress

In order to determine whether the cell wall integrity or responses to oxidative stress were compromised in the mutant strains, spot plate assays were carried out using different concentrations of Congo Red, Calcofluor White and H_2O_2. From the results seen in figure 4.15, cell wall integrity appeared affected in the Δ*rhb1* strain when compared with WT SC5314 and Δ*rhb1*::*RHB1*. Increasing concentrations of either Congo Red or Calcofluor White had no effect on the Δ*gtr1* strain. Tsao *et al.* (2009) previously showed that in *C. albicans*, the *RHB1*-mediated pathway is involved in the signaling pathway controlling cell wall integrity, and they suggested that this signaling is via the MAP kinase Mkc1. The results presented here correlate with the observations suggested by Tsao *et al.* (2009). In addition to this, we propose that this pathway may solely be restricted to Rhb1 and not that of Gtr1 mediated Tor1 signaling. Further analysis using qRT-PCR is suggested to confirm this.

Oxidative stress response was also examined using YEPD supplemented with a range

of H_2O_2 concentrations. Unfortunately neither the Δ*rhb1* or Δ*gtr1* mutant appeared significantly effected when subjected to H_2O_2.

Cell wall integrity and responses to oxidative stress were also determined in the doxycycline-regulatable strains. The tetO-ΔN*TOR1* strain JKC1441 failed to grow on Congo Red and Calcofluor White in the absence of doxycycline while the tetO-*TOR1*/*tor1* strain JKC1549 was similar to WT JKC1361 and *tor1*/*TOR1* strain JKC1347 on Congo Red but more susceptible on Calcofluor White (Fig. 4.16) .

It has become evident over the course of the phenotypic tests that the tetO-ΔN*TOR1* strain JKC1441 struggles in every aspect when compared with the intact tetO-*TOR1*/*tor1* strain, regardless of whether *TOR1* is inhibited with doxycycline. These data may suggest a potential role for the HEAT repeat domain as having a key role in Tor1 signaling. Work by Groves *et al.* (1999) looked at the repeated HEAT sequences, specifically the PR65/A subunit of human, budding yeast, drosophila, and *C. elegans*. The group found that 33 % of the human PR65/A subunit residues are invariant across the other organisms. Therefore, 67 % is non-conserved, possibly presenting a target for antifungal substances.

4.4.5 Effects on Susceptibility to Rapamycin & Fluconazole of Δ*rhb1* and Δ*gtr1*

Susceptibility to rapamycin and fluconazole was analysed by means of an MIC assay to determine whether the Δ*rhb1* and Δ*gtr1* mutants were more susceptible than WT SC5314 (Fig. 4.20). The Δ*rhb1* mutant has greater sensitivity to rapamycin than WT SC5314 with an IC_{80} of 6 ng/ml. This sensitivity can be complemented with the re-introduction of the *RHB1* gene. In comparison, the Δ*gtr1* mutant also shows sensitivity to rapamycin but not to the same extent as the Δ*rhb1* mutant, with an of IC_{80} 8.7 ng/ml. When the *GTR1* gene is re-introduced, this sensitivity is reduced slightly with an $IC_{80}$of 9 ng/ml. Both the Δ*rhb1* and Δ*gtr1* mutants demonstrated sensitivity to rapamycin, which suggests an association with the Tor1 pathway. Previous studies have shown

that *RHB1* is associated with the Tor signaling pathway with increased sensitivity to rapamycin in a mutant Δ*rhb1* strain [102]. Our result here confirms this. However, Δ*gtr1* does not show the same sensitivity to rapamycin as the Δ*rhb1* mutant, with an IC_{80} of 8.7 ng/ml. While the P-S6 assay (Fig 4.3) illustrates that Gtr1 is involved in nutrient activation of Tor1, perhaps it is via the Rhb1-Tor activation pathway that rapamycin affects. This could account for the difference in rapamycin sensitivity. In order to confirm this, a double mutant containing Δ*gtr1* and Δ*rhb1* may show equal levels of sensitivity to Δ*rhb1*.

4.4.6 Effects on Biofilm Formation

The formation of biofilm is critical to infection and presents a challenge in drug therapy given that biofilms can withstand high antifungal concentrations [124]. Here, biofilm assays were performed to assess the effects a homozygous *GTR1* and *RHB1* mutant would have on their formation. Assays were performed using the Crystal Violet method to stain biomass in 96 well plates. Figure 4.21 illustrates that in the absence of these genes, biofilm formation is greater than WT SC5314. Furthermore, the Δ*rhb1* mutant exhibited a greater level of biofilm formation compared to the Δ*gtr1* mutant, suggesting a role for the Rhb1-Tor1 signaling for genes associated with biofilm formation.Visual inspection of the 96 well plates showed that the mutant strains had a dense biomass in comparison to WT SC5314 and the complemented strains (Fig. 4.22). WT SC5314 and the complemented strains formed extended hyphae, however the biomass was less than the Δ*gtr1* and Δ*rhb1* mutant strains and exhibited a higher number of yeast cells in comparison.

These data, along with the additional phenotypic tests performed on the mutant strains demonstrate a role for Gtr1/Rhb1-Tor1 signaling in response to nutrient availability. Furthermore, the differences observed between the Δ*gtr1* and Δ*rhb1* mutant suggest that Gtr1 and Rhb1 are involved in different downstream processes, resulting from their signaling to Tor1. Gtr1 appears to have a role in aggregation and flocculation in

addition to biofilm formation according to the data presented, while Rhb1 appears to play a role in cell wall integrity and biofilm formation. DNA microarray analysis of both mutants will provide an insight into the genes differentially expressed between the Δ*gtr1* and Δ*rhb1* mutant strains.

Chapter 5

Expression Analysis of a Homozygous *GTR1* Mutant Strain of *Candida albicans* & Comparative Analysis with a Homozygous *RHB1* Mutant Strain

5.1 Introduction

The putative GTP-binding protein Gtr1 is a GTPase required for the activation of the TOR Complex 1 (TORC1) in *Saccharomyces cerevisiae* [97]. In *S. cerevisiae*, Gtr1 has been shown to be a subunit of the EGO complex and a multifunctional protein that is involved in the acquisition of phosphate through modulation of Pho84 transport activity [125, 126]. The EGO complex is a vacuolar membrane-associated protein complex. Genetic analyses of this complex has confirmed the existence of a growth control mechanism that originates at the vacuolar membrane. Furthermore, it has pinpointed glutamine as a key metabolite in Tor1 signaling [127]. An additional activator of TORC1 is Rhb1, a G-protein of the RAS superfamily. As stated in chapter 1, Rhb1-Tor1 signaling in *C. albicans* is involved in nitrogen starvation-induced morphogenesis. This is believed to occur via *MEP2*, an ammonium permease.

Tor1 is a conserved protein from yeast to mammals. Mammalian Tor (mTor) is involved in many cellular responses such as growth, proliferation and homeostasis [128]. Therefore, targeting Tor1 with antifungals in an effort to prevent filamentation and virulence of *C. albicans* is problematic. Previously, we examined the effects of over-expressing the upstream regulators of Tor1 as well as *TOR1* itself (Chapter 3). The findings showed that the overexpression of these promotors and of *TOR1* resulted in a Tor1 "hyperactive" phenotype. Hyphal formation on nutrient poor solid medium was reduced in comparison to wild-type cells. Furthermore, a reduction was observed in aggregation and flocculation of these overexpressed strains and a decrease in biofilm was also observed. These phenotypic tests were also performed on homozygous *GTR1* and *RHB1* mutant strains (Chapter 4). The results showed that deletion of *GTR1* resulted in greater aggregation and flocculation when compared with a mutant $\Delta rhb1$ strain. Furthermore, it was observed that the $\Delta rhb1$ stain was more sensitive to cell wall perturbing compounds than $\Delta gtr1$. These data suggest separate roles for the Gtr1 and Rhb1-Tor1 kinase downstream responses.

Here we examine the expression of the entire transcriptome of the $\Delta gtr1$ mutant strain.

Furthermore, the DNA microarray dataset of the Δ*gtr1* mutant strain is compared with previously published DNA microarray data on a Δ*rhb1* mutant [92].

5.2 Materials and Methods

The two-colour microarray-based gene expression protocol was carried out as detailed in section 2.15. The Δ*gtr1* homozygous mutant strain was compared with WT SC5314. A colony of each strain was picked from a 24-48 h old plate and incubated overnight in 4 ml YEPD broths at 37 °C with shaking at 200 rpm. Following incubation, cells were diluted accordingly into 50 ml YEPD to obtain an OD_{600} of 0.1 nm. Both strains were incubated at 37 °C with shaking at 200 rpm in order to reach an OD_{600} of 0.8 nm (~ 8 h). Once an OD_{600} of 0.8 nm was obtained, samples were frozen for RNA extractions as detailed in section 2.5.2. A total of four biological replicates per strain were hybridised to the DNA microarray slide and the DNA microarray was carried out as detailed in section 2.14.

5.2.1 Gene Expression Levels of the Δ*gtr1* Mutant Strain

Two-colour DNA microarrays were used to examine the transcription of the Δ*gtr1* strain. Gene expression profiles were examined at an OD_{600} of 0.8 nm (mid log phase). The fluorescence data of the oligonucleotide probes for each reading frame in the DNA microarray were averaged over 4 microarray slides and classed as single entities. Each entity represented a single probe sequence for an open reading frame. Statistical tests were applied using GeneSpring v13.0 to allow for averaging and normalising of the samples. Further filters were applied to ensure the exclusion of weak fluorescence signals. Additionally, a students T-test was carried out on the averaged biological samples with a p-value cut-off of 0.05. Finally, an asymptotic correction was applied using the "Storey with bootstrapping" method with a q-value cut-off of 0.05.

5.3 Results

5.3.1 Genes Expressed at Higher Levels in the Δ*gtr1* Mutant Strain

Of the differentially expressed genes, 173 were considered to be significantly expressed at a higher level in the Δ*gtr1* strain. These genes had a > 2.0-fold increase in expression. They were submitted to the Gene Ontology (GO)-term slim mapper service on the *Candida* Genome Database, which allowed for the identification of the major branches of the ontologies based on their GO annotations.

First a GO-Slim function was run. This returned genes with increased expression in those associated with molecular function (49.1 %), hydrolase activity (13.3 %), transferase activity (10.4 %), protein binding (4 %) and phosphatase activity (1.7 %). Second, a GO-Slim process was run. Of the 173 genes analysed, this returned genes with increased expression in those associated with biological processes (41.6 %), transport (16.8 %), filamentous growth (6.9 %), pathogenesis (5.8 %), protein catabolic processes (2.3 %) and cell adhesion (2.3 %). A list of all genes can be found on the supplementary CD at the back of this thesis.

5.3.2 Genes Expressed at Lower Levels in the Δ*gtr1* Mutant Strain

Of the differentially expressed genes, 146 were considered to be significantly expressed at a lower level in the Δ*gtr1* strain (< 2.0-fold). These genes were also submitted to the *Candida* Genome Database in order to perform analyses using the GO-term slim mapper tool.

First, a GO-Slim function was run. This returned genes with decreased expression in those that are associated with molecular function (50 %), oxidoreductase activity (13.7 %), transporter activity (8.2 %), hydrolase activity (6.8 %) and protein binding (4.1 %). Second, a GO-Slim process was run. Of the 146 genes analysed, this process returned genes associated with biological processes (44.5 %), transport (13.7 %), response to stress (12.3 %), filamentous growth (8.2 %), ribosome biogenesis (4.1 %), carbohy-

drate metabolic processes (3.4 %) and biofilm formation (1.4 %). A list of all genes can be found on the supplementary CD at the back of this thesis.

5.3.3 Gene Set Enrichment Analysis of the Δ*gtr1* Mutant Strain

Gene set enrichment analysis was performed using the Broad Institute GSEA v2.2.2. The DNA microarray data were inputted into the software and the raw data obtained was exported to Cytoscape v3.3.0 in order to create a network of functional groups of genes that are differentially expressed in the Δ*gtr1* strain. Figure 5.1 illustrates the gene clusters that have increased expression while figure 5.2 illustrates the gene clusters that have a decrease in expression.

Genes that appear to have increased expression in the Δ*gtr1* strain are those associated with oxidative stress, adhesion, glycolysis, biofilm and hyphae production. Genes that appear to have decreased expression levels are those associated with amino acid biosynthesis, metabolism and ribosome biogenesis. Enrichment plots generated using GSEA illustrates this in figure 5.3. The y-axis is the enrichment score which is represented by a green line with a positive normalised enrichment score. This indicates up-regulated gene sets while a negative indicates down-regulated gene sets.

5.3.4 qRT-PCR Confirmation of the Δ*gtr1* DNA Microarray Expression Analysis

In order to confirm the observed gene expressions from the DNA microarray of the Δ*gtr1* strain, qRT-PCR was performed on the the Δ*gtr1* strain and compared to WT SC5314. cDNA was generated from RNA used in the DNA microarray experiment as described in section 2.5.3 and qRT-PCR performed as outlined in section 2.6.3. qRT-PCR was performed on the genes shown in figure 5.4 and confirmed the results seen with the increased and decreased expression of genes in the DNA microarray dataset. *ALS4*, *CAN2*, *GAP1*, *HIP1*, *PHO84* and *PHO112* all showed increased expression compared with WT SC5314.

5.3.5 Differentially Expressed Genes of the Δ*gtr1* Strain Compared with the Δ*rhb1* Strain

The Δ*gtr* and Δ*rhb1* DNA microarray datasets were compared for differences and similarities in the up and down regulation of genes. Upon comparison of both datasets, the Δ*gtr1* strain had 225 specific up-regulated genes in comparison with 55 in the Δ*rhb1* strain (Fig. 5.5). Additionally, down-regulated genes differed with the Δ*gtr1* strain having 183 specifically down-regulated genes in comparison to 30 specifically down-regulated genes in the Δ*rhb1* strain. A list of all increased and decreased genes (2.0-fold) of the Δ*gtr1* mutant can be seen in the supplementary tables S3 and S4.

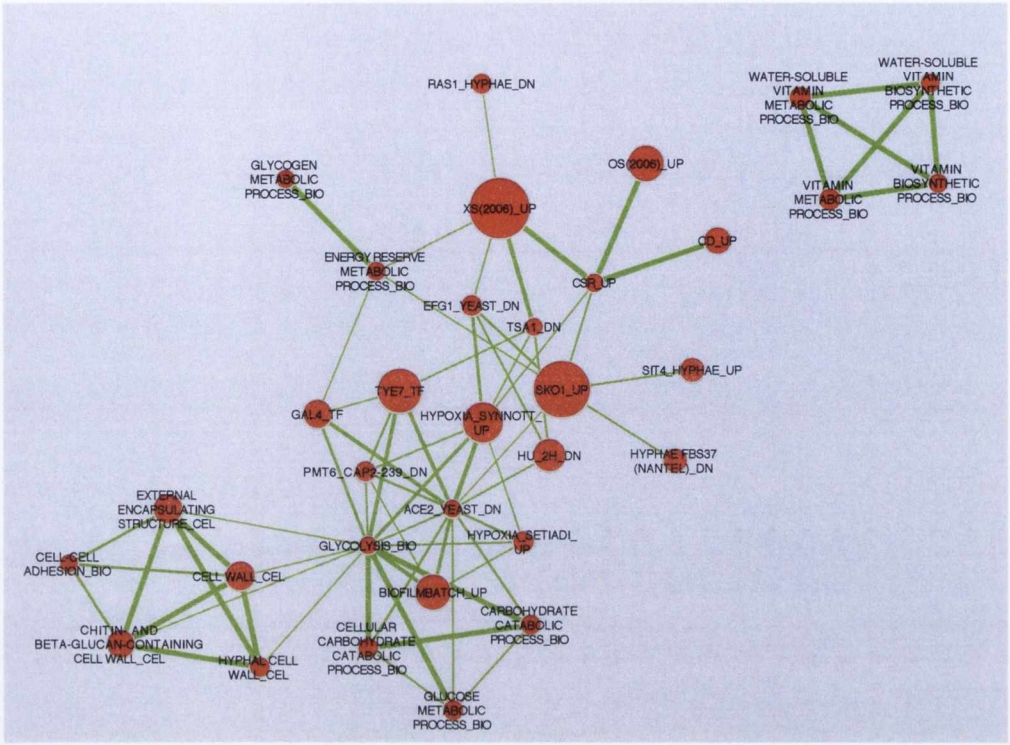

Figure 5.1: **GSEA of the genes differentially increased in the Δ*gtr1* mutant.**

Gene Set Enrichment Analysis (GSEA) v2.2.2 was used in conjunction with Cytoscape v3.3.0 to create a network of functional groups of genes that are differentially expressed in the Δ*gtr1* mutant. The figures above represent enrichment maps of genes differentially increased. Circle diameters reflects the number of modulated gene transcripts in each gene set. A digital copy of these enrichment maps can be found on the attached CD at the back of this thesis.

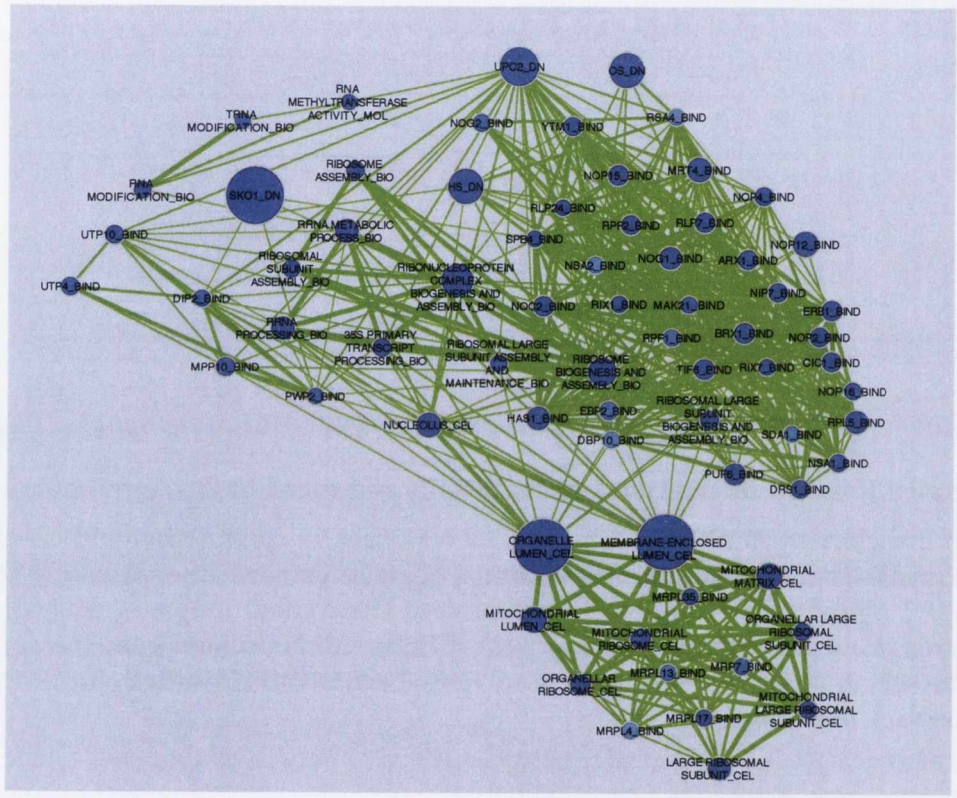

Figure 5.2: **GSEA of the genes differentially decreased in the Δ*gtr1* mutant.**

Gene Set Enrichment Analysis (GSEA) v2.2.2 was used in conjunction with Cytoscape v3.3.0 to create a network of functional groups of genes that are differentially expressed in the Δ*gtr1* mutant. The figures above represent enrichment maps of genes differentially decreased. Circle diameters reflects the number of modulated gene transcripts in each gene set. A digital copy of these enrichment maps can be found on the attached CD at the back of this thesis.

a) Genes Involved in Ribosomal Assembly

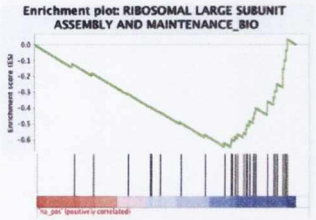

NES= -1.96; p=0.0; FDR=0.011

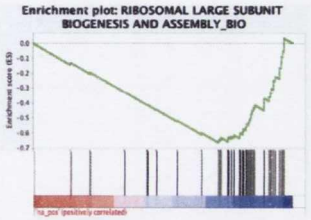

NES= -2.16; p=0.0; FDR=0.004

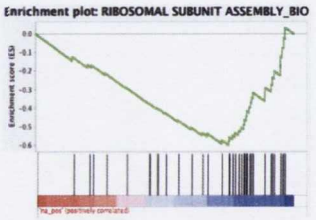

NES= -1.96; p=0.0; FDR=0.235

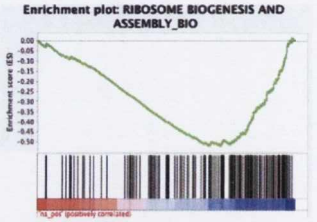

NES= -2.07; p=0.0; FDR=0.028

b) Genes Involved in Glutamine Biosynthesis and Metabolic Processes

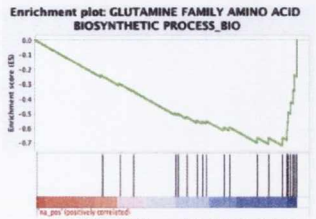

NES= -2.05; p=0.0; FDR=0.055

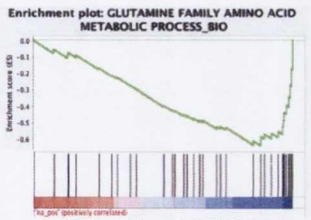

NES= -2.03; p=0.0; FDR=0.08

c) Genes Involved in Biofilm

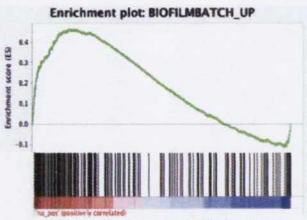

NES= +2.42; p=0.0; FDR=0.002

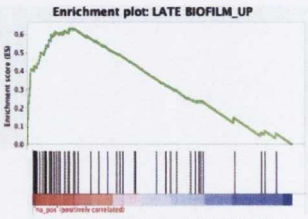

NES= +2.65; p=0.0; FDR=0.0

Figure 5.3: **Enrichment plots of gene sets differentially expressed in Δ*gtr1*.**

Select enrichment plots of gene sets that are differentially expressed. Genes are ranked according to their expression on the x-axis. The up-regulated genes are on the right side and down-regulated genes on the left, indicated by red and blue. The y-axis is the cumulative value of the enrichment score, represented by the green line. A positive normalised enrichment score (NES) indicates enrichment in the up-regulated group of genes in the sample while a negative NES indicates genes in the down-regulated group. The titles indicate the function to which each gene set has been assigned.

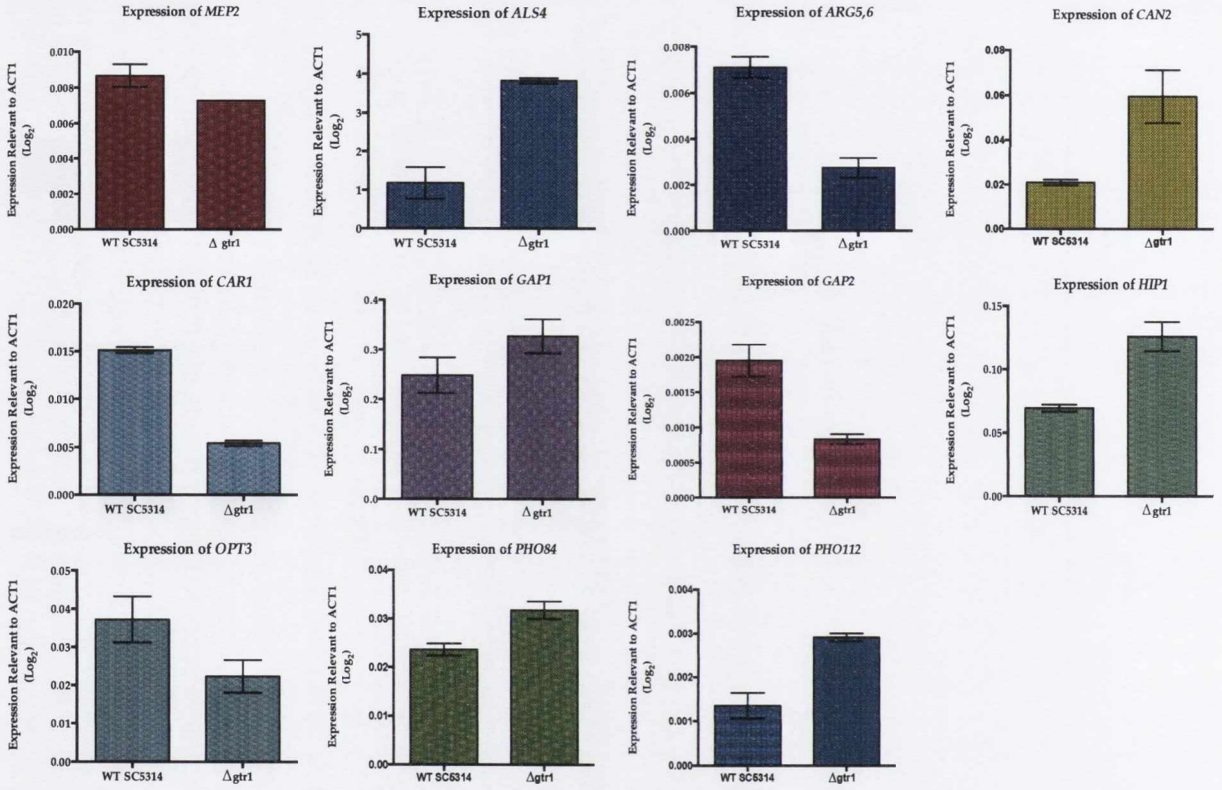

Figure 5.4: **qRT-PCR data of the Δgtr1 mutant DNA microarray.**

qRT-PCR analysis was carried out on a selection of genes in order to compare the up and down expression seen in the Δgtr1 mutant DNA microarray dataset. cDNA was generated from the Δ*gtr1* mutant and WT SC5314 RNA used in the DNA microarray experiment.

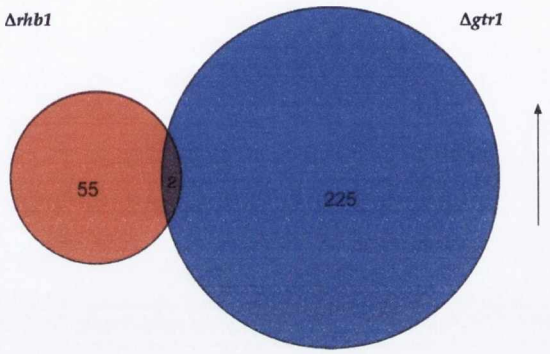

(a)

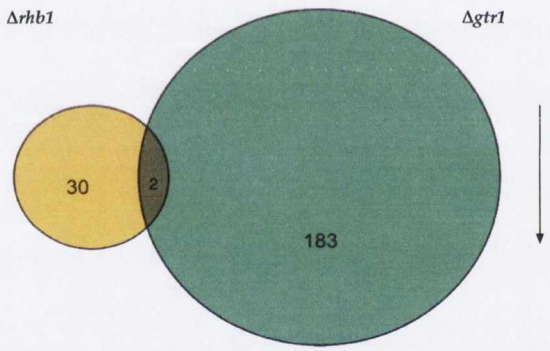

(b)

Figure 5.5: **Overview of overlap (2.0-fold increase & decrease) in DNA microarray data sets.**
Venn diagram showing the common number of genes with a 2.0-fold or more in- crease or decrease between each of the Δ*gtr1* and Δ*rhb1* DNA microarray datasets. (a) represents the up-regulated genes. Δ*gtr1* has 225 genes with a 2.0 fold or more increase compared with 55 in Δ*rhb1*. Both have 2 genes in common with a 2.0 fold or more increase. These are *TNA1* and *ECE1*. (b) represents the down regulated genes. Δ*gtr1* has 183 genes with a 2.0 fold or more decrease compared with 30 in Δ*rhb1*. Both have 2 genes in common with a 2.0 fold or more decrease. These are *CAR1* and *ZCF3*.

5.3.6 Heat Map Analysis

Previously published DNA microarray data on a Δ*rhb1* mutant was obtained from The Gene Expression Omnibus (http://www.ncbi.nlm.nih.gov/geo/) under the accession number GSE29128 and imported into GeneSpring. This was compared with the data obtained for the Δ*gtr1* strain. Heat maps were then generated to compare and contrast differences observed between both microarray datasets.

5.3.6.1 Genes Associated with Cell-Cell Adhesion, Nitrogen Uptake & Phosphate Utilisation

Similarities were observed in the up-regulation of genes associated with cell-to-cell adhesion (Fig. 5.6). The *HWP1*, *ALS3* and *ECE1* genes, critical for biofilm formation, were up-regulated in both the Δ*gtr1* and Δ*rhb1* strains. However, in addition to these genes, further up-regulation of cell-to-cell adhesion genes were observed in the Δ*gtr1* strain that were not observed in the Δ*rhb1* strain. These included additional *ALS* genes along with *UME6*, which is involved in hyphal extension.

The genes associated with nitrogen utilisation were up-regulated in the Δ*rhb1* strain compared with the Δ*gtr1* strain (Fig. 5.6). *MEP2*, *OPT3*, *OPT1* and *SAP2* were greatly up-regulated in the Δ*rhb1* strain and down-regulated in the Δ*gtr1* strain. Additionally, the expression of the gene *DUR1,2* was up-regulated in the Δ*gtr1* strain relative to the Δ*rhb1* strain correlating with the growth in urea in Chapter 4. Furthermore, differences were observed with the genes associated with phosphate uptake (Fig. 5.6). The Δ*gtr1* strain showed increased expression of these genes compared to the Δ*rhb1* strain, specifically the *PHO* genes (*PHO84*, *PHO87*, *PHO89*, *PHO91*, *PHO112* & *PHO113*) which were greatly up-regulated in the Δ*gtr1* strain.

5.3.6.2 Genes Associated with Biofilm Formation, Cell Wall-Associated Proteins, Filamentous Growth, Cellular Amino Acid Biosynthesis & Metabolic Processes

The expression of genes associated with biofilm formation were up-regulated in the Δ*gtr1* strain relative to the expression in Δ*rhb1* which includes *ALS2*, *ALS4* and *PGA1*. However, the Δ*rhb1* strain had similar expression with regards to the genes *HWP1* and *ECE1* (Fig. 5.7). These genes were up-regulated to similar levels in both the Δ*gtr1* and Δ*rhb1* strains. Additionally, differences were observed between genes that code for cell wall-associated proteins (Fig. 5.7). In the Δ*gtr1* strain, these genes were up-regulated compared with the Δ*rhb1* strain and included the genes HEM13, CSP2, DDR48 and GPH1. Furthermore, differences were observed between genes that are associated with amino acid biosynthesis and metabolic processes as well as filamentous growth (Fig. 5.7). Genes associated with amino acid biosynthesis and metabolic processes were more highly expressed in the Δ*rhb1* strain than the Δ*gtr1* strain including *ARG1*, *ARG3*, *ARG4* and *ARG5,6*. Finally, genes associated with filamentous growth were predominantly down-regulated in the Δ*rhb1* strain compared to the expression levels observed in the Δ*gtr1* strain. While there were similarities in the expression levels of *CAR1* and *ZCF3*, the expression of *RHB1*, *ADE5,7*, *CHA1* and *GAP1* was lower in the Δ*rhb1* strain compared to the Δ*gtr1* strain (Fig 5.7).

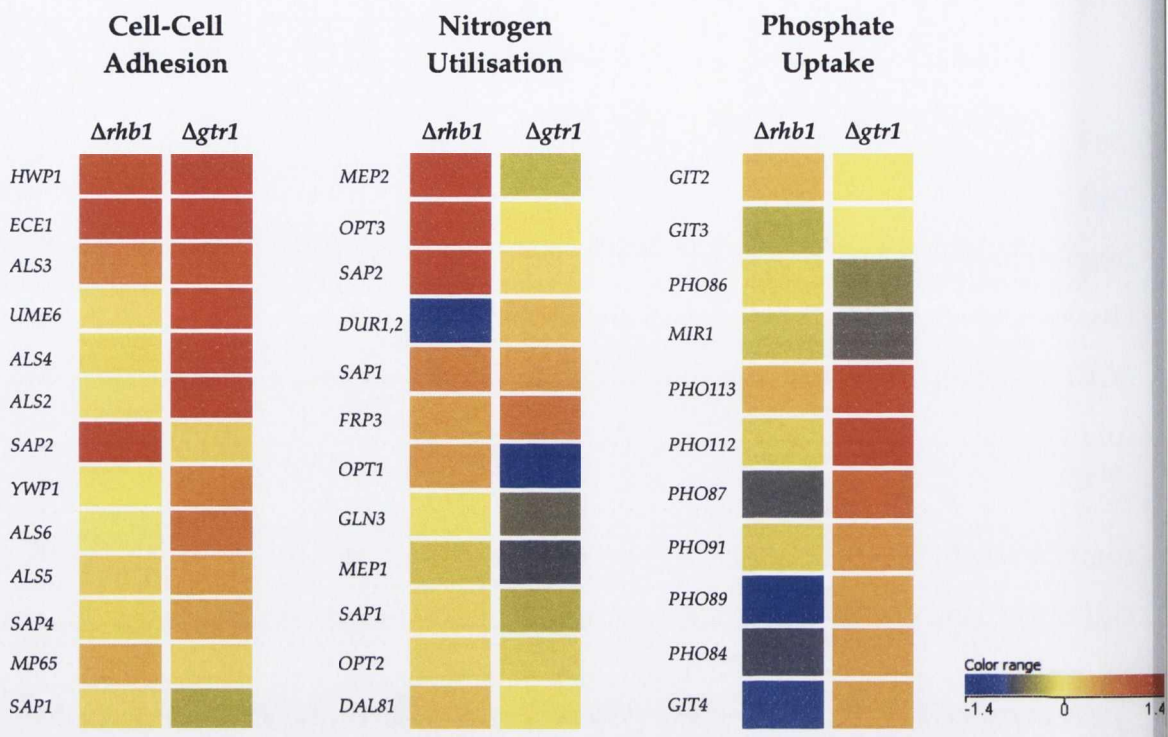

Figure 5.6: **Heat map comparisons of differentially expressed genes involved in adhesion, nitrogen uptake and phosphate utilisation in Δ*gtr1* & Δ*rhb1*.**

Visual heat map showing the expression of genes associated with cell-cell adhesion, nitrogen utilisation and phosphate uptake in the Δ*gtr1* and Δ*rhb1* strains. Each gene is labeled on the left and the legend conveys the relative colouring for the normalised expression level of each gene.

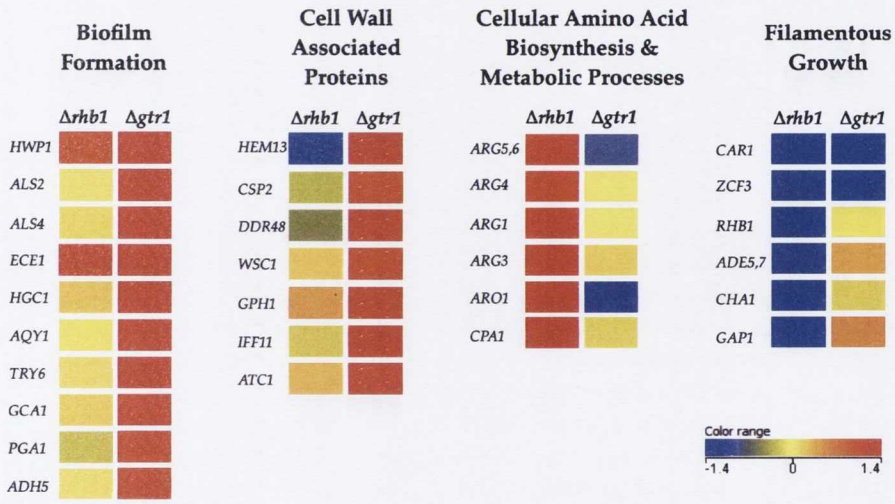

Figure 5.7: **Heat map comparisons of differentially expressed genes involved in biofilm formation, cell wall associated proteins, filamentous growth and amino acid biosynthesis and metabolic processes in Δ*gtr1* & Δ*rhb1*.**

Visual heat map showing the expression of genes associated with biofilm formation, cell wall associated proteins, filamentous growth, cellular amino acid biosynthesis and metabolic processes in the Δ*gtr1* and Δ*rhb1* strains. Each gene is labeled on the left and the legend conveys the relative colouring for the normalised expression level of each gene.

5.4 Discussion

In chapter 4, phenotypic assays demonstrated that homozygous *GTR1* and *RHB1* mutants differ in their ability to aggregate and flocculate. Moreover, these mutants demonstrated differences in growth on medium supplemented with the cell-wall-perturbing compounds Congo Red and Calcofluor White. Furthermore, biofilm assays demonstrated that deletion of both *GTR1* and *RHB1* resulted in an increase in biofilm formed on an abiotic surface. Work by Tsao *et al.* (2009) has linked Rhb1 to *C. albicans* Tor1 signaling in response to nitrogen availability, while work by Mack *et al.* (2000) has demonstrated in fission yeast *S. pombe*, a homozygous *RHB1* mutant resulted in a phenotype similar to nitrogen-starved cells. Much of the work published on *GTR1* has been in the model organism *S. cerevisiae,* demonstrating a role for Gtr1 in the amino acid activation of TORC1. In this chapter, DNA microarray analysis on the Δ*gtr1* strain shows the effects a homozygous *GTR1* mutant have on the downstream signaling of Tor1. The DNA microarray data were also compared with previously published DNA microarray data on a Δ*rhb1* strain in order to determine whether Gtr1 and Rhb1 have similar roles in Tor1 signaling.

5.4.1 Differentially Expressed Genes in a *C. albicans* Homozygous *GTR1* Mutant

Genes with a 2.0-fold increase (173 genes) or decrease (146 genes) in expression were submitted to the *Candida* Genome Database to identify ontologies based on GO annotations. Genes that were up-regulated included those associated with pathogenesis, cell adhesion and filamentous growth, similar to genes expressed during a nitrogen starvation response. Similarly, genes associated with ribosome biogenesis showed a decrease in expression. Gene set enrichment analysis was performed in order to cluster functional groups of genes that were differentially expressed in the Δ*gtr1* strain. Gene set enrchment analysis (Fig. 5.1) illustrated genes up-regulated 2.0-fold in the Δ*gtr1* strain.

These including those associated with biofilm formation, hyphal formation and cellular adhesion. In a nitrogen-limiting environment, signaling to Tor1 is inhibited which results in the expression of genes involved in nitrogen-scavenging (Section 1.6). This suggests a role for Gtr1 in the regulation of these genes via Tor1 signaling.

qRT-PCR was performed on the Δ*gtr1* DNA microarray RNA in order to confirm the gene expression patterns observed in the DNA microarray. Figure 5.4 illustrates the increased expression of the genes *ALS4*, *CAN2*, *PHO84* and *PHO112*. The increased expression of *PHO84* correlates with observations made by Bun-Ya *et al.* (1992). They reported that in *S. cerevisiae*, Gtr1 is associated with the Pho84 P_i (inorganic phosphate) transporter [126]. Furthermore, they suggest that Gtr1 may be involved in the uptake of P_i via Pho84. The DNA microarray analysis presented here confirms the association of Gtr1 with phosphate uptake. Further work should focus on the growth of the Δ*gtr1* and Δ*rhb1* strain in a medium rich in phosphate.

Work by Chen *et al.* (2012) showed that in a Δ*rhb1* mutant, *GAP1* and *HIP1* expression is decreased and *GAP2* expression is increased [92]. The DNA microarray experiment performed here on the Δ*gtr1* strain showed the opposite to that observed by Chen *et al.* (2012). *GAP1* and *HIP1* expression is increased while *GAP2* expression is decreased, suggests that their expression is via Rhb1-Tor1 signaling. These opposing effects seen in the Δ*gtr1* and Δ*rhb1* strains may be due to the availability of excess Tor1 protein that can interact with Rhb1.

5.4.2 Dataset Comparison of the Δ*gtr1* & Δ*rhb1* Mutant Strains

The Δ*gtr1* dataset was compared with the Δ*rhb1* dataset and Venn diagrams generated to illustrate the differences and similarities between both (Fig 5.1). Few similarities were observed between both datasets, with only 2 genes up-regulated and 2 genes down-regulated in both datasets. However, a large difference in gene expression was observed between the datasets. The Δ*gtr1* strain had increased expression of 225 genes compared with 55 in the Δ*rhb1* strain and a decreased expression of 183 compared with

30 in the Δ*rhb1* strain. Heat maps were generated comparing both datasets (Fig. 5.4 & 5.5) and demonstrated that Rhb1 and Gtr1 may control distinct subsets of gene sets via the Tor1 kinase. The data presented here suggest that the expression of genes associated with cell-cell adhesion and phosphate uptake occur via Gtr1-Tor1 signaling. Comparison of the DNA microarray datasets also showed that expression of the *ALS* genes and *PHO* genes, as well as *UME6*, *HWP1* and *ECE1* was increased in the Δ*gtr1* strain. Furthermore, expression of genes associated with biofilm formation and cell wall associated proteins were increased in the Δ*gtr1* strain in comparison to the Δ*rhb1* strain. These differences in gene expression correlate with results seen in chapter 4. Phenotypic analysis of the Δ*gtr1* strain showed that it aggregated and flocculated to a greater extent than the Δ*rhb1* strain. This could be due to the enhanced expression of the *ALS* genes seen in the Δ*gtr1* strain. Additionally, the data above suggests a role for the expression of genes associated with nitrogen utilisation via Rhb1-Tor1 signaling since the Δ*rhb1* strain showed an increase in *MEP2*, *OPT3*, *OPT1*, *SAP2* and *DUR1,2* compared with the Δ*gtr1* strain.

Interestingly, *GLN3* is up-regulated in the Δ*rhb1* strain and down-regulated in the Δ*gtr1* strain, while *GAP1* is down-regulated in the Δ*rhb1* strain and up-regulated in the Δ*gtr1* strain. As discussed previously (chapter 1), *GAP1* is a general amino acid permease that is controlled by NCR, and the transcription of *GAP1* is regulated by the GATA transcription factors Gln3 and Gat1. The expression analysis presented here suggests that Rhb1 appears to be involved in the Tor1 repressed signaling of *GAP1* expression.

These results suggest distinct roles for the Gtr1-Tor1 and Rhb1-Tor1 signaling to express different gene sets when *C. albicans* is grown in unfavorable conditions. Furthermore, these differences observed between the Δ*gtr1* strain and Δ*rhb1* strain may suggest multiple Tor1 complexes involved in the multiple responses due to environmental signals. The construction of a double Δ*gtr1*::Δ*rhb1* mutant may allow further insight into the Gtr1-Tor1 / Rhb1-Tor1 signaling pathway and whether it results in cellular arrest or the identification of other unknown activators of Tor1.

Chapter 6

Transcriptome Analysis of the Doxycycline Regulated Expression of *Candida albicans TOR1*

6.1 Introduction

The target of rapamycin (Tor1), a serine/threonine kinase is a highly conserved eukaryotic kinase. As discussed in chapter 1, the Tor1 kinase is a central regulator in nutrient sensing that was first identified in the analysis of *S. cerevisiae* mutants that conferred resistance to the drug rapamycin. The Tor1 protein is stimulated by nutrients and an active Tor1 kinase in turn phosphorylates target proteins promoting ribosome biogenesis and glycolysis. In an environment rich in nitrogen sources, the GATA transcription factors Gln3 and Gat1 are phosphorylated and restricted to the cytoplasm and the phosphatase Sit4 is inhibited by Tor1 restriction. However, in a nitrogen poor environment Tor1 is inhibited, resulting in the release of Sit4, which in turn dephosphorylates Gln3 and Gat1. These GATA transcription factors are free to translocate to the nucleus and allow for the transcriptional activation of genes involved in the metabolism of poorer nitrogen sources. To date, *S. cerevisiae* has been the model organism for Tor1 research. However, in *C. albicans* nitrogen availability is important in regulating observed phenotypes that are associated with virulence such as protease secretion, filamentation and adhesion.

Previously, data presented here has focused on phenotypic analysis of strains overexpressing the putative activators of Tor1 as well as *TOR1*. Chapter 3 demonstrated that overexpression studies resulted in decreased levels of hyphal formation on nitrogen limiting medium compared to wild-type cells. Additionally, overexpression strains aggregated less and demonstrated a lower level of flocculation compared with wild-type cells. Moreover, the overexpression strains exhibited a decrease in biofilm formation on abiotic surfaces concluding that overexpression resulted in a hyperactive Tor1 phenotype. Furthermore, analyses of a homozygous *GTR1* and *RHB1* mutant revealed that aggregation and biofilm formation were increased in both the Δ*gtr1* and Δ*rhb1* strains while flocculation was only observed in the Δ*gtr1* strain, suggesting distinct roles for Rhb1 and Gtr1 signaling to the Tor1 kinase (Chapter 5).

As *TOR1* is an essential gene, a homozygous mutant could not be generated as it would

result in cellular arrest. In the current study, we have used a heterozygous *tor1* mutant with the tetracycline regulated tetO promoter placed upstream of the intact *TOR1* allele (JKC1549), a gift from Dr. Julia Koehler (Harvard University). Furthermore, we have also examined a second heterozygous mutant where the tetO promoter has been positioned upstream of a truncated copy of *TOR1* where the N-terminal encoding domain (the HEAT repeat domain) has been removed (JKC1441). Here we examine the transcriptome of *C. albicans* when *TOR1* expression is repressed with the inhibitor doxycycline.

6.2 Materials and Methods

The two-colour DNA microarray-based gene expression protocol was carried out as detailed in section 2.15. The JKC1549 (tetO-*TOR1/tor1*) and JKC1441 (tetO-ΔN*TOR1* truncated) mutant strains were compared with the JKC1347 (Heterozygous *TOR1/tor1*) strain. Each strain was plated from frozen onto YEPD containing 100 ng of doxycycline (to initiate *TOR1* inhibition) and incubated for 24 h at 37 °C. Following incubation, cells were washed from plates with 1 ml 1X PBS, centrifuged at 15,000 x g for 1 min and washed once more with 1X PBS. The supernatant was discarded and the pellet resuspended in 1 ml 1X PBS and this suspension was used to inoculate a 50 ml YEPD culture of each strain with an OD_{600} of 0.1 nm. Strains were incubated at 37 °C with shaking at 200 rpm for 2 h and 8 h respectively and each sample was frozen for RNA extractions as detailed in section 2.5.2. A total of four biological replicates per strain were set up side by side for the microarray slides.

6.3 Results

6.3.1 Investigation of the Effects of a Doxycycline-Off *TOR1*

Two-colour DNA microarrays were used to compare gene expression profiles of doxycycline regulatable *TOR1* strains. Gene expression profiles of JKC1549 and JKC1441 were compared to JKC1347 following 2 h and 8h incubation in 30 μg/ml doxycycline. For the DNA microarray, the fluorescence data of the oligonucleotide probes for each reading frame was averaged over 4 microarray slides and classed as single entities. Each entity represented one probe sequence for an open reading frame. Using GeneSpring v13.0, statistical tests were applied to allow for averaging and normalising of samples. Further filters were applied ensuring stringent exclusion of weak fluorescence signals and a Student's t-test was carried out on the averaged biological samples with a p-value cut-off of 0.05. Finally, an asymptotic correction was applied to the data using the Storey with bootstrapping method with a q-value cut-off of 0.05.

6.3.1.1 Genes Expressed at Higher Levels in the tetO-*TOR1*/*tor1* Strain

Of the differentially expressed genes, 366 were considered to be significantly expressed at a higher level in the tetO-*TOR1*/*tor1* strain following 2 h in doxycycline compared with the heterozygous *tor1*/*TOR1* strain. Genes that exhibited a greater than 1.5 fold expression alteration, were submitted to the Gene Ontology (GO)-term slim mapper service on the Candida Genome Database (CGD). This tool allowed for the identification of the major branches of the ontologies common to a list of genes or ORFs, based on their GO annotations.

First, a GO-Slim search for genes associated with the category "biological function" was applied and identified genes with the roles shown in table 6.1a. Second, a GO-Slim search for genes associated with the category "biological process" was run and identified genes with the roles shown in table 6.1b.

6.3.1.2 Genes Expressed at Lower Levels in the tetO-*TOR1*/*tor1* Strain

Of the differentially expressed genes, 339 were significantly expressed at a lower level in the tetO-*TOR1*/*tor1* strain following 2 h in doxycycline compared with the heterozygous *tor1*/*TOR1* strain. These genes were submitted to GO-term slim mapper service on the CGD.

First, a GO-Slim search for genes associated with the category 'biological function' was applied and the results are represented in table 6.2a. Following this, a GO-Slim search for genes associated with the category 'biological process' was run which are shown in table 6.2b.

6.3.1.3 Genes Expressed at Higher Levels in the tetO-ΔN*TOR1* Strain

Following on from the analysis of the tetO-*TOR1* mutant, the functions of genes differentially expressed in the tetO-ΔN*TOR1* strain JKC1441 following growth in doxycycline for 2h were analysed. Of the differentially expressed genes, 534 were considered to be significantly expressed at a higher level (> 1.5-fold) in the tetO-ΔN*TOR1* JKC1441 strain compared with the *tor1*/*TOR1* strain. Genes with greater than 1.5-fold expression were submitted to the GO-Slim mapper service on the Candida Genome Database.

First, a GO-Slim search for genes associated with the category 'biological function' was applied and the results shown in table 6.3a. Following this, a GO-Slim search for genes associated with the category 'biological process' was run and the results shown in table 6.3b.

6.3.1.4 Genes Expressed at Lower Levels in the tetO-ΔN*TOR1* Strain

Of the differentially expressed genes, 475 were considered to be significantly expressed at a lower level (< 1.5-fold) in the tetO-ΔN*TOR1* JKC1441 strain compared with the *tor1*/*TOR1* strain. These genes were submitted to GO-term slim mapper service on the Candida Genome Database.

First, a GO-Slim search for genes associated with the category 'biological function'

was applied and the genes with associated biological function are shown in table 6.4a. Following the Go-Slim function, a GO-Slim search for genes associated with the category 'biological process' was run and the genes associated with biological processes are shown in table 6.4b

6.3.1.5 Genes Expressed at Higher Levels in the tetO-ΔN*TOR1* Compared with the *tor1/TOR1* Strain

Following on from the analysis of the *tetO*-Δ*NTOR1* mutant following doxycycline treatment, we examined the functions of genes differentially expressed between the tetO-Δ*NTOR1* strain and *tor1/TOR1* strain following growth of 2 h without doxycycline. This experiment was designed to determine the role of the N terminal region of the Tor1 protein, specifically that of the HEAT repeat domain. Of the differentially expressed genes, 710 were considered to be significantly expressed at a higher level (> 1.5-fold) in the tetO-Δ*NTOR1* strain compared with the *tor1/TOR1* strain. Genes with greater than 1.5-fold expression were submitted to the GO-Slim mapper service on the Candida Genome Database.

First, a GO-Slim search for genes associated with the category 'biological function' was applied and the results shown in table 6.5a. Following this, a GO-Slim search for genes associated with the category 'biological process' was run and the results shown in table 6.5b.

6.3.1.6 Genes Expressed at Lower Levels in the tetO-ΔN*TOR1* Strain Compared with the *tor1/TOR1* Strain

Of the differentially expressed genes, 710 were considered to be significantly expressed at a lower level (< 1.5-fold) in the tetO-Δ*NTOR1* strain compared with the *tor1/TOR1* strain. These genes were submitted to GO-term slim mapper service on the Candida Genome Database.

First, a GO-Slim search for genes associated with the category 'biological function'

was applied and the genes with associated biological function are shown in table 6.6a. Following the Go-Slim function, a GO-Slim search for genes associated with the category 'biological process' was run and the genes associated with biological processes are shown in table 6.6b

6.3.1.7 Comparison of Differentially Expressed Genes in tetO-*TOR1*/*tor1* and tetO-ΔN*TOR1* Strains and Rapamycin Treated Cells

Next the gene expression changes in the tetO-*TOR1* stains (both tetO-*TOR1* & tetO-Δ*NTOR1*) were compared with published microarray data examining changes in gene expression in *C. albicans* following exposure to rapamycin. All genes exhibiting a 1.5-fold increase (Fig. 6.1) or 1.5-fold decrease (Fig. 6.2) in expression relative to controls in each experiment were compared using Venn diagrams. When all three data sets were compared, 122 rapamycin induced genes were also found to be induced following doxycycline treatment of either tetO-*TOR1* strain. Furthermore, 66 rapamycin repressed genes were found to be repressed following doxycycline treatment of the tetO-*TOR1* strains. A Go-Slim search for genes associated with the category 'biological function' and 'biological process' was run and represented in table 6.7 and 6.8.

Table 6.1: **GO-Slim mapper results of the tetO-*TOR1/tor1* expressed at higher levels.**

(a) GO-Slim Biological Function

Go Term	Frequency
Molecular Function (Unknown)	139 out of 366 genes, 38%
Hydrolase Activity	46 out of 366 genes, 12.6%
DNA Binding	39 out of 366 genes, 10.7%
Transport Activity	29 out of 366 genes, 7.9%
RNA Binding	23 out of 366 genes, 6.3%
Protein Binding	20 out of 366 genes, 5.5%

(b) Go-Slim Biological Process

Go Term	Frequency
Biological Processes (Unknown)	99 out of 366 genes, 27.0%
RNA Metabolic Processes	65 out of 366 genes, 17.8%
Filamentous Growth	49 out of 366 genes, 13.4%
Ribosome Biogenesis	29 out of 366 genes, 7.9%
Carbohydrate Metabolic Processes	20 out of 366 genes, 5.5%
Translation	19 out of 366 genes, 5.2%
Pathogenesis	17 out of 366 genes, 4.6%

Table 6.2: **GO-Slim mapper results of the tetO-*TOR1/tor1* expressed at lower levels.**

(a) GO-Slim Biological Function

Go Term	Frequency
Molecular Function (Unknown)	145 out of 339 genes, 42.8%
Transferase Activity	45 out of 339 genes, 13.3%
Hydrolase Activity	37 out of 339 genes, 10.9%
Oxidoreductase Activity	28 out of 339 genes, 8.3%
Protein Binding	25 out of 339 genes, 7.4%
Phosphatase Activity	8 out of 339 genes, 2.4%

(b) Go-Slim Biological Process

Go Term	Frequency
Biological Processes (Unknown)	115 out of 339 genes, 33.9%
Response to Stress	32 out of 339 genes, 9.4%
Filamentous Growth	32 out of 339 genes, 9.4%
Response to Chemical	30 out of 339 genes, 8.8%
Cell Cycle	12 out of 339 genes, 3.5%
Pathogenesis	11 out of 339 genes, 3.2%
Biofilm Formation	9 out of 339 genes, 2.7%

Table 6.3: **GO-Slim mapper results of the tetO-ΔN*TOR1* expressed at higher levels.**

(a) GO-Slim Biological Function

Go Term	Frequency
Molecular Function (Unknown)	146 out of 534 genes, 27.3%
Hydrolase Activity	95 out of 534 genes, 17.8%
RNA Binding	79 out of 534 genes, 14.8%
Protein Binding	54 out of 534 genes, 10.1%
Transporter Activity	34 out of 534 genes, 6.4%
Protein Kinase Activity	9 out of 534 genes, 1.7%

(b) Go-Slim Biological Process

Go Term	Frequency
RNA Metabolic Process	141 out of 534 genes, 26.4%
Ribosome Biogenesis	91 out of 534 genes, 17.0%
Response to Stress	80 out of 534 genes, 15%
Filamentous Growth	46 out of 534 genes, 8.6%
Cellular Protein Modification Process	34 out of 534 genes, 6.4%
Pathogenesis	26 out of 534 genes, 4.9%
Biofilm Formation	10 out of 534 genes, 1.9%

Table 6.4: **GO-Slim mapper results of the tetO-ΔN*TOR1* expressed at lower levels.**

(a) GO-Slim Biological Function

Go Term	Frequency
Transferase Activity	73 out of 477 genes, 15.3%
Oxidoreductase Activity	47 out of 477 genes, 9.9%
Transporter Activity	39 out of 477 genes, 8.2%
Protein Binding	32 out of 477 genes, 6.7%
Phosphatase Activity	14 out of 477 genes, 2.9%
Protein Kinase Activity	6 out of 477 genes, 1.3%

(b) Go-Slim Biological Process

Go Term	Frequency
Biological Processes (Unknown)	142 out of 477 genes, 29.8%
Transport	83 out of 477 genes, 17.4%
Regulation of Biological Process	81 out of 477 genes, 17%
Organelle Organisation	50 out of 477 genes, 10.5%
Cellular Protein Modification Process	47 out of 477 genes, 9.9%
Carbohydrate Metabolic Process	36 out of 477 genes, 7.5%
Cell Cycle	17 out of 477 genes, 3.6%

Table 6.5: **GO-Slim mapper results of the tetO-ΔN*TOR1* compared with the *tor1/TOR1* strain expressed at higher levels.**

(a) Go-Slim Biological Process

Go Term	Frequency
Hydrolase Activity	124 out of 749 genes, 16.6%
Transferase Activity	90 out of 749 genes, 12.0%
Protein Binding	65 out of 749 genes, 8.7%
DNA Binding	61 out of 749 genes, 8.1%
Transporter Activity	59 out of 749 genes, 7.9%
Oxidoreductase Activity	46 out of 749 genes, 6.1%

(b) GO-Slim Biological Function

Go Term	Frequency
Ribosome Biogenesis	131 out of 749 genes, 17.5%
Response to Stress	106 out of 749 genes, 14.2%
Filamentous Growth	68 out of 749 genes, 9.1%
Pathogenesis	38 out of 749 genes, 5.1%
Carbohydrate Metabolic Process	24 out of 749 genes, 3.2%
Hyphal Growth	17 out of 749 genes, 2.3%
Biofilm Formation	16 out of 749 genes, 2.1%

Table 6.6: **GO-Slim mapper results of the tetO-ΔN*TOR1* compared with the *tor1/TOR1* strain expressed at lower levels.**

(a) GO-Slim Biological Function

Go Term	Frequency
Transferase Activity	121 out of 710 genes, 17.0%
Oxidoreductase Activity	78 out of 710 genes, 11%
Phosphatase Activity	28 out of 710 genes, 3.9%
Enzyme Regulator Activity	22 out of 710 genes, 3.1%
Peptidase Activity	11 out of 710 genes, 1.5%
Protein Kinase Activity	9 out of 710 genes, 1.3%

(b) Go-Slim Biological Process

Go Term	Frequency
Biological Processes (Unknown)	198 out of 710 genes, 27.9%
Transport	129 out of 710 genes, 18.2%
Regulation of Biological Process	117 out of 710 genes, 16.5%
Carbohydrate Metabolic Process	62 out of 710 genes, 8.7%
Vesicle-Mediated Transport	31 out of 710 genes, 4.4%
Cell Cycle	28 out of 710 genes, 3.9%
Protein Catabolic Process	19 out of 710 genes, 2.7%

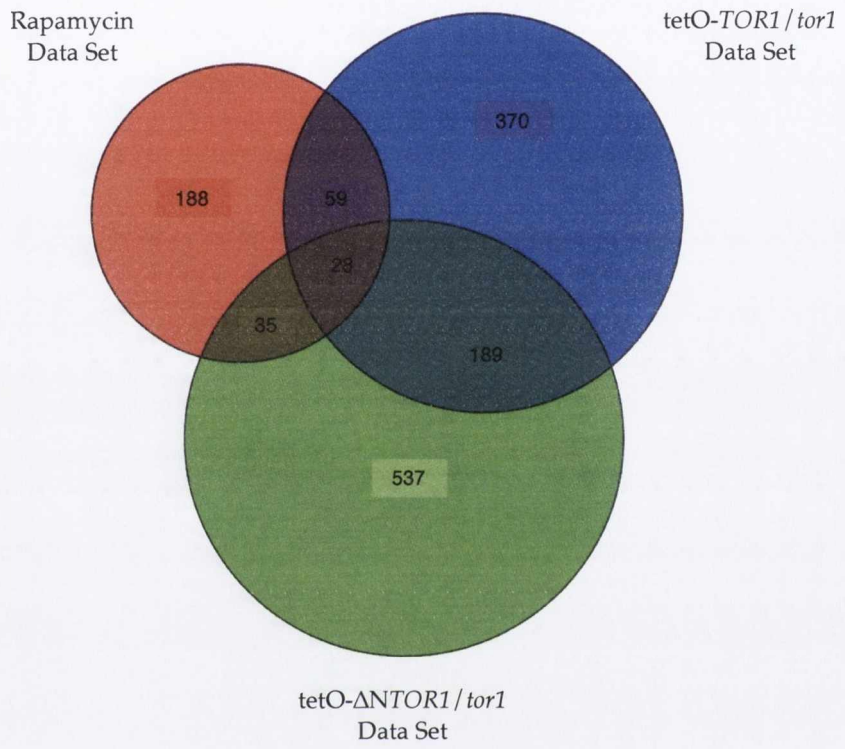

Figure 6.1: **Overview of overlap (1.5-fold increase) in DNA microarray datasets.**

Venn diagram showing the common number of genes with a 1.5-fold or more increase between each of the three DNA microarray datasets.

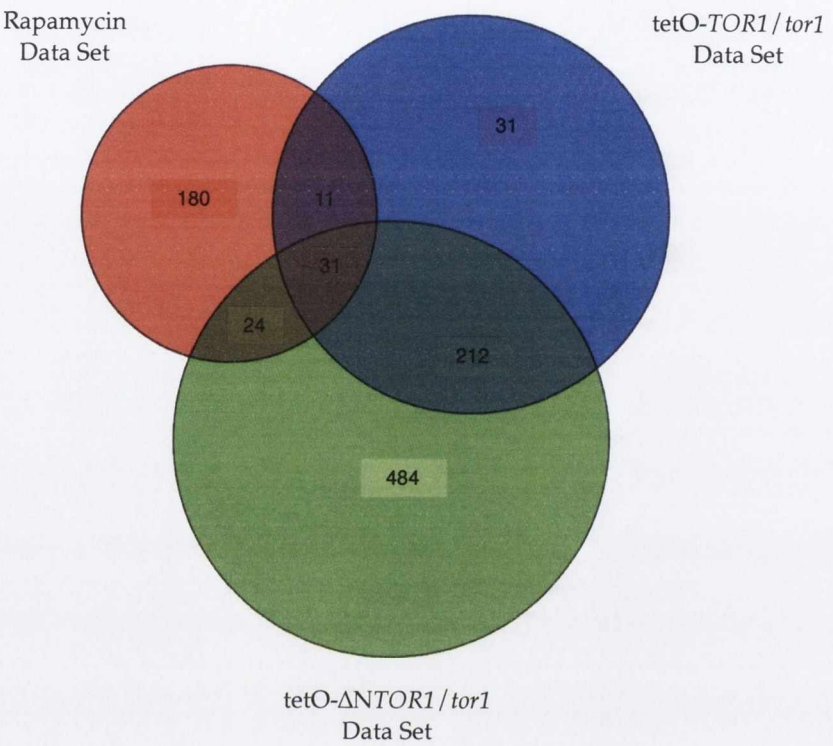

Figure 6.2: **Overview of overlap (1.5-fold decrease) in DNA microarray datasets.**
Venn diagram showing the common number of genes with a 1.5-fold or more decrease between each of the three DNA microarray datasets.

Table 6.7: **GO-Slim mapper results of the tetO-*TOR1* strains with similar gene expression to the rapamycin treated strain (> 1.5-fold).**

(a) GO-Slim Biological Function

Go Term	Frequency
Transporter Activity	35 out of 112 genes, 30.4%
Hydrolase Activity	17 out of 112 genes, 14.8%
Oxidoreductase Activity	11 out of 112 genes, 9.6%
Protein Binding	4 out of 112 genes, 3.5%
Peptidase Activity	4 out of 112 genes, 3.5%
Transferase Activity	4 out of 112 genes, 3.5%

(b) Go-Slim Biological Process

Go Term	Frequency
Transport	40 out of 112 genes, 34.8%
Response to Chemical	27 out of 112 genes, 23.5%
Regulation of Biological Process	26 out of 112 genes, 22.6%
Filamentous Growth	21 out of 112 genes, 18.3%
Response to Drug	20 out of 112 genes, 17.4%
Response to Stress	17 out of 112 genes, 14.8%
Biofilm Formation	8 out of 112 genes, 7%
Cell Adhesion	3 out of 1152 genes, 2.6%

Table 6.8: **GO-Slim mapper results of the tetO-*TOR1* strains with similar gene expression to the rapamycin treated strain (< 1.5-fold).**

(a) GO-Slim Biological Function

Go Term	Frequency
Oxidoreductase Activity	16 out of 66 genes, 26.7%
Transferase Activity	15 out of 66 genes, 25%
Molecular Function Unknown	10 out of 66 genes, 16.7%
Transporter Activity	7 out of 66 genes, 11.7%
Protein Binding	4 out of 66 genes, 6.7%
Phosphatase Activity	1 out of 66 genes, 1.7%

(b) Go-Slim Biological Process

Go Term	Frequency
Transport	11 out of 66 genes, 18.3%
Biological Process (Unknown)	8 out of 66 genes, 13.3%
Generation of Precursor Metabolites & Energy	5 out of 66 genes, 8.3%
Carbohydrate Metabolic Process	4 out of 66 genes, 6.7%
Cellular Homeostasis	3 out of 66 genes, 5%
Protein Catabolic Process	2 out of 66 genes, 3.3%
Lipid Metabolic Process	2 out of 66 genes, 3.3%

6.3.2 Gene Set Enrichment Analysis

6.3.2.1 Analysis of the tetO-*TOR1/tor1* strain by GSEA

Gene set enrichment analyses were performed using the Broad Institute GSEA software v2.2.2. GSEA was used to identify enrichments in our differentially expressed genes with a database of published gene sets including published microarray data, global ChIP data, predicted protein-protein interactions and Gene Ontologies. The data obtained were then exported to Cytoscape v3.3.0 in order to create a visual network of related functional groups of genes that were differentially expressed. Analysis of the tetO-*TOR1/tor1* strain JKC1349 following 2 h growth in doxycycline identified several networks of related gene sets that exhibited increased expression (Fig 6.3). These included gene sets associated with ribosome biogenesis (Fig. 6.3a), cell wall, adhesion and pathogenesis (Fig. 6.3b) and nutrient transport (Fig. 6.3c). A further analysis was performed on the tetO-*TOR1/tor1* strain comparing differences in gene expression between 2 h and 8 h doxycycline exposure. Selected functional gene clusters of the 2 h and 8 h comparison can be seen in figure 6.4. Genes involved in cell wall and adhesion processes that were induced at 2h (denoted by red centre; Fig. 6.4a) exhibited no increase or decreased expression at 8h (denoted by circle border, white [no increase] or blue [decreased expression]; Fig. 6.4a). Some genes associated with nutrient transport exhibited decreased expression by 8 h (Fig. 6.4b). Genes associated with carbohydrate catabolism and biosynthetic processes exhibited a general shut down at 8 h (Fig. 6.4c). A full representation of all the functional clusters can be seen in figure S1.

6.3.2.2 Analysis of the tetO-ΔN*TOR1* JKC1441 strain by GSEA

Gene set enrichment analysis were also performed on the tetO-ΔN*TOR1* strain following 2 h growth in doxycycline. The data obtained from GSEA was exported to Cytoscape v3.3.0 and a network of functional groups of genes that were differentially expressed were constructed (Fig 6.5). This analysis identified several gene sets similar to those identified in JKC1549. Genes involved in purine and ribonucleotide biosynthesis

were down-regulated in JKC1441 (Fig 6.5a). In addition, genes associated with amino acid biosynthesis were shut down and amino acid uptake functions were induced (Fig 6.5b). Genes associated with biofilm formation, pathogenesis, adhesion, biological processes and host interaction were all induced (Fig. 6.5c). In addition stress responses and Ras1/cAMP regulated genes were induced (6.5d).

A further analysis was performed on the tetO-Δ*NTOR1* strain datasets comparing differentially expressed genes following 2 h and 8 h growth in doxycycline. Selected functional gene clusters identified in the 2 h and 8 h comparison can be seen in figure 6.6. Many genes associated with cell wall adhesion, pathogenesis and host defenses exhibited increased expression at 8 h (Fig. 6.6a). Genes associated with ribosome biogenesis exhibited an increase in expression by 8 h, as denoted by the red circle borders (Fig. 6.6b). Genes associated with carbohydrate catabolism and amino acid biosynthesis exhibited further decreased expression at 8 h (Fig. 6.6c) and many stress responses induced at 2 h were down-regulated at 8 h (Fig. 6.6d). A full representation of all the functional clusters can be seen in figure S2.

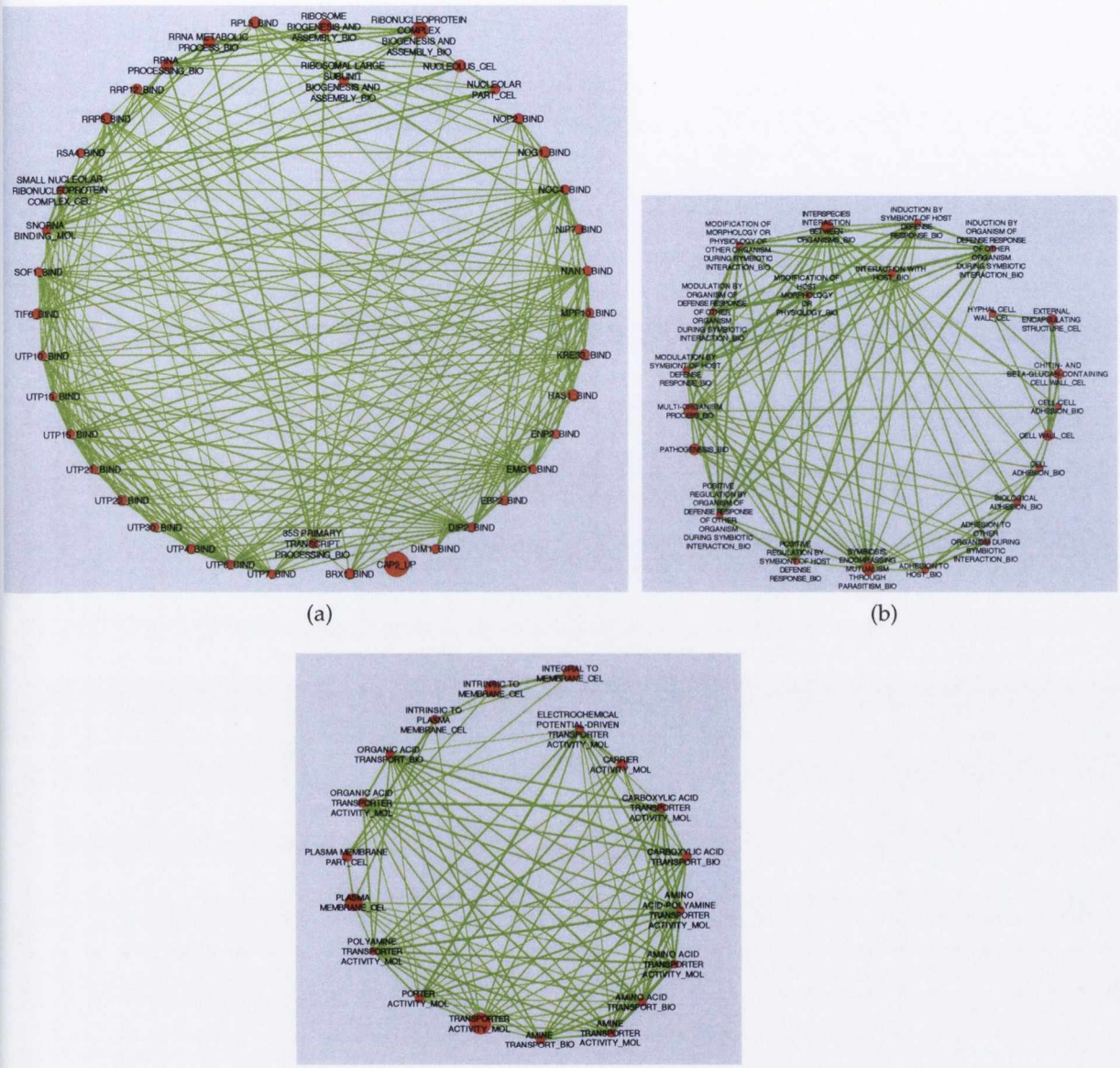

Figure 6.3: **Enrichment map of the genes differentially expressed in the tetO-*TOR1/tor1* strain at 2 h.**

Significantly enriched gene sets were identified with GSEA and visualised using Cytoscape. Circle diameters reflects the number of modulated gene transcripts in each gene set. Red indicates upregulated gene categories and blue downregulated. The thickness of the green connecting lines indicates the degree of similarity between categories. (a) Genes sets associated with ribosome biogenesis. (b) Gene sets associated with cell wall adhesion, pathogenesis and host defenses. (c) Gene sets associated with transport. A full representation of all the functional clusters can be seen on the accompanying CD at the back of this thesis

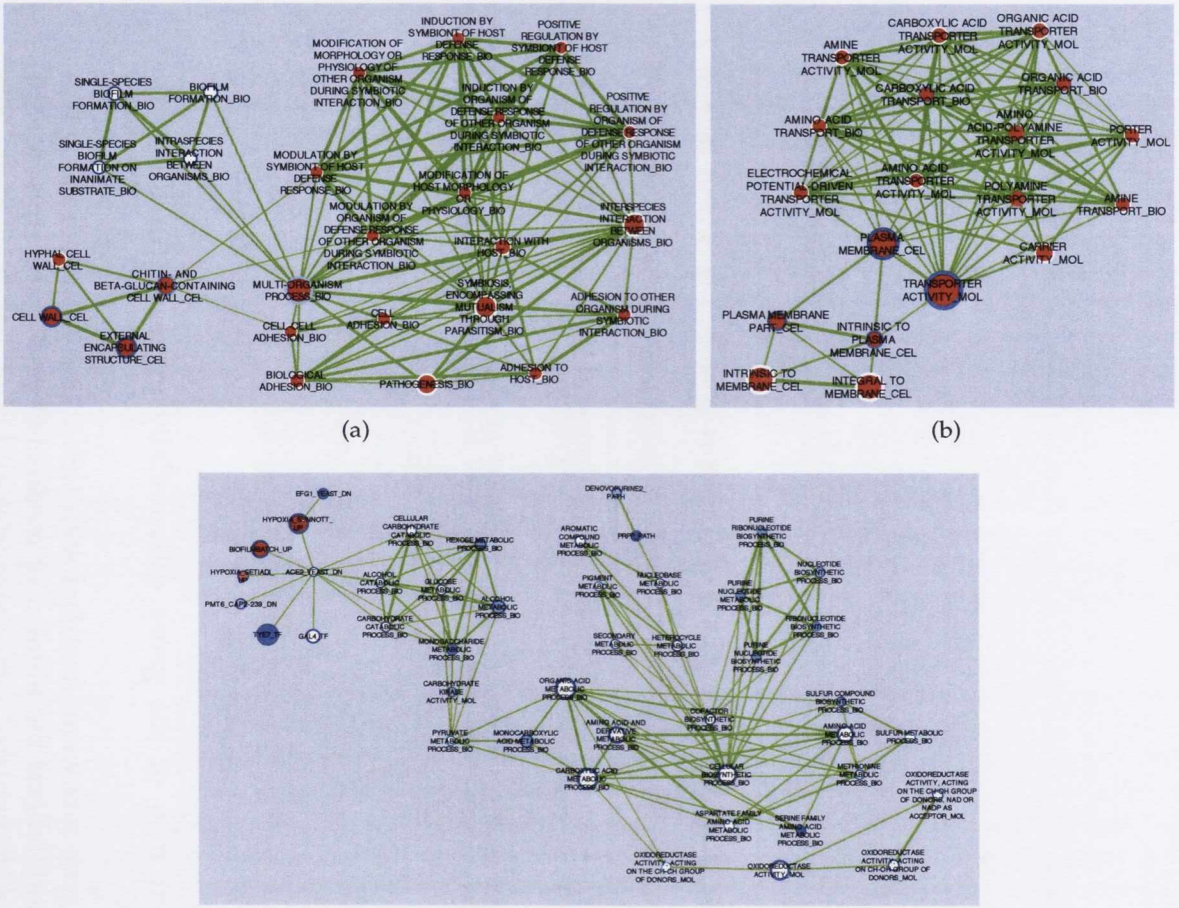

Figure 6.4: **Enrichment map of the genes differentially expressed (2 h v 8 h) in the tetO-*TOR1*/*tor1* strain.**

Significantly enriched gene sets were identified with GSEA and visualised using Cytoscape. Circle diameters reflects the number of modulated gene transcripts in each gene set. Red and blue centers indicate categories up or down-regulated at 2 h, respectively and red and blue circle borders indicate up or down regulation of the category at 8 h, respectively. The thickness of the green connecting lines indicates the degree of similarity between categories. White indicated no significant enrichment at that time point. (a) Genes associated with adhesion, pathogenesis and cell wall. (b) Genes associated with ribosome biosynthesis. (c) Genes associated with amino acid biosynthesis and carbohydrate catabolism. A full representation of all the functional clusters can be

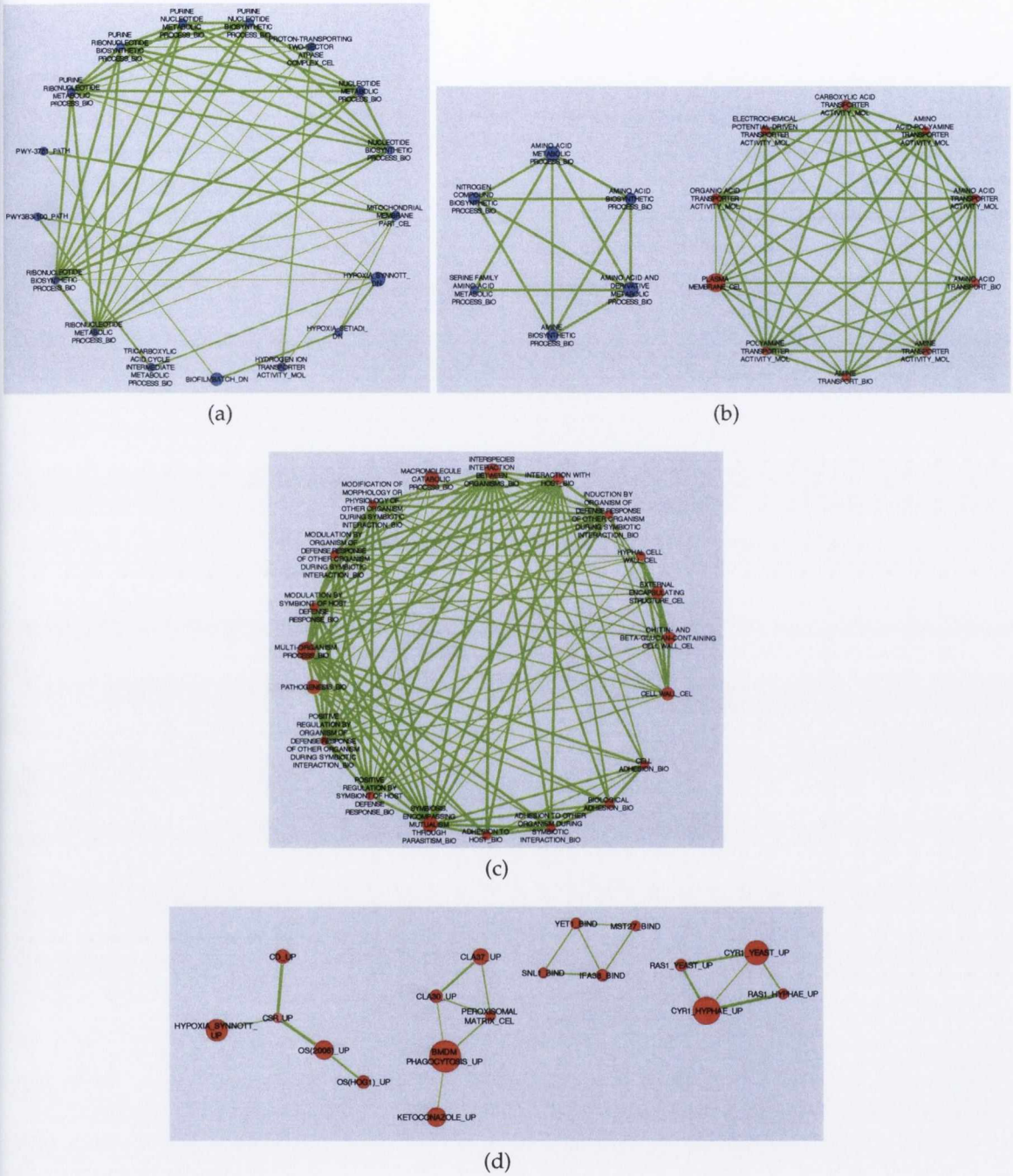

(a) (b) (c) (d)

Figure 6.5: **Enrichment map of the genes differentially expressed in the tetO-ΔN*TOR1* strain at 2 h.**
Significantly enriched gene sets were identified with GSEA and visualised using Cytoscape. Circle diameters reflects the number of modulated gene transcripts in each gene set. Red, up-regulated gene categories and blue down-regulated. The green connecting lines indicate the degree of similarity between categories. (a) Genes associated with ribonucleotide biosynthesis (b) Genes associated with amino acid biosynthesis and transport. (c) Genes associated with biofilm formation, pathogenesis, adhesion and biological processes. (d) Genes associated with stress responses and the Ras1/cAMP pathway. Full representation of all functional clusters can be seen on the accompanying CD at the back of this thesis

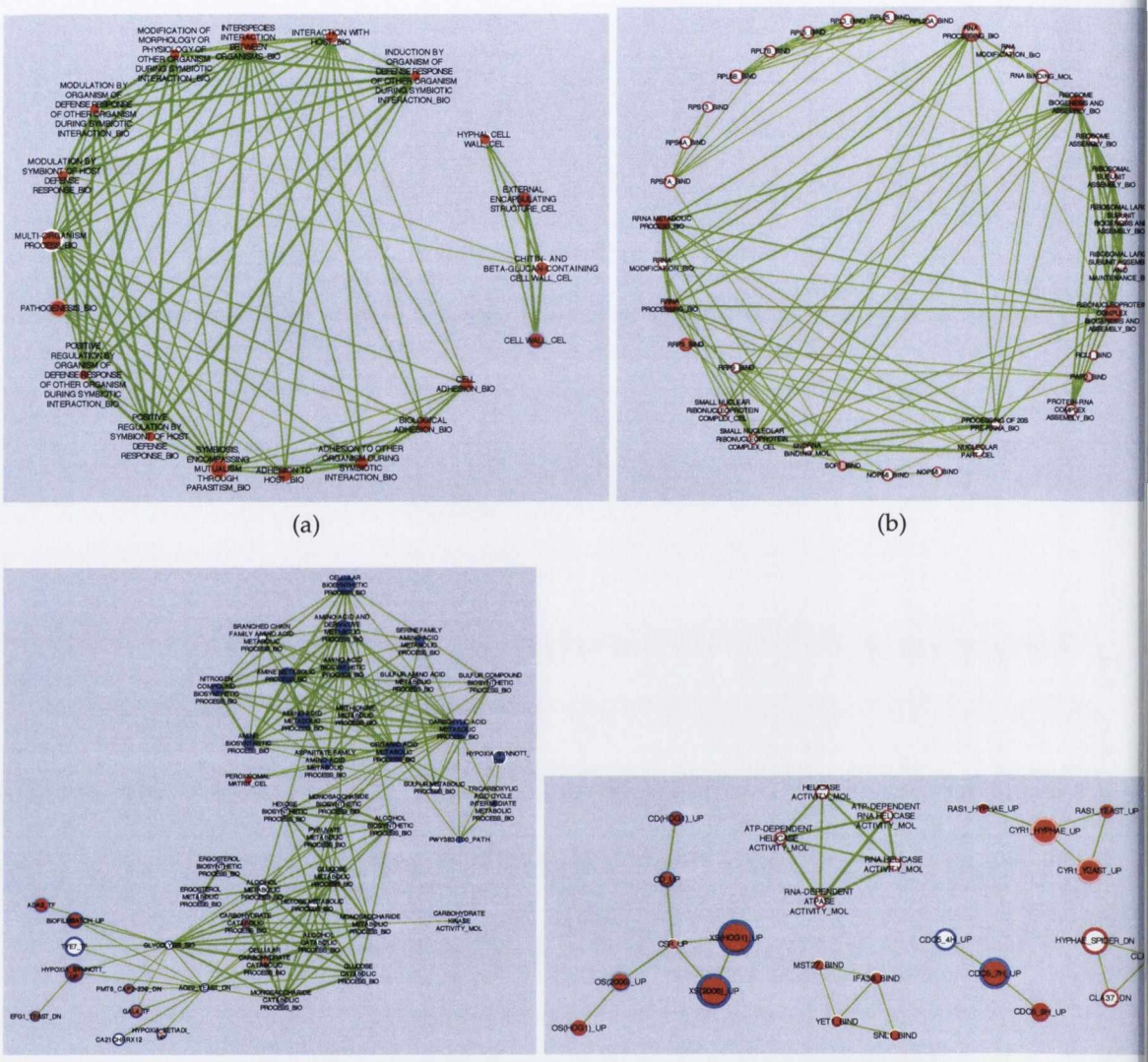

Figure 6.6: **Enrichment map of the genes differentially expressed (2 h v 8 h) in the tetO-ΔN*TOR1* strain.**
Significantly enriched gene sets were identified with GSEA and visualised using Cytoscape. Circle diameters reflects the number of modulated gene transcripts in each gene set. Red and blue centers indicate categories up or down-regulated at 2 h. Red and blue circle borders indicate up or down-regulation at 8 h. White illustrates no difference in expression level. Green connecting lines indicate the degree of similarity between categories. (a) Genes associated with cell wall adhesion, pathogenesis and host defenses. (b) Genes associated with ribosome biogenesis. (c) Genes associated with metabolic processes, amino acid biosynthesis and biofilm. (d) Genes associated with stress and the Ras1/cAMP pathway. A full representation of all the functional clusters can be seen on the accompanying CD at the back of this thesis

6.3.3 Heat Map Analysis

Further analyses were performed using the microarray software package GeneSring GX v13.0 to compare and contrast the differences observed in gene expression identified by GSEA. Heat maps were generated using the DNA microarray data of the tetO-*TOR1/tor1* and truncated JKC1441 strain at 2 h and 8 h. Furthermore, previously published DNA microarray data on rapamycin treatment and a Δ*rhb1* mutant (section 5.3.4) were imported to GeneSpring and compared alongside the tetO-*TOR1/tor1* and truncated JKC1441 strain.

6.3.3.1 Genes Associated with Ribosome Biogenesis & pre-RNA Processing & Assembly

As increased expression of genes involved in ribosome biogenesis was identified by GSEA (Fig 6.3a), we compared the expression of genes associated with the GO term "ribosome biogenesis and assembly" as shown in figure 6.7. The tetO-*TOR1/tor1* and tetO-Δ*NTOR1* strains both exhibited an increase in the expression of these genes, notably the tetO- Δ*NTOR1* strain at 8 h. These genes were most strongly induced following 8 h exposure to doxycycline. In contrast, the previously published rapamycin DNA microarray data show that rapamycin treatment results in decreased expression in genes associated with ribosome biogenesis. Additionally, differences were seen in the expression of genes associated with pre-RNA processing and assembly (Fig 6.8). These genes exhibited decreased expression in the rapamycin treated strain compared with increased expression in the tetO-TOR1 strains.

6.3.3.2 Genes Associated with Oxidative and Osmotic Stress

Similarities and differences were exhibited in genes associated with oxidative stress as shown in figure 6.9. The most notable differences occurred between the tetO-*TOR1* strains at 8 h. The tetO-Δ*NTOR1* strain exhibited an increase in the expression of genes *HNM3*, *MSN4*, *BIG1*, *UBA4* and *RAD16* relative to the expression of the expression

of these genes in the tetO-*TOR1/tor1* strain. Additionally, at 2 h the tetO-*TOR1/tor1* strain exhibited greater expression of genes *SSU1*, *SAP9*, *CDC4*, *AUR1*, *MOH1*, *TPO4* and *ECM22* relative to the expression of these genes in the tetO-ΔN*TOR1* strain. The genes associated with osmotic stress exhibited similar expression levels in all strains with the exception of those seen in figure 6.10. These included the genes *RVS162* at 2 h between the tetO-*TOR1/tor1* strains and *MYO1*, *PBS2*, *ZNC1*, *CMP1* and *YPD1* between the rapamycin treated strain and all tetO-*TOR1/tor1* strains. These genes are involved in the regulation of HOG1, signal transduction pathways and resistance to high pH, Na(+), Li(+) and Mn(2+).

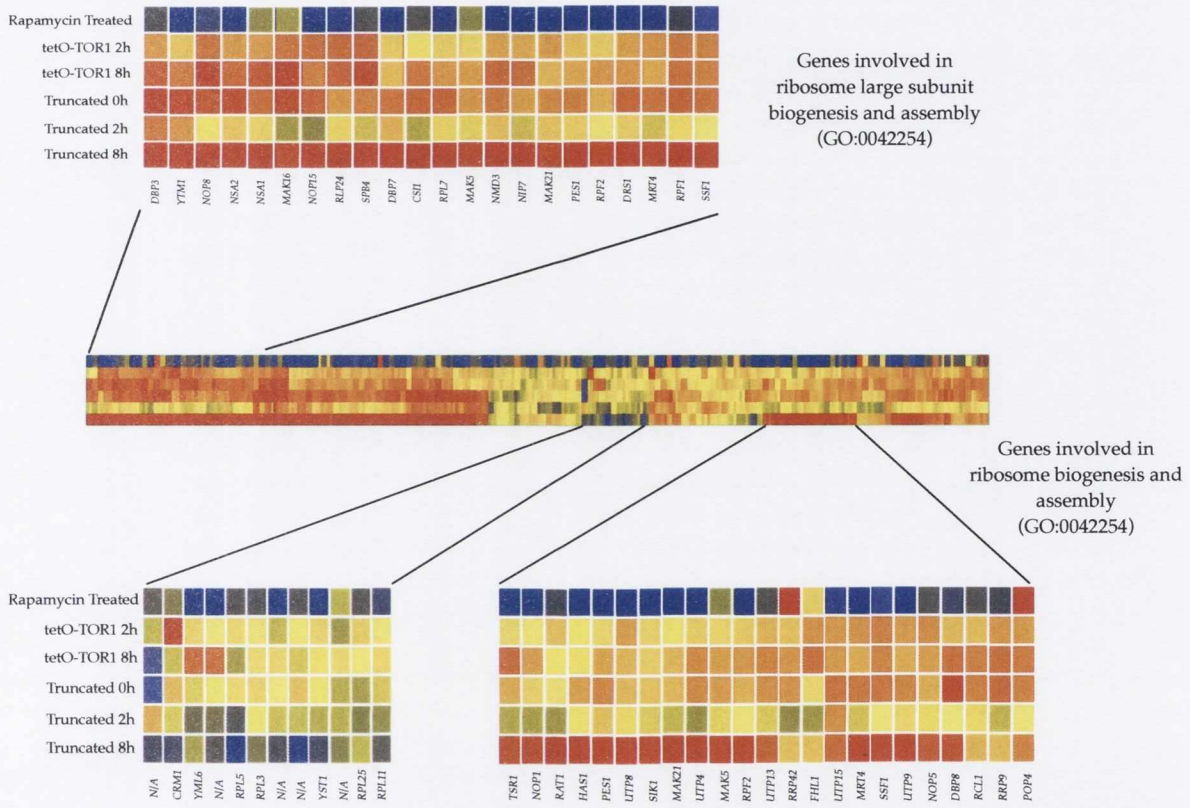

Figure 6.7: **Heat maps of differentially expressed genes involved in ribosomal biogenesis and assembly.**

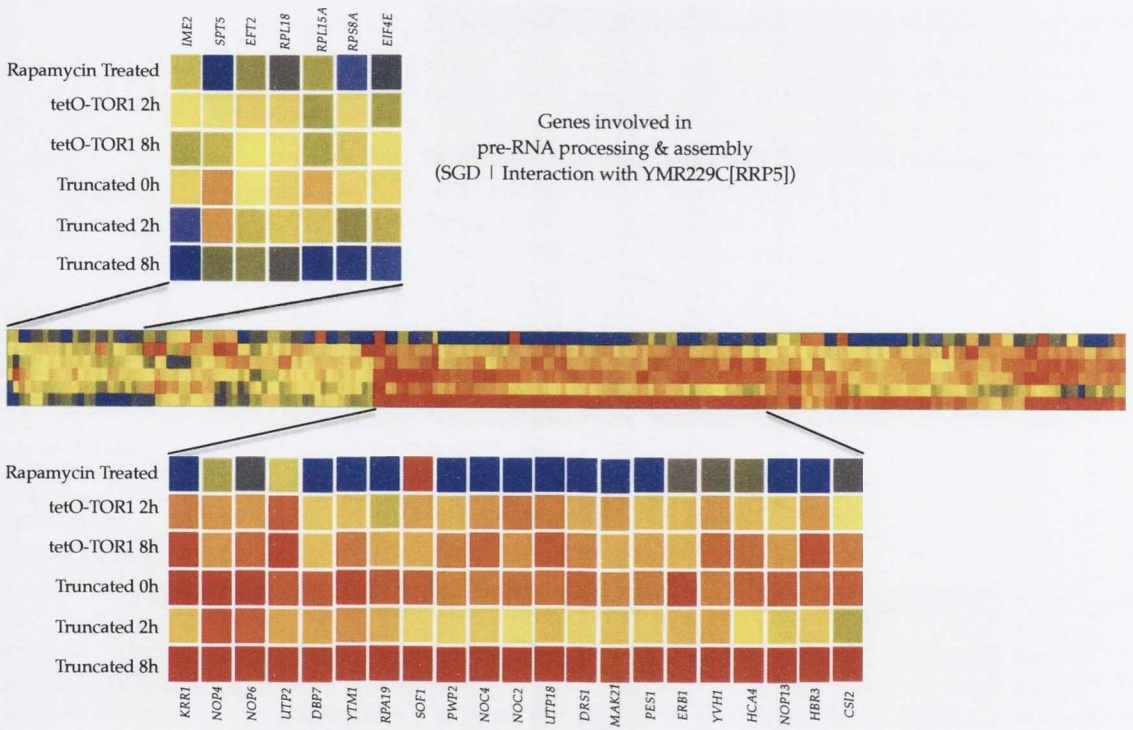

Figure 6.8: **Heat maps of differentially expressed genes involved in pre-RNA processing and assembly.**

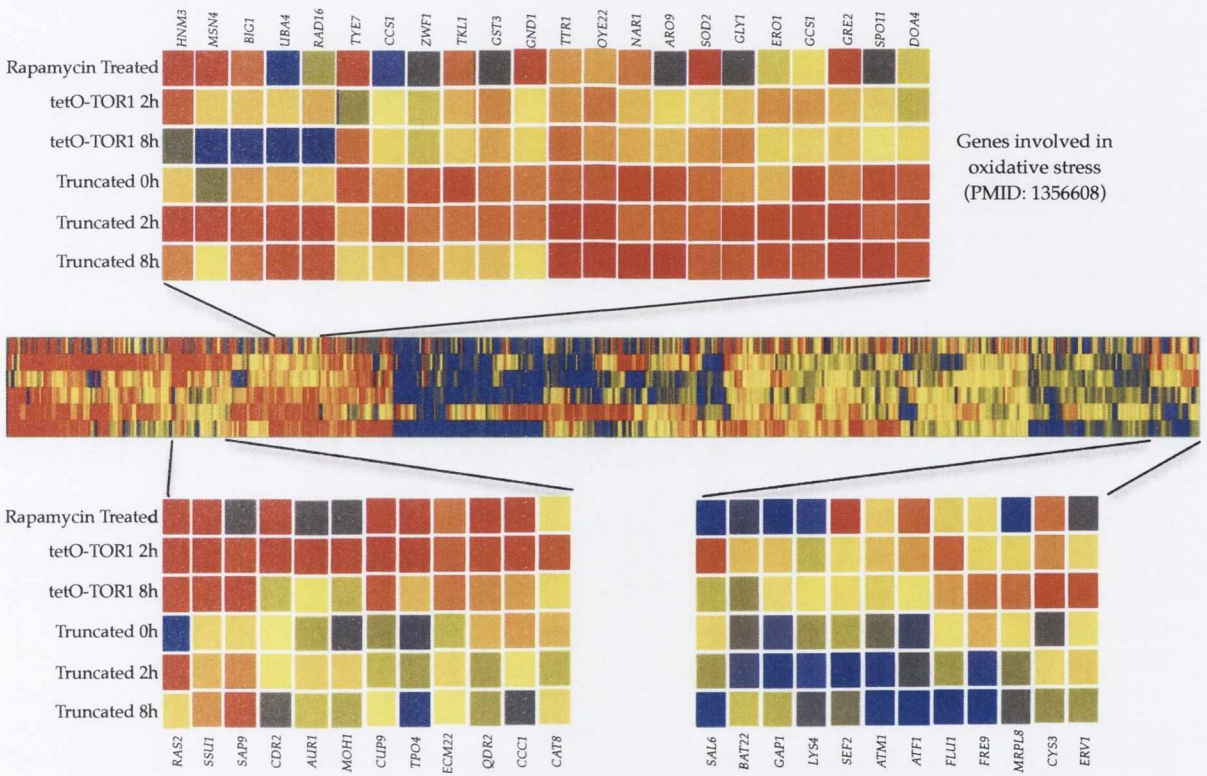

Figure 6.9: **Heat maps of differentially expressed genes involved in oxidative stress.**

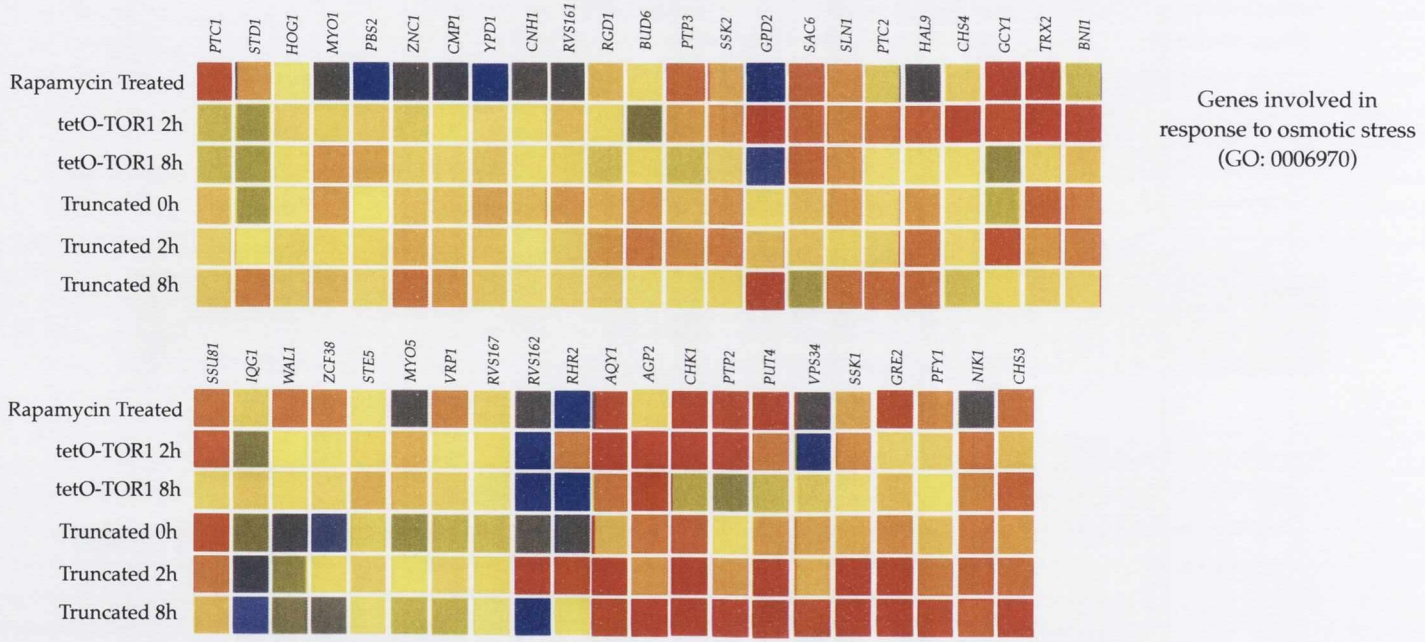

Figure 6.10: **Heat maps of differentially expressed genes involved in osmotic stress.**

6.3.4 qRT-PCR Confirmation of the DNA Microarray Expression Analysis

In order to confirm the observed gene expression from the DNA microarrays of the tetO-*TOR1* strains, qRT-PCR was performed on the RNA used for each strain in the DNA microarray. cDNA was generated as described in section 2.5.3 and qRT-PCR carried out as outlined in section 2.6.3. The qRT-PCR was performed on a selection of genes as shown in figure 6.11, confirming the results seen with the increased and decreased expression of genes in the DNA microarray data set. Analysis of the expression of *CAN2* and *MEP2* confirmed the observed pattern of induction of genes involved in nitrogen and amino acid uptake. Similarly, the phosphate transport genes (*PHO84* and *PHO112*) that were shown to be regulated by Gtr1 (Chapter 5 Fig. 5.5) were induced. We confirmed that genes involved in ribosome biogenesis exhibited increased expression in the case of *DIM1* (18s rRNA demethylase), *PES1* (large subunit maturation) and *RPF2* (ribosomal RNA processing) were induced by doxycycline and in that case of *DIM1* and *RPF2* exhibited higher levels of expression in JKC1441 even prior to doxycycline treatment. *RPS2* and *RPS3* were among the minority of ribosome associated genes showing decreased expression following doxycycline treatment (Fig. 6.9) and this could be confirmed by qRT-PCR.

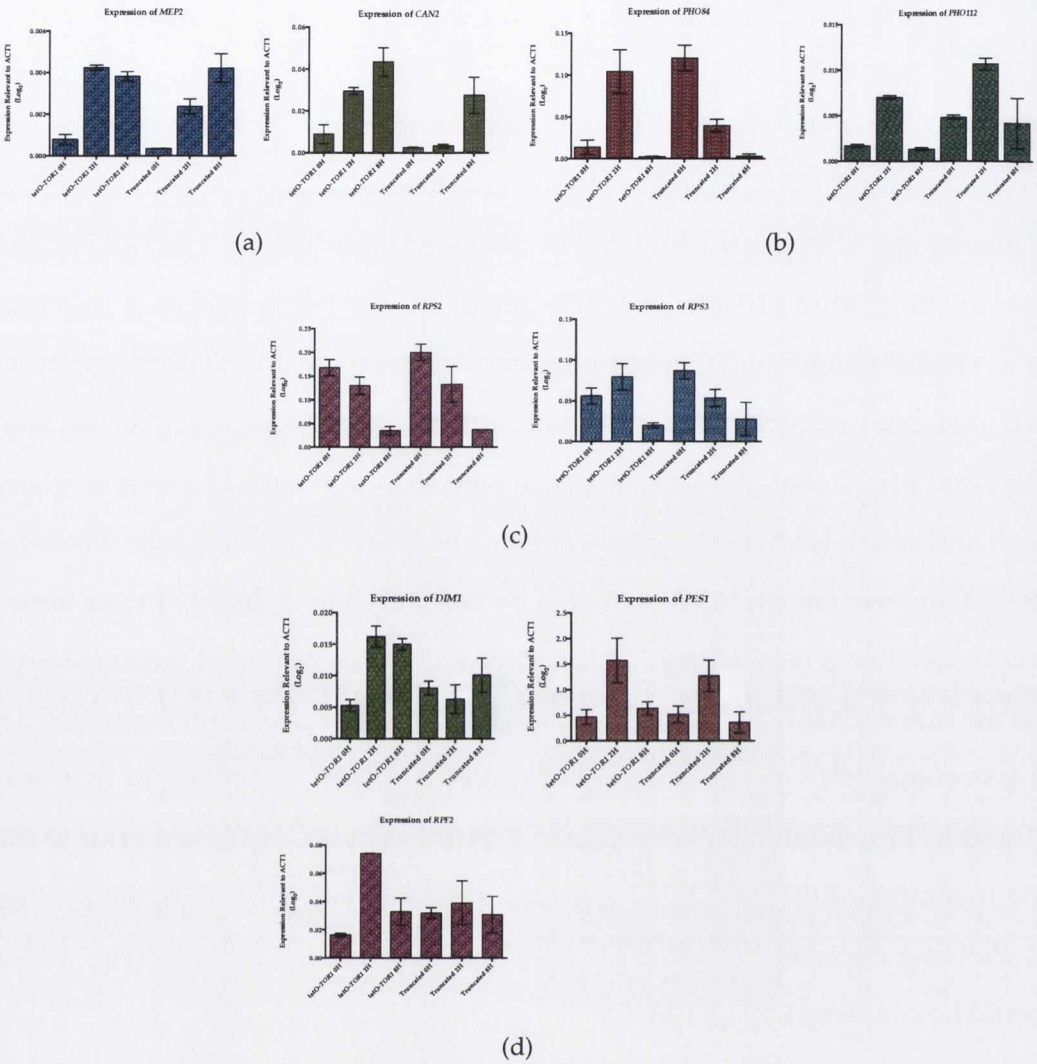

Figure 6.11: **qRT-PCR data of the DNA microarray.**

qRT-PCR analysis of a selection of genes differentially expressed in the DNA microarrays of the tetO-*TOR1* data sets.

6.4 Discussion

Virulence in *C. albicans* is a complex phenotype and is associated with the genes involved in adherence, hyphal formation and biofilm formation and basic metabolic flexibility to allow use of available nutrients in the host. Mutant strains of *C. albicans* that exhibit defects in hyphal formation show a reduction in virulence. Similarly, mutants unable to use alternative carbon or nitrogen sources are also less virulent [129, 123]. In Chapter 3 it was shown that over expression of the Tor1 activators had a constitutively active Tor1 phenotype. This phenotype resulted in a reduction in hyphal formation on medium containing a poor source of nitrogen and in some cases the inability to utilize BSA as a sole nitrogen source. Furthermore, in Chapter 4, phenotypic assays demonstrated that homozygous Δ*gtr1* and Δ*rhb1* mutants exhibited greater aggregation, flocculation and biofilm formation compared with a wild-type strain and in the case of the Δ*rhb1* mutant, a reduced capacity to grow in urea. These data suggests a role for Tor1 in regulating adherence and nutrient acquisition, which are key virulence traits in *C. albicans*. Here, we directly examined the effects of reducing the expression of *TOR1* itself using doxycycline-regulatable *TOR1* alleles, including a full length tetO-*TOR1*/*tor1* and truncated tetO-ΔN*TOR1* allele.

Upon comparison of the DNA microarray data sets, it is clear that Tor1 is involved in the activation of genes required for amino acid biosynthesis and nucleotide metabolism. Both of these categories were down-regulated in the full length tetO-*TOR1*/*tor1* strain and truncated tetO-ΔN*TOR1* strain treated with doxycycline. Activation of genes involved in nitrogen uptake was also observed in both strains following doxycycline treatment. Both of these responses (i.e. activation of nitrogen uptake and suppression of biosynthesis) are indicative of a starvation response which would be expected following suppression of Tor1 activity. There data also show a clear role for Tor1 in regulating virulence and pathogenesis. The addition of doxycycline to YEPD containing the tetO-*TOR1*/*tor1* strain resulted in the expression of genes associated with biological processes such as pathogenesis and filamentous growth (Table 6.1). These

processes were induced in both the full length tetO-*TOR1/tor1* and truncated tetO-ΔN*TOR1* strain following doxycycline treatment indicating that starvation responses and virulence functions are closely regulated.

Most of these starvation responses are induced to some extent in strain JKC1441, even without the addition of doxycycline, indicating that the N-terminal region is required for proper function of the protein. It is difficult to assign specific functions to this domain from the current data, although the fact that the strain is viable suggests that the kinase activities are functional, indicating that the truncated version of the protein may be compromised in interactions with other nutrient sensing molecules, hence the constitutive starvation phenotype.

Perhaps the most unexpected result of the current study is the increased expression of genes associated with ribosomal biogenesis and assembly, in particular the biogenesis and assembly of the large ribosomal subunit. Heat map analysis (Fig. 6.8 & 6.9) shows that these genes were expressed at higher levels in the tetO-*TOR1* strains, in particular the tetO-*TOR1/tor1* strain at 8 h. In rapamycin treated cells, the expression of these genes are decreased, and this is the effect that would be expected upon Tor1 depletion. The opposite effect observed here is unexpected and indicates that regulation of ribosome biogenesis is more complex than previously thought. Depletion of Tor1 kinase would be expected to decrease phosphorylation of the transcriptional factor Sfp1, resulting in reduced transcription of genes involved in ribosome biogenesis. It is difficult to speculate on the mechanism at action here, but it suggests that when ribosomal production is compromised that a stress response mechanism may be activated to boost levels of ribosomal gene transcription. Disruption of translation by cycloheximide also increases transcription of ribosomal genes by an unknown mechanism. The effects of chronic disruption of rRNA gene transcription may exert a similar effect on translation and induce a similar stress response by this unknown mechanism.

These results presented here suggest the role of Tor1 in pathogenesis since the doxycycline inhibition of *TOR1* resulted in the expression of genes associated with filamenta-

tion and pathogenesis. Furthermore, the data suggests that ribosomal biogenesis may be governed by alternate pathways to Tor1 due to either limiting nutrient availability or stress responses exerted on the cells.

Chapter 7

General Discussion

7.1 General Discussion

This study aimed to examine the role of the Tor1 kinase in the virulence of the opportunistic pathogen *C. albicans*. As previously stated, *C. albicans* is an opportunistic pathogen that can cause life-threatening infections in at risk patients, including those who are immunocompromised due to chemotherapy, immunosuppressive drugs, HIV infection or AIDS and those who have undergone invasive surgery. It is believed that the ability to cause an invasive infection is due to the dimorphic trait of *C. albicans*. The organism can exist in three states, yeast, pseudohyphae and true hyphae. The filamentous hyphal form can penetrate tissues and the bloodstream allowing for the dissemination of cells to other locations of the body. Further understandings of how the organism can switch between these different morphological forms may prove beneficial in combating infection.

It is believed that the Tor kinase plays an important role in the switch from yeast-to-hyphae. As discussed in Chapter 1, the Tor kinase is involved in the regulation of nitrogen metabolism. In a limiting nutrient environment, the GATA transcription factors Gln3 and Gat1, both of which are activated by Tor1, regulate the expression of *MEP2* (ammonium permease) and *SAP2* (oligopeptide transporter). These genes, along with *DUR3*, involved in the transport of urea, are important in the pathogenicity of *C. albicans* and the ability of the organism to utilise different nitrogen sources. *MEP2* is a regulator of nitrogen starvation-induced filamentation, *SAP2* is involved in the degradation of protein as a nitrogen source such as host proteins and *DUR3* is involved in the uptake of urea [102, 115, 92].

Tor is a highly conserved protein and has been demonstrated in mammalian cells to be involved in growth. Moreover, in mammalian cells, mTor plays a critical role in embryogenesis and cellular morphogenesis in neurons and T-cells [130, 131]. In the yeast *S. cerevisiae*, Tor has been shown to play a role in the proliferation of cells in a nutrient rich environment while suppressing genes involved in pseudohyphal growth [132]. Furthermore, the activity of Tor can be blocked by the drug rapamycin which

in *C. albicans* induces the expression of adhesins, and in *C. albicans* has been shown to extend hyphal growth in a rich medium. To date, *S. cerevisiae* has been the model organism to study Tor biology.

Gtr1 is an Upstream Activator of the Tor1 Kinase

Gtr1 and Gtr2 are GTPases that form a heterodimer, signaling amino acid availability and function upstream of the TORC1 complex in *S. cerevisiae.* These are orthologs of the mammalian RAG GTPases that function in the activation of mTor via amino acid sensing [133, 134]. We hypothesised that, seeing as these mechanisms are conserved between *S. cerevisiae* and mammalian cells, this mechanism of nutrient sensing may also be conserved in *C. albicans.*

An overexpressed P_{ENO}*GTR1* allele and a Δ*gtr1* mutant were generated in *C. albicans* SC5314 and sent to Dr. Julia Koehler's laboratory in Boston. An assay to investigate the phosphorylation status of Rps6 was performed in order to determine whether the *C. albicans* Gtr1 was a regulator of Tor1 kinase activity. Figure 4.2 illustrated the results of the P-S6 assay. WT SC5314 and heterozygous Δ*gtr1* showed equal band intensities while the P_{ENO}*GTR1* strain had the greatest band intensity. Homozygous Δ*gtr1* had little, if any, visible band indicative of greatly reduced Tor1 activity.

The Putative Activators of Tor1 Play a Role in Adhesion, Hyphal Formation & Biofilm Formation

Upon successfully generating overexpression strains where P_{ENO} was placed upstream of *VAM6*, *GTR1*, *RHB1* and *TOR1*, an array of phenotypic tests were performed to determine the effects on filamentation in nitrogen limiting environments. Firstly, we noted that P_{ENO} strains were capable of forming hyphae in a hyphal inducing medium (Fig. 3.7). Of the tests performed however, the main observation was that P_{ENO} strains lacked the ability to form hyphae as readily as WT SC5314 cells on solid medium and they aggregated less than WT SC5314 in liquid medium.

Figure 3.6 illustrates the lack of hyphae on YNB agar without amino acids and supplemented with either 100 μM urea or $(NH_4)_2SO_4$. This phenotype has previously been shown by Chen *et al.* (2012) were an overexpressed *RHB1* strain attenuates filamentous growth on nitrogen limiting medium [92]. Moreover, in the current study, the addition of 0.5 nM of rapamycin to the medium reveresed the non-filamentous phenotype observed, supporting the role of Tor1 in mediating the phenotype. Furthermore, when Δ*rhb1* and Δ*gtr1* where grown on 100 μM $(NH_4)_2SO_4$, these strains showed equal if not more hyphae surrounding the colonies.

The ability to adhere to the mucosal surface and switch from yeast-to-hyphal cells is a contributing factor to the pathogenicity of *C. albicans* [135]. Therefore, the ability of P_{ENO} strains to aggregate and flocculate were examined. In order to investigate the aggregation and flocculation, P_{ENO} strains were grown in liquid YEPD supplemented with 10 % serum (v/v). As illustrated in figure 3.10, P_{ENO} strains aggregated to a lesser extent than WT SC5314, suggesting genes involved in adhesion are suppressed. In order to quantify this observed phenotype, a semi-quantitative assay was developed involving the filtration of samples to remove hyphal aggregates enabling yeast cells to be counted. These data showed that there was a statistically significant increase in free yeast cells at 2 h, suggesting that P_{ENO} strains, in a strong hyphal inducing medium, are slow to express genes involved in adhesion. Furthermore, upon the addition of 0.5 nM rapamycin the phenotype was reversed resulting in similar cell counts similar to WT SC5314, thus suggesting a role for Vam6, Gtr1 and Rhb1 upstream of Tor1. Additionally, when the assay was performed on the Δ*gtr1* and Δ*rhb1* strains, both mutants aggregated to a greater degree than WT SC5314 (Fig. 4.5) and showed a significantly reduced number of free yeast cells counted at the 2 h and 4 h time points (Fig. 4.6). These data suggest a role for Gtr1 and Rhb1 in the expression of adhesin genes via Tor1. Examination of the DNA microarray performed in Chapter 5 suggests that Gtr1, to a greater extent than Rhb1, regulates the expression of these adhesins. Although similarities were observed in the expression level of *HWP1* and *ECE1* between the two

strains, a large number of genes associated with cell adhesion were up-regulated in the Δ*gtr1* strain compared to the Δ*rhb1* strain. This included the agglutinin encoding *ALS* genes, *ALS2*, *ALS3* and *ALS4*, as well as the filamentous growth regulator *UME6*, which were all up-regulated in the Δ*gtr1* strain. The *ALS* family in *C. albicans* encode large cell-surface glycoproteins. These proteins have been associated with a role in the adhesion to the surface of host cells [136]. Furthermore, this family of genes is associated with pathogenicity in *C. albicans*. The comparative DNA microarray data correlates with the phenotypes observed in Chapter 4. The Δ*gtr1* mutant aggregated and flocculated to a greater extent than the the Δ*rhb1* mutant strain. Furthermore, genes associated with biofilm formation were up-regulated in the Δ*gtr1* strain compared to the Δ*rhb1* strain (Fig. 5.3).

Previous work by Bastidas *et al.* (2009) showed that a rapamycin resistant Tor1 strain was unable to flocculate when grown in Spider medium [90]. Therefore, flocculation of the constitutively active Tor1 P_{ENO} strains was examined in Spider medium. It was observed that the P_{ENO} strains exhibited reduced flocculation in Spider medium compared with WT SC5314 (Fig. 3.12). This provides further evidence of the inhibition of adhesin expression suggesting a Tor1 hyperactive phenotype. Moreover, flocculation of Δ*gtr1* and Δ*rhb1* demonstrated that Δ*gtr1* flocculates when compared with WT SC5314 (Fig. 4.9) while Δ*rhb1* did not. Furthermore, upon examining the flocculate, it was evident that Δ*gtr1* aggregated to a greater degree than the other strains and formed pseuduhyphae, which may be the result of increased *UME6* expression. These data are further evidence to support a role for Gtr1-Tor1 downstream signaling in adhesin expression. These observations regarding the reduced aggregation and flocculation of the P_{ENO} strains led to the hypothesis that a Tor1 hyperactive phenotype would result in a decrease in biofilm formation and adherence of cells to an epithelial monolayer.

Biofilm assays were therefore performed using a crystal violet staining method to stain biomass. After 24 h, a significant reduction in biofilm biomass was observed in the P_{ENO}*TOR1*, P_{ENO}*GTR1* and P_{ENO}*RHB1* strains compared with WT SC5314. Moreover,

at 48 h, $P_{ENO}GTR1$ continued to demonstrate a significant reduction in the level of biofilm formed, suggesting a greater role for Gtr1-Tor1 signaling to genes associated with adherence. This correlates with aggregation and flocculation assays performed earlier, suggesting a role for Gtr1-Tor1 signaling in maintaining biofilm adherence. Furthermore, biofilm assays performed on $\Delta gtr1$ and $\Delta rhb1$ mutants showed an increase in biofilm formation that was significant when compared with WT SC5314. The assays in the current study were carried out in 96 well plates. It would be of interest to repeat these experiments using a flow model that would be more representative of biofilms forming on implanted devices such as catheters. Nonetheless, plates were washed to remove non-adherent cells and statistical significance was observed. Unfortunately, unlike the biofilm assays, epithelial cell adherence assays were non-reproducible resulting in no discernible differences between WT SC5314 and P_{ENO} strains.

The results observed with the P_{ENO} strains suggest that they mimic a Tor1 hyperactive phenotype resulting in the lack of adherence, aggregation and ultimately the reduced ability to form biofilms. These data suggest a role for Vam6, Gtr1 and Rhb1 in signaling to the Tor1 kinase. Further experiments need to be carried out to determine the effects of biofilm assays in a flow system to assess the ability of P_{ENO} strains to adhere to inorganic material. Moreover, when phagocytosed, the cell wall of *C. albicans* is subjected to H_2O_2 stress and an unfavorable environment resulting in the morphological shift from yeast-to-hyphal forms which is an important virulence factor [137]. Genomic transcript profiling by Lorenzo *et al.* (2004) has shown that there are two successive steps in the reprogramming of the transcription in *C. albicans*. The first, a starvation response resulting in down-regulation of translation and activation of the glyoxylate cycle to metabolise alternative carbon sources. Additionally, oxidative stress responses and morphogenetic transcriptional programs are initiated. In the second stage, after hyphal growth has enabled escape from the macrophage, the fungal cells can resume with glycolytic growth [138]. As the Tor1 mutants described here are compromised in starvation induced morphogenesis and nutrient acquisition, analysis of the ability of

strains to survive following macrophage phagocytosis should be carried out to assess the ability of the P_{ENO} strains to survive phagocytosis. Ultimately, in vivo infection models using the organism *Galleria mellonella* would prove beneficial in determining the degree of pathogenicity. This infection model would be less costly and would provide proof of concept before advancing to murine infection models.

GTR1 and *RHB1* Interact with Tor1 and Result in Different Downstream Effects

As discussed, some similarities and differences were observed between the Δ*gtr1* and Δ*rhb1* mutants with regards to flocculation, aggregation and biofilm formation. The Δ*gtr1* mutant flocculated and aggregated to a greater extent than the Δ*rhb1* mutant which may be due to the greater expression of the *ALS* genes in this mutant. In order to investigate the differences in gene regulation further, we compared our DNA microarray data generated with the Δ*gtr1* mutant with previously published DNA microarray data on a Δ*rhb1* mutant strain. Unexpectedly, upon comparing both DNA microarray data sets, only four genes were consistently differentially expressed between the two experiments (Fig 5.1). The Δ*gtr1* strain had 225 genes that were up-regulated compared with only 55 in Δ*rhb1*. Similarly, Δ*gtr1* had 183 down-regulated genes compared with 30 in the Δ*rhb1* mutant. Upon comparing DNA microarray datasets, genes associated in cell-cell adhesion, nitrogen utilisation and phosphate uptake showed significant differences between the Δ*gtr1* mutant and Δ*rhb1* mutant (Fig. 5.2). It should be noted that the Rhb1 experiments were performed and analysed in a different laboratory using a different DNA microarray platform. The DNA microarray of the Δ*rhb1* mutant was performed in SD medium rather than YEPD. This may partly account for some of the difference in transcription observed. However, as indicated below, we carried out qRT-PCR experiments to compare expression of selected genes (n = 11) in both the Δ*gtr1* and Δ*rhb1* mutants an in each case the differential expression patterns identified in the microarray analysis was confirmed. As discussed, genes associated with cell-cell adhesion

(*HWP1, ECE1*) were up-regulated in both strains. Additionally, when analysing genes associated with the utilisation of nitrogen and phosphate uptake, genes associated in nitrogen utilisation were up-regulated in Δ*rhb1* compared with Δ*gtr1*, while genes associated with phosphate uptake were up-regulated in the Δ*rhb1* strain compared with the Δ*gtr1* strain. The genes *MEP2*, *SAP2*, *OPT1*, *OPT2* and *DUR1,2*, associated with the utilisation of alternative nitrogen sources, were all up-regulated in the Δ*rhb1* strain compared with the Δ*gtr1* strain. However, the *PHO* genes, *PHO84*, *PHO87*, *PHO89*, *PHO91*, *PHO112* and *PHO113*, were only up-regulated in the Δ*gtr1* strain compared to the Δ*rhb1* strain.

Additional differences observed between the DNA microarray datasets including genes associated with cell wall functions, amino acid biosynthesis, metabolic processes and genes associated with filamentous growth.

The genes *HGC1* and *UME6* with roles in filamentous growth, were up-regulated in the Δ*gtr1* strain compared to the Δ*rhb1* strain. This correlates with the pseudohyphal morphology of the flocculates seen in Chapter 4, where the flocculate from the Δ*gtr1* strain had extended hyphae in comparison to the yeast cell morphology of the Δ*rhb1* strain.

These data suggest separate roles for Gtr1 and Rhb1 sensing and signaling to Tor1, resulting in different downstream effects. Furthermore, the data suggest there may be multiple Tor complexes, each involved in multiple responses to different environmental signals (Fig 7.1). It is suggested that future work using the Phospho-RPS6 be carried out on the Δ*rhb1* strain and Δ*gtr1* strain subjected to a medium rich in phosphate prior to growth in YNB (without amino and ammonium sulfate) and 1 % glucose.

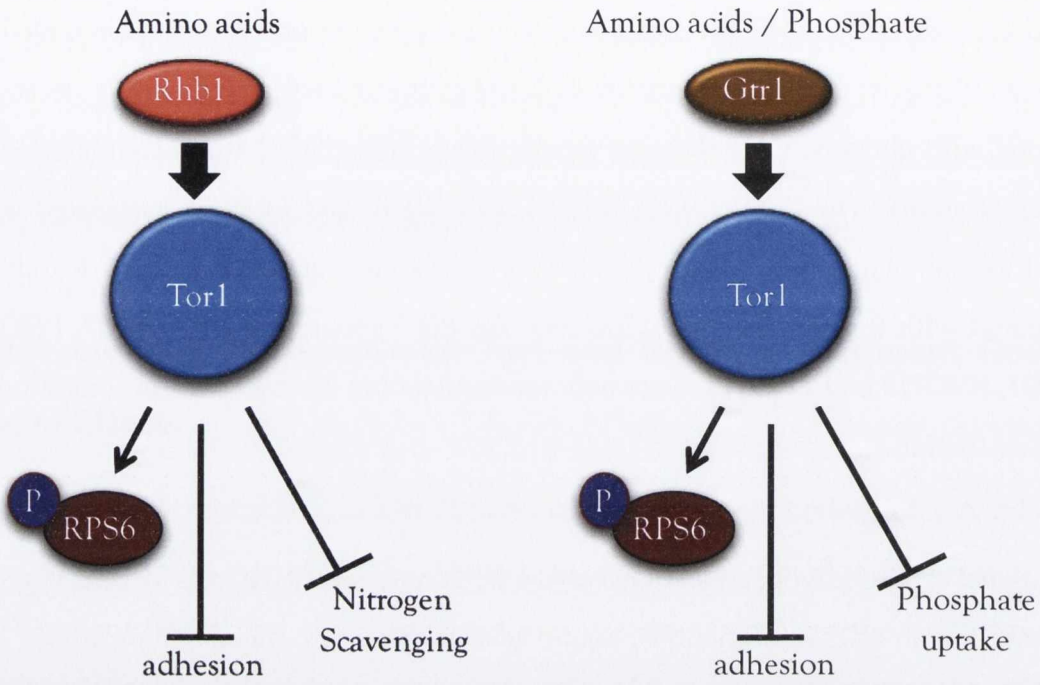

Figure 7.1: **Suggested Gtr1 and Rhb1 down stream targets via the Tor1 kinase.**

The data suggests different responses due to the activation of Tor1 via Gtr1 or Rhb1. Activation by both results in the regulation of ribosome biogenesis and suppression of adhesins. However Gtr1 appears to regulate the uptake of phosphates while Rhb1 regulates nitrogen uptake via the Tor1 kinase.

Tor1 is Involved in the Expression of Genes Associated with Virulence

Genes that are associated with adherence, hyphal formation and biofilm formation are linked to the virulence and pathogenicity of the organism. As stated in Chapter one, mutant strains that have a defect in hyphal formation are less virulent and it is possible that Tor1 may play a role in adhesion and hyphal elongation of *C. albicans*. Furthermore, mutants with a defect in nitrogen uptake result in the loss of hyphal formation. In *S. cerevisiae*, Lorenzo *et al.* (1998) demonstrated that a Δ*mep2* mutant abolished hyphal growth [139]. Furthermore, Δ*sap2* and Δ*dur1,2* mutants have been shown to attenuate the virulence of *C. albicans* [69, 123]. In Chapter 3, we have shown that overexpression of the activators of Tor1 as well as the Tor1 gene resulted in a hyperactive Tor1 phenotype, which led to reduced hyphal formation on nutrient poor solid medium. Furthermore, these overexpression strains were less capable of aggregating and flocculating compared with WT SC5314. This suggests that a hyperactive Tor1 results in the suppression of genes associated with adhesion and hyphal formation. DNA microarray analysis was also performed on a doxycycline-regulatable Tor1 strain. These data showed that in nutrient rich YEPD, when Tor1 is inhibited with doxycycline, genes associated with hyphal formation, biofilm formation and adhesion are all up-regulated (Chapter 6), suggesting that the Tor1 kinase controls the expression of these genes. Some of the genes up-regulated include *ALS3*, *HDA1*, *HSP21*, *SOD4*, *HYR1* and *HGC1*. *ALS3*, *HSP21*, *HYR1* and *HGC1* are also up-regulated in the rapamycin treated strain correlating with the data presented here, further suggesting the role of the Tor1 kinase in the expression of these genes. A full list of the up-regulated genes can be seen in the supplemental table S7.

The N-terminal of Tor1 Plays a Role in Starvation Responses

Full length tetO-*TOR1/tor1* (JKC1549) was compared with the tetO-Δ*NTOR1* JKC1441 strain in Chapters 4 and 6. JKC1441 has a truncated N-terminal, resulting in the loss of the HEAT repeat domain of the Tor1 protein. As previously stated in Chapter 1,

HEAT repeat domains may be involved in localisation or in protein-protein interactions. In phenotypic analysis, while both the tetO strains aggregated to a greater extent compared to WT JKC1361, the tetO-Δ*NTOR1* strain JKC1441 showed a significant decrease in the amount of free yeast following filtration of the hyphal aggregates (Fig 4.10). Furthermore, this was observed qualitatively in figure 4.8. The data suggests that the HEAT repeat domains are an important domain, and loss of this domain impacts significantly on Tor1 function. If this truncation resulted in loss of Tor1 activity, it is possible that cells of the tetO-Δ*NTOR1* strain would mimic those in a nutrient poor environment. On nutrient rich YEPD agar, JKC1441 growth is reduced in comparison to JKC1549. Moreover, in flocculation assays, JKC1441 flocculates to a greater extent than JKC1549 (Fig. 4.12) and upon visual inspection, cells have extended hyphal growth (Fig 4.13). Furthermore, a DNA microarray was performed on JKC1441 without the addition of doxycycline and compared to the intact WT JKC1361 (Fig. 7.2). The analysis showed that genes associated with carbohydrate metabolism and amino acid biosynthesis were down-regulated, which is indicative of a starvation response. Finally, genes associated with stress and starvation responses, as well as filamentation, were all up-regulated. This suggests a role for the N-terminal in Tor1 signaling in *C. albicans*. In order to investigate this, it is suggested that tandem affinity purification is used to study the protein-protein interactions of tetO-Δ*NTOR1* and compare it to an intact Tor1 protein.

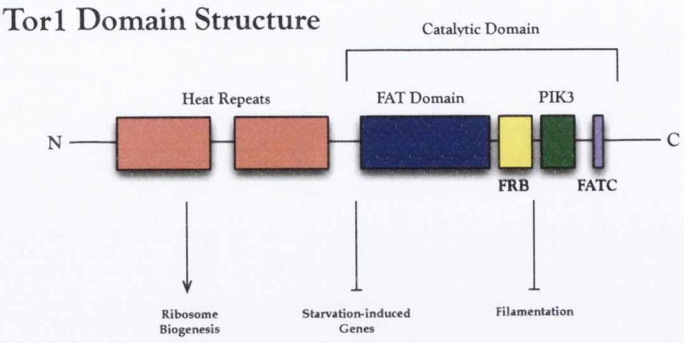

(a)

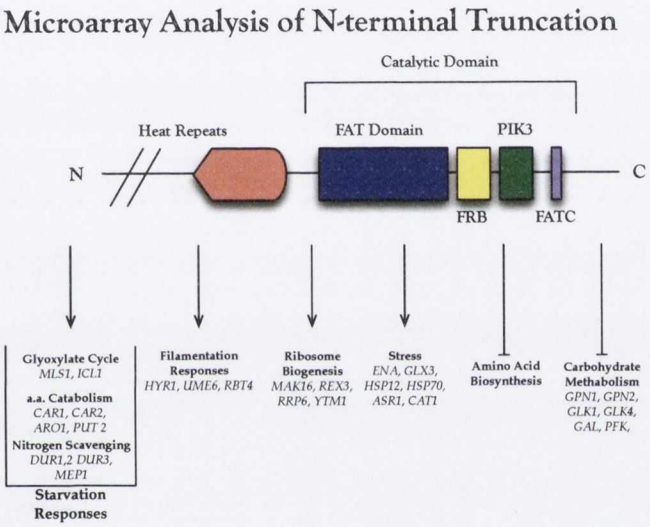

(b)

Figure 7.2: **DNA microarray comparison of the tetO-ΔN*TOR1* and *tor1/TOR1* strains.**

(a) Domain structure of Tor1. In nutrient rich YEPD, starvation response genes were suppressed as well as genes involved in filamentation while genes associated with ribosome biogenesis and glycolysis were expressed. (b) Domain structure of the Tor1 protein in the tetO-ΔN*TOR1* strain. DNA microarray analysis of the tetO-ΔN*TOR1* strain in YEPD without doxycycline revealed that expression of genes associated with carbohydrate metabolism and amino acid biosynthesis were down-regulated. Expression of genes associated with stress and starvation responses as well as filamentation were all increased. Expression of genes associated with ribosome biogenesis were also increased.

Ribosome Biogenesis May Be Controlled via Alternate Pathways to the Tor1 Kinase Pathway

As previously stated in Chapter 1, Tor1 is involved in cellular proliferation, and active growth requires numerous ribosomes. This is an energy-heavy process and therefore promotion of ribosome biogenesis is only observed in nutrient rich conditions, while in nutrient poor conditions, ribosome production is reduced [78, 98]. Therefore, in a doxycycline-regulatable *TOR1* strain, we hypothesised that decreased Tor1 activity would also result in decreased ribosomal activity. A DNA microarray carried out on a doxycycline-regulatable *TOR1* strain was compared with previously published DNA microarray data on a rapamycin treated strain.

Comparative DNA microarray studies revealed a large number of differences between the two datasets. In rapamycin treated cells, genes associated with ribosome biogenesis and assembly, along with those associated with biogenesis and assembly of the large subunit, were down-regulated, as expected in a Tor1 inhibited strain. However, the doxycycline-regulatable strain exhibited an opposite effect. Upon suppression of *TOR1* expression, ribosomal genes were up-regulated as shown in the heat maps in figure 6.5. This difference could suggest that rapamycin treatment and *TOR1* depletion have different effects on Tor1 signaling. Some studies have shown that the effects of rapamycin are very different compared to other methods of *TOR1* inhibition. For example, nutrient removal or stress, both of which inhibit Tor1, have been shown to signal different responses than that caused by rapamycin. Sfp1 and Sch9 are TORC1 substrates involved in activating transcription of genes involved in ribosome biogenesis. Work by Urban *et al.* (2007) showed that TORC1 association with Sfp1, as well as its phosphorylation, was greatly inhibited by rapamycin but unaffected by nutrient deprivation or osmotic stress [77]. There are also data to suggest that impairment of ribosome biogenesis or translation can activate a feedback mechanism to boost expression of ribosomal genes. Firstly, deletion of Sch9 or Sfp1 increases expression of genes involved in ribosome biogenesis. Secondly, treatment with cycloheximide or impairment of the ribosome also

increases the expression of ribosomal genes [140]. These feedback mechanisms are uncharacterized and are presumed to involve Tor1 activation. The increased transcription of rRNA genes observed after *TOR1* suppression may also be the result of a feedback mechanism activated in response to a reduction in rRNA gene transcription. To characterise this response, it may be necessary to examine transcription of these genes at an earlier time-point, prior to the 2 h time-point examined here to determine if the increased transcription of rRNA genes is proceeded by a period of inhibition that may trigger this response.

Candida albicans Tor1 and the Activators Gtr1 and Rhb1.

In this study, we aimed to determine the role of upstream promotors of the *C. albicans* Tor1 kinase and whether they could act as possible antifungal targets. From the data presented here, it is clear that Gtr1 is an upstream activator of the *C. albicans* Tor1 kinase. DNA microarray analysis showed that both Gtr1 and Rhb1 have distinct outcomes in the downstream effects of the Tor1 kinase. Genes associated with cell-cell adhesion, biofilm formation and phosphate uptake were all up-regulated in the Δ*gtr1* mutant suggesting a role for Gtr1-Tor1 signaling of these gene sets. However, genes associated with nitrogen utilisation were up-regulated in the Δ*rhb1* mutant suggesting a role for Rhb1-Tor1 signaling of these gene sets. Not only do these DNA microarrays suggest separate roles for both Gtr1 and Rhb1, they suggest that there might be multiple Tor complexes involved in multiple responses to environmental signals.

Additionally, we have shown that overexpression of these activators resulted in a hyperactive phenotype, resulting in the reduction of hyphal formation when grown on nitrogen poor medium. However, in a strong hyphal inducing medium (YEPD with 10 % v/v serum), overexpression strains were still capable of forming true hyphae, albeit aggregation was less than WT SC5314. Nonetheless, targeting Gtr1 or Rhb1 alone may not be of benefit in reducing infection. Although a reduction was observed in the hyphal formation on solid medium in P_{ENO} strains, a complete inhibition of hyphal formation

was not obtained. Moreover, each strain was capable of forming true hyphae although adherence was reduced as observed in flocculation assays. Furthermore, targeting Gtr1 and Rhb1 may not be specific to *C. albicans*. As previously discussed, homologs of these exist in mammalian hosts and are termed RagA and Rheb and Gtr1 shares protein (52 %) and sequence (47 %) similarity with mammalian GTPase RagA. It is suggested however, that future studies examine the effects of a double $\Delta gtr1$::$\Delta rhb1$ mutant. Moreover, murine infection models using these mutant and overexpression strains may give further insight into virulence in an *in vivo* setting. Perhaps targeting both Gtr1 and Rhb1 may result in a significant knockdown in virulence, suggesting the use of combination therapy to maintain Gtr1 and Rhb1 in a GTP active state. This could be achieved using the P_{ENO} strains in a murine infection model. It is suggested that these strains would exhibit a decrease in infection compared with a wild-type strain.

Furthermore, our data suggests that nutrient sensing and adhesion maybe linked. This may be due to competition between *C. albicans* and the microflora on mucosal surfaces. In the GI tract, where nutrient levels are varying, increased bacterial growth may be detected by *C. albicans* as limited nutrient availability. This in turn may result in the expression of adhesins in order to adhere to the mucosal surface in an environment where competition for space is likely to be tightly linked to the acquisition of nutrients. As such, it would be in the interest of *C. albicans* to signal the expression of genes associated with adherence in combination to those associated with the acquisition of nutrients in a nutrient limiting environment. Therefore, our data suggest that this role might be dedicated to the Gtr1 and Rhb1 proteins. Gtr1 and Rhb1 may signal these different responses to the Tor1 kinase, thus activating separate downstream responses.

Finally, along with the analysis of the putative activators of Tor1, doxycycline-regulatable *TOR1* strains were also examined for their ability to form hyphae, aggregate and flocculated. These strains showed a reduction in the number of free yeast observed in aggregation assays and an increase in flocculation. These observations were observed at a greater extent in the tetO-ΔN*TOR1* strain. Furthermore, DNA microarray analysis

were performed and showed that in a nutrient rich environment, and with the addition of doxycycline, the tetO-*TOR1* strains mimic those of wild-type cells in a nutrient poor environment with the up-regulation of genes associated with virulence. Therefore, these data presented here provide further evidence for the role of the Tor1 kinase in nutrient sensing and signaling and the virulence of *C. albicans*.

References

[1] Taylor, J. W, Jacobson, D. J, & Fisher, M. C. (1999) The evolution of asexual fungi: Reproduction, Speciation and Classification. *Annual Review of Phytopathology* **37**, 197–246.

[2] Heitman, J. (2006) Sexual reproduction and the evolution of microbial pathogens. *Current biology : CB* **16**, R711–25.

[3] Heitman, J. (2011) Microbial pathogens in the fungal kingdom. *Fungal Biology Reviews* **25**, 48–60.

[4] Bruns, T. (2006) Evolutionary biology: a kingdom revised. *Nature* **443**, 758–761.

[5] Lindahl, B. D, Ihrmark, K, Boberg, J, Trumbore, S. E, Högberg, P, Stenlid, J, & Finlay, R. D. (2007) Spatial separation of litter decomposition and mycorrhizal nitrogen uptake in a boreal forest. *New Phytologist* **173**, 611–620.

[6] Gadd, G. M. (2007) Geomycology: biogeochemical transformations of rocks, minerals, metals and radionuclides by fungi, bioweathering and bioremediation. *Mycological Research* **111**, 3–49.

[7] Huang, B, Guo, J, Yi, B, Yu, X, Sun, L, & Chen, W. (2008) Heterologous production of secondary metabolites as pharmaceuticals in Saccharomyces cerevisiae. *Biotechnology Letters* **30**, 1121–1137.

[8] Christian, V, Shrivastava, R, Shukla, D, & Modi, H. A. (2005) Degradation of xenobiotic compounds by lignin-degrading white-rot fungi: Enzymology and mechanisms involved. *Indian J Exp Biol* **43**, 301–302.

[9] Becker, H. (1998) Setting the stage to screen biocontrol. *Agricultural Research.*

[10] Perlroth, J, Choi, B, & Spellberg, B. (2007) Nosocomial fungal infections: epidemiology, diagnosis, and treatment. *Medical Mycology* **45**, 321–346.

[11] Coleman, D. C, Bennett, D. E, Sullivan, D. J, Gallagher, P. J, Henman, M. C, Shanley, D. B, & Russell, R. J. (2008) Oral Candida in HIV Infection and AIDS: New Perspectives/New Approaches. *Critical Reviews in Microbiology* **19**, 61–82.

[12] Shapiro, R. S, Robbins, N, & Cowen, L. E. (2011) Regulatory circuitry governing fungal development, drug resistance, and disease. *Microbiology and Molecular Biology Reviews* **75**, 213–267.

[13] Wilson, L. S, Reyes, C. M, & Stolpman, M. (2002) The direct cost and incidence of systemic fungal infections. *Value Health* **5**, 26–34.

[14] Zhou, C.-H & Wang, Y. (2012) Recent researches in triazole compounds as medicinal drugs. *Current medicinal chemistry* **19**, 239–280.

[15] Sorgo, A. G, Heilmann, C. J, Dekker, H. L, Bekker, M, Brul, S, De Koster, C. G, de Koning, L. J, & Klis, F. M. (2011) Effects of fluconazole on the secretome, the wall proteome, and wall integrity of the clinical fungus *Candida albicans. Eukaryotic Cell* **10**, 1071–1081.

[16] Ostrosky-Zeichner, L, Casadevall, A, Galgiani, J. N, Odds, F. C, & Rex, J. H. (2010) An insight into the antifungal pipeline: selected new molecules and beyond. *Nature Reviews Drug Discovery* **9**, 719–727.

[17] Douglas, C. M. (2001) Fungal beta(1,3)-D-glucan synthesis. *Medical Mycology* **39 Suppl 1**, 55–66.

[18] Berman, J & Sudbery, P. E. (2002) Candida albicans: a molecular revolution built on lessons from budding yeast. *Nat Rev Genet* **3**, 918–30.

[19] Anderson, J. B. (2005) Evolution of antifungal-drug resistance: mechanisms and pathogen fitness. *Nature Publishing Group* **3**, 547–556.

[20] Cannon, R. D, Lamping, E, Holmes, A. R, Niimi, K, Tanabe, K, Niimi, M, & Monk, B. C. (2007) Candida albicans drug resistance another way to cope with stress. *Microbiology (Reading, England)* **153**, 3211–3217.

[21] White, T, Marr, K, & Bowden, R. (1998) Clinical, cellular, and molecular factors that contribute to antifungal drug resistance. *Clin Microbiol Rev.* **11**, 382–402.

[22] Cowen, L, Sanglard, D, Calabrese, D, Sirjusingh, C, Anderson, J, & Kohn, L. (2000) Evolution of drug resistance in experimental populations of candida albicans. *Journal of Bacteriology* **182**, 1515–1522.

[23] Ferrer, J. (2000) Vaginal candidosis: epidemiological and etiological factors. *International Journal of Gynecology & Obstetrics* **71**, 21–27.

[24] Fidel Jr, P. L, Vazquez, J. A, & Sobel, J. D. (1999) *Candida glabrata*: Review of epidemiology, pathogenesis, and clinical disease with comparison toc. albicans. *Clinical Microbiology Reviews* **12**, 80–96.

[25] Hube, B. (2004) From commensal to pathogen: stage- and tissue-specific gene expression of Candida albicans. *Current opinion in microbiology* **7**, 336–341.

[26] Arendrup, M, Horn, T, & Frimodt-Møller, N. (2002) In Vivo Pathogenicity of Eight Medically Relevant Candida Species in an Animal Model. *Infection* **30**, 286–291.

[27] Verstrepen, K. J & Klis, F. M. (2006) Flocculation, adhesion and biofilm formation in yeasts. *Molecular Microbiology* **60**, 5–15.

[28] King, R. D, Lee, J. C, & Morris, A. L. (1980) *Adherence of Candida* albicans and other candida species to mucosal epithelial cells. *Infection and Immunity* **27**, 667–674.

[29] Brand, A. (2012) Hyphal growth in human fungal pathogens and its role in virulence. *International journal of microbiology* **2012**, 517529.

[30] Morrell, M, Fraser, V. J, & Kollef, M. H. (2005) Delaying the empiric treatment of candida bloodstream infection until positive blood culture results are obtained: a potential risk factor for hospital mortality. *Antimicrob Agents Chemother* **49**, 3640–5.

[31] Magee, B & Magee, P. (1987) Electrophoretic karyotypes and chromosome numbers in candida species. *Journal of General Microbiology* **133**, 425–430.

[32] Selmecki, A, Forche, A, & Berman, J. (2010) Genomic plasticity of the human fungal pathogen candida albicans. *Eukaryot Cell* **9**, 991–1008.

[33] Hickman, M. A, Zeng, G, Forche, A, Hirakawa, M. P, Abbey, D, Harrison, B. D, Wang, Y.-M, Su, C.-h, Bennett, R. J, Wang, Y, & Berman, J. (2013) The 'obligate diploid' candida albicans forms mating-competent haploids. *Nature* **494**, 55–9.

[34] Anaul Kabir, M, Hussain, A, Mohammad, & Ahmad, Z. (2012) *Candida albicans*: A model organism for studying fungal pathogens. *ISRN Microbiol* **2012**, 538694.

[35] Jones, T, Federspiel, N, Chibana, H, Dungan, J, Kalman, S, Magee, B, Newport, G, Thorstenson, Y, Agabian, N, Magee, P, Davis, R, & Scherer, S. (2004) The diploid genome sequence of candida albicans. *Proc. Natl. Acad. Sci. U.S.A* **101**, 7329–7334.

[36] Gow, N. A. R, van de Veerdonk, F. L, Brown, A. J. P, & Netea, M. G. (2012) Candida albicans morphogenesis and host defence: discriminating invasion from colonization. *Nat Rev Microbiol* **10**, 112–22.

[37] Chang, W, Li, Y, Zhang, L, Cheng, A, & Lou, H. (2012) Retigeric acid b attenuates the virulence of candida albicans via inhibiting adenylyl cyclase activity targeted by enhanced farnesol production. *PLoS ONE* **7**, e41624.

[38] Gudlaugsson, O, Gillespie, S, Lee, K, Vande Berg, J, Hu, J, Messer, S, Herwaldt, L, Pfaller, M, & Diekema, D. (2003) Attributable mortality of nosocomial candidemia, revisited. *Clinical Infectious Diseases* **37**, 1172–1177.

[39] Fanning, S & Mitchell, A. P. (2012) Fungal biofilms. *PLoS Pathog* **8**, e1002585.

[40] Calderone, R. A & Fonzi, W. A. (2001) Virulence factors of Candida albicans. *Trends in microbiology* **9**, 327–335.

[41] Su, C, Lu, Y, & Liu, H. (2013) Reduced tor signaling sustains hyphal development in candida albicans by lowering hog1 basal activity. *Mol Biol Cell* **24**, 385–97.

[42] Lo, H.-J, Köhler, J. R, DiDomenico, B, Loebenberg, D, Cacciapuoti, A, & Fink, G. R. (1997) Nonfilamentous C. albicans Mutants Are Avirulent. *Cell* **90**, 939–949.

[43] Sudbery, P, Gow, N, & Berman, J. (2004) The distinct morphogenic states of Candida albicans. *Trends in microbiology* **12**, 317–324.

[44] Sudbery, P. E. (2011) Growth of *Candida albicans* hyphae. *Nature Publishing Group* **9**, 737–748.

[45] Finkel, J. S & Mitchell, A. P. (2011) Genetic control of *Candida albicans* biofilm development. *Nat Rev Microbiol* **9**, 109–18.

[46] Nobile, C. J, Nett, J. E, Andes, D. R, & Mitchell, A. P. (2006) Function of candida albicans adhesin hwp1 in biofilm formation. *Eukaryot Cell* **5**, 1604–10.

[47] Nobile, C, Schneider, H, Nett, J, Sheppard, D, Filler, S, Andes, D, & Mitchell, A. (2008) Complementary adhesin function in *C. albicans* biofilm formation. *Curr Biol.* **18**, 1017–1024.

[48] Nobile, C. J & Mitchell, A. P. (2005) Regulation of cell-surface genes and biofilm formation by the c. albicans transcription factor bcr1p. *Curr Biol* **15**, 1150–5.

[49] Nobile, C. J, Andes, D. R, Nett, J. E, Smith, F. J, Yue, F, Phan, Q.-T, Edwards, J. E, Filler, S. G, & Mitchell, A. P. (2006) Critical role of bcr1-dependent adhesins in c. albicans biofilm formation in vitro and in vivo. *PLoS Pathog* **2**, e63.

[50] Hornby, J. M, Jensen, E. C, Lisec, A. D, Tasto, J. J, Jahnke, B, Shoemaker, R, Dussault, P, & Nickerson, K. W. (2001) Quorum sensing in the dimorphic fungus candida albicans is mediated by farnesol. *Appl Environ Microbiol* **67**, 2982–92.

[51] Ramage, G, Saville, S, Wickes, B, & López-Ribot, J. (2002) Inhibition of *Candida albicans* biofilm formation by farnesol, a quorum-sensing molecule. *Applied and Environmental Microbiology* **68**, 5459–5463.

[52] Peleg, A. Y, Hogan, D. A, & Mylonakis, E. (2010) Medically important bacterial-fungal interactions. *Nat Rev Microbiol* **8**, 340–9.

[53] Heitman, J, Movva, N, & Hall, M. (1991) Targets for cell cycle arrest by the immunosuppressant rapamycin in yeast. *Science* **253**, 905–909.

[54] Schmeizie, T & Hall, M. (2000) Tor, a central controller of cell growth. *Cell* **103**, 253–262.

[55] Richardson, C, Schalm, S, & Blenis, J. (2004) Pi3-kinase and tor: Piktoring cell growth. *Seminars in Cell and Developmental Biology* **15**, 147–159.

[56] Andrade, M & Bork, P. (1995) Heat repeats in the huntingtons disease protein. *Nat. Genet.* **11**, 115–116.

[57] Groves, M, Hanlon, N, Turowski, P, Hemmings, B, & Barford, D. (1999) The structure of the protein phosphatase 2a pr65/a subunit reveals the conformation of its 15 tandemly repeated heat motifs. *Cell* **96**, 99–110.

[58] Stanbrough, M & Magasanik, B. (1995) Transcriptional and posttranslational regulation of the general amino acid permease of *Saccharomyces cerevisiae*. *Journal of Bacteriology* **177**, 94–102.

[59] Beck, T & Hall, M. (1999) The tor signalling pathway controls nuclear localization of nutrient-regulated transcription factors. *Nature* **402**.

[60] Kuruvilla, F, Shamji, A, & Schreiber, S. (2001) Carbon- and nitrogen-guality signaling to translation are mediated by distinct gata-type transcription factors. *Proc. Natl. Acad. Sci. U.S.A* **98**, 7283–7288.

[61] Debailleul, F, Trubbia, C, Frederickx, N, Lauwers, E, Merhi, A, Ruysschaert, J.-M, André, B, & Govaerts, C. (2013) Nitrogen catabolite repressible gap1 promoter, a new tool for efficient recombinant protein production in *S. cerevisiae*. *Microbial Cell Factories* **12**, 1.

[62] Magasanik, B & Kaiser, C. A. (2002) Nitrogen regulation in *Saccharomyces cerevisiae*. *Gene* **290**, 1–18.

[63] Dabas, N & Morschhäuser, J. (2007) Control of Ammonium Permease Expression and Filamentous Growth by the GATA Transcription Factors GLN3 and GAT1 in Candida albicans. *Eukaryotic Cell* **6**, 875–888.

[64] Kriel, J, Haesendonckx, S, Rubio Texeira, M, Van Zeebroeck, G, & Thevelein, J. M. (2011) From transporter to transceptor: Signaling from transporters provokes re-evaluation of complex trafficking and regulatory controls. *BioEssays* **33**, 870–879.

[65] Van Nuland, A, Vandormael, P, Donaton, M, Alenquer, M, Lourenço, A, Quintino, E, Versele, M, & Thevelein, J. M. (2006) Ammonium permease-based sensing mechanism for rapid ammonium activation of the protein kinase A pathway in yeast. *Molecular Microbiology* **59**, 1485–1505.

[66] Van Zeebroeck, G, Bonini, B. M, Versele, M, & Thevelein, J. M. (2009) Transport and signaling via the amino acid binding site of the yeast Gap1 amino acid transceptor. *Nature Chemical Biology* **5**, 45–52.

[67] Morschhäuser, J. J. (2011) Nitrogen regulation of morphogenesis and protease secretion in Candida albicans. *International Journal of Medical Microbiology* **301**, 390–394.

[68] Paul, J. A, Barati, M. T, Cooper, M, & Perlin, M. H. (2014) Physical and genetic interaction between ammonium transporters and the signaling protein Rho1 in the plant pathogen Ustilago maydis. *Eukaryotic Cell* **13**, 1328–1336.

[69] Hube, B, Sanglard, D, Odds, F. C, Hess, D, Monod, M, Schäfer, W, Brown, A. J, & Gow, N. A. (1997) Disruption of each of the secreted aspartyl proteinase genes sap1, sap2, and sap3 of *Candida albicans* attenuates virulence. *Infection and Immunity* **65**, 3529–3538.

[70] Staib, P, Lermann, U, Blass-Warmuth, J, Degel, B, Würzner, R, Monod, M, Schirmeister, T, & Morschhäuser, J. (2008) Tetracycline-inducible expression of individual secreted aspartic proteases in *Candida albicans* allows isoenzyme-specific inhibitor screening. *Antimicrobial Agents and Chemotherapy* **52**, 146–156.

[71] Martínez, P & Ljungdahl, P. O. (2005) Divergence of Stp1 and Stp2 Transcription Factors in Candida albicans Places Virulence Factors Required for Proper Nutrient Acquisition under Amino Acid Control. *Molecular and Cellular Biology* **25**, 9435–9446.

[72] Reuß, O & Morschhauser, J. (2006) A family of oligopeptide transporters is required for growth of candida albicans on proteins. *Molecular Microbiology* **60**, 795–812.

[73] Warner, J. R. (1999) The economics of ribosome biosynthesis in yeast. *Trends in biochemical sciences* **24**, 437–440.

[74] Powers, T & Walter, P. (1999) Regulation of Ribosome Biogenesis by the Rapamycin-sensitive TOR-signaling Pathway in Saccharomyces cerevisiae. *Molecular Biology of the Cell* **10**, 987–1000.

[75] Cardenas, M. E, Cutler, N. S, Lorenz, M. C, Di Como, C. J, & Heitman, J. (1999) The TOR signaling cascade regulates gene expression in response to nutrients. *Genes & development* **13**, 3271–3279.

[76] Loewith, R & Hall, M. (2011) Target of rapamycin (tor) in nutrient signaling and growth control. *Genetics* **189**, 1177–1201.

[77] Urban, J, Soulard, A, Huber, A, Lippman, S, Mukhopadhyay, D, Deloche, O, Wanke, V, Anrather, D, Ammerer, G, Riezman, H, Broach, J. R, De Virgilio, C, Hall, M. N, & Loewith, R. (2007) Sch9 is a major target of TORC1 in Saccharomyces cerevisiae. *Molecular Cell* **26**, 663–674.

[78] LempiAinen, H, Uotila, A, Urban, J, Dohnal, I, Ammerer, G, Loewith, R, & Shore, D. (2009) Sfp1 Interaction with TORC1 and Mrs6 Reveals Feedback Regulation on TOR Signaling. *Molecular Cell* **33**, 704–716.

[79] Ly, C, Arechiga, A. F, Melo, J. V, Walsh, C. M, & Ong, S. T. (2003) Bcr-Abl Kinase Modulates the Translation Regulators Ribosomal Protein S6 and 4E-BP1 in Chronic Myelogenous Leukemia Cells via the Mammalian Target of Rapamycin. *Cancer Research* **63**, 5716–5722.

[80] Ruvinsky, I, Sharon, N, Lerer, T, Cohen, H, Stolovich-Rain, M, Nir, T, Dor, Y, Zisman, P, & Meyuhas, O. (2005) Ribosomal protein S6 phosphorylation is a determinant of cell size and glucose homeostasis. *Genes & development* **19**, 2199–2211.

[81] Chowdhury, T & Köhler, J. R. (2015) Ribosomal protein s6 phosphorylation is controlled by tor and modulated by pka in *Candida albicans*. *Molecular Microbiology* **98**, 384–402.

[82] Raught, B, Gingras, A.-C, & Sonenberg, N. (2001) The target of rapamycin (TOR) proteins. *Proceedings of the National Academy of Sciences of the United States of America* **98**, 7037–7044.

[83] Thomas, G & Hall, M. N. (1997) TOR signalling and control of cell growth. *Current Opinion in Cell Biology* **9**, 782–787.

[84] Lu, Y, Su, C, & Liu, H. (2012) A gata transcription factor recruits hda1 in response to reduced tor1 signaling to establish a hyphal chromatin state in candida albicans. *PLoS Pathog* **8**, e1002663.

[85] Cleary, I. A, Lazzell, A. L, Monteagudo, C, Thomas, D. P, & Saville, S. P. (2012) Brg1 and nrg1 form a novel feedback circuit regulating *Candida albicans* hypha formation and virulence. *Mol Microbiol* **85**, 557–73.

[86] Alonso-Monge, R, Navarro-García, F, Molero, G, Diez-Orejas, R, Gustin, M, Pla, J, Sánchez, M, & Nombela, C. (1999) Role of the mitogen-activated protein kinase hog1p in morphogenesis and virulence of candida albicans. *Journal of Bacteriology* **181**, 3058–3068.

[87] Enjalbert, B, Smith, D, Cornell, M, Alam, I, Nicholls, S, Brown, A, & Quinn, J. (2006) Role of the hog1 stress-activated protein kinase in the global transcriptional response to stress in the fungal pathogen candida albicans. *Mol Biol Cell* **17**, 1018–1032.

[88] Zacchi, L. F, Gomez-Raja, J, & Davis, D. A. (2010) Mds3 Regulates Morphogenesis in Candida albicans through the TOR Pathway. *Molecular and Cellular Biology* **30**, 3695–3710.

[89] Lee, C. M, Nantel, A, Jiang, L, Whiteway, M, & Shen, S. H. (2004) The serine/threonine protein phosphatase sit4 modulates yeast-to-hypha morphogenesis and virulence in *Candida albicans*. *Molecular Microbiology* **51**, 691–709.

[90] Bastidas, R. J, Heitman, J, & Cardenas, M. E. (2009) The Protein Kinase Tor1 Regulates Adhesin Gene Expression in Candida albicans. *PLoS Pathogens* **5**, e1000294.

[91] Binda, M, Péli-Gulli, M.-P, Bonfils, G, Panchaud, N, Urban, J, Sturgill, T. W, Loewith, R, & De Virgilio, C. (2009) The Vam6 GEF controls TORC1 by activating the EGO complex. *Molecular cell* **35**, 563–573.

[92] Chen, Y.-T, Lin, C.-Y, Tsai, P.-W, Yang, C.-Y, Hsieh, W.-P, & Lan, C.-Y. (2012) Rhb1 regulates the expression of secreted aspartic protease 2 through the tor signaling pathway in *Candida albicans*. *Eukaryot Cell* **11**, 168–82.

[93] Long, X, Lin, Y, Ortiz-Vega, S, Yonezawa, K, & Avruch, J. (2005) Rheb binds and regulates the mtor kinase. *Curr Biol* **15**, 702–13.

[94] Alonso-Monge, R, Román, E, Arana, D. M, Prieto, D, Urrialde, V, Nombela, C, & Pla, J. (2010) The sko1 protein represses the yeast-to-hypha transition and regulates the oxidative stress response in candida albicans. *Fungal Genet Biol* **47**, 587–601.

[95] Biswas, K & Morschhäuser, J. (2005) The mep2p ammonium permease controls nitrogen starvation-induced filamentous growth in candida albicans. *Mol Microbiol* **56**, 649–69.

[96] Gong, R, Li, L, Liu, Y, Wang, P, Yang, H, Wang, L, Cheng, J, Guan, K.-L, & Xu, Y. (2011) Crystal structure of the Gtr1p–Gtr2p complex reveals new insights into the amino acid-induced TORC1 activation. *Genes & development* **25**, 1668–1673.

[97] Sengottaiyan, P, Spetea, C, Lagerstedt, J. O, Samyn, D, Andersson, M, Ruiz-Pavón, L, & Persson, B. L. (2012) The intrinsic GTPase activity of the Gtr1 protein from Saccharomyces cerevisiae. *BMC Biochemistry* **13**, 11–11.

[98] Loewith, R & Hall, M. N. (2011) Target of rapamycin (TOR) in nutrient signaling and growth control. *Genetics* **189**, 1177–1201.

[99] Kim, J & Guan, K.-L. (2011) Amino Acid Signaling in TOR Activation. *Annual review of biochemistry* **80**, 1001–1032.

[100] Valbuena, N, Guan, K.-L, & Moreno, S. (2012) The Vam6 and Gtr1-Gtr2 pathway activates TORC1 in response to amino acids in fission yeast. *Journal of cell science* **125**, 1920–1928.

[101] Manning, B. (2003) Rheb fills a GAP between TSC and TOR. *Trends in biochemical sciences* **28**, 573–576.

[102] Tsao, C.-C, Chen, Y.-T, & Lan, C.-Y. (2009) A small g protein rhb1 and a gtpase-activating protein tsc2 involved in nitrogen starvation-induced morphogenesis and cell wall integrity of *Candida albicans*. *Fungal Genetics and Biology* **46**, 126–136.

[103] Naglik, J. R, Challacombe, S. J, & Hube, B. (2003) Candida albicans Secreted Aspartyl Proteinases in Virulence and Pathogenesis. *Microbiology and molecular ...* **67**, 400–428.

[104] Sullivan, D, Moran, G, & Colman, D. (2007) Differential regulation of the transcriptional repressor nrg1 accounts for altered host cell interactions in candida albicans and candida dubliniensis. *Molecular Microbiology* **66**, 915–929.

[105] O'Connor, L, Caplice, N, Coleman, D. C, Sullivan, D. J, & Moran, G. P. (2010) Differential Filamentation of Candida albicans and Candida dubliniensis Is Governed by Nutrient Regulation of UME6 Expression. *Eukaryotic Cell* **9**, 1383–1397.

[106] Gillum, A, Tsay, E, & Kirsch, D. (1984) Candida albicans gene for orotidine-5'-phosphate decarboxylase by complementation of s. cerevisiae ura3 and e. coli pyrf mutations. *Mol Gen Genet* **198**, 179–182.

[107] Cruz, M. C, Goldstein, A. L, Blankenship, J, Del Poeta, M, Perfect, J. R, McCusker, J. H, Bennani, Y. L, Cardenas, M. E, & Heitman, J. (2001) Rapamycin and less

immunosuppressive analogs are toxic to *Candida albicans* and *Cryptococcus neoformans* via fkbp12-dependent inhibition of tor. *Antimicrob Agents Chemother* **45**, 3162–70.

[108] Staib, P, Moran, G. P, Sullivan, D. J, Coleman, D. C, & Morschhäuser, J. (2001) Isogenic strain construction and gene targeting in *Candida dubliniensis*. *J Bacteriol* **183**, 2859–65.

[109] Berger, J. A, Hautaniemi, S, Järvinen, A.-K, Edgren, H, Mitra, S. K, & Astola, J. (2004) Optimized LOWESS normalization parameter selection for DNA microarray data. *BMC bioinformatics* **5**, 194.

[110] Li, L & Guan, K.-L. (2009) Amino Acid Signaling to TOR Activation: Vam6 Functioning as a Gtr1 GEF. *Molecular Cell* **35**, 543–545.

[111] Reinke, A, Chen, J. C. Y, Aronova, S, & Powers, T. (2006) Caffeine Targets TOR Complex I and Provides Evidence for a Regulatory Link between the FRB and Kinase Domains of Tor1p. *Journal of Biological Chemistry* **281**, 31616–31626.

[112] Song, W, Wang, H, & Chen, J. (2011) *Candida albicans* sfl2, a temperature-induced transcriptional regulator, is required for virulence in a murine gastrointestinal infection model. *FEMS Yeast Research* **11**, 209–222.

[113] Martin, R, Moran, G. P, Jacobsen, I. D, Heyken, A, Domey, J, Sullivan, D. J, Kurzai, O, & Hube, B. (2011) The Candida albicans-Specific Gene EED1 Encodes a Key Regulator of Hyphal Extension. *PLoS ONE* **6**, e18394.

[114] Milne, S. W, Cheetham, J, Lloyd, D, Aves, S, & Bates, S. (2011) Cassettes for pcr-mediated gene tagging in *Candida albicans* utilizing nourseothricin resistance. *Yeast* **28**, 833–41.

[115] Navarathna, D. H. M. L. P, Das, A, Morschhäuser, J, Nickerson, K. W, & Roberts, D. D. (2011) Dur3 is the major urea transporter in candida albicans and is co-regulated with the urea amidolyase dur1,2. *Microbiology* **157**, 270–9.

[116] Dabas, N, Schneider, S, & Morschhäuser, J. (2009) Mutational analysis of the candida albicans ammonium permease mep2p reveals residues required for ammonium transport and signaling. *Eukaryot Cell* **8**, 147–60.

[117] Vinod, P. K, Sengupta, N, Bhat, P. J, & Venkatesh, K. V. (2008) Integration of global signaling pathways, camp-pka, mapk and tor in the regulation of flo11. *PLoS One* **3**, e1663.

[118] Murai, T, Nakase, Y, Fukuda, K, Chikashige, Y, Tsutsumi, C, Hiraoka, Y, & Matsumoto, T. (2009) Distinctive responses to nitrogen starvation in the dominant active mutants of the fission yeast Rheb GTPase. *Genetics* **183**, 517–527.

[119] Sekiguchi, T, Hayashi, N, Wang, Y, & Kobayashi, H. (2008) Genetic evidence that ras-like gtpases, gtr1p, and gtr2p, are involved in epigenetic control of gene expression in *Saccharomyces cerevisiae*. *Biochemical and Biophysical Research Communications* **368**, 748–754.

[120] Soulard, A, Cohen, A, & Hall, M. N. (2009) TOR signaling in invertebrates. *Current Opinion in Cell Biology* **21**, 825–836.

[121] Eaton, K. A, Brooks, C. L, Morgan, D. R, & Krakowka, S. (1991) Essential role of urease in pathogenesis of gastritis induced by Helicobacter pylori in gnotobiotic piglets. *Infection and Immunity* **59**, 2470–2475.

[122] Cox, G. M, Mukherjee, J, Cole, G. T, Casadevall, A, & Perfect, J. R. (2000) Urease as a virulence factor in experimental cryptococcosis. *Infection and Immunity* **68**, 443–448.

[123] Navarathna, D. H. M. L. P, Lionakis, M. S, Lizak, M. J, Munasinghe, J, Nickerson, K. W, & Roberts, D. D. (2012) Urea amidolyase (dur1,2) contributes to virulence and kidney pathogenesis of *Candida albicans*. *PLoS ONE* **7**, e48475–15.

[124] Taff, H. T, Mitchell, K. F, Edward, J. A, & Andes, D. R. (2013) Mechanisms of Candidabiofilm drug resistance. *Future Microbiology* **8**, 1325–1337.

[125] Gao, M & Kaiser, C. A. (2006) A conserved GTPase-containing complex is required for intracellular sorting of the general amino-acid permease in yeast. *Nature cell biology* **8**, 657–667.

[126] Bun-Ya, M, Harashima, S, & Oshima, Y. (1992) Putative GTP-binding protein, Gtr1, associated with the function of the Pho84 inorganic phosphate transporter in Saccharomyces cerevisiae. *Molecular and Cellular Biology* **12**, 2958–2966.

[127] Dubouloz, F, Deloche, O, Wanke, V, Cameroni, E, & De Virgilio, C. (2005) The TOR and EGO protein complexes orchestrate microautophagy in yeast. *Molecular Cell* **19**, 15–26.

[128] Laplante, M & Sabatini, D. M. (2012) mTOR signaling in growth control and disease. *Cell* **149**, 274–293.

[129] Ramírez, M. A & Lorenz, M. C. (2007) Mutations in alternative carbon utilization pathways in *Candida albicans* attenuate virulence and confer pleiotropic phenotypes. *Eukaryotic Cell* **6**, 280–290.

[130] Han, J, Wang, B, Xiao, Z, Gao, Y, Zhao, Y, Zhang, J, Chen, B, Wang, X, & Dai, J. (2008) Mammalian target of rapamycin (mTOR) is involved in the neuronal differentiation of neural progenitors induced by insulin. *Molecular and cellular neurosciences* **39**, 118–124.

[131] Delgoffe, G. M, Kole, T. P, Zheng, Y, Zarek, P. E, Matthews, K. L, Xiao, B, Worley, P. F, Kozma, S. C, & Powell, J. D. (2009) The mTOR kinase differentially regulates effector and regulatory T cell lineage commitment. *Immunity* **30**, 832–844.

[132] Wullschleger, S, Loewith, R, & Hall, M. N. (2006) TOR Signaling in Growth and Metabolism. *Cell* **124**, 471–484.

[133] Kim, E, Goraksha-Hicks, P, Li, L, Neufeld, T. P, & Guan, K.-L. (2008) Regulation of TORC1 by Rag GTPases in nutrient response. *Nature cell biology* **10**, 935–945.

[134] Sancak, Y & Sabatini, D. M. (2009) Rag proteins regulate amino-acid-induced mTORC1 signalling. *Biochemical Society Transactions* **37**, 289–290.

[135] Mayer, F. L, Wilson, D, & Hube, B. (2013) Candida albicans pathogenicity mechanisms. Virulence. 2013; 4: 119–28.

[136] Hoyer, L. L. (2001) The als gene family of *Candida albicans*. *Trends in microbiology* **9**, 176–180.

[137] Lewis, L. E, Bain, J. M, Lowes, C, Gillespie, C, Rudkin, F. M, Gow, N. A. R, & Erwig, L.-P. (2012) Stage specific assessment of *Candida albicans* phagocytosis by macrophages identifies cell wall composition and morphogenesis as key determinants. *PLoS Pathogens* **8**, e1002578.

[138] Lorenz, M. C, Bender, J. A, & Fink, G. R. (2004) Transcriptional response of Candida albicans upon internalization by macrophages. *Eukaryotic Cell* **3**, 1076–1087.

[139] Lorenz, M. C & Heitman, J. (1998) The MEP2 ammonium permease regulates pseudohyphal differentiation in Saccharomyces cerevisiae. *The EMBO journal* **17**, 1236–1247.

[140] Liu, R, Iadevaia, V, Averous, J, Taylor, P. M, Zhang, Z, & Proud, C. G. (2014) Impairing the production of ribosomal RNA activates mammalian target of rapamycin complex 1 signalling and downstream translation factors. *Nucleic Acids Research* **42**, 5083–5096.

Appendices

Table S1. List of oligonucleotide sequences used in the transformation of WT SC5314

Transformation Oligopeptide	Oligopeptide Sequence
CaTOR Mut 1	GTGAGTCGAGAACTCGTCCGAGTTGCAGTTTTATGGCA CGAACAATGGCACGATGCTTTGGAAGATGCTAGCAGG TTTTTC
CaTOR Mut 2	GTGAGTCGAGAACTCATCCGAGTTGTAGTTTTATGGCA CGAACAATGGCACGATGCTTTGGAAGATGCTAGCAGG TTTTTC
CaTOR Mut 3	GTGAGTCGAGAACTCGTCCGAGTTGTAGTTTTATGGCA CGAACAATGGCACGATGCTTTGGAAGATGCTAGCAGG TTTTTC
ENOp/VAM6 Mut F1	TTTGAACAATTGGTTATATATAGTCTTCAATGTATATTT ACAGAATTTAAATATATTACACTGTATTTGTCTTTTAAA TGGAAATCGTAGCGTTAGTATCGAATCGACAGC
ENOp/VAM6 Mut R1	GATATCTTGTTATTCTTAATCTCATTTGAAGAAATTCTT ATTCTATCCAAAGGCTCTATCACATCTATATTCATTACC ATTGTTGTAATATTCCTGAATTATC
ENOp/TOR Mut F1	TTTTTTTCAACCCCGAAATTTGTTCTTCTGATTTTTTGAC TCCATTACCTACCGTTGTGGACCAAGTGATTCGTTAGT ATCGAATCGACAGC
ENOp/TOR Mut R1	TCCTTTGAAAATCTCTGTTAGAGCAACACCATCAACCA CTTGTAGTTGTGCTGATGTAGATGCTGATGCTGACATTG TTGTAATATTCCTGAATTATC
ENOp/RHB1 Mut F1	TTTGATAACCACCACCACCAAGTGAAGCAAGCAAGCA GCCAAACAAAAAAAAAATTTTCTATTATTTTATTGTTGTC CTTTTTTTTTTCGTTAGTATCGAATCGACAGC
ENOp/RHB1 Mut R1	TCTTCAACAAATCGAACGGTGATGGAGGATTTTCCAAC TGAACGAGATCCAACCACTGCTATCTTACGGGCTTTGA CCAGCATTGTTGTAATATTCCTGAATTATC
ENOp/GTR1 Mut F1	AAGTATAGTCATATCATATTTATAATTCTACAAATAAG GTCAAAAAATAAATATAAAAAACCAAAAATACGAAC ACCTAACGTTAGTATCGAATCGACAGC
ENOp/GTR1 Mut R1	AAGTATAGTCATATCATATTTATAATTCTACAAATAAG GTCAAAAAATAAATATAAAAAACCAAAAATACGAAC ACCTAACGTTAGTATCGAATCGACAGC

SAT1/GTR1 F1	CAAAATGTCAATCTCTCGTGTATAACATTTACACTAAT TTATACTCAATCTTAACTATCATCATCATCATTAACAAC AACAGTAAAACGACGGCCAGT
SAT1/GTR1 R1	ATAGAAACTGATTCGTGATTTTGTTAATAGTTTTAATTA CAGATTAAAACTTAAAACTCCCACCTGTTAAGTTTGAC TCTGGAAACAGCTATGACCATG
SAT1/GTR1 2ND F1	TAATCATAATCATTTCTATTTAAATTTAAATTATTGAAA ACAAAACAATCTCACTTTTTTCATCTTATAACTAGTAA AACGACGGCCAGT
SAT1/GTR1 2ND R1	TGTTTTACTCATTATTTTCAATTTTTTCAAACCATCTTCT AGCAGCTTTAATATTATCTAAAATCAATAATTCTTCAT GTGGAAACAGCTATGACCATG
GTR1 Reint F1	CCGCTCGAGGAAGTTATACCACTTCTATG
GTR1 Reint R1	GGGAAGCTTACGCGCGTGACACTCTTCGG

Table S2. List of oligonucleotide sequences used though during this research

Oligopeptide Name	Oligopeptide Sequence
ENOp Con F1	TTGATAATTCAGGAATATTACAAC
VAM6 Con R1	CCCATCCTTAGTTATATTAC
TOR1 Con R1	TTTGAAGCCATTCAATAGCTCTTTT
RHB1 Con R1	TCATTTTTGTTACCAACAAG
GTR1 Con R1	TAATGCTGAATAATTGGAAA
RT VAM6 F1	GGACGCTGCAATGGAATACT
RT VAM6 R1	TTGGCACCGTGTTCTGATAA
RT TOR1 F1	TGTTGAAGGTCAGAGCGTTG
RT TOR1 R1	ATTTGGGCGTAAACGACTTG
RT RHB1 F1	TGTAATGCCAAAAGCATCCA
RT RHB1 R1	CCAAACAAATGGGACTACCTG
RT GTR1 F1	ATGGGATTGTGGAGGTCAAA
RT GTR1 R1	CCCCTGGCAGATATTGTTGT
ACT1 F1	AGCTCCAGAAGCTTTGTTCAGACCAG
ACT1 R1	TGCATACGTTCAGCAATACCTGGG
GTR1/SAT1 FLIP F1	ATTATTGTTTATTGTAAGAT
GTR1/SAT1 FLIP R1	AGTGGGCTGGCAGTAATTTC
ARG5,6 F1	ACCAAGGTAAGTTGGCATCG
ARG5,6 R1	TGGAGACGAACCTTTGGAAG
PES1 F1	AAGGAAGACGGTGAAGCTGA
PES1 R1	TTTGTTGGAAGTTCCCTTCG
DIM1 F1	GGCCCAAGGAATTGTTGATA
DIM1 R1	TTAATTCCGCTGCCATTCTT

GAP2 F1	GTTGGCCTTGTCTGGTTTGT
GAP2 R1	ACTTGGGGAAGAATGCAATTG
CAN2 F1	GCTATTGTTGGGTGGCTCAT
CAN2 R1	TGCACTACGGATTGCTCTTG
RPS3 F1	CCGGTGCTAAAGGTGTTGAA
RPS3 R1	GCATCTGGTAAAGCTCTTGGA
RPF2 F1	TTCCGTGGTGAAGAAACTGA
RPF2 R1	GGACCAATTTCATCCAATTCA
HIP1 F1	GGACAGCATTGTTCCCCTTG
HIP1 R1	GTTTTCGGCATGGCCTTTACC
ALS4 F1	ATTGCCACGCTTGTTTTACC
ALS4 R1	TCCACAGTTTCTCGTCCACA
OPT3 F1	TTCTGCCACCATGCTTCATA
OPT3 R1	CAAGAAATGGGGACCAAGAA
GAP1 F1	ATAGCACTTATGGCCCATGC
GAP1 R1	TCAACATCAATGCTGCCAAT
CAR1 F1	GAATTTTCTTGGGTGCCTCA
CAR1 R1	CCAAGGCCATTTCAACAACT
PHO84 F1	TTTGTTGGGTTTGTTCGTCA
PHO84 R1	GCAATAATGGCACCGACTTT
PHO112 F1	TCATGGTGCTGCGTTTATAT
PHO112 R1	TGGAACATGCACTTCTTGGA
MEP2 F1	GGAAGCAATTGGGGTATCAG
MEP2 R1	TGGTTTCAGGATCGTCATCA